Connection Details and Field Implementation of UHPC Piles – Phase II

Final Report
September 2019

BRIDGE ENGINEERING CENTER

IOWA STATE UNIVERSITY
Institute for Transportation

About BEC

The mission of the Bridge Engineering Center (BEC) is to conduct research on bridge technologies to help bridge designers/owners design, build, and maintain long-lasting bridges.

About InTrans

The mission of the Institute for Transportation (InTrans) at Iowa State University is to develop and implement innovative methods, materials, and technologies for improving transportation efficiency, safety, reliability, and sustainability while improving the learning environment of students, faculty, and staff in transportation-related fields.

ISU Nondiscrimination Statement

Disclaimer Notice

Iowa DOT Statements

Technical Report Documentation Page

1. Report No. IHRB Project TR-615	2. Government Accession No.	3. Recipient's Catalog No.	
4. Title and Subtitle Connection Details and Field Implementation of UHPC Piles – Phase II		**5. Report Date** September 2019	
		6. Performing Organization Code	
7. Author(s) Jessica Garder (orcid.org/0000-0001-7345-9267), Sriram Aaleti (orcid.org/0000-0002-8738-454X), Liang Zhong (orcid.org/0000-0002-4669-1885), and Sri Sritharan (orcid.org/0000-0001-9941-8156)		**8. Performing Organization Report No.** InTrans Project 09-363	
9. Performing Organization Name and Address Bridge Engineering Center Iowa State University 2711 South Loop Drive, Suite 4700 Ames, IA 50010-8664		**10. Work Unit No. (TRAIS)**	
		11. Contract or Grant No.	
12. Sponsoring Organization Name and Address Iowa Highway Research Board Iowa Department of Transportation 800 Lincoln Way Ames, IA 50010		**13. Type of Report and Period Covered**	
		14. Sponsoring Agency Code IHRB Project TR-615	

15. Supplementary Notes

Visit www.intrans.iastate.edu for color PDF files of this and other research reports.

16. Abstract

With 21% structurally deficient and 6% functionally obsolete bridges, Iowa ranks among the bottom states in bridge infrastructure quality. Extending the service life of new and existing bridges through the development of new solutions has, therefore, been one of the principal challenges of the state. Given that 30% of the overall cost of bridges is directed toward the foundation and the difficult accessibility of foundation elements for maintenance, creative solutions are needed to lengthen the service life of bridge substructures.

The recent advancements in ultra-high-performance concrete (UHPC) offer great potential to overcome this challenge. The durability and high strength properties of UHPC offer a superior advantage over other types of material commonly used in bridge foundations. The use of UHPC for piles was investigated in a previous project, where a UHPC pile cross-section was designed and optimized. Through analytical and experimental investigations, the study demonstrated UHPC as a practical alternative for bridge piles.

To advance the UHPC pile design previously developed, this study aimed to develop connection details, improve drivability and installation, and conduct field performance verification. New splice details were developed, and their performance was evaluated in various laboratory and field tests. Additionally, the suitability of the Iowa Department of Transportation's (DOT's) current pile-to-abutment connection details for the UHPC pile was investigated in laboratory experiments. After completing a vertical and lateral load test in the field on two UHPC piles to optimize pile design and evaluate the performance of the splice, a UPHC production pile was implemented in an actual bridge abutment foundation, and its performance under the cyclic lateral movement of the bridge was monitored over two years.

The new splice design details performed adequately in both laboratory and field experiments, and they are recommended for implementation. The completed tests also demonstrated that current Iowa DOT pile-to-abutment connection details are adequate for utilizing UHPC piles in routine design. The field implementation and monitoring of the UHPC production pile indicated satisfactory performance and showed that UHPC piles can be used in place of the commonly used steel piles, thereby increasing durability of foundations in Iowa bridges.

17. Key Words bridge abutment foundations—bridge infrastructure—bridge piles—concrete durability—pile-to-abutment connections—splice details—ultra-high-performance concrete piles		18. Distribution Statement No restrictions.	
19. Security Classification (of this report) Unclassified.	**20. Security Classification (of this page)** Unclassified.	**21. No. of Pages** 309	**22. Price** NA

Form DOT F 1700.7 (8-72)   **Reproduction of completed page authorized**

CONNECTION DETAILS AND FIELD IMPLEMENTATION OF UHPC PILES – PHASE II

Final Report
September 2019

Principal Investigator
Sri Sritharan, Wilkinson Chair Professor
Civil, Construction, and Environmental Engineering, Iowa State University

Research Assistants
Jessica A. Garder and Liang Zhong

Authors
Jessica Garder, Sriram Aaleti, Liang Zhong, and Sri Sritharan

TABLE OF CONTENTS

LIST OF FIGURES

LIST OF TABLES

ACKNOWLEDGMENTS

EXECUTIVE SUMMARY

With an increasing rate of bridges becoming structurally deficient or functionally obsolete, the need for innovative solutions to improve the service life of bridges and reduce maintenance costs has become paramount. Given that a significant portion of bridge cost is allocated to the substructure and the difficulty associated with the maintenance of underground structural systems, such solutions should be designed to improve foundation performance as well. In the current practice in Iowa, bridges are generally founded on piles made of commonly used materials, including precast, prestressed concrete or steel. However, such piles are susceptible to damage from stresses induced during driving as well as accented deterioration when exposed to harsh environmental conditions.

In a previous study, ultra-high-performance concrete (UHPC) was investigated as an alternative material for piles. Given its strength and durability properties, UHPC has the potential to overcome the limitations of traditional materials. In that study, a UHPC pile cross-section was developed, and its performance was successfully verified through laboratory and field tests.

The objective of the research presented in this report was to further improve the design of piles using UHPC by developing suitable connection details, optimizing the geotechnical pile design, and implementing and monitoring the performance of a UHPC production pile in an actual bridge foundation. To achieve this goal, a new splice detail was developed to accommodate the UHPC pile cross-section. The performance of the splice was then verified through tensile, shear, and flexural tests in the laboratory, and a lateral load test in the field. The splice performed well in all tests, and results showed that stresses in the splice are well below the allowable limits.

Then, the suitability of Iowa Department of Transportation (DOT) abutment connection details for the UHPC was investigated in the laboratory. The pile-to-abutment connection was tested in weak-, strong-, and 30º skew-axis bending. A weak-axis bending test was also conducted on a steel H-pile-to-abutment connection for comparison. Test results showed that the current Iowa DOT pile-to-abutment connection details are adequate for the UHPC pile.

Finally, an instrumented UHPC production pile was implemented in an actual bridge foundation. Two of the HP 10×57 steel piles included in the foundation were also instrumented. The response of the piles under cyclic lateral movements resulting from thermal effects was monitored over an extended period. Recorded strains indicated that the UHPC pile would not crack under the maximum displacement of 0.20 in. experienced by the bridge, neither would the steel pile experience yielding. Given that the UHPC pile and the connection details developed in this research performed well in all tests and field implementation, UHPC piles can be satisfactorily used in place of steel piles.

CHAPTER 1: INTRODUCTION

1.1. Introduction to UHPC and AASHTO Strategic Plan

In 2005, the American Association of State Highway Transportation Officials (AASHTO) identified grand challenges that should be addressed through more research advancement (AASHTO 2005). Two of these challenges focus on extending the service life of bridges and optimizing structural systems. Currently, AASHTO calls for a 75-year service life for bridges and highway structures. In recent years, some bridges in the US have been designed with a 100- to 150-year service life (Freyermuth 2009). The service life of new bridge foundations may be increased due to the desirable qualities of the ultra-high-performance concrete (UHPC) materials.

In 2008, a report entitled "Iowa's Deficient Bridges" identified Iowa as having 21% of its bridges (i.e., 5,153) in the structurally deficient category, which is the fourth-highest percentage in the nation (TRIP 2008). A bridge is considered structurally deficient when there is a significant amount of deterioration to any of the bridge's major components, such as the deck or supports. An additional 6% of Iowa's bridges (i.e., 1,455) were classified as functionally obsolete (TRIP 2008), which includes any bridge that was built to standards that are not used in today's design. For example, a bridge having a vertical clearance that does not adequately serve the current traffic demand would be considered functionally obsolete.

To keep up with the rate of bridges becoming structurally deficient or functionally obsolete and to start reversing the percentage of structurally deficient bridges, the Iowa Department of Transportation (DOT) and other local agencies are looking for solutions to extend the service life of new and existing bridges as well as reduce or eliminate maintenance costs. As the service life of a bridge is improved, its foundation performance also should be enhanced, because a major portion of bridge construction costs lies in the foundation. The average cost of a bridge substructure is 30% of the total bridge cost (Menn 1990).

Due to the cost and difficulty of maintaining bridge substructures, creative solutions are needed to extend the service life of structural systems by utilizing existing and new materials more efficiently. The high strength available when using UHPC allows for reduced cross-section design and more efficient use of the material. In addition, the durability of UHPC also indicates the possibility of dramatically reducing or eliminating the deterioration associated with commonly used piles for bridge foundations.

1.2. Current Deep Foundation Practice and Limitations

There are many different types of piles used to support structural loads in the US. The four main categories are concrete, steel, timber, and composite piles, which are then broken up into many subgroups as shown in Figure 1-1.

1

Load Bearing Piles

Concrete   Steel   Timber   Composite

Steel: H, Pipe

Composite: Timber, TPT, Pipe - Shell

Pipe: Filled, Unfilled

Unfilled: Open End, Closed End

Concrete:
Precast   Cast-in-Place

Precast: Prestressed, Reinforced
Prestressed: Pre-tension, Post-tension
Post-tension: Cylinder
Reinforced: Jointed, Non-Jointed

Cast-in-Place: Cased, Uncased
Uncased: Compacted, Drilled / Bored
Drilled / Bored: ACIP, Micropile, Drilled Shaft, Helical Screw

Cased:
Driven w/ Mandrel   Driven / Pushed w/o Mandrel   Drilled / Bored
Driven w/ Mandrel: Pipe Cased, Shell Cased
Driven / Pushed w/o Mandrel: Pipe, Monotube, Fundex, Tubex or Grout-injected Tubex
Drilled / Bored: Micropile, Drilled Shaft

Hannigan et al. 2006a, modified from Naval Facilities Engineering Command 1982

Figure 1-1. Deep foundation type options

The most common deep foundation chosen for bridge foundations are steel H-piles and precast, prestressed concrete piles, which is the focus of this chapter as a comparison to UHPC piles. Both of these piles have certain limitations when it comes to durability and drivability, which are outlined in the following sections.

1.2.1.   Precast, Prestressed Concrete Piles

Commonly, precast concrete piles are used in marine environments on the coast. One disadvantage associated with precast, prestressed concrete piles is the fact that the ends of the piles are not effectively prestressed due to the development length of the prestressing strands to make them fully effective, thus causing a reduced tensile capacity in these regions. Tensile stresses can be developed in concrete piles during diving in certain soil conditions. For example, driving of a concrete pile in a hard soil layer that is overlying a soft layer can induce tensile stresses in the pile. Once the pile breaks through the hard layer, a tension stress develops at the

pile toe. Another example is when driving a concrete pile in soft clay conditions. At the beginning of drive, the pile is susceptible to a tensile stress at the pile head as a result from the reflected wave of the hammer blow.

Concrete piles can fail as a result of large compressive stresses developed during driving. This can be attributed to an excessively large driving hammer used during installation or when driving through hard soil conditions. Figure 1-2 illustrates the crushing of concrete due to hard driving conditions for normal concrete piles.

DiMillio 1999

Figure 1-2. Concrete piles damaged by difficult driving conditions

It is important to perform an accurate drivability analysis to ensure that damage does not occur during driving of concrete piles.

In addition to the disadvantages during installation, precast concrete piles must be handled carefully in order to avoid cracking when picking up the pile during loading and unloading as well as picking up for field installation. Improper lifting procedures can crack or even break precast concrete piles.

Precast concrete piles that are subjected to sulfate ions undergo an expansive chemical reaction, which leads to cracking and spalling of the concrete and ultimately a reduction in available structural capacity (Moser et al. 2011). When concrete piles are subjected to chlorides, it is the steel reinforcement that will corrode instead of the concrete itself. As the reinforcement steel expands from corrosion, the concrete bursts. This type of corrosion leads to loss of bond between steel and concrete as well as a reduction in pile capacity (Moser et al. 2011). Figure 1-3 depicts the bursting of the concrete due to corrosion of the reinforcement steel as well as the abrasion of the water.

Moser et al. 2011

Figure 1-3. Damage to prestressed concrete pile due to corrosion

1.2.2.   Steel H-Piles

Steel H-piles are commonly used in Iowa for integral abutment bridges. During driving, the disadvantages of steel H-piles include buckling under harsh driving conditions, as well as the tendency to deviate from the designed location when obstructions are encountered, such as boulders. When driving steel H-piles through very dense gravels or soils containing boulders, the toe of the pile may severely deform and separation of the flanges and web may occur as shown in Figure 1-4.

Hannigan et al. 2006b

Figure 1-4. Damaged H-pile toe

Additionally, the Iowa DOT requires the top 12 in. of all steel piles to be trimmed due to the expected deformation of the pile head during driving (Iowa DOT 2011), which is depicted in Figure 1-5.

Ng et al. 2011

Figure 1-5. Typical damage to top steel H-piles due to driving

Not only can the driving conditions influence the performance of steel H-piles but also the corrosion as the bridge service life is dramatically influenced when the corrosion of steel piles occurs. Corrosion is also a major problem for steel piles embedded in fill materials or above the water table. The water table fluctuation zone (Decker et al. 2008) is the zone in which the most corrosion occurs on steel H-piles. A summary of the maximum corrosion rate observed for various conditions was completed by Decker et al. (2008) and corrosion rate corresponding to number of years exposed, pH, resistivity, and chloride content is summarized in Table 1-1 along with the associated references.

Table 1-1. Corrosion rate of steel piles with various soil conditions

Corrosion rate, in./yr	Years exposed	pH	Resistivity, Ω in.	Chloride, ppm	Reference
0.0007	22	5.1–6.0	19685–27559	16–59	Wong and Law 1999
0.0019	7	7.4–8.2	335–2756	0.3	Romanoff 1962
0.0032	11	6.9	1693–4331	0.6	Romanoff 1962
0.0019	11	8.1	315–508	0.5	Romanoff 1962
0.0006	12	7.7–8.4	136–512	0.5	Romanoff 1962
0.0007	34	8.2	118110	17.8	Decker et al. 2008
0.0005	35	7.7	59055	256	Decker et al. 2008
0.0006	38	7.5	59055	444	Decker et al. 2008

Corrosion of steel piles does not only happen beneath the soil; Figure 1-6 indicates severe corrosion to the steel H-piles used in a bridge in St. Louis, Missouri located above the soil.

Figure 1-6. Corroded steel H-pile

1.3. Benefits of UHPC Related to Piling

UHPC is a cement matrix often used with steel fibers with a compressive strength ranging from 22 ksi to 36 ksi (Resplendino 2012). UHPC has several advantages including strength, ductility, durability, and aesthetic design flexibility, which were achieved by eliminating the characteristic weaknesses of normal concrete.

Taking advantage of the engineering and durability properties, a UHPC pile was developed in Phase I of this project, which can be found in the final report written by Vande Voort et al. (2008). A comparison between a UHPC pile section, comparable steel HP 10×57 pile section, and concrete pile section is presented in Figure 1-7.

(a) (b) (c)
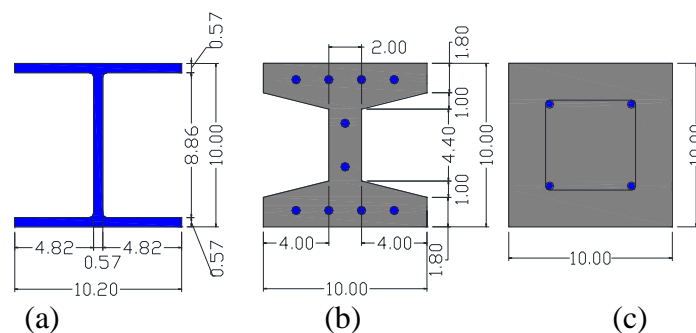
Figure 1-7. Cross-sections of (a) steel HP 10×57, (b) UHPC, and (c) 10 x 10 in. normal concrete piles

Note that all dimensions in Figure 1-7 are in inches, and notice that the UHPC pile has similar outer dimensions as the HP 10×57 pile to allow for the same driving equipment to be used during installation. Additionally, the reduced cross-section when compared to the normal concrete pile allows for easier driving.

6

1.3.1. *Durability*

The tightly packed nature of the mix design gives UHPC its excellent durability characteristics. As a result of the low water-binder-ratio, the capillary porosity of an uncracked UHPC specimen is much less than that of normal concrete (NC) or high-performance concrete (HPC), and also has the benefit of a greatly reduced chloride permeability (Scheydt and Müller 2012).

Because UHPC is very durable material, the required concrete cover thickness for steel reinforcement is typically reduced, allowing for a further reduction in section size, thus resulting in an efficient use of the material. An additional benefit resulting from the durability of the material is its potential to extend the lifespan of bridges and lower the maintenance costs.

1.3.2. *Strength*

UHPC exhibits very high strength characteristics when compared to HPC or NC, which are given in Table 1-2.

Table 1-2. Strength characteristics of UHPC vs. HPC and NC

Property	UHPC	HPC	Normal concrete
Compressive strength, ksi	26–30	12–18	4–8
Tensile strength, ksi	1.7	0.8–0.9	0.3–0.7
Elastic modulus, ksi	8,000	4,800–6,400	3,600–5,100

Due to the high strength of UHPC, the cross-section could be designed efficiently to reduce the amount of material needed for fabrication and to withstand both the compressive and tensile stresses developed during driving. From the casting of the ¾-scale test units and the full-scale test piles, the proposed UHPC piles with the tapered H-section can be cast successfully in a precasting plant and can achieve the required high strength of 26 to 29 ksi, as long as the recommended heat treatment procedures are employed (Vande Voort et al. 2008).

1.4. UHPC Pile

The UHPC pile was designed as described by Vande Voort et al. in 2008 as Phase I of the project. A brief summary of the research is given in this section.

During Phase I of the project, the design of the UHPC pile cross-section was optimized and is reproduced in Figure 1-8a.
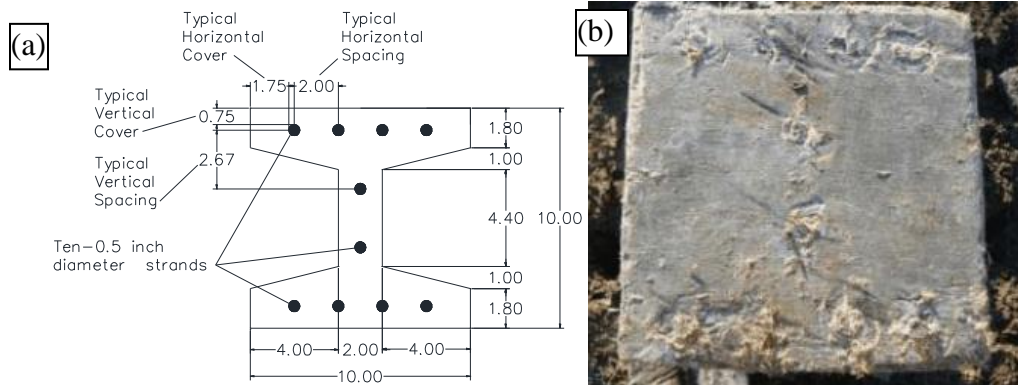
Figure 1-8. (a) Cross-section of UHPC pile and (b) top 18 in. of test pile

There were some concerns regarding the effectiveness of the prestressing in the head and toe of the pile and the performance of the pile due to driving stresses. It was decided that the top 9 in. would be cast as a solid 10 in. by 10 in. block as shown in Figure 1-8b that was tapered into the designed cross-section. The moment-curvature response of the UHPC pile was predicted and confirmed in the laboratory flexural test. A vertical load test was performed on two test piles driven in the field after the laboratory testing and results were then compared to the performance of a steel HP 10×57. Additionally, a lateral load test was completed between the two UHPC test piles.

1.5.   Scope of Research

The successful completion of Phase I of the UHPC project was a stepping stone toward Phase II of the project, in which the options to improve the drivability, installation, connection details, and performance verification in the field were planned. The objectives of this thesis included the following:

- Predict the performance of a UHPC pile in an integral bridge abutment
- Perform a laboratory test on typical pile-to-abutment connection by subjecting it to axial and cyclic lateral loading
- Perform a lateral load test in the field on the splice connection designed to extend the length of UHPC piles
- Perform a vertical load test to failure in the field
- Instrument and install a UHPC pile as part of a bridge foundation and compare its driving behavior to that of a steel H-pile

1.6.   Report Layout

This report has eight chapters describing the development of various connection details and both laboratory and field testing of UHPC piles. A summary of each chapter's content is presented below.

- **Chapter 1 – Introduction:** A brief introduction to the limitations of traditional concrete and steel piles and details of the UHPC pile

- **Chapter 2 – Literature Review:** A review of published studies describing the composition, microstructure, durability, material properties, applications, practice for splicing details and pile-to-abutment connections, integral abutments, and analysis procedures for drivability and lateral loading

- **Chapter 3 – Analysis of UHPC Piles in Integral Abutments:** Description of the results from the analysis of the pile section in weak-axis bending comparing it to strong-axis bending for moment-curvature response analysis and lateral load parametric study

- **Chapter 4 – UHPC Splice Design and Testing:** Description of the fabrication and casting of the UHPC test units and abutment cap, weak-axis bending on a short HP 10×57 pile and a short UHPC pile anchored to the abutment cap

- **Chapter 5 – Pile-to-Abutment Connection Testing:** Description of the fabrication and casting of the UHPC test piles, driving of the UHPC test piles, vertical load test, lateral load test, and analysis of the weak-axis bending performance of the UHPC pile during the lateral load test

- **Chapter 6 – Field Testing of UHPC Test Piles:** Description of the fabrication and casting of the UHPC test piles, driving of the UHPC test piles, vertical load test, lateral load test, and analysis of the weak-axis bending performance of the UHPC pile during the lateral load test

- **Chapter 7 – Field Implementation and Monitoring of a UHPC Production Pile:** Description of the fabrication and casting process of the UHPC production pile, instrumentation plan, the driving of the three instrumented HP 10×57 piles and the UHPC production pile, and an analysis predicting the performance of the UHPC and HP 10×57 piles

- **Chapter 8 – Summary, Conclusions, and Future Research:** A summary of the results on UHPC piles found from casting, field testing, and long-term monitoring, and a description of future research potential

9

CHAPTER 2: LITERATURE REVIEW

2.1.   Introduction

This chapter introduces the history, background, material properties, and applications of UHPC in order to characterize the material being used in the pile project as well as the deep foundation design methods used to design the UHPC test piles and UHPC production piles. Because the UHPC production pile will be installed in an integral abutment for long-term monitoring, current design guidelines are identified, along with a summary of previous research on long-term monitoring of integral abutments. Finally, to predict the behavior of the test and production piles during driving, testing, and monitoring, two computer software packages LPILE and GRLWEAP were used, and they are described in detail in Section 2.7.1 and Section 2.7.2, respectively.

2.2.   History and Background

Relatively recent advances in concrete technology have introduced UHPC. Despite efforts to create new concrete mixes with higher strength over the past 150 years, structural applications using the improved concrete have often lagged due to the high cost of material and lack of design guidelines for the new material (Tang 2004). Four milestones have been key to the development of UHPC, which includes the development of the cement matrix, the fiber, the bond at the interface between fiber and matrix, and the resulting composite (Naaman and Wille 2012). Naaman and Wille (2012) have identified the achievements of each milestone in chronological order as well as giving consideration to different geographical regions.

Richard and Cheyrezy (1995) outlined the basic design principles that should be followed when designing UHPC materials, which are: (1) ensuring homogeneity of the material by eliminating coarse aggregates, (2) providing a compacted density by optimizing particle sizes, (3) achieving a good microstructure by subjecting the material to heat treatment, and (4) providing ductility of the material by adding steel fibers.

Normal concrete is a heterogeneous material. In order to reduce the effects of the problems related to the non-uniformity in concrete, coarse aggregates are replaced by fine sands, the paste is mechanically improved by forming a more tightly packed mix design, and the aggregate ratio is decreased (Richard and Cheyrezy 1995). The small diameter of the aggregates used in UHPC causes the aggregate to behave integrally in a continuous matrix instead of as a rigid skeleton in a normal concrete. This quality allows UHPC to accommodate a much larger compressive force that is transmitted by the matrix of material (Vande Voort et al. 2008). Figure 2-1 compares the representation of the force transfer between normal concrete and UHPC.
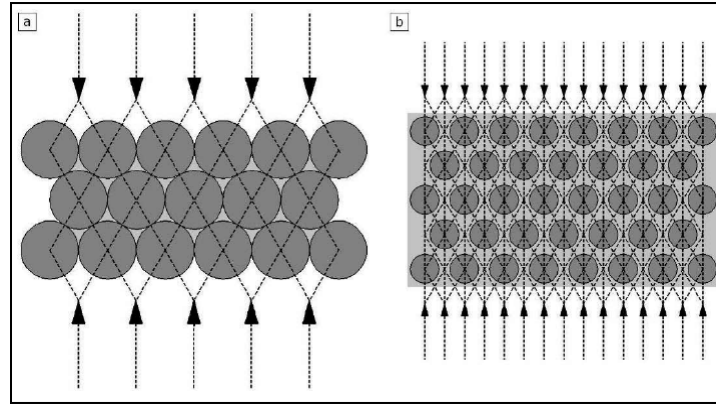
After Walraven 2002

Figure 2-1. Depiction of force transfer through (a) normal concrete and (b) UHPC

There are several types of UHPC used around the world. The main difference between each is the type and quantity of fibers used in the mix design. A summary of the advantages and disadvantages of UHPC is given in Table 2-1.

Table 2-1. Advantages and disadvantages of UHPC

Advantages	Disadvantages
High compressive strength	Short-term costs
High tensile strength	Material cost
High shear strength	Mixing time
High impermeability	Casting bed time
High durability	Heat treatment
Self-leveling	Cast-in-place construction may not be feasible
Self-healing of unhydrated cement	
Long-term costs	
Eliminate labor installing stirrups	
Fewer deck replacements	
Reduced weight for shipping	

Source: Wipf et al. 2009

The four main types of UHPC are BSI/CERACEM, compact reinforced composites (CRC), multi-scale cement composite (MSCC), and reactive powder concrete (RPC) (Vande Voort et al. 2008).

BSI/CERACEM was developed by Sika Corp. and Eiffage S.A. and includes coarse aggregates unlike the other three types of UHPC (Jungwirth and Muttoni 2004). Both CRC and MSCC use larger amounts and different sizes of fiber when compared to RPC (Vande Voorte et al. 2008). RPCs typically contain steel fibers that occupy 2% of the volume to gain ductility (Richard and Cheyrezy 1995). A form of RPC is Ductal, which is produced by the French companies LafargeHolcim and Bouygues S.A. A composition of UHPC is provided in Table 2-2.

Table 2-2. Common UHPC mix components

Component	Weight per cubic foot, lb	Mass ratio /Cement	Volume fraction, %
Sand	61.9	1.430	38.8
Cement	42.3	1.000	22.7
Silica fume	14.0	0.325	10.6
Crushed quartz/Fly ash	13.0	0.300	8.1
Fibers	9.4	0.218	2.0
Superplasticizer*	0.9	0.021	1.4
Water	9.9	0.229	16.5

Source: Cheyrezy and Behloul 2001
*Superplasticizer is expressed as the weight of the solid fraction; the liquid fraction is included in the water weight.

Because of its availability and use in several bridge research and implementation projects in the US, including Iowa, and abroad (e.g., Perry and Seibert 2011, Behloul et al. 2006, FHWA 2010, Sritharan 2015), the UHPC used in the current and previous phase of the pile project is Ductal. Unless otherwise noted, the UHPC in the remainder of the report refers specifically to Ductal, while the research outcomes are applicable to any form of UHPC with engineering properties comparable to those of Ductal.

2.3.   Material Properties

An extensive literature review was completed by Vande Voort et al. (2008) on the material properties of UHPC. This section includes a brief summary of Vande Voort's literature review with appropriate updates for the material properties of UHPC used for Phase II of the UHPC pile project, which include compressive strength, tensile strength, shrinkage and creep, elastic modulus, strain limits, and allowable driving limits. Additional information provided below was found with regard to standard and calculation method manuals and tolerances for prefabrication of structural elements using UHPC.

2.3.1.   *Compressive Strength*

UHPC does not have any compressive strength for almost 1 day after pouring, and a set time of 17 hours is recommended (Graybeal 2006). After the set time, UHPC develops its compressive strength very rapidly. Thus, the majority of the strength is gained in the first seven days of curing when heat treatment is not applied. The influence of heat treatment applied during the curing process of UHPC structural elements plays a large role in developing the compressive strength. The rate of strength gain for heat treated UHPC, from 7 to 56 days, is only 5% of the compressive strength (Vande Voort et al. 2008). Heat treatment allows the structural elements to reach their final maturity before the typical 28-day strength that is required for normal concrete (AFGC 2002). In addition, the final compressive strength of UHPC is typically 10% higher for heat-treated UHPC elements than non-heat-treated UHPC elements (Graybeal 2005). The effect of delaying the heat treatment only slightly decreases the compressive strength than if applied right after stripping the forms (Graybeal 2005).

In comparison, normal concrete has a compressive strength within the range of 4 to 8 ksi, and HPC has a compressive strength between 12 and 18 ksi. Heat-treated UHPC has a compressive strength approximately two times that of HPC and five times that of normal concrete (Vande Voort et al. 2008).

2.3.2. Tensile Strength

Normal concrete has a tensile strength in the range of 300 to 700 psi, and HPC has a tensile strength in the range of 800 to 900 psi. In comparison, UHPC develops more tensile strength than normal concrete and HPC, even beyond the development of micro-cracking, which is due to the steel fibers effectively spanning the cracks. Additionally, UHPC can also experience strain-hardening between the first tensile crack strength and the ultimate tensile strength (Vande Voort et al. 2008). Heat treatment decreases the amount of time it takes to reach the tensile strength and typically increases the tensile capacity by about 10% (AFGC 2002). After exposing cracked UHPC cylinders to harsh environments, no noticeable decrease in peak tensile load-carrying capacity was observed (Graybeal 2005).

The behavior of UHPC can be described based on the crack width. UHPC can be characterized as elastoplastic up to a crack width of around 0.012 in. (Chanvillard and Rigaud 2003). The same crack width of 0.012 in. corresponds to the stress associated with the basis for fiber tensile strength (AFGC 2002).

2.3.3. Shrinkage and Creep

Shrinkage is the loss of free water through evaporation, which leads to the gradual shortening of the element with time. Heat treatment substantially reduces the effects of delayed shrinkage and creep (AFGC 2002), which allows for the valid assumption that there will not be any shrinkage of the concrete after heat treatment. If no heat treatment is performed on the material, the shrinkage can be assumed to be 550 μm (AFGC 2002).

Creep is an additional time dependent strain added to the concrete due to sustained load on the concrete matrix. The ultimate creep coefficient for untreated UHPC is 0.8 and drops to 0.2 for heat-treated UHPC (AFGC 2002).

2.3.4. Elastic Modulus

Normal concrete has an elastic modulus within a range of 3,500 to 5,100 ksi, and HPC has an elastic modulus of approximately 4,800 to 6,400 ksi (Vande Voort et al. 2008). AFGC recommends using a modulus of elasticity of 8,000 ksi during the design stage when experimental information is not available on the UHPC material, as well as an initial modulus of 5,700 ksi. The modulus of elasticity of UHPC is linear elastic for both compression and tension until specific strain limits are reached. For compression, the elastic portion limit is approximately 80 to 90% of the compressive strength of heat-treated UHPC with only a 5% deviation from the stress-strain linearity (Graybeal 2007). A delay in the heat treatment of the UHPC material is a

factor that will affect the modulus of elasticity, which causes the modulus of elasticity to be slightly reduced, rather than for full steam treatment (Graybeal 2005).

Many equations have been developed to estimate the modulus of elasticity of concrete. Four equations were specifically developed for UHPC and are given below as equations (2-1) through (2-4); all based on the compressive strength, where E is the elastic modulus in psi and f_c' is the compressive strength in psi. Vande Voort et al. (2008) recommended the use of equation (2-2) to estimate the elastic modulus of UHPC based on laboratory tests completed in Phase I of the pile project.

$$E = 50,000\sqrt{f_c'} \qquad \text{(Sritharan et al. 2003)} \qquad (2\text{-}1)$$

$$E = 46,000\sqrt{f_c'} \qquad \text{(Graybeal 2007)} \qquad (2\text{-}2)$$

$$E = 2,373,400\ln(f_c') - 468,010 \qquad \text{(Ma and Schneider 2002)} \qquad (2\text{-}3)$$

$$E = 525,000\sqrt[3]{f_c'} \qquad \text{(Ma et al. 2004)} \qquad (2\text{-}4)$$

2.3.5.   Strain Limits

Compression

Vande Voort et al. (2008) found several variations for the compression strain limit of UHPC in various studies. The compression limits range from 3,200 to 4,400 microstrains. The compression strain limit recommended by Sritharan et al. (2003) and Dugat et al. (1996) for elastic behavior of 3,200 microstrains is used to characterize the limits in compression of heat-treated UHPC in this study.

Flexural Tension

There is a close agreement for the cracking tensile strain, which ranges from 300 to 330 microstrains (Vande Voort et al. 2008). However, the ultimate tensile strain has some noticeable variation between various reported results. An ultimate tensile strain ranging from 5,000 to 7,000 microstrains was reported by Richard and Cheyrezy (1995), while an ultimate tensile strain of 7,500 microstrains was reported by Dugat et al. (1996).

AFGC (2002) proposed the relationship given in Figure 2-2 for crack width versus stress.
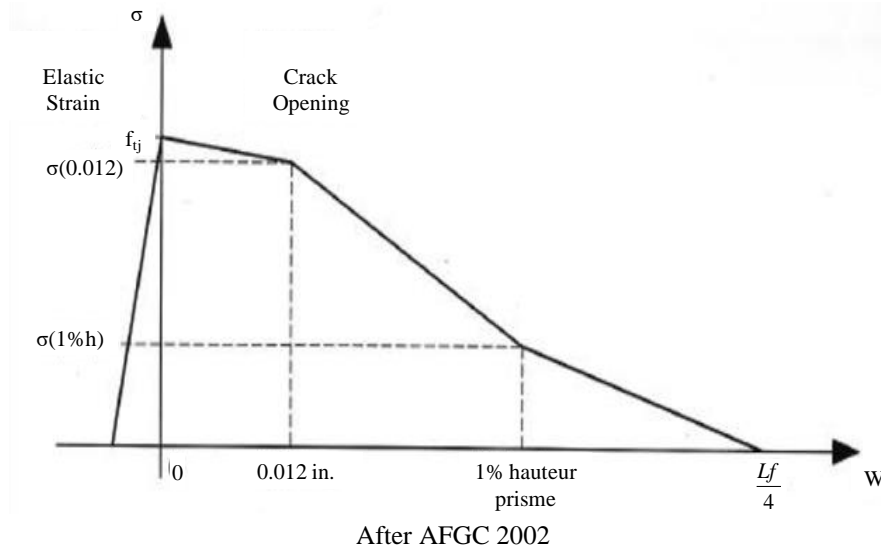
Figure 2-2. Simplified tensile-strength law

Vande Voort et al. (2008) reported the corresponding strains with cracking width for various locations on the relationship for Ductal. Micro-cracking begins at 160 microstrains, cracking starts at 1,350 microstrains and the limit where cracks start exceeding the 0.012 in. limit is at 2,400 microstrains.

2.3.6.   *Allowable Driving Stresses*

In many cases, a pile may experience the highest tensile stress during driving. AASHTO (2007) limits the compression and tension driving stresses to $0.9f_y$ for H-piles, where f_y is the yield strength of the steel. For concrete piles, equation (2-5) gives the limit on compression stresses, and equation (2-6) limits the tension driving stresses.

$$\sigma_c = 0.85 f_c' - f_{pe} \qquad \text{(psi)} \qquad\qquad (2\text{-}5)$$

$$\sigma_t = 3\sqrt{f_c'} + f_{pe} \qquad \text{(psi)} \qquad\qquad (2\text{-}6)$$

where,
f_c' = concrete compressive strength
f_{pe} = effective prestressing after losses

It is important to control the driving stresses when driving the pile though a hard layer above a weaker soil for concrete piles. As the pile punches through the hard layer during driving, the pile toe experiences less resistance, resulting in large tension stresses in this region. Also, concrete piles are at risk from tensile stresses at the beginning of drive in soft clays due to the compressive stress wave that is reflected up the length of pile as a tension wave.

15

2.3.7.   Standards and Calculation Methods

Because UHPC is a fairly new material, there is no united standard design procedure or recommendations available. Many countries have developed their own recommendations and guides for the design of UHPC structural elements. A brief description of the recommendations from Australia, France, Japan, and the US are made for each of these countries in this section.

Australia developed design guidelines for using Ductal in prestressed concrete beams in 1999 based on research completed at the University of New South Wales (Gowripalan and Gilber 2000). The intentions of these guidelines were made to relate design of members with Ductal to prestressed structural members. The design limits of Ductal for preventing tension and compression failure, as well as defining the strength in flexure, shear and torsion, crack control, deflections, fire resistance, fatigue, prestressing losses, and anchorage zones were provided.

France first developed interim recommendations in 2002 and the guide is broken into three main parts: (1) characterize the material performance, (2) structural element design, and (3) durability of the material (AFGC 2002). Recommendations for how to perform checks and inspections on finished products are also included. The recommendations allow for designers to predict the behavior of UHPC members that incorporate no reinforcement, mild steel reinforcement or prestressing steel.

New AFGC recommendations have been proposed based on major research and feedback to better characterize the characteristics of ultra-high-performance fiber-reinforced concrete (UHPFRC) or UHPC (Resplendino 2012). Some of the recommendations that have been improved regard the characterization of fire behavior of UHPC, punching resistance, abrasion, shear resistance, and tensile strength.

Recommendations for high-performance fiber-reinforced cement composites (HPFRCC), which are essentially UHPC, were developed in Japan by the Concrete Committee in the Japan Society of Civil Engineers in 2004 (JSCE 2008). The recommendations satisfy the safety, serviceability, recoverability, and compatibility to the environmental performance requirements by proposing methods for uniaxial tensile tests and crack width measurements. Additionally, recommendations were made for the design tensile strength, design tensile strain, and design crack width.

The Federal Highway Administration (FHWA) developed guidelines for the material property characterization of UHPC materials in 2006 (Graybeal 2006). Both experimental phases as well as an analytical phase were completed during the research. Through this research, recommendations were made to define the behaviors of UHPC compared to those of normal concrete.

2.3.8.   Tolerances

In order to ensure the quality of UHPC when mixing and pouring, certain tolerances are required. When mixing UHPC at a batch plant, a tolerance of ±2% for each weighed ingredient should be

used and reduced to ±1% for powders (AFGC 2002). The drop height when placing the UHPC should not exceed more than about 1.5 ft to ensure that no segregation or clustering of fibers occurs (AFGC 2002). It is recommended that no delay in-between batches be allowed because a skin can form on the surface of the last concrete layer. If a delay does occur, the two layers must be joined together by raking the interface surface (AFGC 2002).

UHPC is sensitive to temperatures, so recommended minimum and maximum temperatures are given for which no additional steps are required. The minimum temperature recommended is 41ºF. If the temperature is below this minimum, additional steps, such as heating the aggregate or mix water, using insulated forms, or using setting or hardening accelerators should be used (AFGC 2002). If the temperature is above 95°F, precautions similar to those used for normal concrete should be taken (AFGC 2002).

2.4.   Applications

Since UHPC was developed in the 1990s, it has been used for various applications ranging from designing architectural elements to structural elements. Vande Voort et al. (2008) provides a detailed list of applications for UHPC up until 2008. This section summarizes a few of the applications listed by Vande Voort relative to the control study, and some of the new project that have been completed since 2008.

2.4.1.   Structural Members

Bridge Components

Research related to completed or ongoing projects on UHPC bridge applications are as follows:

- UHPC joint fill for precast concrete accelerated bridge construction – UHPC was used to fill the voids between the precast abutments and steel H-pile foundations, joints between the precast deck panels, and joints between the precast approach slab panels (Young et al. 2012)
- UHPC waffle deck panel – The benefits of UHPC and precasting were combined to create durable deck and optimize design (Aaleti et al. 2011)
- UHPC to normal concrete deck interface – Developing shear friction interfaces that are appropriate for overlaying UHPC on new and existing normal concrete bridge decks (Sritharan et al. 2012)
- UHPC bridge bearings – UHPC was used to create a new generation of sliding bearing joint for bridge applications to replace single steel slide bearings (Hoffmann and Weiher 2012)
- Second generation of Pi-shaped girder – The girder was developed for short- and medium-span highway bridges similar to the prototype UHPC Pi-girder but with an increased deck thickness and width, increased web thickness, decreased web spacing, and rounded reentrant corners to improve upon the first generation of girders (Graybeal 2009)
- Super Bridge 200 – The bridge is a cable-stayed bridge with the purpose of developing technologies to improve UHPC behavior, construct girders and plates, construct a UHPC deck, and develop a UHPC cable-stayed bridge system (Kim et al. 2012)

2.4.2.   *Field Implementation*

Bridges

Several traffic and foot bridges have been constructed around the world using UHPC for design and construction of the structural components. The first of these bridges was the Sherbrooke pedestrian bridge shown in Figure 2-3, which was constructed in Quebec, Canada in July of 1997.

© Ductal 2012, https://www.ductal.com/en

Figure 2-3. Sherbrooke pedestrian bridge, Quebec, Canada

It is the world's first pedestrian bridge to have RPC components. The deck and the top and bottom chord of the open-web space trusses were made with RPC, which had a 29 ksi compressive strength. The web of the truss contained RPC but was confined by stainless steel tubes (Blais and Couture 1999). To date, two other pedestrian bridges with UHPC structural members have been constructed in Canada (Perry and Seibert 2011).

The first UHPC bridge in the US was a 110 ft single-span bridge built in Wapello County, Iowa in 2006 using UHPC bridge beams as shown in Figure 2-4.

Wipf et al. 2009

Figure 2-4. The UHPC girder bridge in Wapello County, Iowa

The bridge project allowed researchers to develop a shear design procedure, evaluate the performance of the UHPC girder, and evaluate the structural performance of the bridge (Wipf et al. 2009).

In Mayenne, France, the Saint Pierre La Cour Bridge was built in 2005 with two lanes for traffic and one lane for pedestrians and is pictured in Figure 2-5.

Behloul et al. 2006

Figure 2-5. Saint Pierre La Cour Bridge in France after completion

Ductal was used for the pretensioned beams and thin precast deck. The bridge was designed by VSL International and Bouygues Travaux Publics S.A.S. using the new recommendations for the use of ultra-high strength concretes reinforced with fibers (Behloul et al. 2006).

The Cat Point Creek Bridge was constructed in 2008 and was the first bridge involving UHPC structural components to be constructed in Richmond County, Virginia. One of the 10 spans of the bridge contains UHPC girders, as shown in Figure 2-6, which were monitored over a period for performance compared to the HPC girders for the other 9 spans (Ozyildirim 2011).

© Ductal 2019, https://www.ductal.com/en

Figure 2-6. Cat Point Creek Bridge with UHPC girders on one span in Virginia

Jakway Park Bridge was built using UHPC Pi-girders in Buchanan County, Iowa. This was the first highway bridge using UHPC batched in a ready-mixed truck. The bridge was open to traffic in November 2008 (PCA 2012). A picture of the Jakway Park Bridge is shown in Figure 2-7.

FHWA 2010

Figure 2-7. Jakway Park Bridge in Iowa using Pi-girders

Columns

The Queen Sofia Museum in Madrid, Spain underwent an expansion by adding three new buildings on a support structure consisting of 24 slender steel columns in 2005. To support the new structures, Ductal was poured directly inside of the steel columns (Ductal 2012). Figure 2-8 shows how the UHPC was handled for the onsite mix and pour of the tall, thin columns.

Figure 2-8. Onsite pour for UHPC columns during Queen Sofia Museum expansion

Other Structures

Due to the superior qualities of UHPC compared to normal concrete, many other structures have been designed and constructed using this material. One example of the innovative uses for UHPC is stairs, which are used at Roissy Airport in Paris and at the LafargeHolcim office in Birmingham, Alabama. Additionally, the durability of the material makes UHPC a good option for corrosive environments such as the Cattenom Nuclear Power Plant cooling tower in France, which used UHPC beams and girders to support the structure. Two other structures that have used UHPC are a retained earth anchorage system used in Réunion Island in France and the gold bar troughs at the Gold Bar Wastewater Treatment Plant in Edmonton, Alberta, Canada (Behloul et al. 2008).

2.4.3. Deep Foundations

Prefabricated Concrete Sheet Piles

Grünewald (2004) designed prefabricated concrete sheet piles with steel fibers after developing a self-compacting, fiber-reinforced concrete (SCFRC) mix for precast sheet piles. Grünewald's concrete sheet piles limited the length of the steel fibers as well as the maximum aggregate size as is typically done in UHPC. Each sheet pile segment was prestressed with eighteen ½ in. prestressing strands, with a flange thickness of 2.0 in. and a web thickness of 1.8 in. Three of the six SCFRC sheet piles that were cast were driven into the ground with a vibratory hammer, and it was reported that they performed as expected (Grünewald 2004).

UHPC Pile Project - Phase I

As introduced in Section 1.4, a UHPC pile was designed and tested in Phase I of the UHPC pile project at Iowa State University (ISU). The cross-section was designed, and a prediction of the moment-curvature response was calculated and then verified in the laboratory. After laboratory testing, the pile was field tested as part of Phase I (Vande Voort et al. 2008).

The cross-section of this pile was designed keeping in mind that solid sections would use too much of the expensive UHPC material and hollow sections are difficult to construct. Therefore, an H-shaped pile section was explored for designing the UHPC piles. Finally, a tapered H-shaped section was decided upon, taking advantage of the several inherent benefits, as shown in Figure 1-8.

Due to the high compressive strength of UHPC, ten ½ in. diameter, 270 ksi low relaxation prestressing strands were used to increase the tensile capacity of the pile. A ¾ in. cover thickness for the ½ in. prestressing strands was used in the design based on research at minimum spacing and cover requirements for UHPC. The minimum strand spacing used in the design of the UHPC pile was 2.0 in. center-to-center.

To predict the moment-curvature response for strong-axis bending of the UHPC pile, a section analysis spreadsheet was developed for various axial loads using Microsoft Excel. The results from the analysis were used in LPILE to estimate the behavior of the UHPC pile for the soil conditions at the location of the field test. Seven assumptions were used for the section analysis calculations, which are: (1) plane sections remain plane, (2) prestress losses occur due to only elastic shortening and shrinkage of UHPC, (3) strands have perfect bonding to UHPC outside the transfer regions resulting in the change in strain in the prestressing strands and concrete being equal at a given location, (4) effective prestressing is applied at the centroid of the section, (5) bending only occurs about the major flexural axis, (6) initial prestressing does not induce any inelastic strains on the strands, and (7) axial loads on the pile are applied through the centroidal axes with no eccentricity. The effect of creep was not considered in the section analysis due to the loads during testing having a relatively short duration.

A drivability analysis was conducted using GRLWEAP on the proposed cross-section. The analysis was completed to ensure the driving stresses under various parameters were well below the allowable limits for UHPC. The results for the UHPC pile were compared to the performance of NC, HPC, and HP 10×57 piles.

To characterize moment-curvature response of the UHPC pile section and verify the analysis procedures, two tests on a ¾-scale UHPC test specimen were completed. The first test unit was tested with an axial load of 80 kips and a cyclic lateral load in a push-pull manner. Cracking in the welds of the test setup occurred during testing and resulted in a slight modification of the test setup for the second test specimen. The second specimen was tested in a similar push-pull protocol but had an increased axial load of 200 kips.

The results from the first laboratory test provided a good correlation between the test results and the predicted moment-curvature response. No reliable curvature data was obtained from the instrumentation of the second specimen due to premature diagonal cracking occurring during the test, which is believed to be caused by the small scale used for the test specimen and lack of steel fibers bridging the cracks. For the design of the ¾-scale test specimen, the fibers were not scaled in size accordingly, which presumably did not allow the fibers to flow freely. The full-scale UHPC pile should allow the fibers to pass more freely to avoid this problem.

Driving stresses calculated using GRLWEAP for a variety of cushions, soils, and driving hammers were found to be well below the allowable stress limits for UHPC piles, resulting in the possible elimination of a pile cushion. UHPC piles exhibited an increased drivability over normal concrete piles due to the reduced cross-sectional area and increased strength characteristics of the material. Through the field testing, it was confirmed that the same driving equipment can be used for UHPC piles as used for steel H-piles of the same size and weight, except for the helmet used to drive the pile.

To verify the potential benefits of UHPC piles for bridge substructure applications, two full-scale 35 ft long UHPC test piles were driven next to a bridge being constructed in Oskaloosa, Iowa. Additionally, a steel HP 10×57 test pile was installed and tested to provide a performance comparison. The soil at the site consisted of 15 ft of a loess soil, 20 ft of Pre-Illinoian glacial till, and bedrock with a water table located at approximately 10 ft from the ground surface.

The test piles and reaction frame anchor piles were driven using a DELMAG D19-42 hammer. A lifting hook was cast into the UHPC piles 7 ft from the pile head but could not be utilized due to the risk of the pile head colliding with the hammer leads. To remedy this problem, a lifting strap was connected to the pile head and to the hammer and helmet. The contractor suggested improving the lifting procedure of the UHPC pile by moving the lifting hook closer to the pile head. No visible damage to the UHPC pile heads were observed after driving of the test piles.

Once the test piles were installed, a vertical load test was performed on one of the UHPC test piles. The predicted failure load of both test piles was between 150 kips and 179 kips depending on which method was used to calculate the estimated axial load capacity. A vertical load of 200 kips was applied to the test pile but was not able to fail the pile based on Davisson's criteria (1972). A second vertical load test was performed on the UHPC test pile that was loaded until 300 kips, which was the limit for the test setup. Again, this magnitude of load was unable to fail the UHPC pile. Using an extrapolation of the load test results, the theoretical ultimate load was found to be 368 kips for the second UHPC test pile.

The axial load capacity of the UHPC pile was 86% greater than that of the steel HP 10×57 pile, as measured from the vertical load test of the steel pile performed in the field. The increase in capacity of the UHPC pile was attributed to the increased cross-sectional area of the UHPC pile and possible increase in perimeter when compared to the steel test pile, resulting in an increased toe resistance and skin friction. It was determined that it may be possible to reduce the length or number of UHPC piles in comparison to HP 10×57 piles in bridges due to the increased capacity.

Following the vertical load tests, the two UHPC test piles were then used for a lateral load test. A horizontal actuator was positioned between the two UHPC test piles so that both could be tested simultaneously. Each test pile was subjected to a lateral load so that the pile sections were subjected to bending about the strong-axis direction. LPILE was used to predict the maximum lateral load that the test piles would develop in the soil before experiencing structural failure or exceed the limitations set by the equipment used.

Shear failure occurred in one of the tests piles at 22.8 kips, which was much less than the predicted ultimate lateral load for the UHPC test piles. The reason given for the failure of the first test pile was thought to be that the critical section for shear was weakened by a significant portion of the web rendered ineffective due to the instrumentation bundle passing through the location. As a result of the first test pile failure, the second test pile was not pushed to failure because the displacement could not be increased past 2.54 in.

2.5.   Pile Design Method

Typically, for integral bridges, a single row of piles are used to support the abutments (Iowa DOT 2011). Thus, the pile is designed based on the capacity of a single pile and not a group because there is sufficient distance between piles.

2.5.1.   Geotechnical Resistance

There are many different static methods used to design the ultimate capacity of single piles. Commonly, all of the methods use the same basic equations to calculate the ultimate bearing capacity of a single pile, which are given in equations (2-7) through (2-9).

$$Q_u = R_s + R_t \qquad \qquad \text{(Hannigan et al. 2006a)} \qquad \qquad \text{(2-7)}$$

$$R_s = f_s A_s \qquad \qquad \text{(2-8)}$$

$$R_t = q_t A_t \qquad \qquad \text{(2-9)}$$

where,
Q_u = ultimate bearing capacity
R_s = shaft resistance
R_t = toe bearing resistance
f_s = unit shaft resistance
A_s = pile shaft surface area
q_t = unit toe resistance
A_t = pile toe area

The methods have developed different approaches to calculate f_s and q_t. Frequently used methods that have been developed for cohesionless soils are the Meyerhof method (Meyerhof 1976), Brown method (Brown et al. 2001), Nordlund method (Nordlund 1963), effective stress method (Fellenius 1991), L.P.C. method (Bustamante and Gianeselli 1983), and Nottingham and Schmertmann method (Nottingham and Schmertmann 1975, Schmertmann 1978). Additionally, methods that have been developed for cohesive soils are the total stress analysis (α-Method) (Tomlinson 1994), effective stress method (Fellenius 1991), and λ-Method (API 1993). A detailed description of the methods and how to calculate f_s and q_t are given by Hannigan et al. (2006a). The Iowa Blue Book Method (Iowa DOT 2011) was used for the design of the test and production piles during this portion of the research project and is outlined here.

Table 2-3 shows the load and resistance factor design (LRFD) recommended nominal resistance values for end bearing of steel H-piles, prestressed concrete piles, and steel pipe piles.

Table 2-3. LRFD driven pile foundation end bearing geotechnical resistance chart

Soil description	Blow count			Estimated nominal resistance values for end bearing pile in kips [ksi]									
	N-value		Wood pile[(1),(3)]	Steel "H" Grade 50			Prestressed concrete[(2)]			Steel pipe[(4)]			
	Mean	Range		10	12	14	12	14	16	10	12	14	18
Granular material													
	<15	---	(5)	(5)	(5)	(5)	(5)	(5)	(5)	(5)	(5)	(5)	(5)
Fine or medium sand	15	---	32	(5)	(5)	(5)	60	84	108	32	48	64	108
Coarse sand	20	---	44	(5)	(5)	(5)	84	116	148	44	64	88	144
Gravelly sand	21	---	44	(5)	(5)	(5)	84	116	148	44	64	88	144
	25	---	56	(5)	(5)	(5)	(6),(7)	(6),(7)	(6),(7)	(7)	(7)	(7)	(7)
	---	25–50	(6)	[2–4]	[2–4]	[2–4]	(7)	(7)	(7)	(7)	(7)	(7)	(7)
	---	50–100	(6)	[4–8]	[4–8]	[4–8]	(6)	(6)	(6)	(7)	(7)	(7)	(7)
	---	100–300	(6)	[8–16]	[8–16]	[8–16]	(6)	(6)	(6)	(7)	(7)	(7)	(7)
	---	>300	(6)	[18]	[18]	[18]	(6)	(6)	(6)	(7)	(7)	(7)	(7)
Bedrock													
	---	100–200	(6)	[12]	[12]	[12]	(7)	(7)	(7)	(7)	(7)	(7)	(7)
	---	>200	(6)	[18]	[18]	[18]	(7)	(7)	(7)	(7)	(7)	(7)	(7)
Cohesive material													
	12	10–50	16	(5)	(5)	(5)	28	40	52	16	24	62	52
	20	---	24	[1]	[1]	[1]	44	64	84	28	36	52	84
	25	---	32	[2]	[2]	[2]	60	84	108	32	48	64	108
	50	---	(6)	[4]	[4]	[4]	116[(6)]	164[(6)]	212[(6)]	56	96	128	212
	100	---	(6)	[7]	[7]	[7]	(6)	(6)	(6)	(6)	(6)	(6)	(6)

Source: After Iowa DOT 2011

Table notes: (1) Wood piles shall not be driven through soils with N > 25. (2) With prestressed concrete piles the preferred N for soil at the tip ranges from 25 to 35. Prestressed concrete piles have been proven to be difficult to drive in very firm glacial clay and very firm sandy glacial clay. Prestressed concrete piles should not be adjusted for a different tip area. (3) End bearing resistance values for wood piles are based on a tip area of 72 in^2. Values shall be adjusted for a different tip area. (4) Steel pipe piles should not be driven in soils with consistent N > 40. See the 1994 soils information chart [BDM 6.2.1.5] for end bearing when a conical driving point is used. (5) Do not consider end bearing. (6) Use of end bearing is not recommended for timber piles when N > 25 or for prestressed concrete piles when N > 35 or for any condition identified with this note. (7) End bearing resistance shall be 0.0389 x N value [ksi].

Based on standard penetration test (SPT) data from the site and type of pile used, the R_t value can be found using equation (2-9). When Table 2-3 has square brackets around the number, the value given is q_t and should be used in conjunction with equation (2-9). To calculate R_s, Table 2-4 and Table 2-5 are used along with equation (2-10).

Table 2-4. LRFD driven pile foundation friction geotechnical resistance chart for alluvium

	Blow count			Estimated nominal resistance values for friction pile in kips/ft									
				Steel "H" Grade 50			Prestressed concrete			Steel pipe			
	N-value		Wood										
Soil description	Mean	Range	pile[1],[3]	10	12	14	12	14	16	10	12	14	18
Alluvium													
Very soft silty clay	1	0–1	0.8	0.4	0.8	0.8	0.8	0.8	0.8	0.4	0.4	0.4	0.8
Soft silty clay	3	2–4	1.2	0.8	1.2	1.2	0.8	0.8	0.8	0.8	0.8	0.8	1.2
Stiff silty clay	6	4–8	1.6	1.2	1.6	2.0	1.2	1.6	2.0	1.2	1.2	1.6	2.0
Firm silty clay	11	7–15	2.4	2.0	2.4	2.8	2.4	2.8	3.2	1.6	2.0	2.4	2.8
Stiff silt	6	3–7	1.6	1.2	1.6	1.6	1.6	1.6	1.6	1.2	1.2	1.6	1.6
Stiff sandy silt	6	4–8	1.6	1.2	1.6	1.6	1.6	1.6	1.6	1.2	1.2	1.6	1.6
Stiff sandy clay	6	4–8	1.6	1.2	1.6	2.0	2.0	2.0	2.4	1.2	1.6	1.6	2.0
Silty sand	78	3–13	1.2	1.2	1.2	1.6	1.6	1.6	1.6	0.8	0.8	1.2	1.6
Clayey sand	13	6–20	2.0	1.6	2.0	2.8	2.4	2.4	2.8	1.6	2.0	2.4	2.8
Fine sand	15	8–22	2.4	2.0	2.4	2.8	2.4	2.8	3.2	1.6	2.0	2.4	2.8
Coarse sand	20	12–28	3.2	2.8	3.2	3.6	3.2	3.6	4.0	2.0	2.4	2.8	3.6
Gravely sand	21	11–31	3.2	2.8	3.2	3.6	3.6	3.6	4.0	2.0	2.4	2.8	3.6
Granular material	> 40	---	[2]	4.0	4.8	5.6	[2]	[2]	[2]	[2]	[2]	[2]	[2]

Source: After Iowa DOT 2011

Table notes: (1) For double entries, the upper value is for an embedded pile within 30 ft of the natural ground elevation, and the lower value [ ] is for depths more than 30 ft below the natural ground elevation. (2) Do not consider the use of this pile type for this soil condition, wood with N > 25, prestressed concrete with N > 35, or steel pipe with N > 40. (3) Prestressed concrete piles have proven difficult to drive in these soils. Prestressed piles should not be driven in glacial clay with consistent N > 30 to 35.

Table 2-5. LRFD driven pile foundation friction geotechnical resistance chart for glacial clay

Soil description	Blow count N-value Mean	Range	Wood pile[1],[3]	Steel "H" Grade 50 10	12	14	Prestressed concrete 12	14	16	Steel pipe 10	12	14	18
Glacial clay													
Firm silty glacial clay	11	7–15	2.8	2.4	2.8	3.2	2.8	3.2	3.6	2.0	2.4	2.4	3.2
Firm clay (gumbotil)	12	9–15	2.8	2.4	2.8	3.2	2.8	3.2	3.6	2.0	2.4	2.4	3.2
Firm glacial clay[1]	11	7–15	2.4 [3.2]	2.8 [3.2]	3.2 [4.0]	3.6 [4.4]	3.2 [4.0]	3.6 [4.4]	4.0 [4.8]	2.0 [2.4]	2.4 [2.8]	2.8 [3.2]	3.6 [4.4]
Firm sandy glacial clay[1]	13	9–15	2.4 [3.2]	2.8 [3.2]	3.2 [4.0]	3.6 [4.4]	3.2 [4.0]	3.6 [4.4]	4.0 [4.8]	2.0 [2.4]	2.4 [2.8]	2.8 [3.2]	3.6 [4.4]
Firm –very firm glacial clay[1]	14	11–17	2.8 [3.6]	2.8 [4.0]	3.2 [4.8]	3.6 [5.6]	4.0 [4.8]	4.4 [5.2]	4.8 [5.6]	2.4 [3.2]	2.8 [3.6]	3.2 [4.0]	4.0 [5.2]
Very firm glacial clay[1]	24	17–30	2.8 [3.6]	2.8 [4.0]	3.2 [4.8]	3.6 [5.6]	3.2[3] [4.8]	3.6[3] [5.6]	4.4[3] [6.4]	2.4 [3.2]	2.8 [3.6]	3.2 [4.0]	4.0 [5.2]
Very firm sandy glacial clay[1]	25	15–30	3.2 [4.0]	2.8 [4.0]	3.2 [4.8]	3.6 [5.6]	3.2[3] [4.8]	3.6[3] [5.6]	4.4[3] [6.4]	2.4 [3.2]	2.8 [3.6]	3.2 [4.0]	4.0 [5.2]
Cohesive or glacial material[1]	> 35	---	[2]	2.8 [4.0]	3.2 [4.8]	3.6 [5.6]	[2]	[2]	[2]	2.0[4] [3.2]	2.4[4] [4.0]	2.8[4] [4.4]	3.6[4] [5.6]

Source: After Iowa DOT 2011

Table notes: (1) For double entries the upper value is for an embedded pile within 30 ft of the natural ground elevations, and the lower value [ ] is for depths more than 30 ft below the natural ground elevation. (2) Do not consider the use of this pile type for this soil condition, wood with N > 25, prestressed concrete with N > 35, or steel pipe with N > 40. (3) Prestressed concrete piles have proven difficult to drive in these soils. Prestressed piles should not be driven in glacial clay with consistent N > 30 to 35. (4) Steel pipe piles should not be driven in soils with consistent N > 40.

$$R_s = f_s^* l \qquad (2\text{-}10)$$

where,
f_s^* = unit shaft resistance, kips/ft
l = length of soil layer

The Iowa DOT (2011) uses equation (2-11) to design the pile to satisfy the design requirements for a downward load.

$$\sum \eta_i \gamma_i P_i \le \varphi_c Q_u \qquad (2\text{-}11)$$

where,
$\sum \eta_i \gamma_i P_i$ = total factored load per pile
γ_i = average load factor, $\gamma_i = 1.45$
η = number of piles
φ_c = soil resistance factor

The Iowa Highway Research Board recently sponsored a project to calibrate resistance factors for the state of Iowa. The interim soil resistance factor was taken as 0.725. AbdelSalam et al. (2012) made recommendations for improved resistance factors for the Iowa Blue Book Method that accounted for construction control and setup. Table 2-6 includes the recommended resistance factors based on soil type, construction control, and setup.

Table 2-6. Resistance factors for single pile in axial compression

Theoretical analysis[c]	Construction control [a]					Resistance factor [b]				
	Driving criteria basis		PDA/CAPWAP	Retap Test 3-Days After EOD	Static Pile Load Test	Cohesive			Mixed	Non-cohesive
	Iowa DOT ENR formula	WEAP				φ	φ_{EOD}	φ_{setup}	φ	φ
Iowa Blue Book	Yes	-	-	-	-	0.60	-	-	0.60	0.50
	-	Yes[d]	-	-	-	0.65	-	-	0.65	0.55
			Yes	-	-	0.70[e]	-	-	0.70	0.60
				Yes	-	0.80	-	-	0.70	0.60
			-	-	Yes	0.80	-	-	0.80	0.80

Source: Green et al. 2012
Table notes: (a) Determine the construction control that will be specified on the plans to achieve the target nominal driving resistance. (b) Resistance factors presented in Table E1 are for redundant pile groups (minimum of 5 piles). (c) Use BDM Article 6.2.7 to estimate the theoretical nominal pile resistance, based on the Iowa Blue Book. (d) Use the Iowa Blue Book Soil input procedure to complete WEAP analysis. (e) Setup effect has been included when WEAP is used to establish driving criteria and CAPWAP is used as a construction control.

Table 2-7 provides guidelines to assist in classifying the soil type.

Table 2-7. Soil classification method

Generalized soil category	AASHTO	USDA textural	BDM 6.2.7 geotechnical resistance chart	
Cohesive	A-4, A-5, A-6, and A-7	Clay Silty clay Silty clay loam Silt Clay loam Silt loam Loam Sandy clay	Loess	Very soft silty clay Soft silty clay Stiff silty clay Firm silty clay Stiff silt Stiff sandy clay
			Glacial clay	Firm silty glacial clay Firm clay (gumbotil) Firm glacial clay Firm sandy glacial clay Firm-very firm glacial clay Very firm glacial clay Very firm sandy glacial clay Cohesive or glacial material
Non-Cohesive	A-1, A-2, and A-3	Sandy clay Loam Sandy loam Loamy sand Sand	Alluvium or Loess	Stiff sandy silt Silty sand Clayey sand Fine sand Coarse sand Gravelly sand Granular material (n > 40)

Source: Green et al. 2012

2.5.2.   *Structural Resistance*

Vande Voort et al. (2008) summarize the compressive stress limits used between 1983 and 2008 by state DOTs, AASHTO, and American Society of Civil Engineers (ASCE) for steel H-piles and precast, prestressed concrete piles. Specifically, Table 2-8 outlines the current compressive stress limits for steel H-piles and precast, prestressed concrete piles used by the Iowa DOT, which still follow the AASHTO allowable stress design (ASD).

Table 2-8. Compressive stress limits for steel H-piles in precast, prestressed concrete piles in Iowa

Steel H-pile	Precast, prestressed concrete piles
6.0 ksi – typical design 9.0 ksi – design stress allowed for end bearing piles on rock with SPT N-values of 100–200 or combined end bearing and friction piles on rock with N-values ≥ 200 12.0 ksi – design stress is permitted for the same cases as above, except it may only be used for piers and with approval from the soil Soil Design Section and Assistant Bridge Engineer	$0.33f_c' - 0.27f_{pe}$ (For 12 in. square pile only)

Source: Iowa DOT 2011

2.6. Integral Abutments

Integral bridges are bridges that have no movement joints and have foundations that accommodate the superstructure deformation due to temperature, creep, and shrinkage effects causing the bridge to expand or contract with time (Kamel et al. 1996). The changes in length cause the bridge to increase and decrease, which results in a push-pull effect on abutments and pile heads. To minimize the cost of construction and maintenance, the Iowa DOT prefers to use integral abutments whenever possible in design (Iowa DOT 2011).

2.6.1. Current Integral Abutment Design Guidelines

Many research projects were conducted to provide maximum bridge lengths for integral abutment bridges. One such study was completed by Dicleli and Albhaisi (2004) and gives the recommendations based on climate as shown in Table 2-9.

Table 2-9. Recommendations for maximum bridge length

Pile size	Steel bridges		Concrete bridges	
	Moderate climate length, ft	Cold climate length, ft	Moderate climate length, ft	Cold climate length, ft
HP 12 × 84	722	476	1,050	869
HP 12 × 74	673	443	984	820
HP 10 × 57	525	461	787	640

Source: After Dicleli and Albhaisi 2004

Abendroth and Greimann (2005) recommended including a prebored hole filled with a material that has low stiffness and orienting the piles such that they are subjected to weak-axis bending during bridge movement. These changes are intended to improve the performance of the foundations in integral abutments.

Typically, each state DOT has developed its own design guidelines, including for integral abutments Table 2-10 briefly summarizes the integral abutment guidelines for eight state DOTs.

Table 2-10. Summary of eight DOT design guidelines for integral abutments

State	Girder type	Max bridge length limit, ft	Max. skew, º	Prebore hole length, ft	Pile orientation	Reference
IA	Concrete	575	45	10	0 to 30º skew: Parallel to abutment 31 to 45º skew: weak-axis bending	Iowa DOT 2011
	Steel	400				
NY	Concrete Steel	330	45	8	Weak-axis bending	NYSDOT 2011
ME	Concrete Steel	330 200	25	-	Weak-axis bending	Maine DOT 2003
MA	Concrete	590	30	10	Web parallel to centerline of the abutment	Mass DOT 2009
	Steel	330				
RI	Concrete Steel	600 350	30	10	Weak-axis bending	Rhode Island DOT 2007
VT	Concrete Steel	695 395	20	-	Weak-axis bending	VTrans 2008
CO	Concrete Steel	790 640	-	-	-	CDOT 2009
MN	Concrete Steel	300	45	-	-	MnDOT 2011

When comparing the recommendations by Dicleli and Albhaisi (2004) to the maximum bridge length limits for HP 10×57 steel piles in Iowa, the maximum bridge length for steel bridges in Iowa is about 13% less in the study and 10% less for concrete bridges than recommended by Dicleli and Albhaisi (2004). The Minnesota DOT (MnDOT) uses a maximum bridge length for integral abutments 35% lower than the value given in the study by Dicleli and Albhaisi (2004) for steel bridges and 53% lower for concrete bridges.

Minnesota does not differentiate between types of bridges and none of the DOTs appear to differentiate between size and type of pile used for the guidelines given in Table 2-10. Additionally, not all DOTs specify the maximum skew, prebored holes, or orientation of the pile in integral bridges. Consequently, it may be stated that the design guidelines for many DOTs, with regard to integral abutments, can be improved to help reduce construction and maintenance costs.

2.6.2.   Long-Term Field Monitoring

When monitoring an integral bridge, it should be noted that many factors influence the continuous movement of the bridge superstructure and substructure. A parametric study was completed by Huang et al. (2004) that looked at many variables and validated their effects on integral abutments through long-term monitoring of an integral abutment. Some of the key variables noted in this study were pile orientation, soil conditions, predrilled holes, pile head condition, and bridge length. Findings from this parametric study are as follows:

- H-piles in strong-axis bending improve the piles performance but increase the concrete tensile stresses in the superstructure
- Stiffer soils cause larger stresses in the superstructure and piles
- Prebored holes are effective at reducing the stresses in the superstructure and piles
- A hinged connection at the pile head may cause the stresses in the superstructure to decrease, but rotation of the pile cap may cause large pile curvatures during expansion and contraction of the bridge
- Increases in bridge length increase the stresses the superstructure develops correspondingly

Abendroth and Greimann (2005) also recommended that the abutment piles have a weak-axis orientation to provide the least resistance to the longitudinal expansion and contraction of the bridge superstructure.

In a few studies as listed in Table 2-11, integral bridges were continuously monitored in the field for long periods of time to determine the performance of integral abutments.

Table 2-11. Summary of long-term monitoring of integral abutment bridges

| Name | Length, ft | Skew, ° | Girder type | Prebore hole length, ft | Longitudinal displacement, in. | | Rotation, ° | Pile orientation | Reference |
					Contraction	Expansion			
Boone River Bridge	324.5	45	Concrete	9	1.2	0.8	-	Weak-axis	Girton et al. 1991
Maple River Bridge	320	30	Steel	12	1.6	0.9		Weak-axis	
Bridge #55555 (North)	216.5	0	Concrete	None	1.41	0.3	0.11	Weak-axis	Huang et al. 2004
Bridge #55555 (South)	216.5	0	Concrete	None	1.98	0.3	0.095	Weak-axis	
Tama County Bridge, West	110	20	Concrete	None	negligible		-	Weak-axis	Abendroth et al. 2007
Tama County Bridge, East	110	20	Concrete	None	0.11	0.043	-	Weak-axis	
Guthrie County Bridge	318	30	Concrete	10	1.25	0.5	-0.056 to 0.032	Weak-axis	Abendroth and Griemann 2005
Story County Bridge	201.3	15	Concrete	8	1.3	0.46	-0.014 to 0.061	Weak-axis	
Mississinewa River Bridge	367	8	Concrete	None	0.59	0	1.5	Weak-axis	Frosch et al. 2005
Orange-Wendell Bridge, North	270		Steel	10	0.5	0.18	-0.15 to 0.13	Weak-axis	Bonczar et al. 2005
Orange-Wendell Bridge, South	270		Steel	10	0.28	0.34	-0.15 to 0.1	Weak-axis	
Scotch Road Bridge	298	15	Steel	0	0.5	0.55	-0.07 to 0.1	Weak-axis	Hassiotis 2007
Knox County Bridge	415.92	59.09	Steel	0	0.781		0.013	Strong-axis	Oesterle and Lotfi 2005

35

In these investigations, long-term monitoring programs measured bridge temperatures, longitudinal displacement, soil pressures behind the abutments, strains in the bridge girders, vertical rotation of the abutments, and vertical-temperature gradients through the depth of the bridge girders (Abendroth and Greimann 2005). In most of these studies, an analytical model was validated by the performance of the monitored bridge.

In many instances, the movement of one integral abutment in a bridge does not equal the movement of the integral abutment on the other side (Abendroth and Greimann 2005, Jorgenson 1983). Abendroth et al. (2007) found the reasons for these phenomena to be due to the difference in soil type, compaction of backfill, moisture content of backfill, vertical alignment of the roadway, geometric configuration of the bridge, and the bridge pitch at the two abutments. Another common finding from this study is that the contraction mode of displacement for the bridge induces slightly higher stresses than for the expansion displacements (Duncan and Arsoy 2003).

The seasonal expansion and contraction of integral abutment bridges are controlled by the ambient temperature, solar radiation, and relative humidity (Huang et al. 2004). Expansion is when the bridge elongates and is generally assigned the sign convention of positive displacement, while contraction is when the bridge shortens and is assigned a negative displacement.

Through long-term monitoring, it was discovered that longitudinal displacement due to thermal effects are present in a dominant cycle as a result of the seasons, but also a much smaller daily or weekly fluctuation can be visible (Girton et al. 1991). Typically, the abutment tends to rotate away from the river or road the bridge is spanning during the warmer months due to the expansion of the bridge superstructure (Huang et al. 2004). These movements of the bridge cause the bridge to rotate in the vertical direction. The vertical rotations found in integral abutments are responsible for shifting the moments lower into the pile, which was confirmed by Hassiotis (2007) by monitoring the Scotch Road Bridge.

Typically, when modeling the integral connection between abutment and pile head, the piles are assumed to behave in a fully fixed manner. Arsoy et al. (2002) found that the measured stresses in steel H-piles and pipe piles were about half of the theoretical stresses of fully fixed head piles, implying that the piles might not be fully fixed at the pile-to-abutment interface.

The skew of the bridge is also another factor that influences the behavior of the integral abutment. Many DOTs have maximum limits on the allowed skew for an integral abutment. Through long-term monitoring, it was found that if a large skew is present in a bridge, the designer can expect the bridge to rotate in plane about the vertical axis as the bridge expands and contracts with temperature (Abendroth et al. 2007).

Duncan and Arsoy (2003) found by modeling the performance of the piles for integral abutments, the approach fill significantly reduces the loads on the pile. As the abutment expands and contracts due to the bridge movements, the approach fill is dragged across the top of the soil

foundation, thus inducing a displacement in the foundation soil and reducing the relative displacement between the pile and the foundation soil. When not considering the effect of approach fill for modeling, it is considered conservative.

In many of the long-term field monitoring studies, strains were measured along the length of the piles in the integral abutments. Abendroth and Greimann (2005) found that the strains in the H-piles for the Guthrie County bridge exceeded the yield strain of steel. Additionally, the Story County bridge had pile strains that were smaller, but adding the combination of dead, live, and impact loads on the superstructure of the bridge, a portion of the pile flange would exceed the yield strain of steel.

2.7.   Pile Analysis

To predict the performance of UHPC piles in the field, computer software was used to measure the response of the pile when subjected to lateral loading and the response during driving. This section summarizes the basic principles used in LPILE and GRLWEAP, which were used in this study.

2.7.1.   LPILE

LPILE is a computer program created by Ensoft, Inc. to analyze a pile under lateral loading (Reese et al. 2004). Common types of piles subjected to lateral load are transmission towers, offshore structures, bridge foundations, overhead sign foundations, retaining walls, wind generators, poles, anchorages, and marine piers. Specifically for this research, the lateral loads influence on piles due to the expansion and contraction of integral bridges are considered. Many parametric studies using LPILE have been completed in the past. One such study completed by Huang et al. (2004) was mentioned in Section 2.6.2.

The way LPILE analyzes a pile under a lateral load is by using the concept of Winkler analysis. Figure 2-9 illustrates the model used within LPILE.
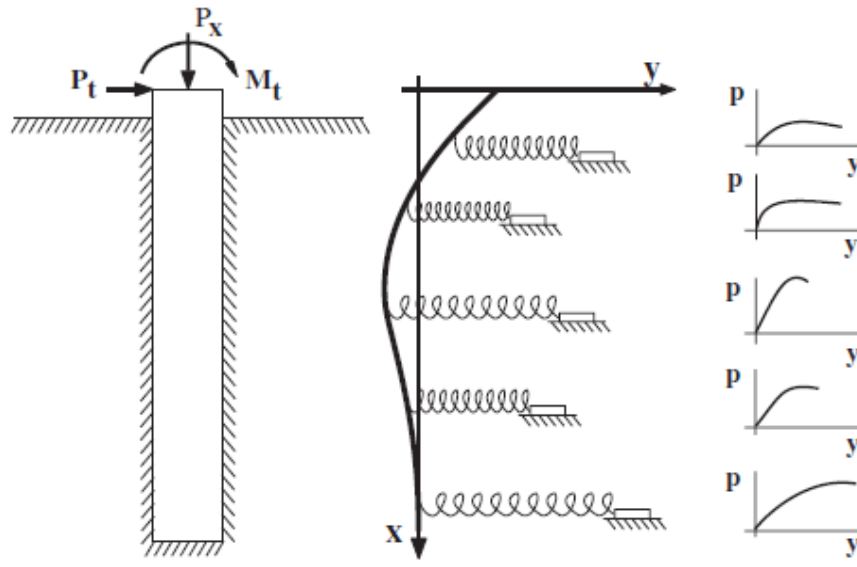
Reese et al. 2004, Ensoft, Inc.

Figure 2-9. Model of a pile subjected to loading

The pile and soil are broken up into a specified number of layers. The soil within each layer is modeled using springs controlled by *p-y* curves allowing for the simulation of nonlinear materials. To solve for the nonlinear response of a laterally loaded pile, a fourth-order differential equation was developed by Hetényi (1946) and is given in equation (2-12).

$$EI\frac{d^4y}{dx^4} + Q\frac{d^2y}{dx^2} - p + W = 0 \qquad (2\text{-}12)$$

where,
EI = flexural rigidity
y = lateral deflection of the pile at a point X along the length of the pile
Q = axial load on the pile
p = soil reaction per unit length
W = distributed load along the length of the pile

Figure 2-10 illustrates the element form of a beam-column that LPILE uses to solve the differential equation by using the finite difference method where the moments can be positive or negative.
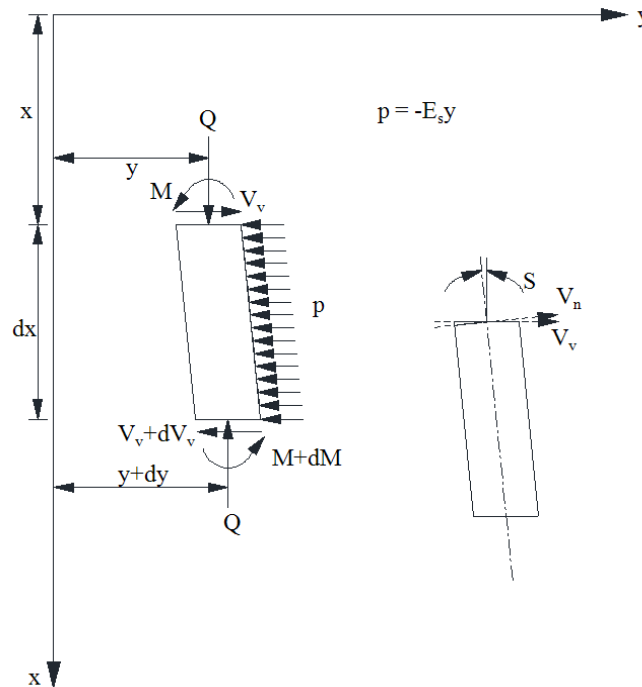
Reese et al. 2004, after Hetényi 1946

Figure 2-10. Element form beam-column

Assumptions made within LPILE by Reese et al. (2004) for a lateral load analysis are as follows:

- The pile is straight and has a uniform cross-section
- The pile has a longitudinal plane of symmetry with the load and reactions lying in that plane
- The pile material is homogeneous
- The proportional limit of the pile material is not exceeded
- The modulus of elasticity of the pile material is the same in tension and compression
- Transverse deflections of the pile are small
- The pile is not subjected to dynamic loading
- Deflections due to shearing stresses are small
- The magnitude of the axial load is constant with depth

The last assumption listed above is not strictly true. However, typically the maximum bending moment occurs close to the ground surface where the axial load is relatively unchanged. If there is concern about allowing this last assumption, the axial load can be varied along the length of the pile by including additional input values through a very lengthy iterative procedure.

Along the length of the pile, LPILE uses equation (2-13) to calculate shear, equation (2-14) to calculate moment, and equation (2-15) to calculate slope for each beam-column element.

$$V = EI \frac{d^3 y}{dx^3} + Q \frac{dy}{dx} \qquad (2\text{-}13)$$

$$M = EI \frac{d^2 y}{dx^2} \qquad (2\text{-}14)$$

$$S = \frac{dy}{dx} \qquad (2\text{-}15)$$

where,
V = shear in the pile
M = bending moment in the pile
S = slope of the elastic curve defined by the axis of the pile

To perform a typical lateral load analysis within LPILE, the user would need to input the analysis type, pile properties, loading type, pile head boundary conditions, and soil conditions. After the analysis is run, the user can obtain the shear, bending moment, and displacement along the length of the pile in a text or graphical file as output.

2.7.2.   GRLWEAP

One of the most common computer programs used by DOTs to perform a wave equation and drivability analysis is GRLWEAP. The current GRLWEAP program was developed from the WEAP program that was created in 1976 by Goble, Rausche, and Likins (PDI 2005). The program simulates the motions and forces attributed with driving of a foundation pile by various types of hammers using a numerical solution. To complete these calculations, time is divided into small intervals. It is assumed that all velocities, forces, and displacement will have constant values during each interval, and the velocities, forces, and displacements at each interval will differ from the previous interval by just enough to represent the change occurring between intervals (Smith 1960).

Figure 2-11 illustrates the model of the hammer, pile, and soil system during driving within GRLWEAP.
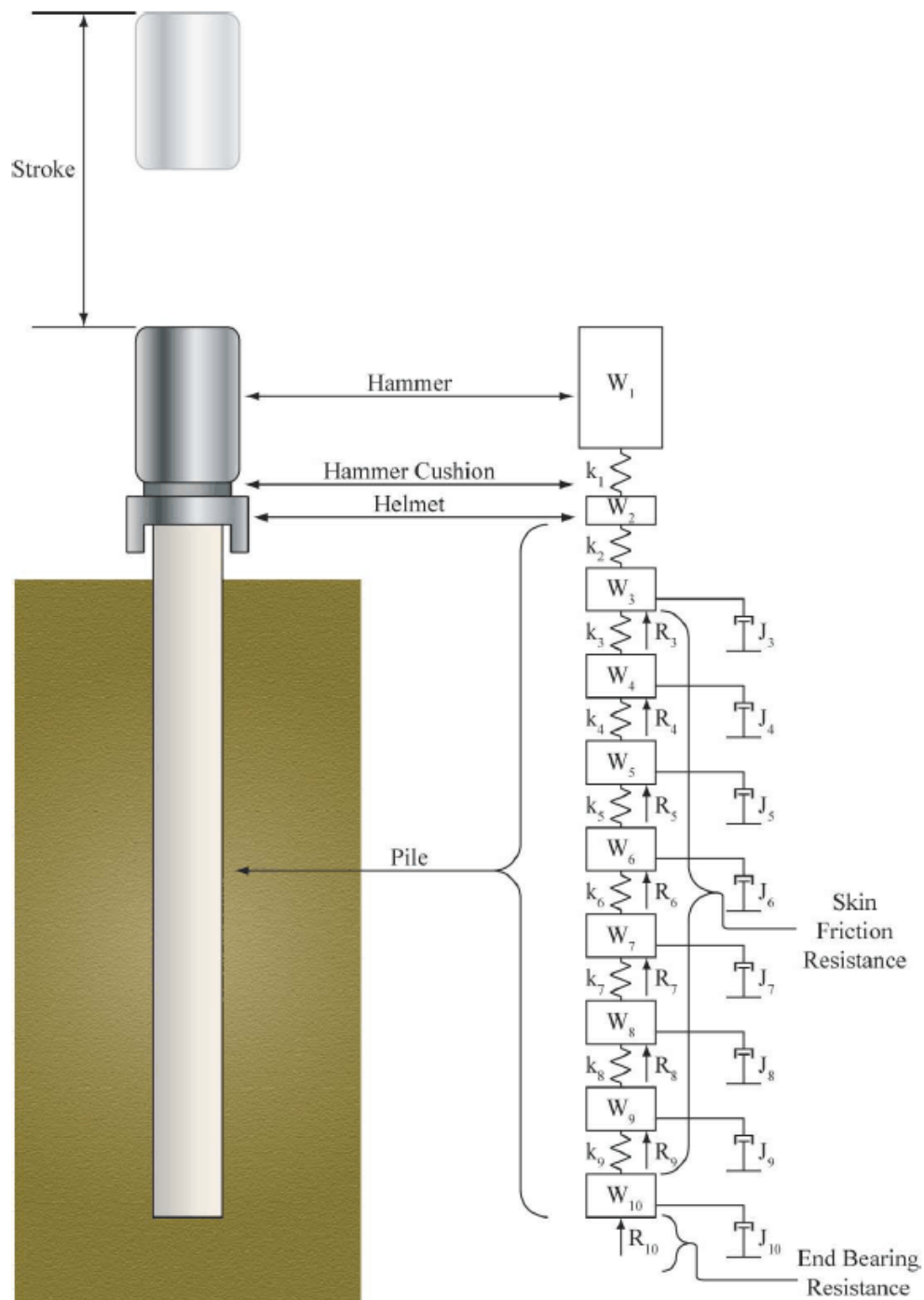
Vande Voort et al. 2008, after Graff 1965

Figure 2-11. Model of hammer, pile, and soil used in the wave equation analysis

W_1 and W_2 represent the weight of the hammer and the weight of the helmet, respectively. The hammer cushion is represented as k_1 and is assumed to have no weight. The pile is modeled by using a series of weights and springs representing the weight and stiffness of the pile, respectively.

The soil resistance is modeled by upward forces on each segment of the pile shown in Figure 2-11 by the symbol, R_i. Dashpots labeled J_i represent the damping within the soil. J_i takes into account the increase in soil resistance as the soil experiences a rapidly applied displacement compared to a slower displacement. Figure 2-12 represents the resistance-displacement diagram for the modeled soil.
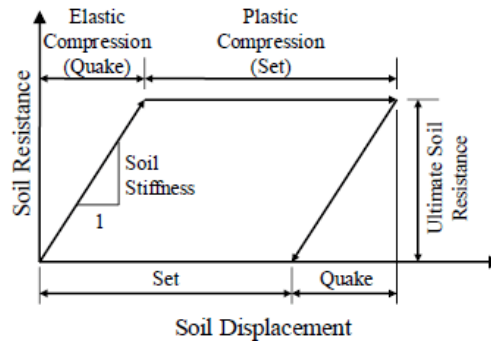
Vande Voort et al. 2008, after Smith 1962

Figure 2-12. Soil resistance-displacement relationship for wave equation analysis

The process of developing the driving forces are represented by the hammer striking the hammer cushion that develops a displacement corresponding to the stiffness of the spring used to model it. This displacement causes a force in the spring that accelerates the weight of the helmet, causing a displacement of the helmet, which then displaces the spring. The process continues along the length of the pile. To accurately calculate the stresses in each increment of pile, a sufficiently small time interval must be used. Smith (1960) recommends using 0.00025 second time interval for steel and timber piles and increases the time interval to 0.00033 seconds for concrete piles.

Input information that is required to run a wave equation analysis is hammer data, driving system data, pile data, and soil information. A library of hammer information is available for use within the program based on manufacturer specifications. If a special hammer is used, a new hammer can be added to the program. The driving system data includes information about the hammer cushion, helmet, and pile cushion. The pile data required to run the analysis is total length, cross-sectional area, elastic modulus, and specific weight as a function of depth. Information about the soil that is needed is input information about each soil layer, which can include SPT N-values, water level, damping factors, and quake factors. Recommended input values for quake and damping factors are given by Smith (1960), GRL Engineers (2001), and Dirks and Kam (2003).

The solution for the wave equation goes through a calculation process by computing the forces, displacements, and velocities of each segment of the driving system at each time interval. The force, displacement, and velocities are assumed constant for each time interval and are used to calculate the new values for the next time interval. The calculation process goes through equations (2-16) through (2-23) for each segment, m, at each time interval, n (Smith 1960).

$$V_{Impact} = \sqrt{\frac{2E_h\phi g}{W_1}} \tag{2-16}$$

$$D_m = d_m + v_m(10\Delta t) \tag{2-17}$$

$$C_m = D_m - D_{m+1} \tag{2-18}$$

$$F_m = C_m K_m \tag{2-19}$$

$$Z_m = F_{m-1} - F_m - R_m \tag{2-20}$$

$$V_m = v_m + Z_m \frac{\Delta t g}{W_m} \tag{2-21}$$

$$R_m = (D_m - D'_m)K'_m(1 + J_m v_m) \tag{2-22}$$

$$R_u = \sum_{m=3}^{s} R_m \tag{2-23}$$

where,
V_{Impact} = velocity of the driving hammer at impact
E_h = rated energy of the driving hammer
φ = efficiency of the driving hammer
g = acceleration of gravity
W_i = weight of pile segment
D_m = displacement of soil and pile segment in time interval, n
d_m = displacement of soil and pile segment in time interval, n-1
V_m = velocity in the time interval, n
v_m = velocity of pile segment in time interval, n-1
Δt = time interval
C_m = Compression in spring in time interval, n
F_m = force exerted by spring in time interval, n
K_m = stiffness of spring in time interval, n
Z_m = accelerating force in time interval n
R_m = soil resistance acting on the pile segment in time interval, n
D'_m = soil plastic displacement in time interval, n
K'_m = stiffness of the soil
J_m = soil damping constant
R_u = total ultimate soil resistance during driving
s = total number of pile segments in model

The available output of GRLWEAP is the blow count, axial stresses, and energy transfer. From these three outputs, the bearing capacity, stresses at an observed blow count, and expected blow count can be determined.

CHAPTER 3: ANALYSIS OF UHPC PILES IN INTEGRAL ABUTMENTS

This chapter focuses on comparing UHPC and HP 10×57 piles. The section behavior of the two piles was evaluated when subjected to different axial loads and then used as input into a lateral load analysis. The goal of the lateral load analysis is to determine the behavior of UHPC piles with respect to steel HP 10×57 piles for various conditions associated with integral abutments and assist with the experimental plan for the field testing and long-term monitoring of UHPC piles. This will be conducted via a moment-curvature analysis of the UHPC and HP 10×57 piles, and a parametric analysis to compare the pile's performance at five key parameters.

3.1.   Moment-Curvature Analysis

In order to perform the moment-curvature analysis for the UHPC pile section, a Microsoft Excel moment-curvature program written by Vande Voort et al. (2008) from Phase I of the project was modified so that the UHPC pile section could be analyzed about the weak axis. To calculate the moment-curvature of an HP 10×57 steel pile section, an open-source computer program package known as OpenSees (McKenna et al. 2006) was used. The program has the capabilities of modeling and analyzing the nonlinear response of systems using a wide range of material models, elements, and solution algorithms. The existing script that was developed for the analysis of the HP 10×57 pile is included in Appendix A.

3.1.1.   Analysis Assumptions

The moment-curvature response program for UHPC piles using Excel is based on the following assumptions, which are modeled after Vande Voort et al. (2008):

- Plane sections remain plane
- Prestress losses occur due only to elastic shortening and shrinkage of UHPC
- Strands have perfectly bonded to UHPC outside of the transfer regions, so the change in strain in prestressing strands is equal to the change in strain in concrete at the strand location
- Effective prestressing is applied at the centroid of the section
- Bending only occurs about the weak flexural axis
- Initial prestressing does not induce any inelastic strains on the strands
- Axial loads on the pile are applied thought the centroidal axis with no eccentricity

3.1.2.   Section Analysis

The moment-curvature program divides the cross-section into 100 small segments and calculates the stresses and strains for each segment at a given curvature. The stress and strains are then converted into forces and moments. The prestressing, prestressing losses, and axial load contribute to the uniform strain in the concrete, and they are referred to as the zero curvature strains for both UHPC and prestressing steel. The equations used in this Excel worksheet were developed by Vande Voort et al. (2008).

Two equations were used to calculate the prestressing losses. Equations (3-1) and (3-2) were used to obtain the prestressing losses due to elastic shortening of the UHPC member and shrinkage of UHPC material, respectively.

$$\Delta f_{pES} = \frac{f_{pi}A_{ps}}{2A_{ps} + A_c\frac{E_{ci}}{E_p}} \tag{3-1}$$

$$\Delta f_{pSH} = \frac{\varepsilon_{SH}A_cE_p}{A_c + A_{ps}\frac{E_p}{E_c}} \tag{3-2}$$

where,
Δf_{pES} = prestress losses due to elastic shortening of UHPC
f_{pi} = initial prestress applied to prestressing strands
A_{ps} = total area of prestressing strands
A_c = total area of UHPC
E_{ci} = elastic modulus of UHPC at time of transfer of prestressing
E_p = elastic modulus of prestressing strands
Δf_{pSH} = prestress losses due to shrinkage of UHPC
ε_{SH} = total shrinkage strain of UHPC
E_c = elastic modulus of cured UHPC

Another factor that affects the zero curvature strain is the free shrinkage of the UHPC. The prestressing strands do not undergo the free shrinkage that the UHPC experiences. The result of this difference is a tensile strain induced in the UHPC, which can be characterized by equation (3-3). The final factor contributing to the zero curvature strain is the strain due to the axial load and can be calculated using equation (3-4).

$$\Delta\varepsilon_{cSH} = \frac{\varepsilon_{SH}A_{ps}}{A_{ps} + A_c\frac{E_c}{E_p}} \tag{3-3}$$

$$\varepsilon_p = \frac{P}{A_cE_c + A_{ps}E_p} \tag{3-4}$$

where,
$\Delta\varepsilon_{cSH}$ = tensile strain in UHPC due to free shrinkage
ε_p = strain in UHPC or prestressing steel caused by axial load
P = applied axial load

The total initial strains or zero curvature strains can be calculated using equation (3-5) and equation (3-6) for the prestressing strands and the UHPC, respectively.

$$\varepsilon_{pZC} = \frac{f_{pi} - \Delta f_{pES} - \Delta f_{pSH}}{E_p} - \varepsilon_p \qquad (3\text{-}5)$$

$$\varepsilon_{cZC} = -\frac{(f_{pi} - \Delta f_{pES})A_{ps}}{A_c E_c} + \Delta \varepsilon_{cSH} - \varepsilon_p \qquad (3\text{-}6)$$

where,
ε_{pZC} = strain in prestressing steel at zero curvature
ε_{cZC} = strain in UHPC at zero curvature

After the zero curvature strains are calculated, the tensile and compressive strains due to curvature are calculated. As mentioned previously, the cross-section of the UHPC pile was divided into 100 evenly spaced horizontal segments. The user of the program is required to input the width of each section as well as the location of the prestressing strands. The strain for each of the horizontal segments of the UHPC and prestressing strands are calculated by using equations (3-7) and (3-8), respectively.

$$\varepsilon_{ct} = \varphi y_{cg} + \varepsilon_{cZC} = \varphi \left(y - \frac{\varepsilon_{cZc}}{\varphi} \right) + \varepsilon_{cZC} = \varphi y \qquad (3\text{-}7)$$

$$\varepsilon_{pt} = \varphi y_{cg} + \varepsilon_{pZC} = \varphi \left(y - \frac{\varepsilon_{cZC}}{\varphi} \right) + \varepsilon_{pZC} = \varphi y - \varepsilon_{cZC} + \varepsilon_{pZC} \qquad (3\text{-}8)$$

where,
ε_{ct} = total strain in UHPC
φ = curvature about horizontal axis
y_{cg} = distance from centroid, measured positive downward
y = distance from neutral axis, measured positive downward
ε_{pt} = total strain in prestressing steel

The variables in these equations are depicted in Figure 3-1.
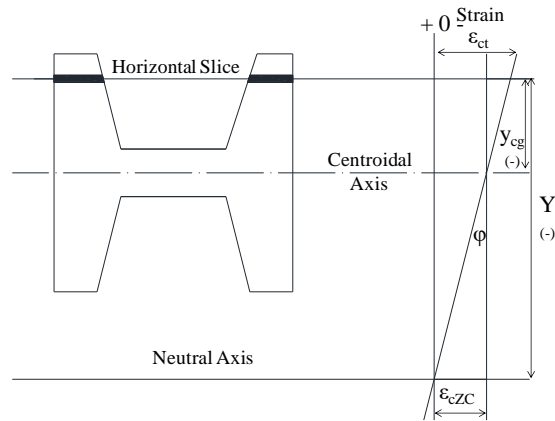
After Vande Voort et al. 2008

Figure 3-1. Definitions of distance from centroid and distance from neutral axis

During each step, the stresses and strains are calculated for each segment of the cross-section using a stress-strain relationship of UHPC and of prestressing strands that are described in Figure 3-2 and Figure 3-3, respectively.
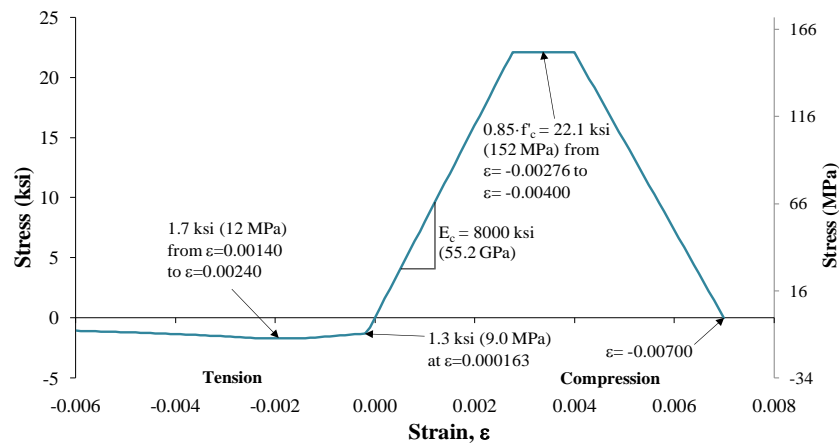
Vande Voort et al. 2008

Figure 3-2. Assumed UHPC monotonic stress-strain behavior
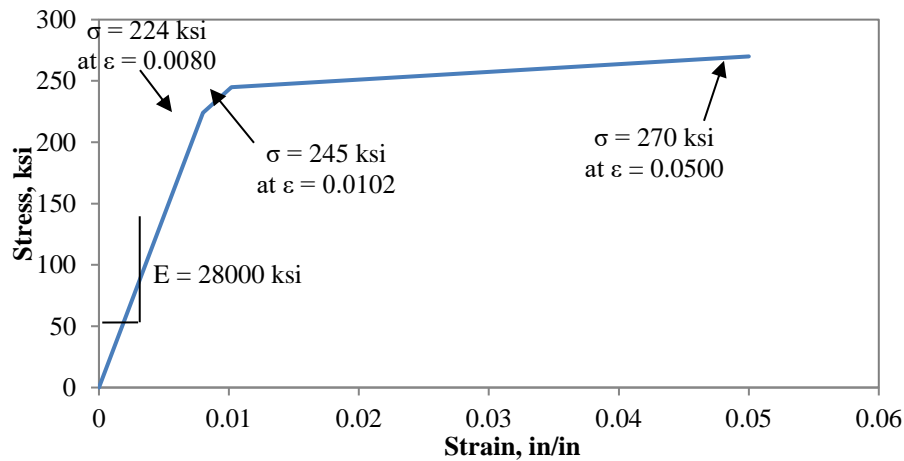
Figure 3-3. Assumed stress-strain behavior for 0.5 in., 270 ksi low relaxation prestressing strand

The forces and moments are then calculated for each segment of the cross-section by manipulating the strains. The spreadsheet solves a series of equations using the solver to calculate the appropriate curvature and neutral axis for each step. When the correct neutral axis is found for a curvature by satisfying the equilibrium condition, the sum of the moments in the section is equal to the total moment resistance associated with the input curvature (Vande Voort et al. 2008).

3.1.3.   Results

The ultimate curvature for each axial load as defined by the Excel moment-curvature program was determined by using one of the four conditions described by Vande Voort et al. (2008), whichever occurs first, as follows:

- The strain in the extreme compression fiber reached the assumed ultimate value of 7,000 microstrains
- The strain in a prestressing strand reached the assumed ultimate value of 50,000 microstrains
- The moment resistance of the section decreased to 80% of its maximum value
- The location of the neutral axis depth changed very suddenly, causing a large drop in moment resistance

Figure 3-4 shows the moment-curvature response of the UHPC pile section in weak-axis bending subjected to various axial loads.
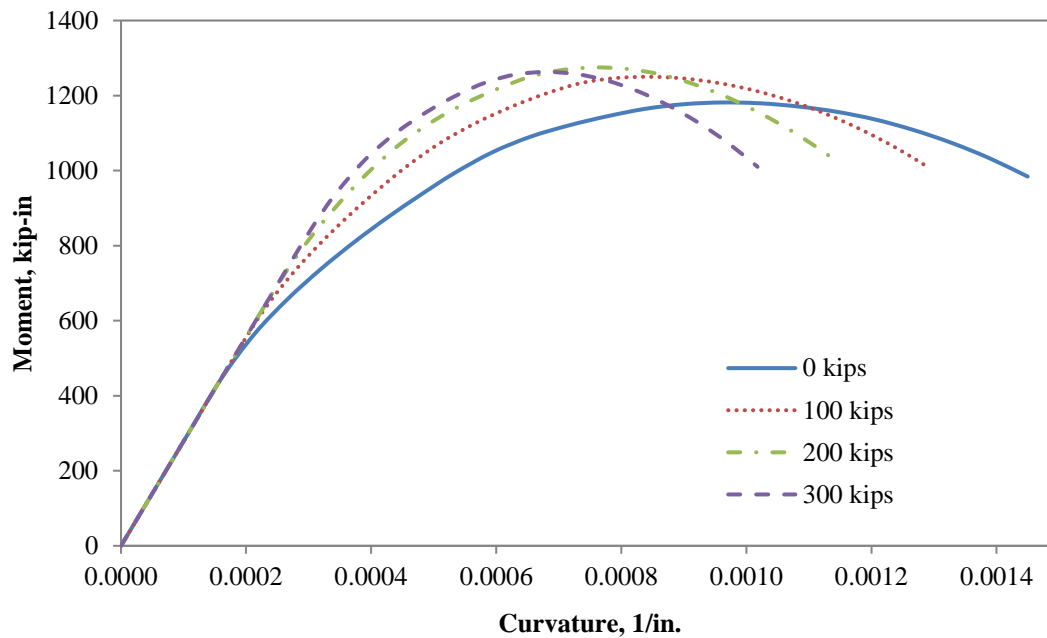
Figure 3-4. Moment-curvature of the UHPC pile section subjected to weak-axis bending with varying axial loads

As the axial load increases, the ultimate curvature decreases. The maximum moment resistance increases slightly for each load, up to 200 kips and stays the same for the axial load of 300 kips. Figure 3-5 shows the moment-curvature of a UHPC pile in strong-axis bending.
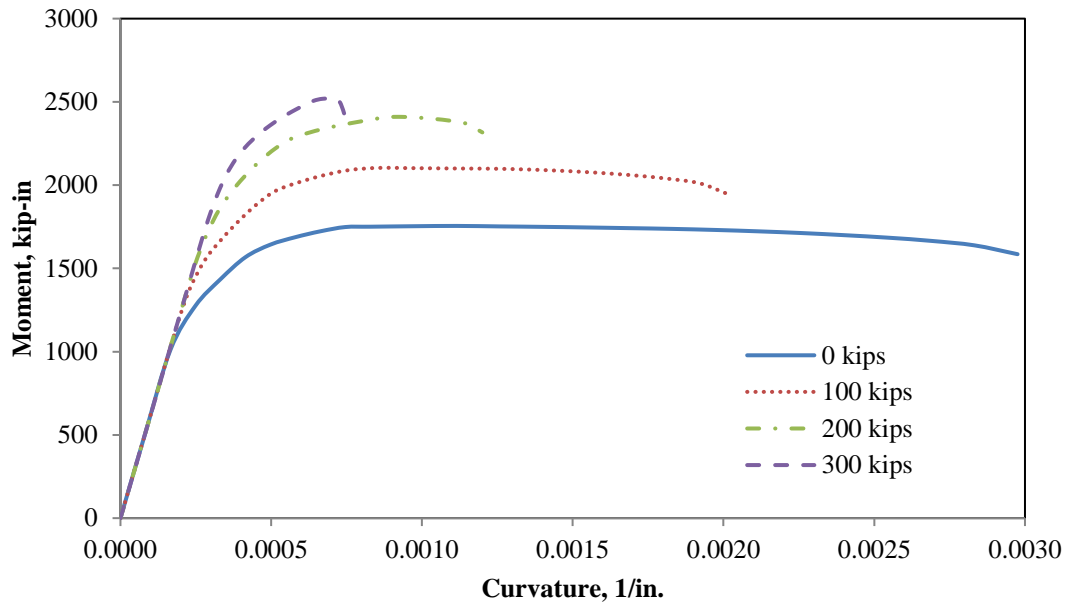
After Vande Voort et al. 2008

Figure 3-5. Moment-curvature of the UHPC pile section subjected to strong-axis bending with varying axial loads

Like the weak-axis bending, the ultimate curvature for UHPC subjected to strong-axis bending decreases as the axial load increases, but the maximum moment increases as the axial load increases.

To compare the moment-curvature response of the section behavior of a UHPC pile in strong-axis bending and weak-axis bending, the response at 100 kip axial load for both is shown in Figure 3-6.
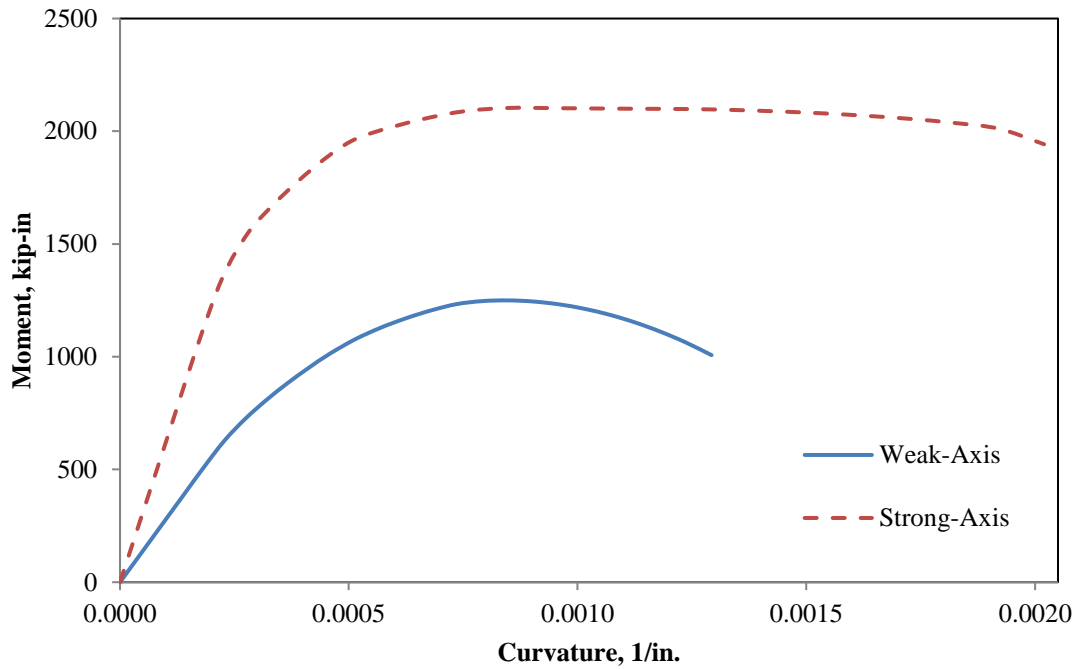
Figure 3-6. Comparison of moment-curvature between strong-axis and weak-axis bending of the UHPC pile sections subjected to a 100 kip axial load

The results from Vande Voort et al. (2008) were used for the UHPC pile section subjected to strong-axis bending. It is worth noting that both the maximum moment resistance and the ultimate curvature are greater for the strong-axis bending. The flexural rigidity and the ultimate moment of a UHPC strong-axis pile are 109% greater and 56% greater than for a UHPC pile in weak-axis bending, respectively.

Like the UHPC pile section, the HP 10×57 pile section was subjected to the same varying axial loads in both strong-axis and weak-axis bending. The weak-axis piles are given in Figure 3-7, and the strong-axis piles are shown in Figure 3-8.
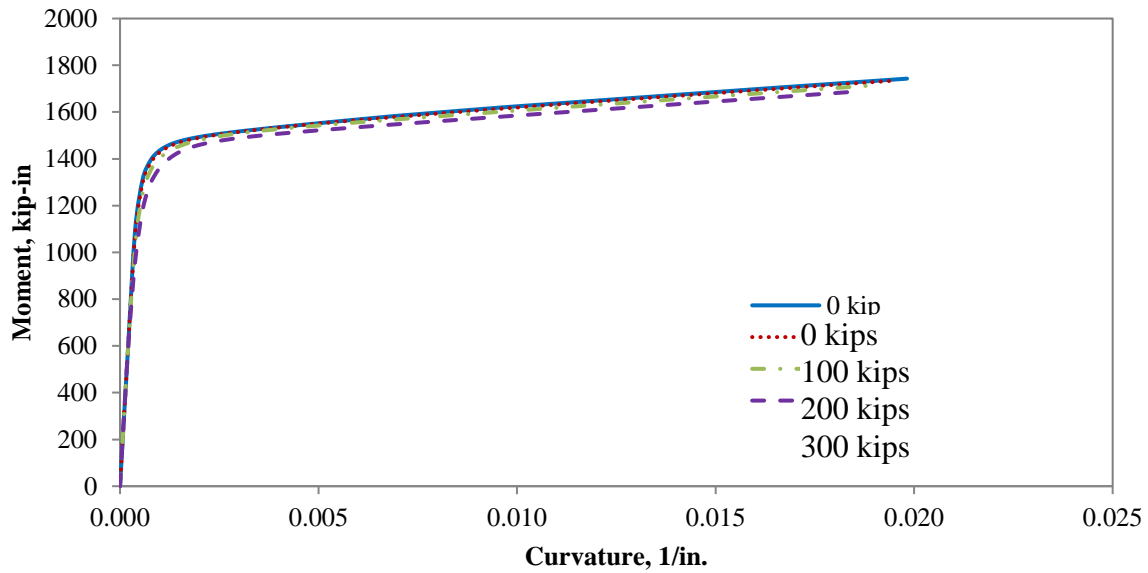
Figure 3-7. Moment-curvature of HP 10 × 57 pile section subjected to weak-axis bending with the varying axial loads
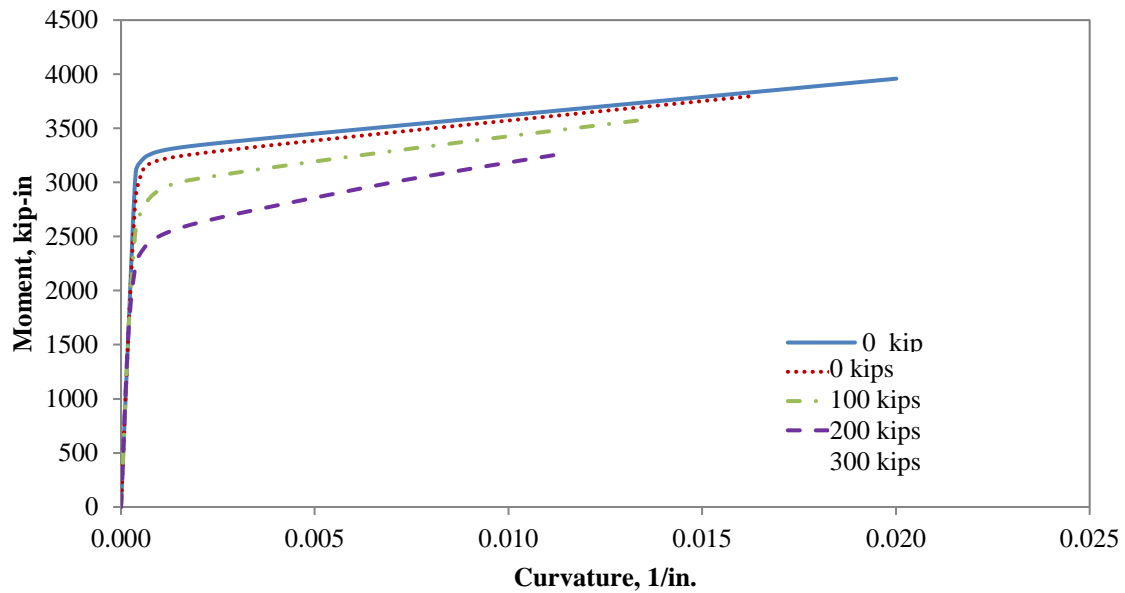
Figure 3-8. Moment-curvature of HP 10 × 57 pile section subjected to strong-axis bending with varying axial loads

As the axial load increases, the ultimate curvature decreases for both cases, but is more pronounced for the strong-axis piles. The maximum moment resistance decreases very slightly as the axial load is increased on the pile subjected to weak-axis bending. In contrast, the pile in

strong-axis bending has a dramatic decrease in the maximum moment resistance for the 200 and 300 kip axial load.

To compare the moment-curvature response of the section behavior of an HP 10 × 57 pile in strong-axis bending and weak-axis bending, the response at 100 kip axial load for both is shown in Figure 3-9.
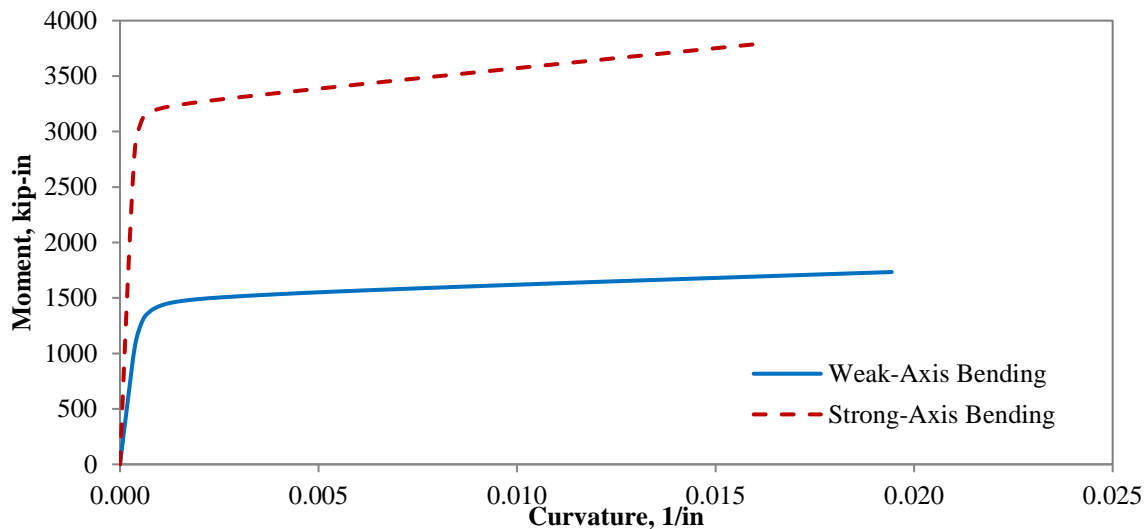
Figure 3-9. Comparison of moment-curvature between strong-axis and weak-axis bending of HP 10 × 57 pile section subjected to a 100 kip axial load

It is worth noting that both the maximum moment resistance and the ultimate curvature are greater for the strong-axis bending. The flexural rigidity and the ultimate moment of a steel pile in strong-axis bending are 191% greater and 17% less than for the steel pile in weak-axis bending, respectively.

A comparison between UHPC piles and steel HP 10 × 57 piles is shown for weak-axis bending in Figure 3-10 at an axial load of 100 kips.

53
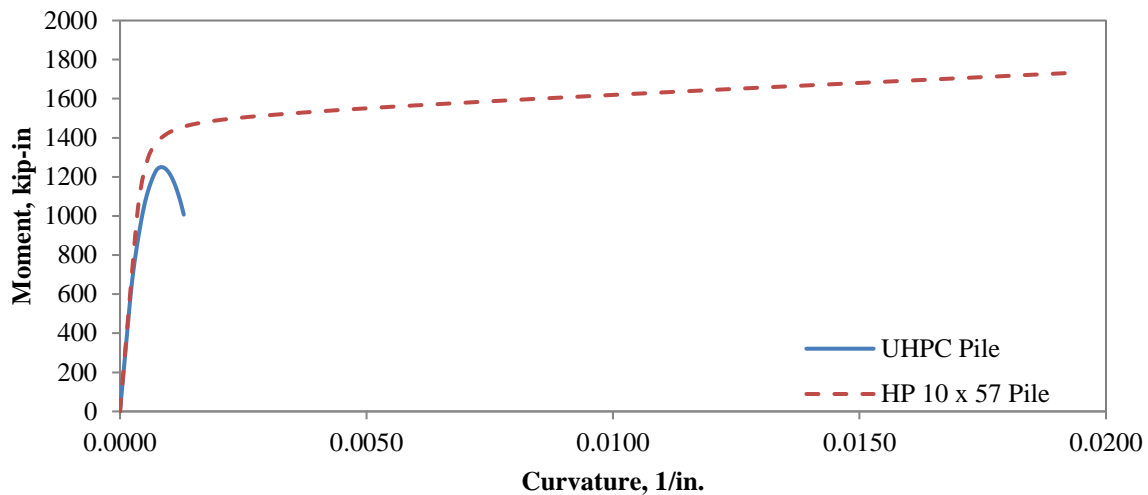
Figure 3-10. Moment-curvature response at 100 kip axial load comparing a UHPC pile and an HP 10 × 57 pile in weak-axis bending

While the two sections show comparable elastic stiffness, the steel pile exhibits higher moment resistance. Since the piles are primarily used for carrying axial loads in Iowa, the UHPC pile was designed for this purpose. The difference in moment resistance is inconsequential. If the serviceability limit state is defined using the yield strain for the H-pile and the crack width is kept to less than 0.0012 in. for UHPC piles, the H-pile section shows an increase in moment resistance of 39%. Finally, the inherent ductility of steel produces ultimate curvature significantly higher than that of the UHPC pile section. The level of ductility is not needed for the pile, and the level shown by the UHPC pile is adequate for piles designed primarily for axial load resistance.

Like the weak-axis bending piles, the maximum moment, ultimate curvature, ultimate moment, and stiffness are higher for a strong-axis bending steel HP 10 × 57 pile than a strong-axis bending UHPC pile, as illustrated in Figure 3-11.
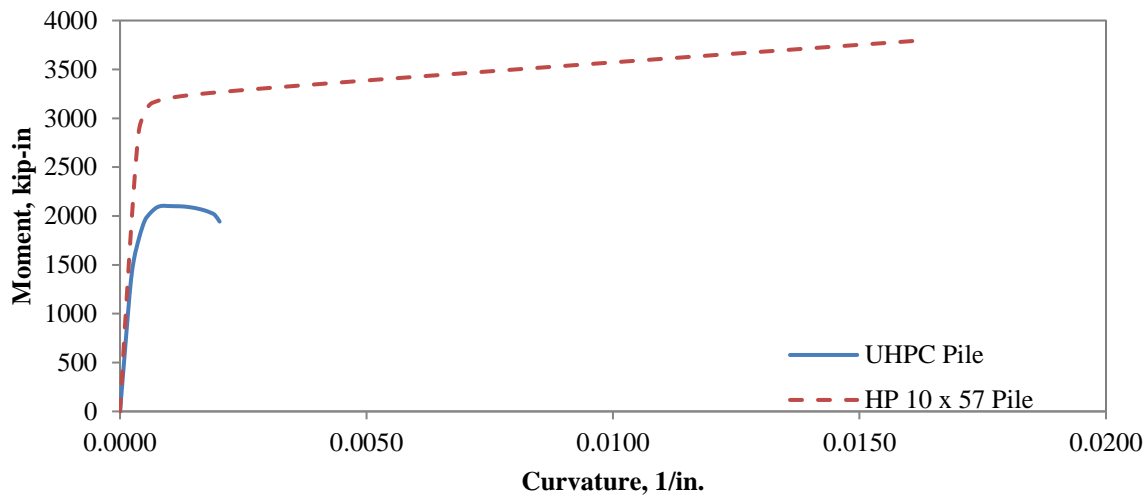
Figure 3-11. Moment-curvature response at 100 kip axial load comparing a UHPC pile and an HP 10 × 57 pile in strong-axis bending

The differences between UHPC and HP 10 × 57 piles are higher for strong-axis bending than for weak-axis bending due to the differences in stiffness between the two types of piles in strong-axis bending, with the HP 10 × 57 pile's stiffness being 38% higher than that of the UHPC pile. If the serviceability limit state is defined using the yield strain for the H-pile and the crack width is kept to less than 0.0012 in. for UHPC piles, the H-pile section shows an increase in moment resistance of 85%.

A moment-curvature analysis of UHPC and HP 10 × 57 piles was compared in strong- and weak-axis bending for four different axial load cases to better understand the section behavior of piles. The section behavior indicates the effect the piles will have on an integral abutment. For example, the HP 10 × 57 pile subjected to strong-axis bending has a much higher maximum resisting moment than for an HP 10 × 57 pile subjected to weak-axis bending. As a result of increasing the maximum resisting moment, the pile will transfer more forces into the abutment and the deck of the bridge, which must be accounted for in the design process to eliminate cracking in the bridge's structural elements.

3.2.   Parametric Analysis

A systematic study was undertaken to examine the lateral load performance of UHPC and HP 10 × 57 piles under various conditions using LPILE[PLUS] 5.0. The analyses were performed for typical integral abutment pile foundation conditions and the deflection, bending moment, and shear profiles along the pile length were compared. Five key parameters were investigated to quantify the behavior of UHPC and HP 10 × 57 in this parametric study.

3.2.1.   Parameters

The first parametric study compared a UHPC pile to a steel HP 10×57 pile by changing various conditions. The key parameters used in the study were soil type, pile head boundary condition, axial load, pile orientation, and displacement. A total of 128 different cases were evaluated for UHPC and steel HP 10×57 piles and various combinations of key parameters. The variations included for each parameter are:

- Soil type: four extreme soil conditions as shown in Table 3-1

Table 3-1. Soil properties used for parametric analyses

Soil type	Density* γ, lb/in^3	Friction angle* φ, degree	Cohesion* c, psi	Subgrade modulus* k_s, lb/in.^{3}	Strain at 50%* $\varepsilon_{50\%}$
Loose sand	0.063	30	-	25	-
Dense sand	.075	40	-	225	-
Soft clay	.063	-	3	30	0.020
Very stiff clay	.075	-	35	800	0.004

* Reese and Matlock 1956, Wang and Reese 1993, Kamel et al. 1996, Reese et al. 1974 and 2004

- Pile head boundary condition: fixed and pinned
- Axial load: 0 kip, 100 kips, 200 kips, and 300 kips
- Pile orientation: weak-axis bending and strong-axis bending
- Lateral displacement: 1.00 in. and 1.55 in.

In Iowa, a 10 ft deep prebored hole is required for abutment piles in integral abutments when the bridge exceeds 130 ft in length (Iowa DOT 2011). As a result, a second study compared the results from the first study to the behavior of a UHPC pile and an HP 10×57 pile with a 10 ft prebored hole for some of the conditions used in the first study. A total of eight cases were evaluated for UHPC and steel HP 10×57 piles as given in Table 3-2.

Table 3-2. Eight load cases investigated in the second parametric study considering a prebored hole

Conditions	Axial load, kips	Soil type	Lateral displacement, in.
Fixed-pile head;	100	Soft clay	1.00
			1.55
		Stiff clay	1.00
			1.55
Weak-axis bending	200	Soft clay	1.00
			1.55
		Stiff clay	1.00
			1.55

3.2.2.   Allowable Tensile Strains

The allowable tensile stress versus crack width for UHPC was given in Figure 2-2. Based on components of UHPC, Vande Voort et al. (2008) reported tensile strain limits for the behavior of UHPC corresponding to the stresses in Figure 2-2. Accordingly, 160 microstrains represents the barrier when micro-cracking begins at the extreme tension fiber, and 1,350 microstrains is when visible cracking begins. The strain limit of the extreme tension fiber to facilitate the fiber to pull out of the UHPC is 2,400 microstrains. The model in Figure 2-2 was updated to include the values as shown in Figure 3-12.
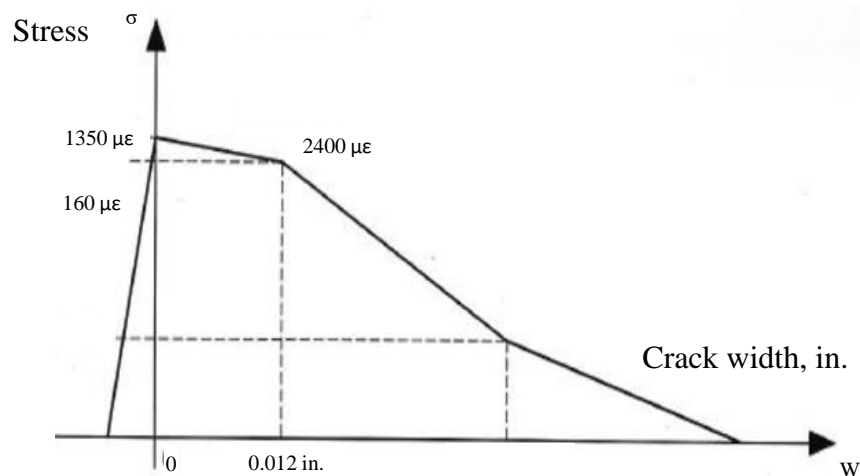
Figure 3-12. Simplified tensile strength law with tensile strain assumptions

In comparison, a value of 1,700 microstrains was used to determine the first yield of the flanges in the steel HP 10×57 piles with an assumed modulus of elasticity of 29,000 ksi and a yield strength of 50 ksi.

3.2.3. *Predicted Width and Location of Cracking along the Piles*

The flexural moment resistance at a given section of pile is the sum of the moments a pile is subjected to at a given location. The flexural moment resistance along the length of each pile was calculated using LPILE for a given lateral displacement and was used to predict the extent of cracking in the UHPC pile, as well as yielding the HP 10 × 57 pile would experience during lateral loading. For UHPC, micro-cracking is considered acceptable, the visible cracking corresponding to 1,350 microstrains is considered undesirable, and cracking that provides widths greater than 0.012 in. is deemed unacceptable. Yielding of the HP 10 × 57 pile is also considered undesirable; therefore, the visible cracking and yield limits are compared between the HP 10 × 57 pile and UHPC pile throughout this section to compare the performance of each pile section.

Potential cracking along the length of the UHPC pile was determined by finding the moment corresponding to the defined tensile strain limits for a given axial load. Using the moment-curvature calculations given in Section 3.1, Table 3-3 lists the moments used to determine the onset of cracking for UHPC piles.

Table 3-3. Assumed flexural cracking moments of UHPC piles in weak-axis bending

Axial load	Moments corresponding to strain limits given in Figure 3-12, kip-in.		
	Micro-cracking	Visible cracking	Crack width > 0.012 in.
100	536	948	1,144
200	660	1,084	1,246

Similarly, Table 3-4 gives the moments where yielding begins in the flanges of steel HP 10 × 57 piles.

Table 3-4. Estimated yielding moments of HP 10 × 57 piles in weak-axis bending

Pile type	Axial load	Yielding moment, kip-in.
HP 10 × 57	100	840
	200	711

Notice that as the axial load is increased from 100 kips to 200 kips, the moments at each of the limits for UHPC increases, while for the steel pile the yielding moment decreases as the axial load increases, giving an advantage to the UHPC pile.

Figure 3-13 through Figure 3-16 illustrate the location and extent of flexural cracking along the length of a UHPC pile as well as the location of yielding for steel HP 10×57 piles under various conditions.
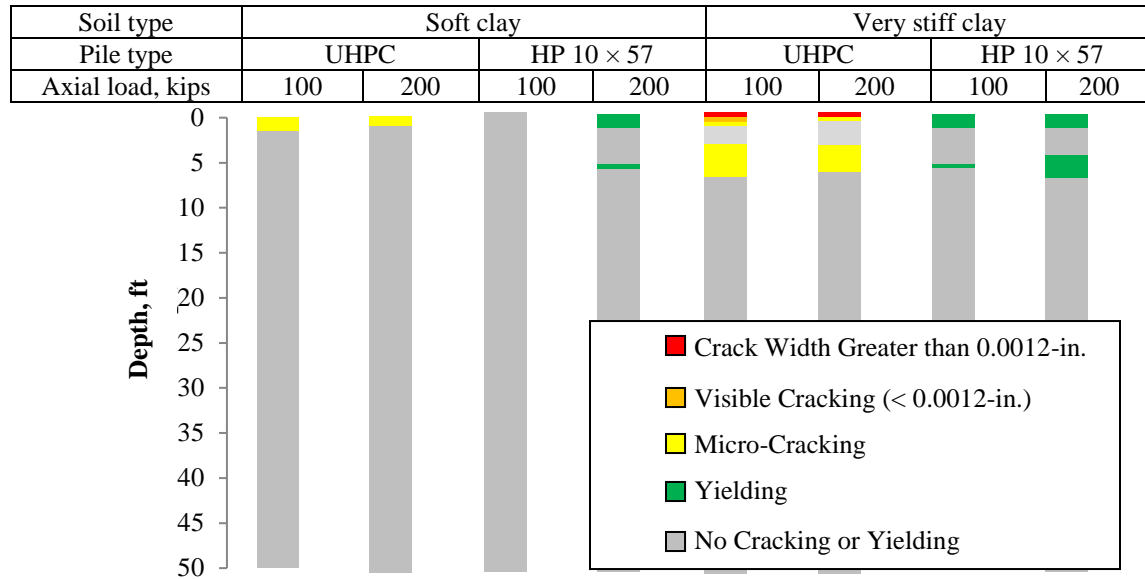
Figure 3-13. Cracking or yielding along the length of piles subjected to 1.00 in. of lateral displacement without a prebored hole
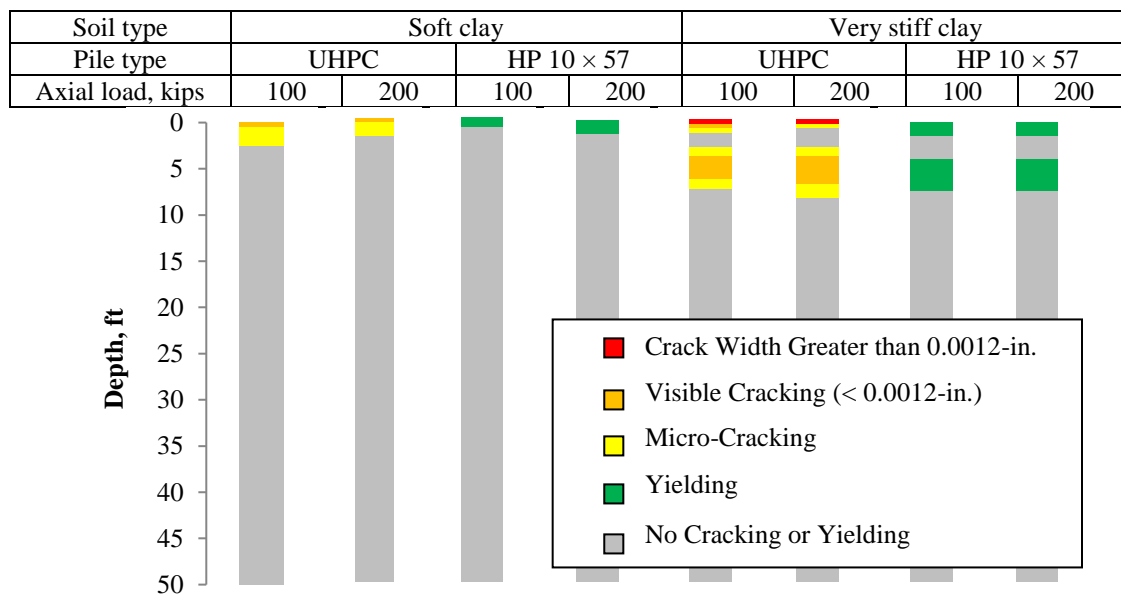
Figure 3-14. Cracking or yielding along the length of piles subjected to 1.55 in. of lateral displacement without a prebored hole

Soil type	Soft clay				Very stiff clay			
Pile type	UHPC		HP 10 × 57		UHPC		HP 10 × 57	
Axial load, kips	100	200	100	200	100	200	100	200
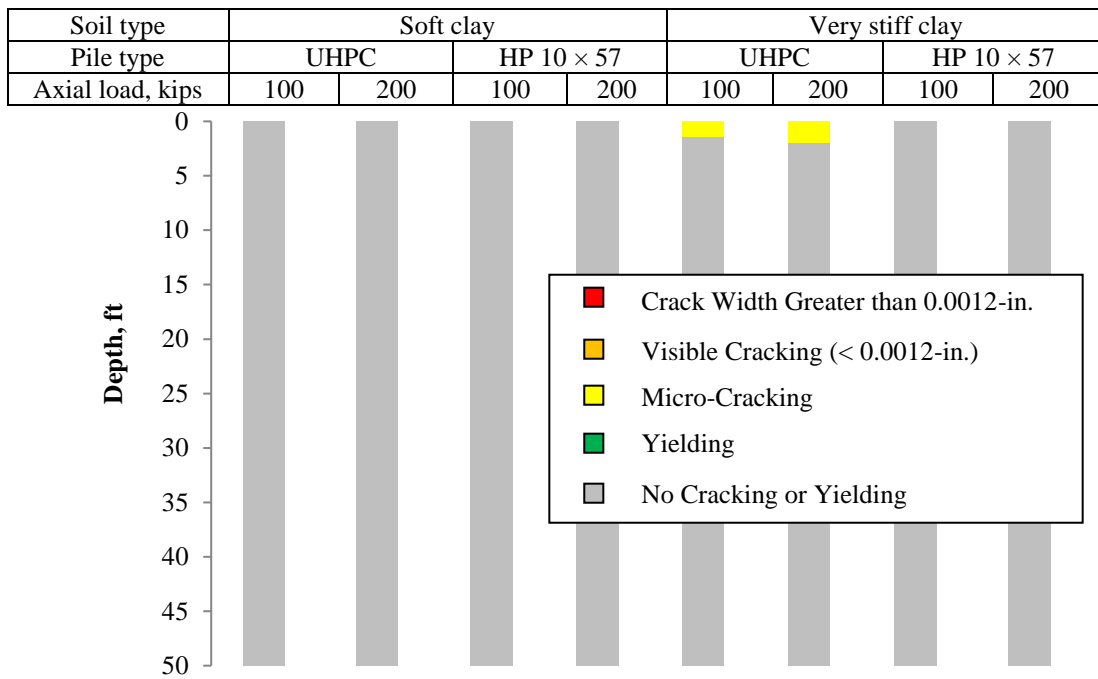
Figure 3-15. Cracking or yielding along the length of piles subjected to 1.00 in. of lateral displacement with a 10 ft deep prebored hole

Soil type	Soft clay				Very stiff clay			
Pile type	UHPC		HP 10 × 57		UHPC		HP 10 × 57	
Axial load, kips	100	200	100	200	100	200	100	200
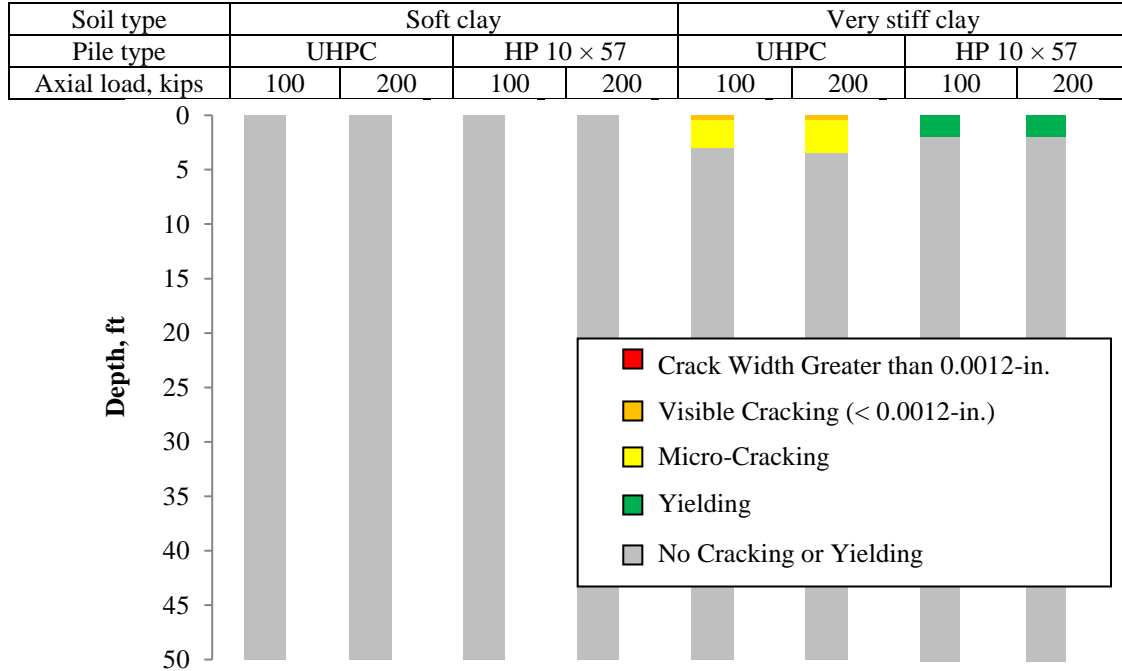
Figure 3-16. Cracking or yielding along the length of piles subjected to 1.55 in. of lateral displacement with a 10 ft deep prebored hole

The boundary conditions are supposed to reflect typical Iowa DOT integral abutment design. As a result, the parameters assumed here include a fixed-pile head condition and weak-axis bending.

Figure 3-13 depicts the type and location of damage that would occur if an integral abutment moved 1.0 in. in the longitudinal direction without having a prebored hole around each of the piles. Yielding is present for the top 6 in. of the HP 10×57 pile for the 200 kip axial load in the soft clay, but no undesirable cracking occurs for the UHPC pile under the same condition. Both visible cracking and cracks with a width greater than 0.012 in. are present for the UHPC pile, and yield is present in the HP 10×57 pile at two different depths.

If the lateral displacement is increased to 1.55 in. in very stiff clay, the UHPC piles are predicted to have unacceptable crack widths larger than 0.0012 in. It is important to note that vertical rotations of the abutment were not taken into account during this analysis, which would reduce the magnitude of flexural moments on the pile head. Additionally, two locations for yielding in the HP 10×57 pile were present for this load case, resulting in a total of 4 ft of the pile being susceptible to yielding within the flanges. The results of 1.55 in. of lateral displacement without a prebored hole are displayed in Figure 3-14.

A more representative model of an integral abutment pile is to take into account the effects of prebored holes. Typically, the Iowa DOT fills the prebored hole with bentonite or polymer slurry and assumes no lateral resistance from such material. Figure 3-15 displays the reduced amount of cracking and no yielding that is predicted to occur in piles that were installed with a prebored hole at 1.0 in. of lateral displacement. No undesirable cracking or yielding is predicted to occur for either soft clays or very stiff clays.

When piles were subjected to 1.55 in. of lateral displacement with a prebored hole condition, a small amount of visible cracking was found in the UHPC pile as well as yielding in the steel HP 10×57 pile as shown in Figure 3-16. When comparing Figure 3-14 to Figure 3-16, it is apparent that the cracking of UHPC piles and yielding of steel piles are noticeably reduced when a 10 ft prebored hole is present.

The point of fixity was also determined for each lateral load case, which was then compared between the UHPC and HP 10×57 piles. The point of fixity is the depth at which the pile behaves fixed. This location was determined by identifying the depth at which the piles' lateral displacement was less than 0.01 in.

3.2.4.   Results

The pile type, soil type, pile head boundary condition, axial load, pile orientation, and presence of a prebored hole were modeled during the parametric study. The findings from changing these parameters are described in this section.

When comparing the differences in performance between the UHPC pile and the HP 10×57 pile while keeping all of the parameters the same, the maximum moments and maximum shear forces induced in both piles are almost identical as shown in Figure 3-17.
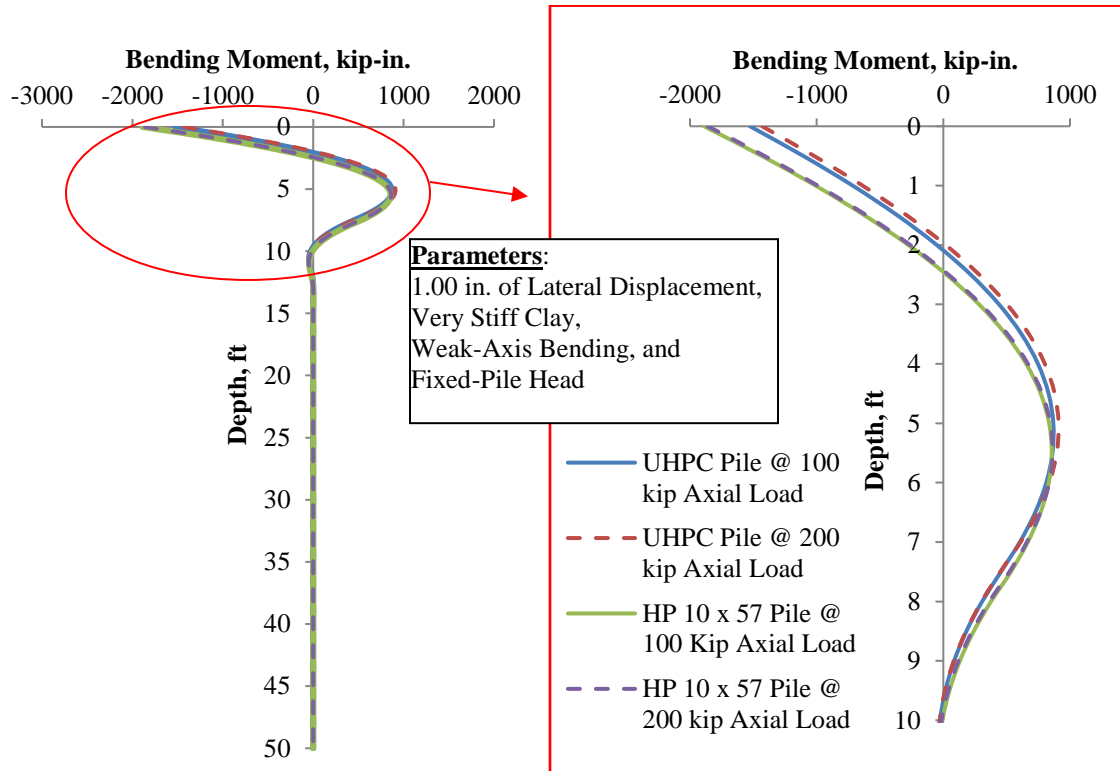
Figure 3-17. Performance difference between a UHPC pile and an HP 10×57 pile

The steel pile has a slightly higher maximum moment and maximum shear as shown in Figure 3-17, which is caused by the slight difference in flexural rigidity (EI). The HP 10×57 pile has a slightly lower EI value than the UHPC pile by 1.0%.

As the soil becomes softer, the location of the second maximum moment for fixed-pile head conditions is deeper than for stiffer or denser soils. Figure 3-18 illustrates the effect the soil has on the pile's bending moments.
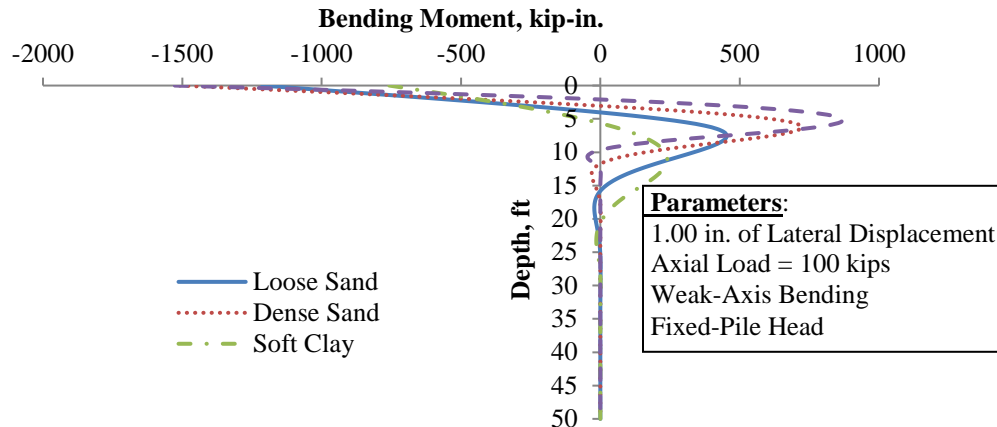
Figure 3-18. Effect of soil type on UHPC pile behavior

When varying the pile head boundary condition of UHPC and steel HP 10×57 piles from fixed to pinned condition, the results were very different as can be expected, and are illustrated in Figure 3-19.
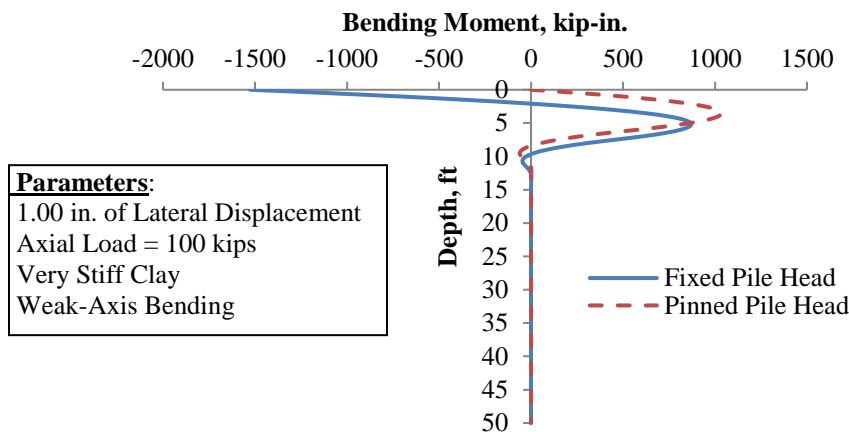
Figure 3-19. Effect of fixed- and pinned-pile head boundary conditions on moment profile for UHPC piles

There are three main differences in performance, which are due to: (1) the magnitude of the maximum bending moments and shear forces being greater for the fixed-pile head condition as compared to the pinned-pile head condition, (2) the location of the second peak moment being much deeper for the pinned-pile head condition than that of the fixed pile, and (3) the point of fixity for the pile with a fixed head connection being deeper than for the pinned connection.

Furthermore, it was found that as the axial load was increased, the maximum bending moment and maximum shear forces decrease for the steel HP 10×57 piles and the UHPC piles subjected

to weak-axis bending but increased for the UHPC pile subjected to strong-axis bending. For strong-axis, HP 10×57 piles, the maximum moment increased from 0 kips to 100 kips but decreased for 200 and 300 kips. Also, the locations of the second maximum moment remains relatively constant, but the magnitude increases as the axial load increases for the weak-axis bending case as shown in Figure 3-20.
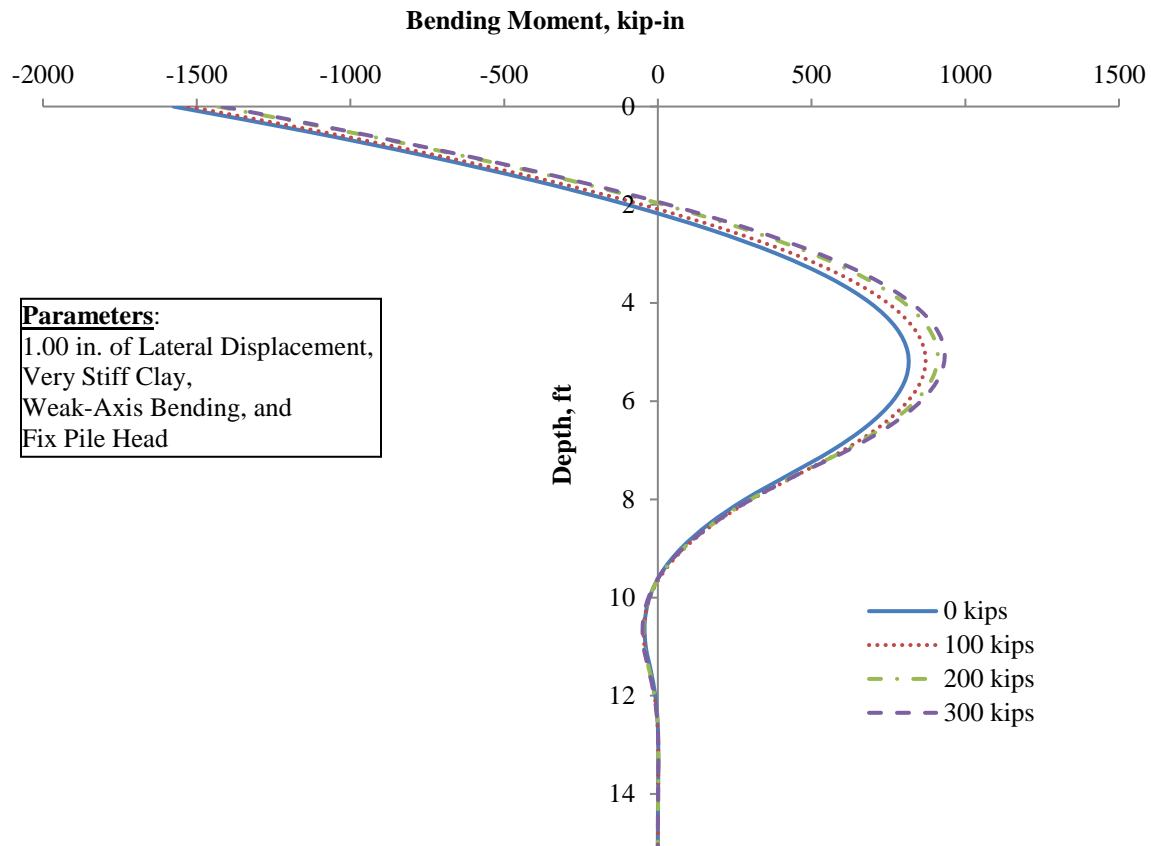
Figure 3-20. Comparison of bending moment when varying the axial load for UHPC piles

The point of fixity stays relatively constant as the axial load increases for all the UHPC and HP 10×57 piles in all soil types.

As the orientation of the pile was changed from strong-axis to weak-axis, three main differences in performance were evident due to the change in stiffness and are depicted in Figure 3-21.
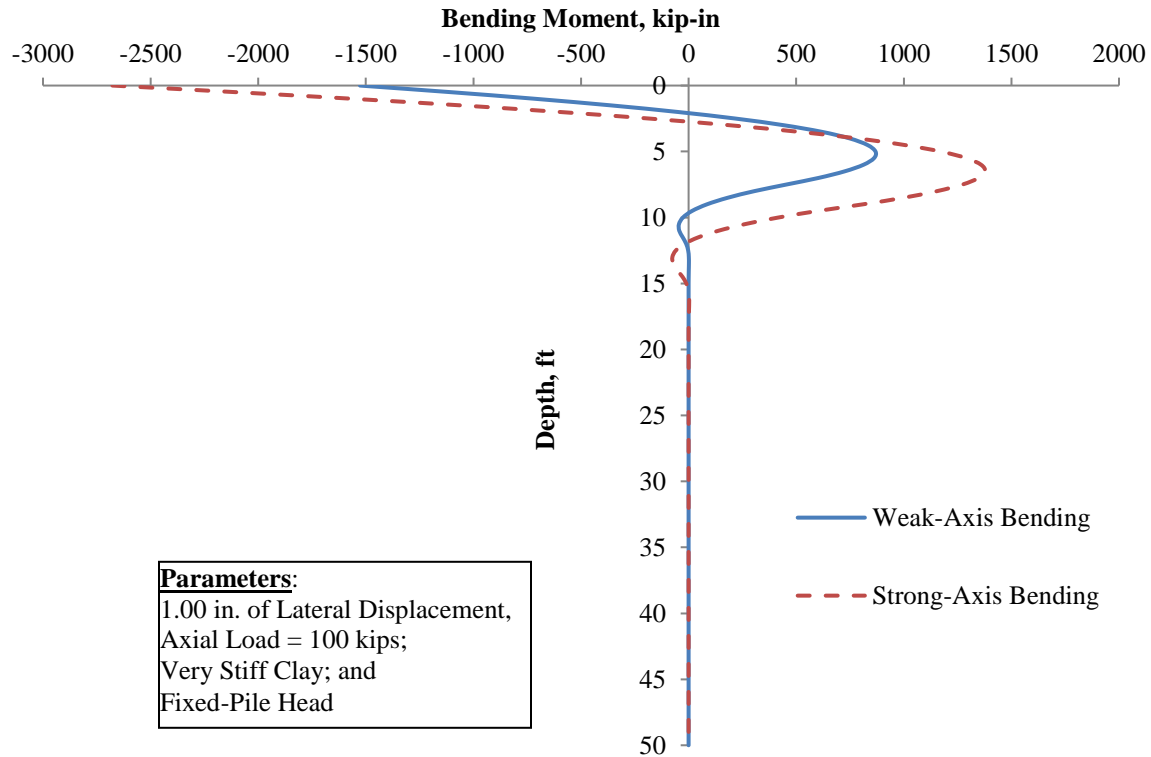
Figure 3-21. Effects of strong-axis vs. weak-axis bending for a UHPC pile

These differences include: (1) the maximum bending moment and maximum shear force were lower for weak-axis bending, (2) the magnitude and location of the second maximum moment is smaller and closer to the pile head for weak-axis bending, and (3) the depth of fixity is closer to the pile head for weak-axis bending.

The presence of a 10 ft prebored hole around the pile decreased the bending moment shear forces that were imposed on the pile. The depth to the second maximum moment and the depth of fixity are deeper than a pile without a prebored hole but not as far as would be expected, which is illustrated in Figure 3-22.
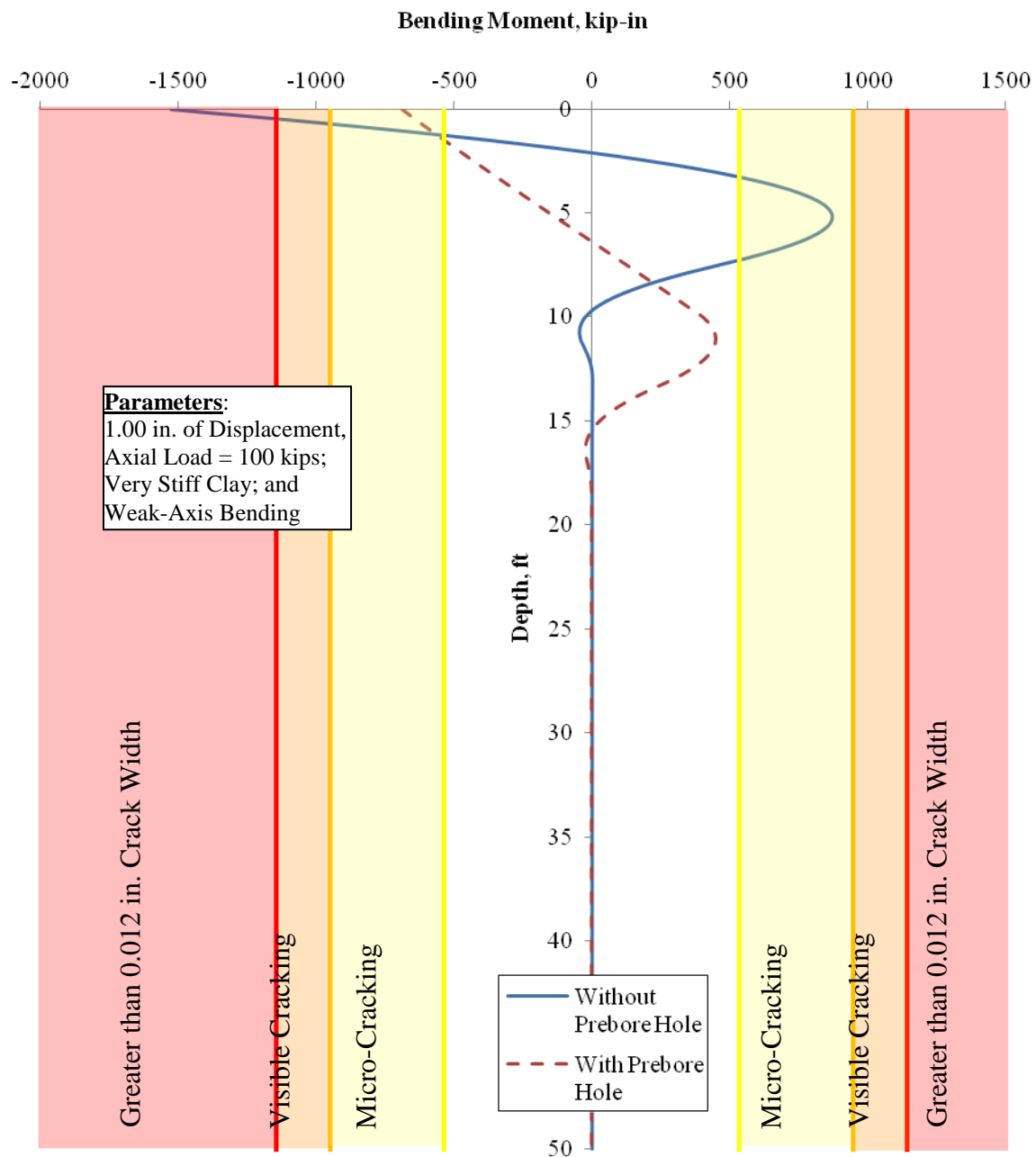
Figure 3-22. Effects of a prebored hole on the imposed performance of a UHPC pile

Also, the maximum shear is not at the pile head for all of the cases where prebored holes were modeled, except for piles in soft clay with a 100 kip axial load. The prebored hole reduced the flexural moment the UHPC pile would be subjected to within the acceptable limits when installed in integral abutments.

A complete set of the tables from the study can be found in Appendix B, which includes tables of the maximum moments and maximum shear. The depth to the second maximum moments and the depth to the point of fixity are also included.

3.3. Experimental Plan

The instrumentation, testing plan, and load increments for the field testing and long-term monitoring were based on the results from Phase I of the UHPC project and the parametric analysis conducted in this study.

Phase I of the project identified a need to improve the location and attachment of the pile driving analyzer (PDA) equipment to produce better results. Also, a smaller cable was used for the instrumentation in order to avoid making a weak zone within the UHPC pile cross-section, and rodding the web of the pile was performed during pouring of UHPC to avoid pocketing within the web of the pile.

The parametric study supports the use of UHPC piles in integral abutments as long as prebored holes are specified. Additionally, the study indicates regions for potential damage and what depth to find it on the pile. A preliminary estimate of the location of instrumentation can be made for the test piles based on the location of the maximum moments.

3.3.1. Field Testing

Two tests were completed in the field. The first field test was a vertical load test, which was completed to verify the performance of the UHPC pile and the specified design length of the UHPC production pile since it was 9 ft shorter than the HP 10×57 piles used for the bridge. The second test performed was designed with the intention of verifying the performance of the splice detail during driving and lateral loading.

3.3.2. Long-Term Monitoring

The long-term monitoring was designed with the intention of verifying the performance of the UHPC pile subjected to cyclic movement due to the abutments movement caused by thermal effects of an integral abutment. Once completed, the performance will be compared to the steel HP 10×57 piles used for the bridge.

CHAPTER 4: SPLICE DESIGN AND TESTING

Splicing of piles is commonly done in practice due to the limitations in handling and transportation of the long piles and the associated costs. Also, splicing of piles is done when the pile lengths required are too long for driving in one piece with the available equipment. Splicing also alleviates the need to calculate exact lengths prior to installation, which reduces the wastage of piles that are too long. However, the splice must be capable of resisting stresses induced by driving and service loads. Splices should be effective without significantly extending the duration of construction, be as durable as the piles, and be inexpensive.

There are several splicing details available in literature for precast concrete piles, especially for square, hexagonal, and circular piles. The splices generally can be categorized into different types based on the splicing procedures and load transfer mechanisms. A schematic description of splice types is shown in Figure 4-1.
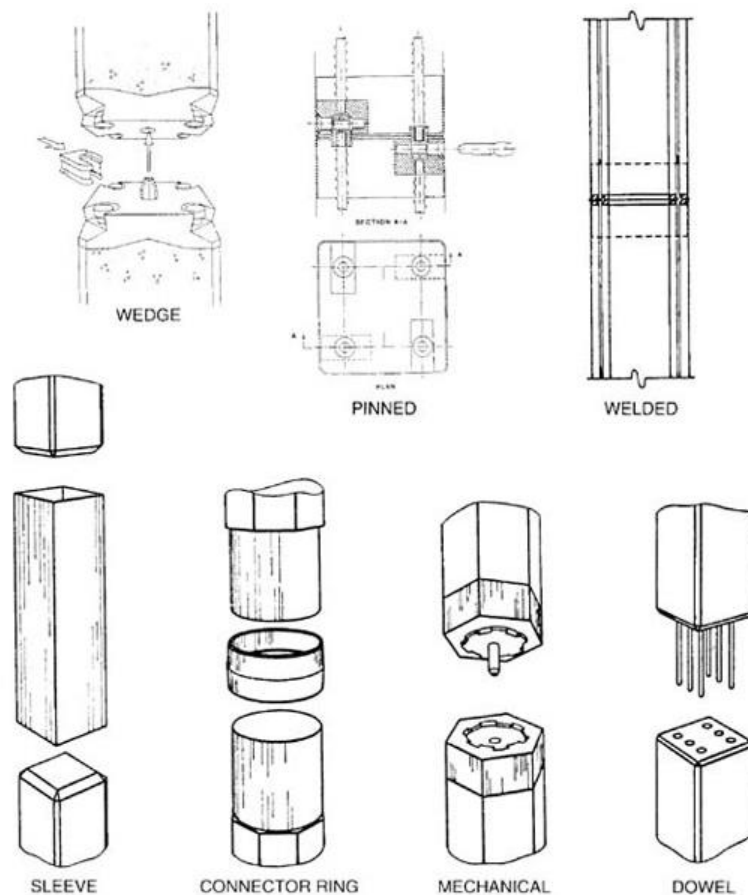
PileBuck 2013, © 2019 Pile Buck International, Inc.

Figure 4-1. Types of pile splices

1. Welded splice: This type of splice consists of steel plates with attached reinforcing steel bar cast into the pile ends, which are field welded together. This method is used in the US for steel piles. However, this type of splicing for concrete piles requires field labor and handling equipment while the weld is performed.
2. Dowel type splice: In this type, holes are cast or field drilled into the top of the bottom pile section. The top pile segment with rebar dowels protruding 3 ft to 6 ft from the end is guided into place and the holes are grouted with quick-set, high-strength grout or epoxy. Although material cost is low, this method is infrequently used in the US as it requires that the pile top segment be supported in place until the epoxy or grout attains necessary strength. However, this type of splicing can be useful for extending a driven pile to a required cut-off elevation with a short precast section.
3. Mechanical splice: Steel plates or castings with attached rebar anchors are precast into the pile ends. Steel bars or "wedges" are inserted into the mating surfaces when the top pile segment is aligned on the driven section. This method is fast and has been widely used in the US for prestressed piles since the 1970s. Proprietary systems that utilize high-strength steel bars to lock machined plates together are predominant. The Sure-Lock mechanical splice is an example and is made for all sizes of prestressed concrete piling (including some cylindrical piles). This splice can equal the pile in bending and tension capacities. This splice is shown in Figure 4-1.
4. Sleeve splice: A "can" of steel 2–3 m long with a stop in the middle is used for this splice. It slides over the driven section, and the top pile section is then lowered into it before driving resumes. The splice is relatively economical and easy to use but has very little bending and no tensile capacity.
5. Wedge splice: This method is generally used with precast piles. An example of this is the Westpile, which utilizes a wedge driven on plates attached to the pile ends. This puts the connection at the corners to develop resistance at the extreme fibers. This is shown in Figure 4-1.
6. Pinned splice: These use a pinned connection to secure the splice. These are generally not used in North America.

4.1.   Design of UHPC Splice

In the design of the splice, several factors were considered. The splice's performance was designed for tension, compression, bending, and shear. The load path for each loading was considered and then designed in order to provide adequate capacity during installation and in service.

Tensile stresses are expected in the piles during the driving process due to the reflection of the impact wave introduced by a pile driving hammer. The tensile forces developed in the pile are first transferred to the shear studs and corner steel angles through bond and shear transfer mechanisms, and then to the welds between the splices. At the splice location, all the tension force is taken by the welds between the splice plates. In order to design the splice for the tension capacity, the forces expected during the driving process should be determined. These forces will depend on the soil properties and hammer type used for pile driving. Tensile stresses are highest when resistance to driving is low and tensile waves are reflected back up the pile. These forces

can be estimated using the WEAP analysis. However, in this project, the pile splice was designed to have a minimum of 50% of the UHPC pile capacity in tension. This value was chosen based on the experience of the research team with the level of tensile stresses observed in piles during driving in Iowa soils in previous research projects. For the bridges designed to Iowa DOT standards, the piles are not expected to see any tension in service. So, the chosen value for the splice capacity in tension is conservative. The cross-section of corner steel angles, weld lengths, and thickness were calculated to meet this strength requirement for the splice and details are shown in Figure 4-2.
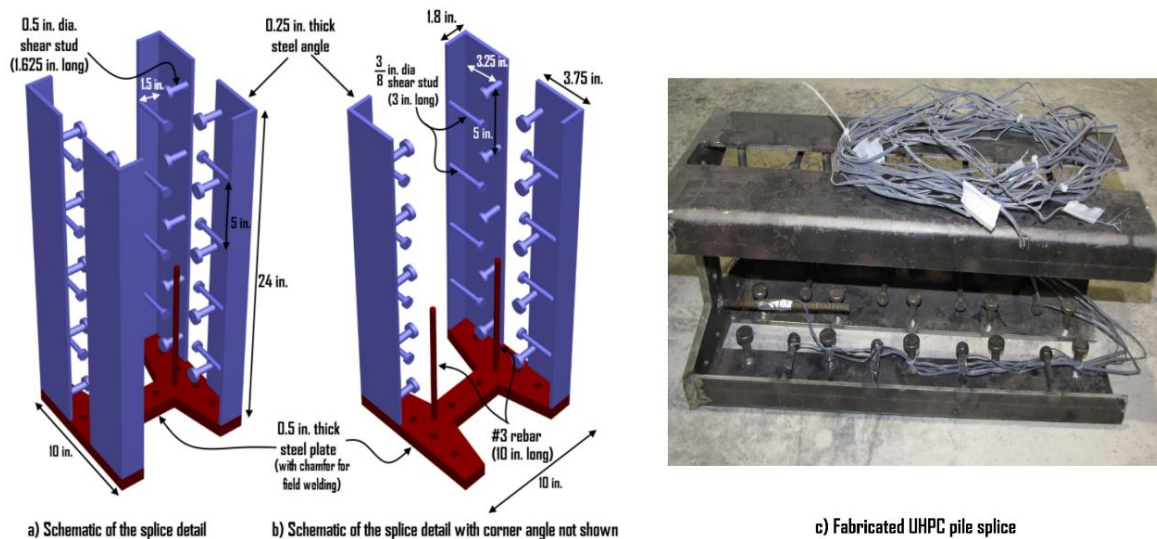
Figure 4-2. Schematic and fabricated UHPC splice embedment details

The moment and shear capacity of the spliced pile section was designed to reach the full moment and shear capacity of the unspliced UHPC H-pile section. The moment capacity of the UHPC H-pile with zero axial load in weak- and strong-axis directions were determined to be 1,200 kip-in. and 1,700 kip-in., respectively. With a 200 kip axial load, the moment capacity of UHPC H-pile in weak- and strong-axis direction increased to 1,300 kip-in. and 2,300 kip-in. respectively. Accordingly, the required weld thicknesses and the lengths were determined. The compressive forces between the spliced pile sections were designed to be transferred via full bearing of end steel plates of the splice.

There are several splicing details available in literature for precast concrete piles. However, with the optimized H-shape of the UHPC pile, there were no suitable splice connection details available for field splicing of the UHPC piles. Based on the literature on available splices, dry connections comprising of welding, bolting, or quick-set grout are typically preferred to extend the piles in the field during driving. Dry connection details for splicing help in reducing construction delays. It is common practice to use welding when steel piles are spliced as this is considered an efficient technique in the field. Consequently, a welded detail was preferred for the splice of the UHPC piles. Figure 4-2 shows the steel embedment used at the ends of UHPC piles, which facilitates welding between two H-shaped steel plates to establish the connection. The

steel embedment consisted of a ½ in. thick, H-shaped A50 steel plate with four ¼ in. thick corner steel angles with shear studs. The corner angles were welded to the H-shaped steel end plates with 3/16 in. thick weld along the entire length of the corner angles. Standard 3 in. long, 3/8 in. diameter shear studs and 1.625 in. long, ½ in. shear studs at 5 in. spacing were used along the long and short sides of the corner angles, respectively. The steel embedment was 24 in. long and the details are shown in Figure 4-2a. Edges of the H-shaped end plate were beveled for accommodating a 5/16 in. full penetration weld along the entire perimeter of the end plate to splice the UHPC piles together. Two 10 in. long, Grade 60, #3 rebar pieces were welded to the end plate at 3.25 in. along the web center line to help distribute the tension forces across the depth of the pile.

4.2.   Design of Test Units and Precast Fabrication

Four full-scale, 4 ft long UHPC test units with the above mentioned splice embedment details were designed and fabricated to experimentally evaluate the performance of the splice connection under tension, shear, and flexural loading. The required number of splice embedments were fabricated by the precast producer. Welding of the corner plates and the shear studs were performed by a certified welding technician at the precast plant. Once the embedments were fabricated, steel strain gages were placed on few long and short shear studs and rebar embedment. One end of the splice specimens was designed to transition into a full 10 in. by 10 in. square cross-section to accommodate four ¾ in. diameter high-strength threaded rods placed in a square pattern. The high-strength threaded rods were inserted in the formwork while specimen casting, and these rods were embedded in UHPC for 9 in. in length.

4.2.1.   Casting Process

When casting the test units, wooden side forms were used for the UHPC test units and were installed by the precast producer at the precast plant. The splice embedment was placed inside the wooden formwork, and prestressing strands were taken through the holes in the splice embedment end plate. The bottom four prestressing strands were first arranged in their proper configuration and stressed to their initial prestress of 202.5 ksi, which is approximately 75% of their ultimate strength. After the bottom row of prestressing strands was stressed, Styrofoam inserts to create the H-shape were secured to the wood forms with double-sided tape and caulking. After the Styrofoam was in place, the final six prestressing strands were arranged and stressed to an initial prestress of 202.5 ksi. The mixing of the UHPC was done using a 4.0 yd^3 mixer at the precast producer. After completing the batching of the UHPC mix, the UHPC was poured into a bin and transported to the bed by the overhead crane, where it was poured into the forms for all of the UHPC laboratory test units while making sure to rod the web to prevent air pockets. Immediately after the UHPC was poured in the forms, the top surface of the test units was covered with plastic wrap to minimize any moisture loss. A tarp was placed over the UHPC test units and propane heaters were used for the initial curing at 86°F. Along with the test units, 3 in. diameter UHPC cylinders were cast with the pour. The precaster tested cylinders periodically during the initial curing of UHPC to determine the compressive strength of the mix. After reaching a compressive strength of 14 ksi, the prestressing strands were cut at the member ends, and the piles were transferred to begin the steam curing.

4.2.2. UHPC Material Properties

The compressive strength of the UHPC was estimated using 3 in. diameter cylinders, which were cast and cured with the UHPC test piles. A total of seven cylinders were tested in compression at the ISU Structural Engineering Research Laboratory using a universal compression machine. The measured strength of the cylinders is given in Table 4-1.

Table 4-1. Measured compressive strength of UHPC used in test units

Cylinder number	f'_c, ksi
1	21.4
2	19.8
3	19.1
4	19.4
5	22.7
6	22.8
7	19.1
Average	20.6

The design strength of the UHPC mix was 26 ksi, and the results show an average strength of only 20.6 ksi was achieved for the UHPC material. Based on the failure mode, it was suspected the measured strength was not achieved due to the end surface of the test cylinders not being perfectly horizontal.

4.3. Experimental Testing

Full-scale laboratory tests have been completed to verify the expected behavior and to ensure adequate capacity of the UHPC splice connections. The laboratory investigation included the testing of the splice region under direct tension as well as critical shear and flexural stresses. A total of six different tests including, weak- and strong-axis bending tests, three shear load tests, and a direct tension test were performed. The details of the load tests conducted are summarized in Table 4-2.

Table 4-2. Details of tests for splice characterization

S.NO	Test type	# of tests conducted	Purpose
1	Direct tension	1	Evaluate the tension capacity
2	Shear	3	Estimate the shear force capacity
3	Flexure	2 (weak- and strong-axis)	Estimate the flexural capacity

Two test units were used for these tests. In each case, two 4 ft long UHPC pile segments with steel splice embedment (see Figure 4-2) were cast and spliced together at the ends using a 5/16 in. weld all around the interface at the splice.

4.3.1.   *Tension Test*

Test Setup and Instrumentation

In order to simulate the stresses encountered by the splice region during driving in the field, a self-reacting test frame with stiff steel end sections was constructed in the ISU structural laboratory. The self-reacting test frame was supported on rollers, and neoprene pads were provided underneath the rollers to minimize friction forces. The schematic of the self-reacting frame is shown in Figure 4-3a.

a) Schematic of Direct Tension Setup

b) Test Setup in the ISU Structural Laboratory
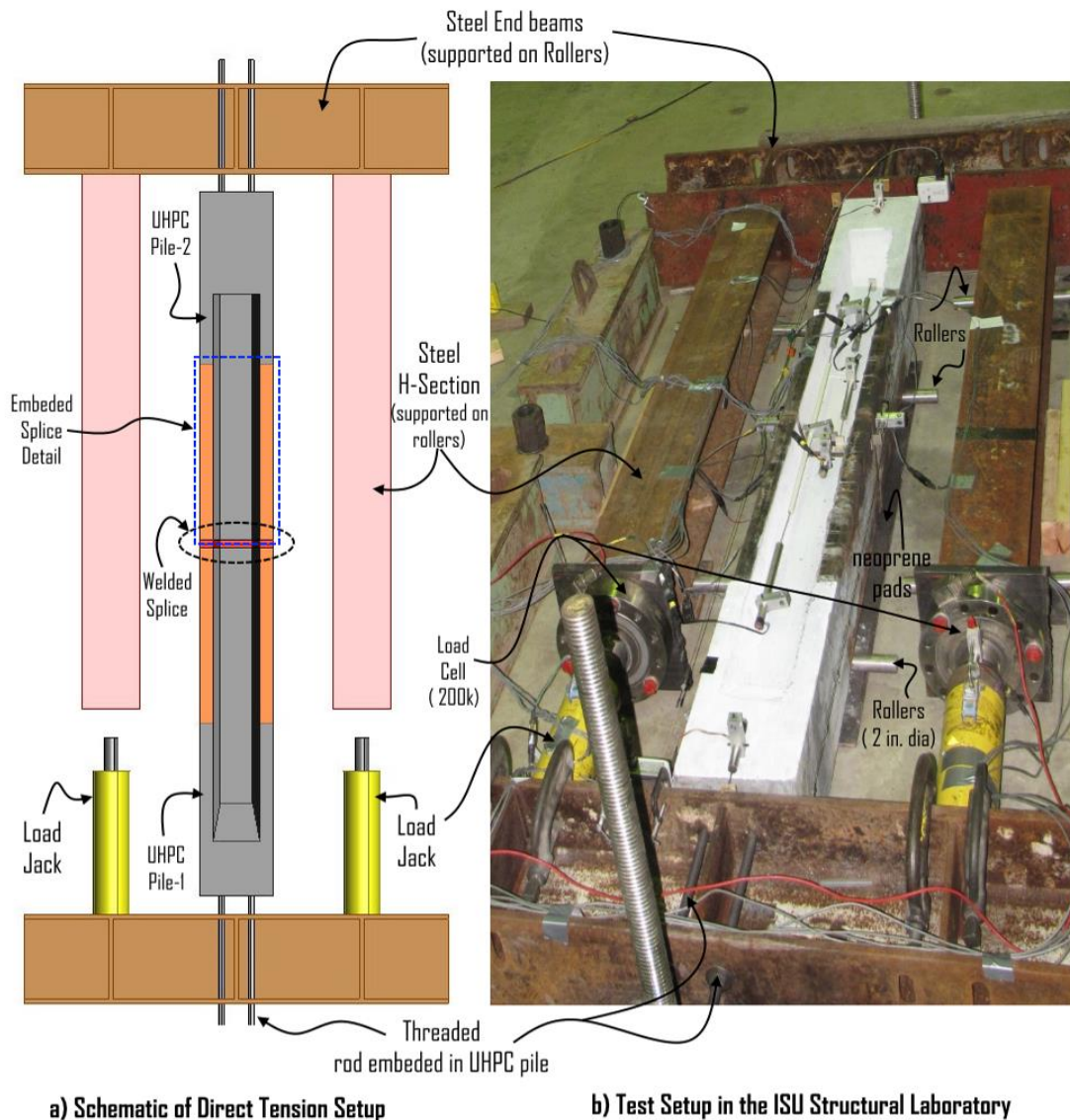
Figure 4-3. Details of the self-reacting test frame and direction tension setup

An 8 ft long UHPC splice pile specimen was produced by welding two 4 ft long UHPC specimens with a splice embedment. The welding was performed by a certified welder. The test specimen was then subjected to direct tension force using the test setup shown in Figure 4-3b.

The UHPC splice pile was attached to the steel end beams of the reacting frame using the 0.75 in. diameter high-strength threaded rod embedded in the UHPC pile at the unspliced end. Two 110 kip hydraulic jacks were used to apply the load onto the steel H-sections on the rollers, which in turn applied the direct tension force on the UHPC pile. The total load applied in each jack was monitored using the load cells mounted on each of the two steel beams of the reaction frame. A large number of instruments, including displacement gages and strain gages, were used to measure the response of the spliced UHPC pile. A total of 10 linear variable differential

transducers (LVDTs) and two string potentiometers were placed along the length of the spliced pile, across the weld splice joint to measure any gap opening between the steel splice details and UHPC. The external instrumentation details are shown in Figure 4-4.
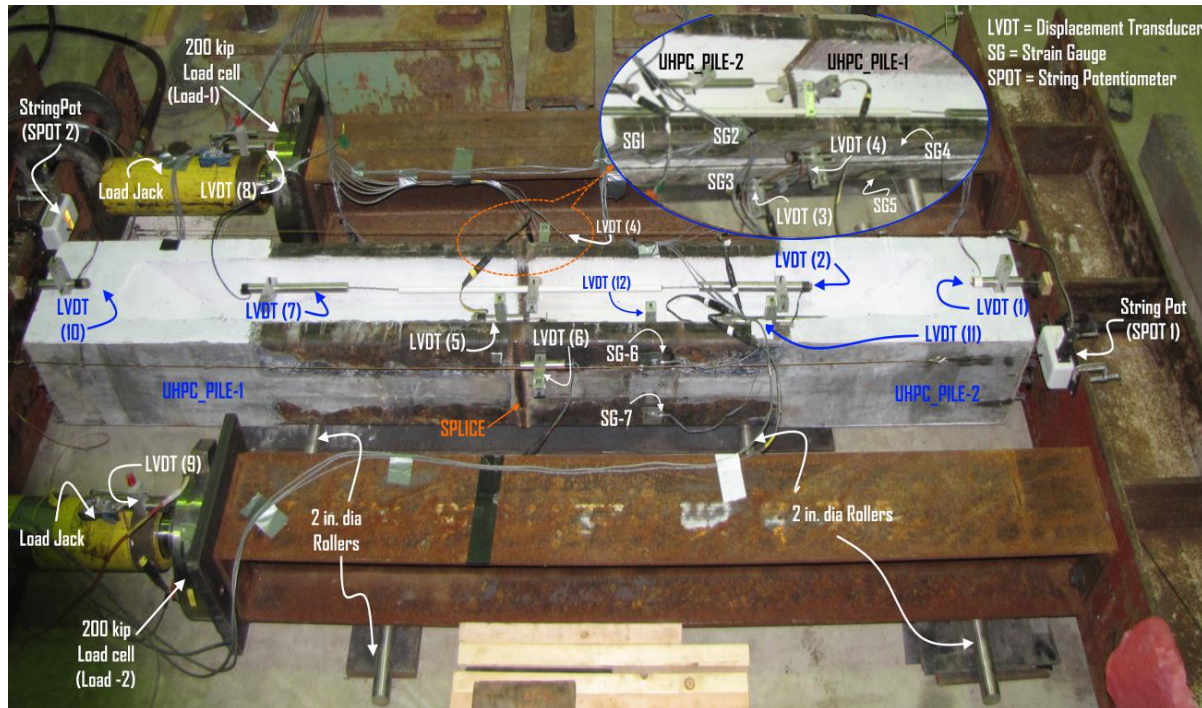
Figure 4-4. Details of the external instrumentation on the UHPC spliced specimen

The corner steel angles of the splice were also instrumented with external steel strain gages (SG 1 to SG 7 in Figure 4-4) to measure the strain demand in the steel angles during loading. The exact locations of these gages are presented in Table 4-3.

Table 4-3. Location of external strain gages on the corner steel angles

Gage name	Distance from splice, in.	Distance from top, in.	Gage name	Distance from splice, in.	Distance from top, in.
SG -1	18.5	1.75	SG-5	12.5	8.25
SG- 2	12.5	1.75	SG-6	12.25	2.375
SG-3	12.5	8.125	SG-7	12.25	8.375
SG-4	12.5	2			

Also, the shear studs and the rebar in the splice embedment were instrumented with strain gages to measure the critical stresses under direct tension loading. The details of the strain gages on the shear studs are provided in Figure 4-5.

a) Strain Gauges on Splice-1   b) Strain Gauges on Splice-2
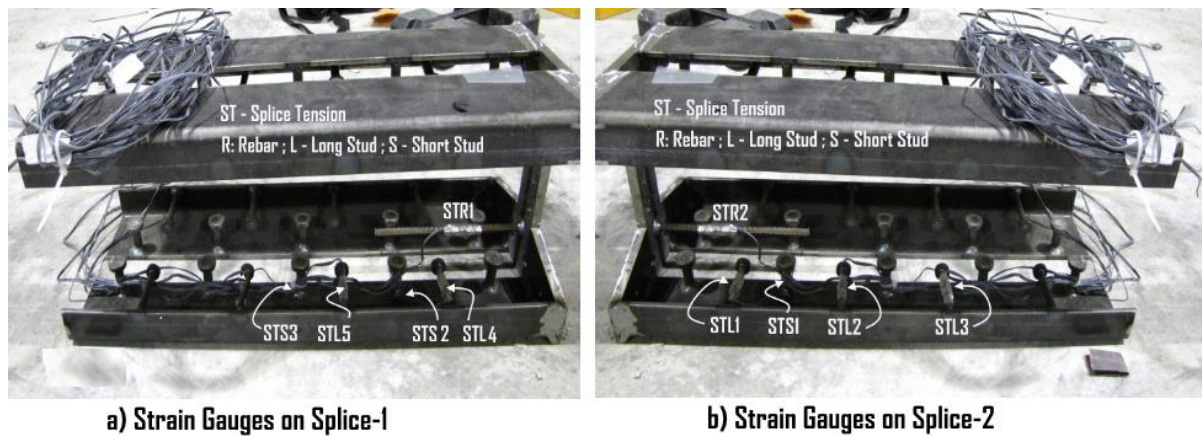
Figure 4-5. Locations of the strain gages on the shear studs and rebar of the UHPC splice

Testing Sequence and Observations

The UHPC spliced pile was subjected to direct tension load at 10 kips increments using the hydraulic jacks. Both hydraulic jacks were controlled using a single pump to have equal displacements in the hydraulic jacks and thus apply pure tension force on the specimen. During the test, the data from all gages and displacement devices were recorded using a computer-based data acquisition system at a 1 Hz frequency. At a total load of 45 kips, oil leakage from one of the hoses connected to loading jacks was observed. The hydraulic jacks were then unloaded to zero force, and the leaking hose was replaced. All the instrumentation was reinitialized before the loading was reapplied. During loading, at a total load of 103 kips, noises were heard and fine hairline cracks appeared at nearly 6 in. from the right end of the specimen (Figure 4-6b), where the cross-section transitioned to a 10 in. square section.

b) Fine cracking at 100 kips of tension force

c) Widened endcarck

d) Closeup of the crack showing absence of steel fiber

a) Spliced UHPC pile test specimen under direct tension loading
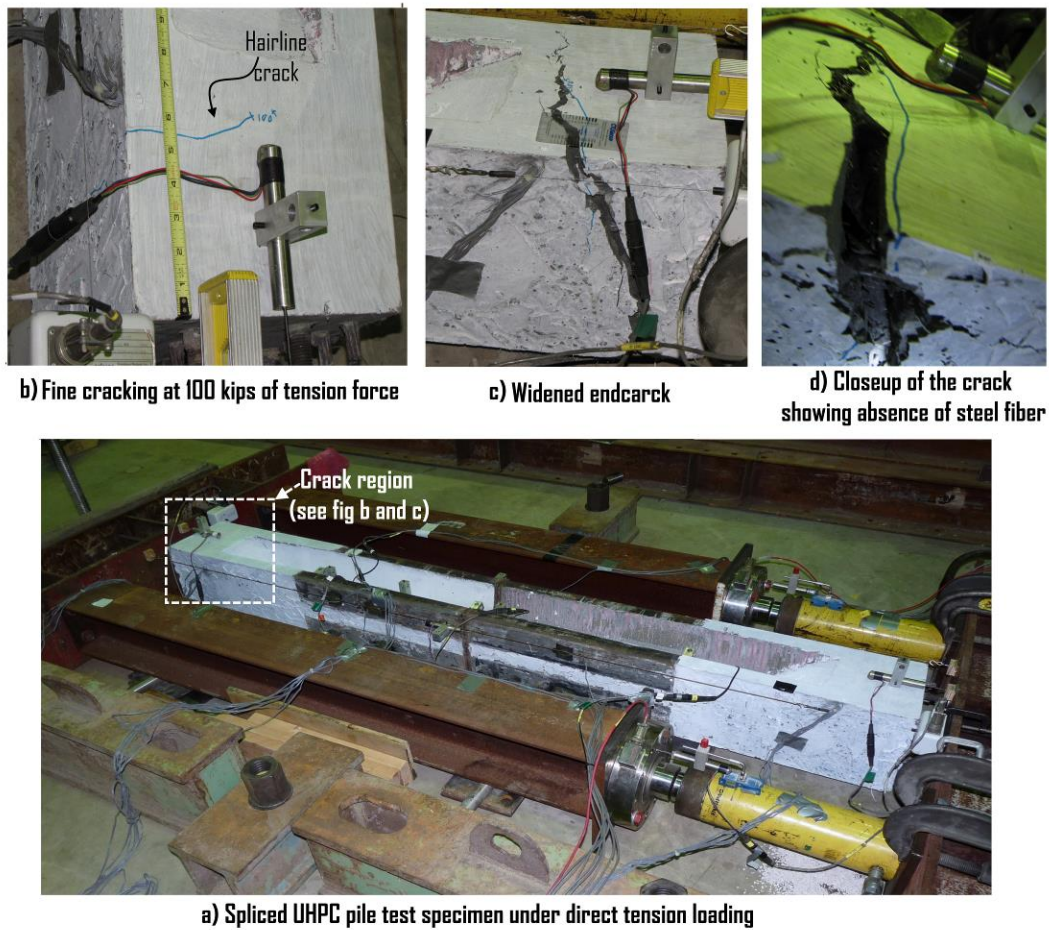
Figure 4-6. Crack formation in the spliced specimen end region at 100 kips of load

Upon continued application of this loading magnitude, the crack widened significantly with the crack width reaching up to 0.5 in. (Figure 4-6c). The loading was stopped, and the load jacks were unloaded to zero force. Following the unloading, a closer inspection revealed the absence of steel fibers at the crack location (Figure 4-6d). The applied maximum load of 103 kips created 1.03 ksi of tensile stress at the crack section location, which is close to the expected cracking strength of UHPC matrix without any fibers reported in literature.

The maximum applied tension load of 103 kips corresponded to 27.4% of the unspliced pile tension capacity. In order to subject the pile splice to tension loads up to 50% of the pile capacity, a retrofit to load application using stiff steel angles was designed and implemented. The retrofit included welding four steel angles to 1 in. thick angles, which were welded to the end beams of the test setup (Figure 4-7a).
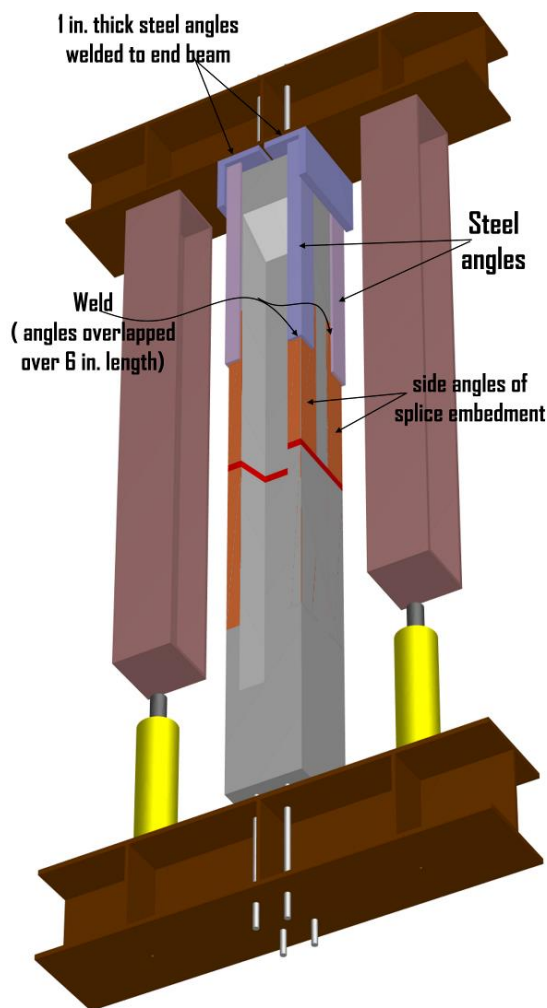
a) Schematic of retrofit to test setup to apply tension loads (retrofit shown on oneside only for clarity)
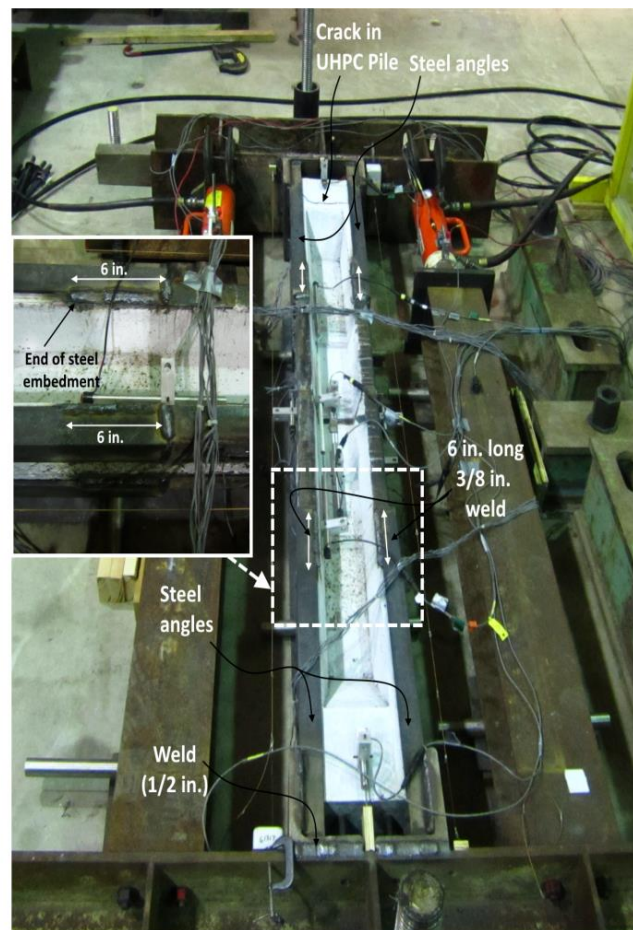
b) Test setup after the retrofit

Figure 4-7. Schematic of the retrofit to setup for load application and retrofitted test setup

The four steel angles were overlapped and welded to the corner angles of the splice embedment over a length of 6 in. This retrofit transferred the load directly from the load jacks to the splice region.

Following the retrofit, all the displacement measuring devices (LVDT and string potentiometers) were reinstalled and reinitialized. The external strain gages on the corner angles of the embedment were damaged during the welding of retrofit angles due to excessive heat. New gages were not installed as the surfaces were not easily accessible for gage installation. The splice specimen was subjected to tension loading with increments of 10 kips. All the data from the instruments were recorded at 1 Hz frequency. From here onward, testing before and after the retrofit are referred as Phase I and Phase II testing, respectively, for the purpose of presenting the results. The pile specimen was subjected to a load of 226 kips, equivalent to 60% of the pile

tension capacity. The test was stopped as the maximum capacity of the hydraulic jacks was reached. There was no observed visible cracking in either the pile or the splice region at the maximum load.

Results

The measured gap/crack opening between the splice end plate and UHPC as a function of load is shown in Figure 4-8.

a) Measured gap width at the splice location (Phase-I)   b) Measured gap width at the splice location (Phase-II)
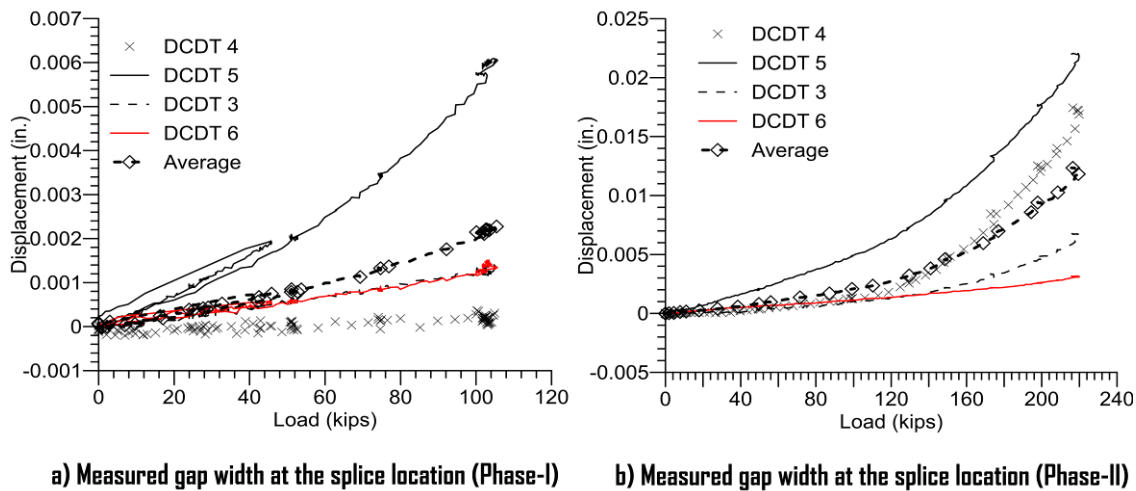
Figure 4-8. Measured gap width between splice end plate and UHPC at the splice location

The measured gap opening in the web region at 187.5 kips of load corresponding to 50% of pile tension capacity was around 0.012 in., whereas the measured gap opening on the flange side was less than 0.005 in. These crack widths are much smaller than crack widths allowed in bridge elements. This observation supports that the splice detail performed sufficiently and will not cause any durability issues. The total elongation of the pile in the splice region over a 4 ft length during both phases of testing is shown Figure 4-9.
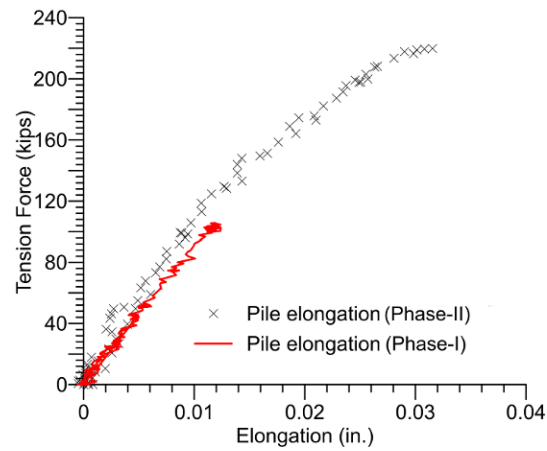
Figure 4-9. Elongation of UHPC over the splice region

The stiffness of the splice region is nearly the same in both phases, indicating that the retrofit applied the tension forces as expected in the field.

The measured strains in the long and short shear studs along the corner angles with respect to applied loading is shown in Figure 4-10.

**a) Measured strains in corner angle shear studs
(Phase-I)**

**b) Measured strains in corner angle shear studs
(Phase-II)**
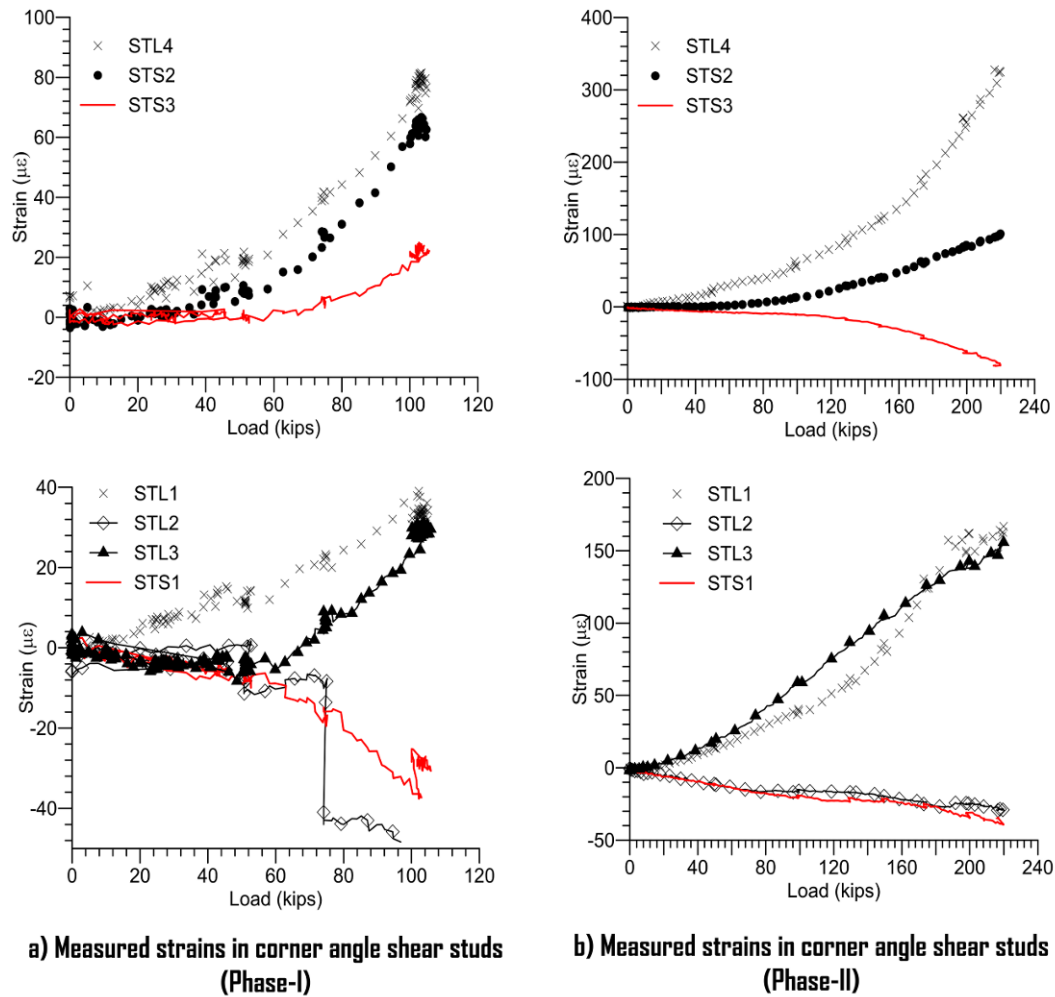
Figure 4-10. Measured strains in shear studs along the corner angles in splice detail

The measured maximum strain in shear studs at the peak load of 226 kips was 330 microstrains, corresponding to 15% of the yield strain of the shear studs. This indicates that the number of shear studs or diameter of the shear studs provided are more than required and could be reduced in future splice details. Reducing the number of shear studs can decrease the length of the splice embedment by 24 in. and could minimize the total cost of the splice detail.

The measured strain in the #3 rebar welded to the splice end plate is shown in Figure 4-11.

81

a) Measured strains in splice bar (Phase-I)   b) Measured strains in splice bar (Phase-II)
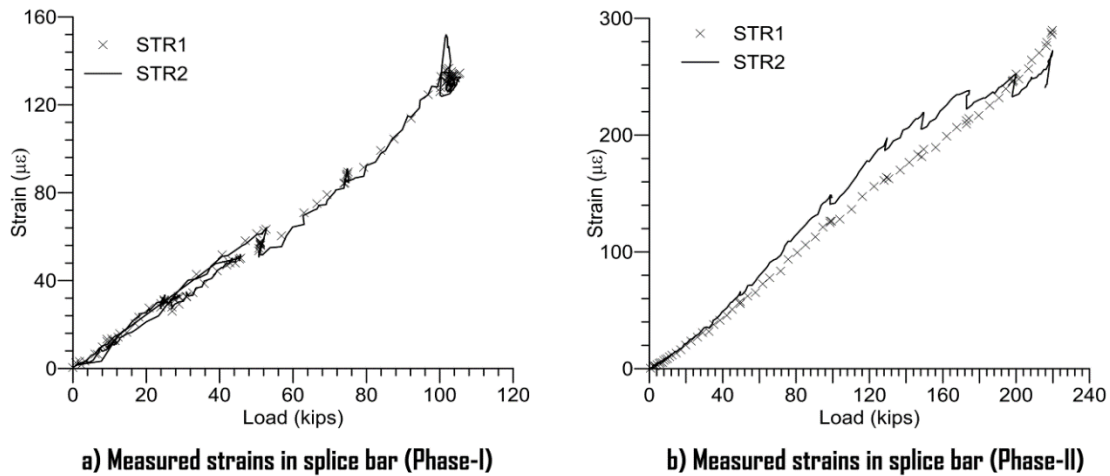
Figure 4-11. Measured strains in the #3 rebar in the splice detail

The maximum strain measured in the rebar was 290 microstrains, 14% of the rebar yield strain. This indicates that the bar size could be reduced. However, it is not recommended to reduce the bar size or eliminate the bar as it helps to contain the gap opening between the end plate and UHPC in the web region (see Figure 4-8). Further, the research team believes that the gap opening could be reduced by using a higher diameter rebar rather than the #3 bar.

4.3.2.   *Shear and Flexure Test*

Shear Test Load Frame and Test Setup

The shear capacity of the splice connection was evaluated with a spliced UHPC pile subjected to a point load about strong axis in a simply supported configuration as shown in Figure 4-12a.

a) Splice shear testing test setup   b) Schematic of the test setup and instrumentation
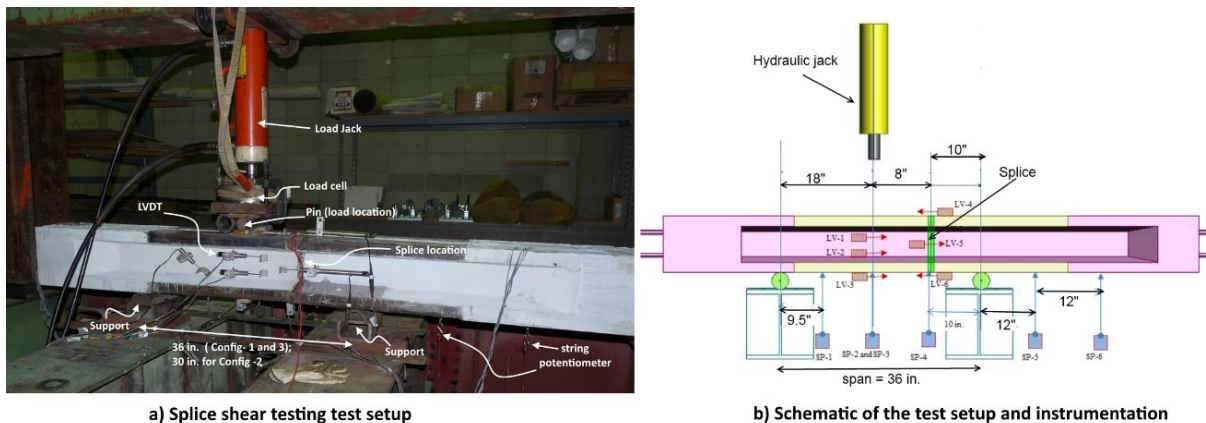
Figure 4-12. Test setup for splice shear testing

The 8 ft long spliced pile was simply supported over a 3 ft span and was subjected to a three-point bending using a 120 kip hydraulic jack. The load point was located at a distance of 8 in. from the splice location, subjecting the splice to a combined shear force and moment. In order to capture the effect of different moment to shear ratio (s) on splice performance, shear tests were done in three different configurations, obtained by varying the distance between the supports and the load point. These different configurations simulated the expected moment and shear demands at the various locations along the pile length in the prototype bridge. The specimen span length and load location points for each of the three load configurations are given in Table 4-4.

Table 4-4. Details of load configurations

Load configuration	Span, in.	Location of the splice from the right support, in.	Load location from the right support, in.
Configuration 1	36	10	18
Configuration 2	30	4	12
Configuration 3	36	15	23

Several different types of instruments were used for this study, including LVDTs and string potentiometers to capture deflections and curvature at the splice and load locations. A total of six string potentiometers were used to measure vertical displacements along the span of the spliced specimens. Two string potentiometers were located at the load application location and one at the splice location. The locations and identifications used for these string potentiometers are shown in Figure 4-12b. Three LVDTs at each of the load application points and the splice location along the height of the section were used to measure the average strains and their distribution. During testing, data from all the instrumentation was captured at 1 Hz frequency.

4.3.3.   Testing Sequence and Observations

The loading was applied in 5 kip increments until hairline shear cracking was observed in the pile web region. The maximum load applied in all the load configurations was 110 kips. The observed shear force versus displacement under point load for different load configurations is shown in Figure 4-13a.
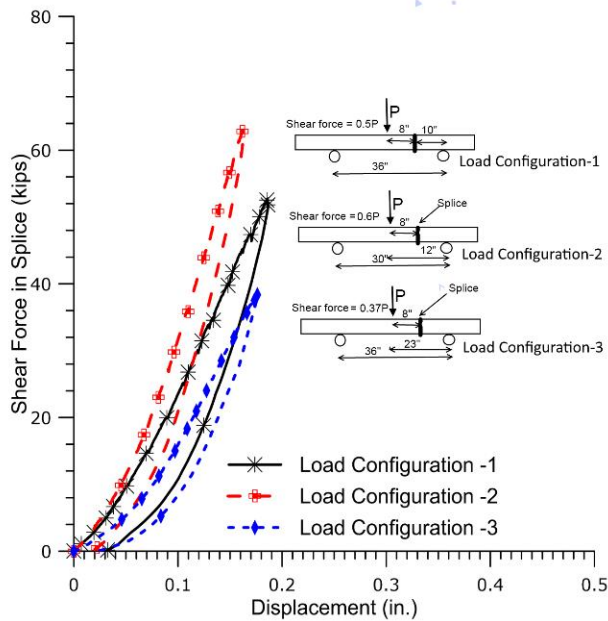
a) Shear force -displacement response   b) Shear cracking in web region of pile

Figure 4-13. Observed shear force vs. displacement behavior and shear cracking

During all the load configurations tests, hairline shear cracks were observed in the web region at a shear force of 48 kips. However, the cracks closed completely upon load removal. The splice region was subjected to a maximum shear of 66 kips in load configuration 2, which is nearly 200% more than the typical shear force in the UHPC pile in the prototype bridge. This value is also 37% more than the shear corresponding to web shear cracking capacity.

4.3.4.   *Flexural Tests Load Frame and Test Setup*

The flexural capacity of the splice connection in both weak- and strong-axis directions were evaluated using a simply supported configuration as shown in Figure 4-14.
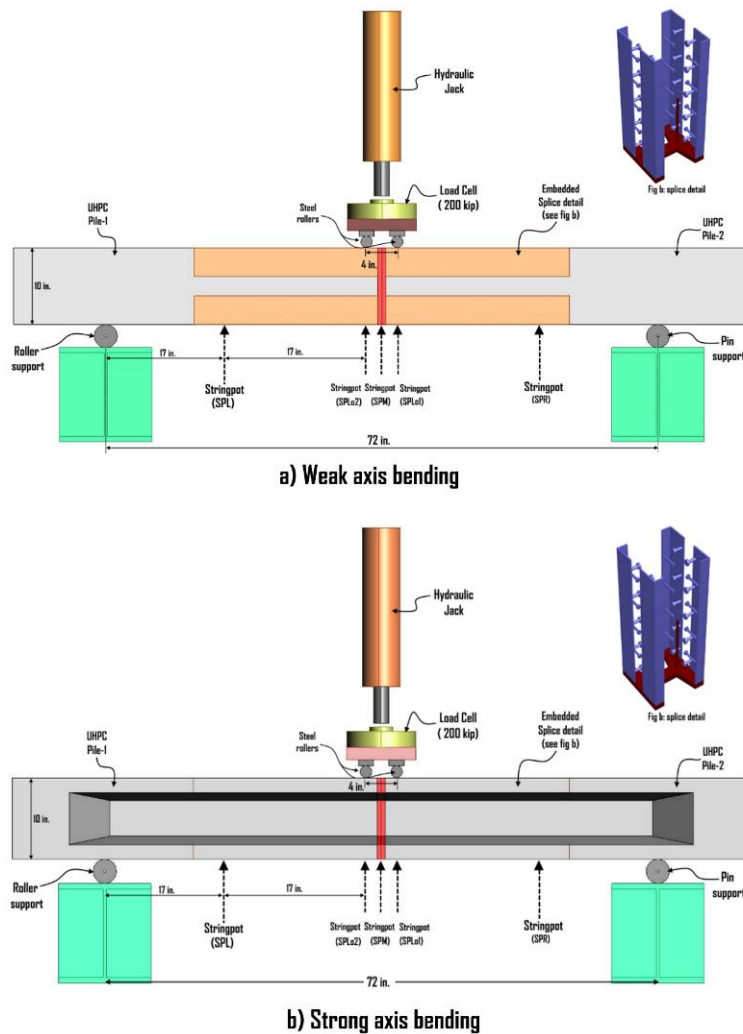
Figure 4-14. Schematic of the test setup for bending test of splice UHPC pile

The 8 ft long spliced pile was simply supported over a 6 ft span and was subjected to a four-point bending using a 120 kip hydraulic jack. The load points were located 2 in. on either side of the splice, subjecting the splice region to pure moment. The loading was applied in 5 kip increments until the specimens experienced failure.

Several different types of instruments were used for this study, including LVDTs and string potentiometers to capture deflections and curvature at the splice locations. A total of five string potentiometers were used to measure vertical displacements along the span of the spliced specimens. The string potentiometers were located at the quarter points (i.e., 17 in. from the supports), at the load points (i.e., at 2 in. from center), and at the center (i.e., splice location). The locations and identifications used for these string potentiometers are shown in Figure 4-14 and Figure 4-15.
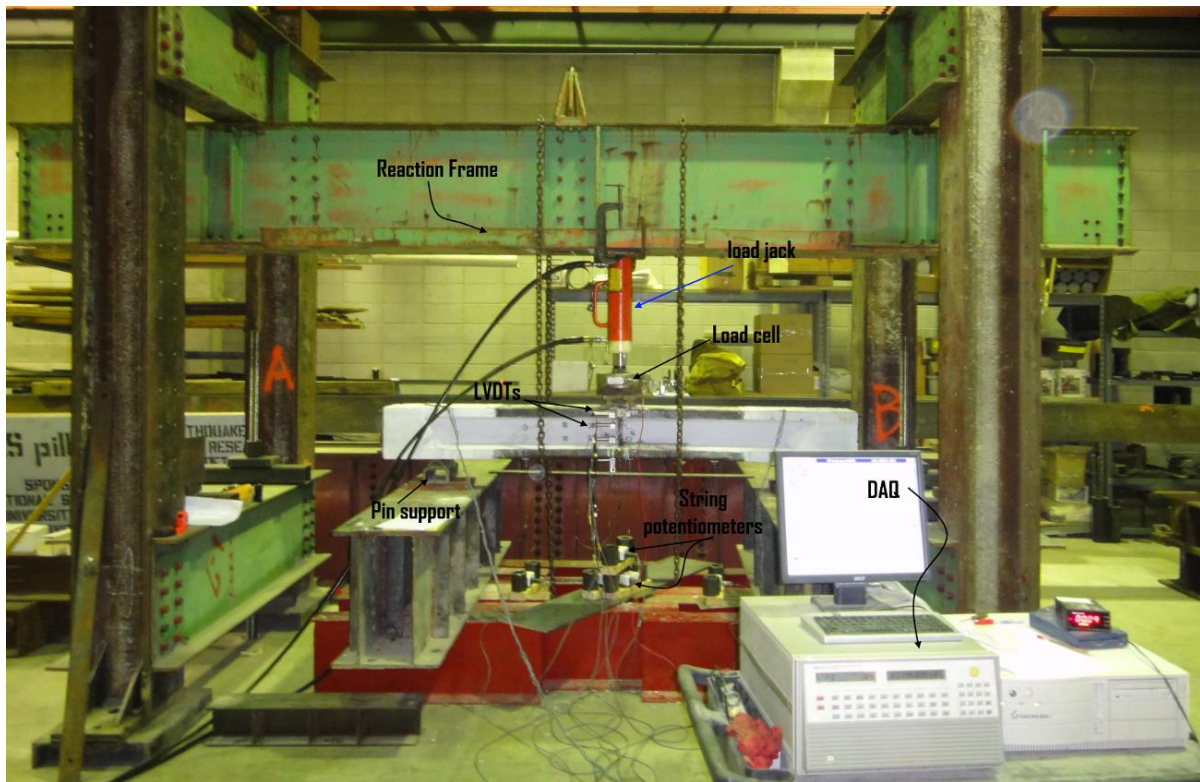
Figure 4-15. Test setup used for splice bending test in the ISU structural laboratory

Four LVDTs were used at the center of the specimen along the height of the section to measure the average strains and their distribution in the constant bending region. During testing, data from all the instrumentation were captured at 1 Hz frequency.

Weak-Axis Bending Test Observations and Results

The spliced UHPC pile specimen tested under direct tension loading was used to evaluate the performance of the splice in weak-axis bending direction. Reusing the test specimen for this bending test was deemed acceptable as the splice region didn't experience any noticeable damage during the previous tension tests. The end crack observed in the tension pile had no effect on the overall response of the specimen since, as the crack falls outside the support locations.

The measured force-displacement and moment-curvature responses of the splice region in the weak direction are shown in Figure 4-16a, and Figure 4-16b, respectively.

a) Force-displacement response b) Moment - curvature response
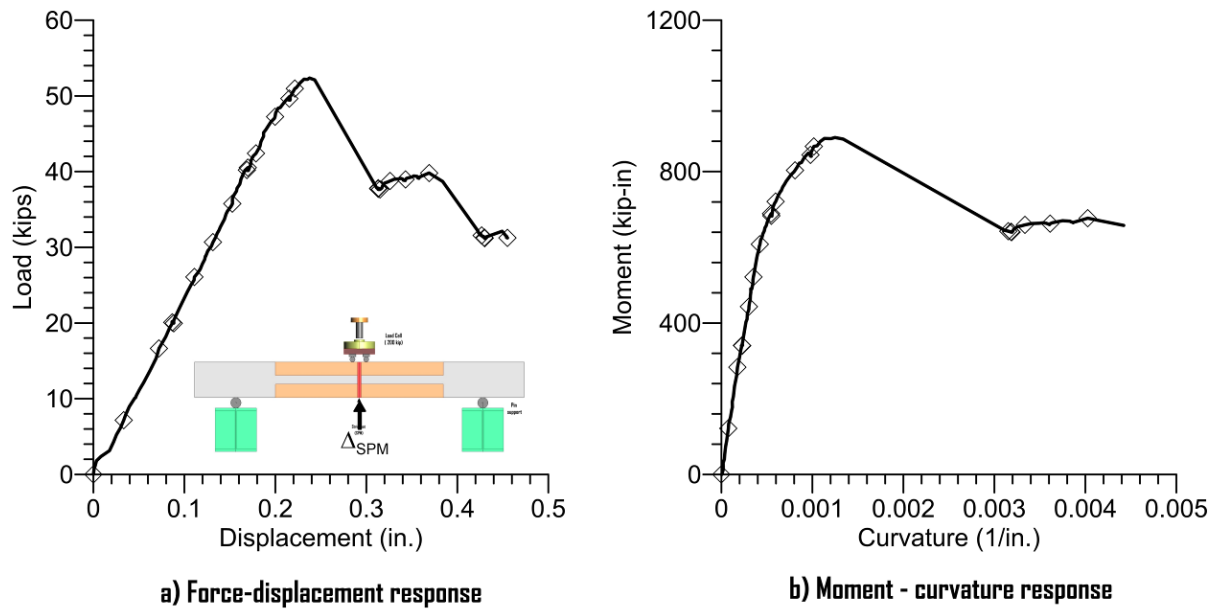
Figure 4-16. Observed force-displacement and moment-curvature response of splice region in weak-axis direction

The curvature at the splice location was calculated using the LVDTs along the height of the splice region. The splice region experienced failure at a maximum load of 52 kips with the fracture of the weld between the corner angles and the ½ in. end plate (Figure 4-17).

Figure 4-17. Failure of test specimen in weak-axis bending and close-up of the failed welds

This load corresponds to a bending moment value of 918 kip-in. on the splice region. This value, when compared to the bending capacity of the unspliced pile section, represents 76.5% and 70.6% of the capacities at zero kip and 200 kips axial load. On further inspection of the failure

surface, it was observed that the shop welding at the precast plant did not adhere to the requirements and resulted in the shorter weld length between the corner angles and the plate, leading to the failure of the splice (See close up in Figure 4-17). However, it is worth noting that the weld between the two pile pieces did not experience any damage, indicating that the connection will have sufficient strength. Based on the observed damage mode, a full penetration weld between edge angles and the end plate is recommended for future splice details.

Strong-Axis Bending Test Observations and Results

The spliced UHPC pile specimen tested under shear loading was used to evaluate the performance of the splice in strong-axis bending direction. Reusing the test specimen for this bending test was deemed acceptable as the splice region didn't experience any noticeable damage during the shear loading tests.

The measured force-displacement and moment-curvature responses of the splice region in the weak direction are shown in Figure 4-18a and Figure 4-18b, respectively.

a) Force-displacement response

b) Moment - curvature response
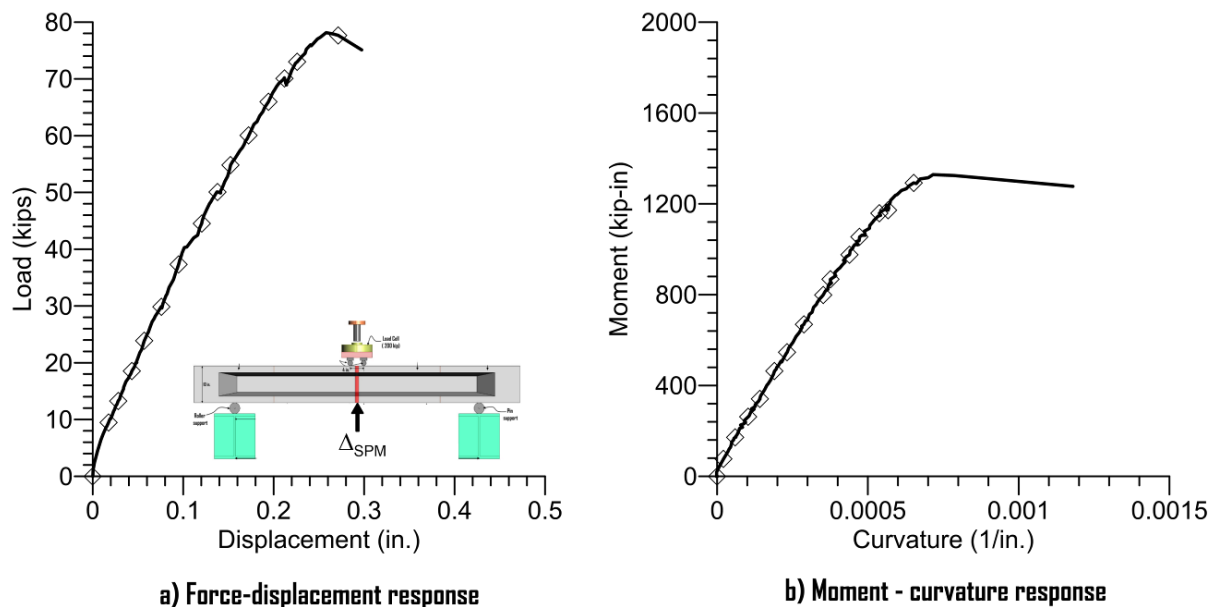
Figure 4-18. Observed force-displacement and moment-curvature response of splice region in strong-axis direction

The curvature at the splice location was calculated using the LVDTs along the height of the splice region. Similar to the weak-axis bending specimen, the splice region experienced failure at a maximum load of 78 kips with the fracture of the weld between the corner angles and the ½ in. end plate (Figure 4-17). This load corresponds to a bending moment value of 1,326 kip-in. on the splice region. This value, when compared to the bending capacity of the unspliced pile section, represents 78% and 57.6% of the capacities at zero kip and 200 kips axial load, respectively. On further inspection of the failure surface, weld length between the corner angles was found to be

shorter than the required minimum similar to the weak-axis bending specimen. It is worth noting that the weld between the two pile pieces did not experience any damage, indicating that the connection will have sufficient strength. Based on the observed damage mode, a full penetration weld between edge angles and the end plate is recommended for future splice details.

CHAPTER 5: PILE-TO-ABUTMENT CONNECTION TESTING

The lateral load behavior of a typical pile-to-abutment connection was tested in the laboratory to verify the performance of the abutment, pile, and connection. The laboratory tests were designed and completed by using an inverted test setup in comparison to actual field conditions for ease of construction and testing. A total of four laboratory tests, including a reference steel HP 10×57 pile testing in weak-axis bending and three UHPC piles testing in weak-, strong-, and 30° skew-direction bending were performed. Full-scale cross-sections for the UHPC and HP 10×57 test units and a full-scale section of an abutment were used for these tests. This chapter describes the design, casting, testing, and results of all the test specimens: SPAC-1, UPAC-1, UPAC-2, and UPAC-3.

5.1.   Design of Test Units

Three full-scale, 8 ft long UHPC test units and one 8 ft long steel HP 10×57 test unit were designed to test the piles and their connection to abutments using the typical Iowa DOT pile-to-abutment connection detail. The UHPC test units were given the names L7, L8, and L9. The HP 10×57 pile was identified as S1, which provided a comparison for the UHPC piles. The HP 10×57 pile is a common bridge foundation choice used by the Iowa DOT.

Test units L8 and L9 were cast for future laboratory testing that focused on the performance of precast pile-to-abutment connections when the pile is subjected to strong-axis bending and to a pile subjected to loading at a 30° skew. The focus of this chapter, however, is on S1 and L7, with each having a cast-in-place abutment cap. Both of these test units were subjected to weak-axis bending for the duration of the test because typical integral abutment piles are oriented to experience weak-axis bending in order to increase lateral flexibility of the bridge foundation.

Typical Iowa DOT abutment details were used as the basis for building the test specimen. Figure 5-1 shows the typical plan view of the abutment details while Figure 5-2 shows a cross-section view of the abutment and the reinforcement details.
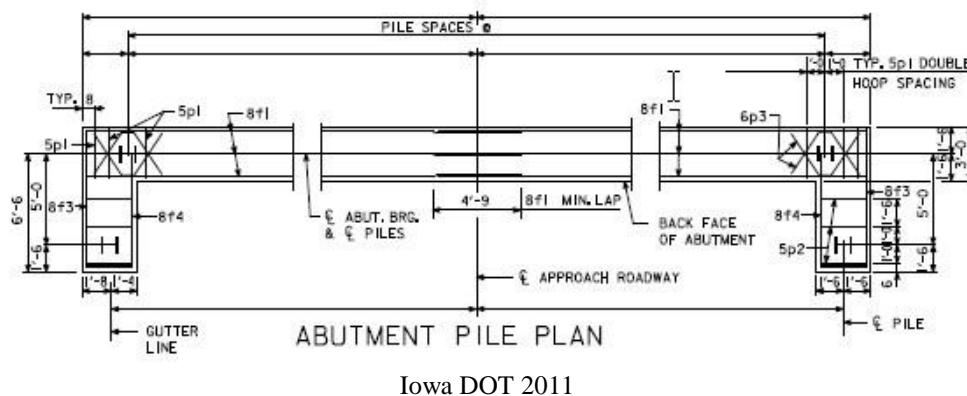
Iowa DOT 2011

Figure 5-1. Plan view of a typical integral abutment
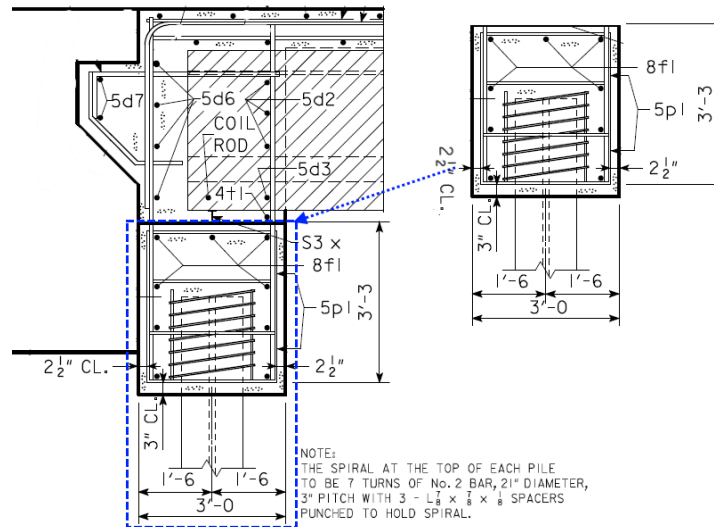
Iowa DOT 2011

Figure 5-2. Elevation view of a typical integral abutment detail

The portion of the section modeled in the laboratory is the blue dotted line box found in Figure 5-2, and it was rotated 180º for ease of construction and testing, which is shown in Figure 5-3.
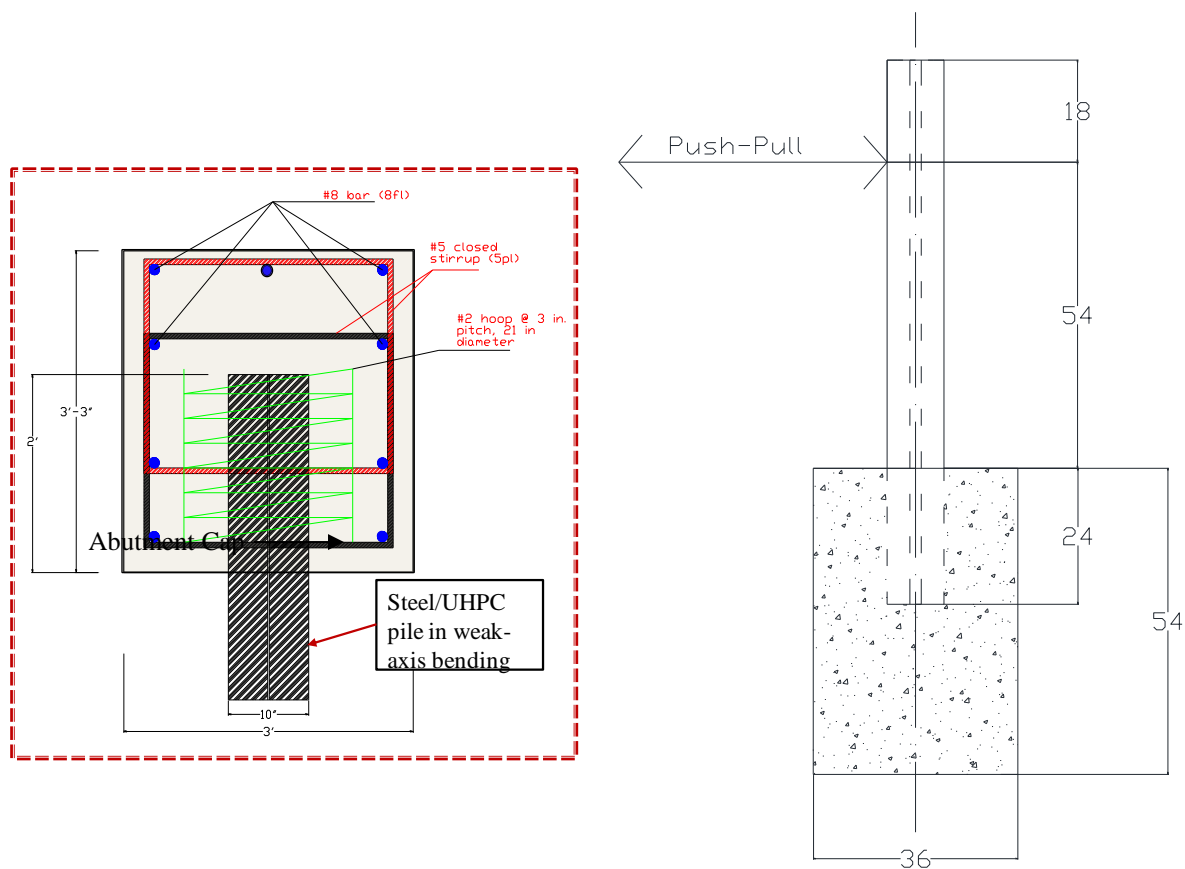
Figure 5-3. Outer dimensions of the abutment block for SPAC-1 and UPAC-2

Note in Figure 5-3 that all dimensions are in inches.

The 8 ft length of the test unit was chosen to meet the expectations of the test based on the LPILE analysis in Section 5.3. The test unit was embedded into the abutment cap at 24 in. as is commonly used for abutment design. Additionally, 18 in. was needed at the end of the pile to ensure that the prestressing strands were fully developed at the location where the lateral load was applied, thus leaving a maximum lever arm of 54 in. The cross-section of the test unit was uniform except along the top 18 in. There was a solid block for the first 9 in., which was tapered into an H-shape over the remaining 9 in. as shown in Figure 5-4.
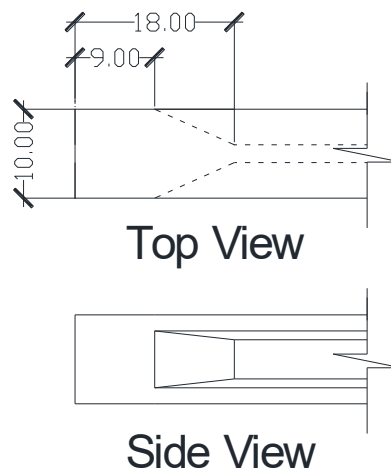
Figure 5-4. Change in cross-section of the top 18 in. on the UHPC test unit

Note in Figure 5-4 that all dimensions are in inches.

5.2. Fabrication of UHPC Pile

5.2.1. Embedded Instrumentation and Formwork Setup

The UHPC laboratory test pile units were instrumented with strain gages on February 8, 2011 at Coreslab Structures, Inc. in Bellevue, Nebraska. The instrumentation scheme for the steel and UHPC test units under weak-axis bending were kept identical and determined from the LPILE analysis results described in Sections 3.2 and 5.3, and the test setup, which is described in Section 5.5. The UHPC pile tests with precast abutment have slightly different instrumentation compared to the weak-axis bending tests. All the UHPC piles were cast with ¼ in. embedded threaded couplers to attach various instruments during testing, as shown in Figure 5-5.

Figure 5-5. Threaded ¼ in. coupler inserts in the UHPC pile formwork to attach instrumentation

Each test specimen had three rotation meter inserts (ID-1 through 3) and 20 LVDT (ID-4 through 23), which were used to attach instrumentation during the performance evaluation of the test units. A total of 12 strain gages (ID-24 through 35) were also used for instrumentation. Table 5-1 lists all of the instrumentation used and the labels for each.

Table 5-1. Instrumentation of UHPC laboratory test pile

ID	Label	ID	Label	ID	Label	ID	Label
1	RM01	10	LV07	19	LV16	28	SGP05
2	RM02	11	LV08	20	LV17	29	SGP06
3	RM03	12	LV09	21	LV18	30	SGP07
4	LV01	13	LV10	22	LV19	31	SGP08
5	LV02	14	LV11	23	LV20	32	SGP09
6	LV03	15	LV12	24	SGP01	33	SGP10
7	LV04	16	LV13	25	SGP02	34	SGP11
8	LV05	17	LV14	26	SGP03	35	SGP12
9	LV06	18	LV15	27	SGP04		

RM – insert for rotation meter. LV – insert for LVDT. SGP – strain gage on prestressing strand

The exact locations of the instrumentation attached to the prestressing strands and the inserts in concrete forms are shown in Figure 5-6.
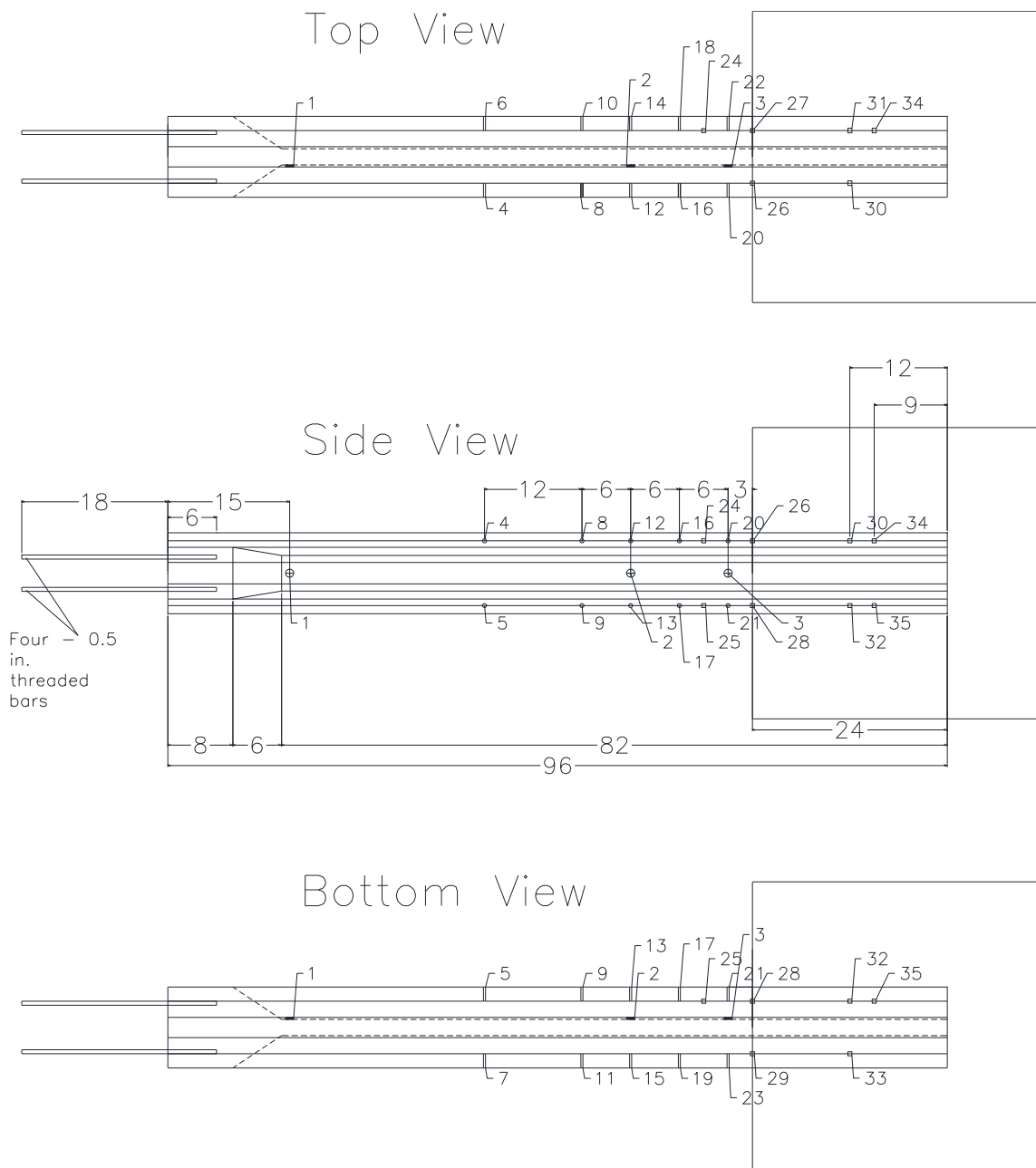
Figure 5-6. Instrumentation plan used for UHPC laboratory test units

5.2.2. Casting Process

When casting the test units, wooden side forms were used for the UHPC test units and were installed before the ISU research team arrived at the precast plant. The bottom four prestressing strands were arranged in their proper configuration and stressed to their initial prestress of 202.5 ksi, which is approximately 75% of their ultimate strength. The strain gages located on the bottom strands were installed as shown in Figure 5-7.

Figure 5-7. Instrumented bottom prestressing strands in the form

After the bottom row of prestressing strands was instrumented, the Styrofoam inserts were secured to the wood forms with double-sided tape and caulking.

After the Styrofoam was in place, the final six prestressing strands were arranged and stressed to their initial prestress of 202.5 ksi, as shown in Figure 5-8.

Figure 5-8. Prestressing strands layout at the anchorage end

The rest of the gages were installed to the prestressing strands. Initial readings of the strain gages were taken and the side forms were locked in place. Threaded coupler inserts for instrumentation were then glued to the formwork at the locations presented in Figure 5-6. The mixing of the UHPC ensued at the precaster's batch plant in a 4.0 yd^3 mixer.

After completing the batching of the UHPC mix, the concrete was poured into a bin and transported to the bed by the overhead crane, where it was poured into the forms for all of the UHPC laboratory test units while making sure to rod the web to prevent air pockets. Immediately

after the UHPC was poured in the forms, the top surface of the test units was covered with plastic wrap to minimize any moisture loss. A tarp was placed over the UHPC test units and propane heaters were used for the initial curing at 86°F. Along with the test units, 3 in. diameter UHPC cylinders were cast with the pour, which were periodically tested during the initial curing of UHPC to determine the compressive strength of the mix. After reaching a compressive strength of 14 ksi, the prestressing strands were cut at the member ends and the piles were transferred to a location where the steam curing was completed.

5.2.3.   Details of Test Units Pour

The UHPC laboratory test units were cast at Coreslab Structures, Inc. in Bellevue, Nebraska on February 10, 2011. Figure 5-9 depicts how the test piles were lined up in a single line along the length of the precast bed to utilize as much of the prestressing strand as possible.
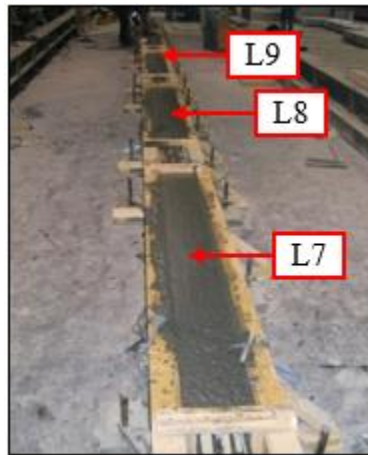
Figure 5-9. Layout of UHPC test units

5.2.4.   Casting Process of Abutment Cap

The casting of the abutment specimens was done in two phases. In Phase I, abutments for steel pile (SPAC-1) and UHPC pile in weak-axis direction (UPAC-1) were cast. In Phase II, abutments for the UHPC piles in strong-axis (UPAC-2) and skew-axis bending (UPAC-3) were cast. Phase I abutment caps were cast on May 9, 2011 in the ISU structural laboratory along with two base blocks. The reinforcement cages were built as per Iowa DOT standard and are shown in Figure 5-10a.
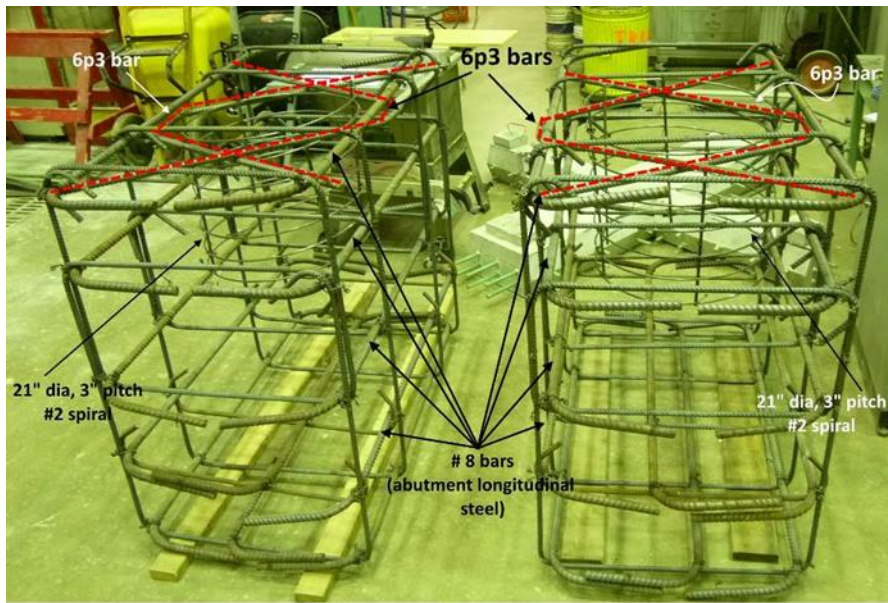
a) Reinforcement cage for abutments for steel and UHPC pile (UPAC-1) specimens
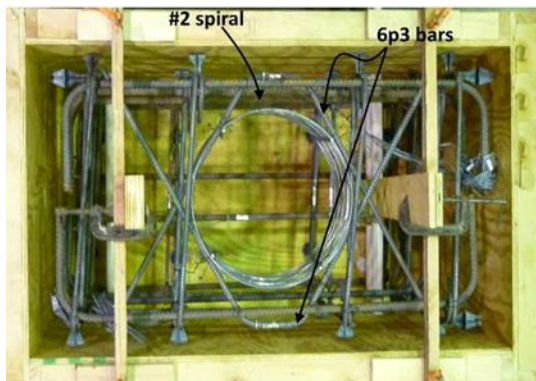
b) Reinforcemet in the abutment formwork

c) Casting setup for Steel and UHPC pile

Figure 5-10. Reinforcement and construction of abutment specimens for steel and UHPC piles in weak-axis bending

The formwork for the abutments were made out of plywood and had the specified steel reinforcement inside as shown in Figure 5-10b. The pile specimens were attached to a steel beam and hung in the desired location with 2 ft of the pile head embedded in the pile cap as shown in Figure 5-10c. The abutment caps were constructed using standard Iowa DOT concrete mix with 4 ksi compressive strength. The concrete was batched at Iowa State Ready Mix Concrete plant and transported to the structural engineering laboratory by a concrete truck. The base blocks were constructed on the same day using a 5 ksi concrete, early strength mix. Since the base blocks don't have any influence on the performance of the pile-to-abutment connections, a standard mix design available at the local ready-mixed plant was used. The concrete from the ready-mixed truck was first poured into a concrete bucket, which was lifted with the overhead

crane to the location of the forms. The concrete was then poured and vibrated in a series of lifts to get full consolidation. Once the abutment cap forms were filled, the top surface of the concrete was finished. A similar finish was also completed for the base blocks.

In Phase II of construction, two precast abutment caps with full-depth void were constructed following Iowa DOT design standards on February 10, 2012.
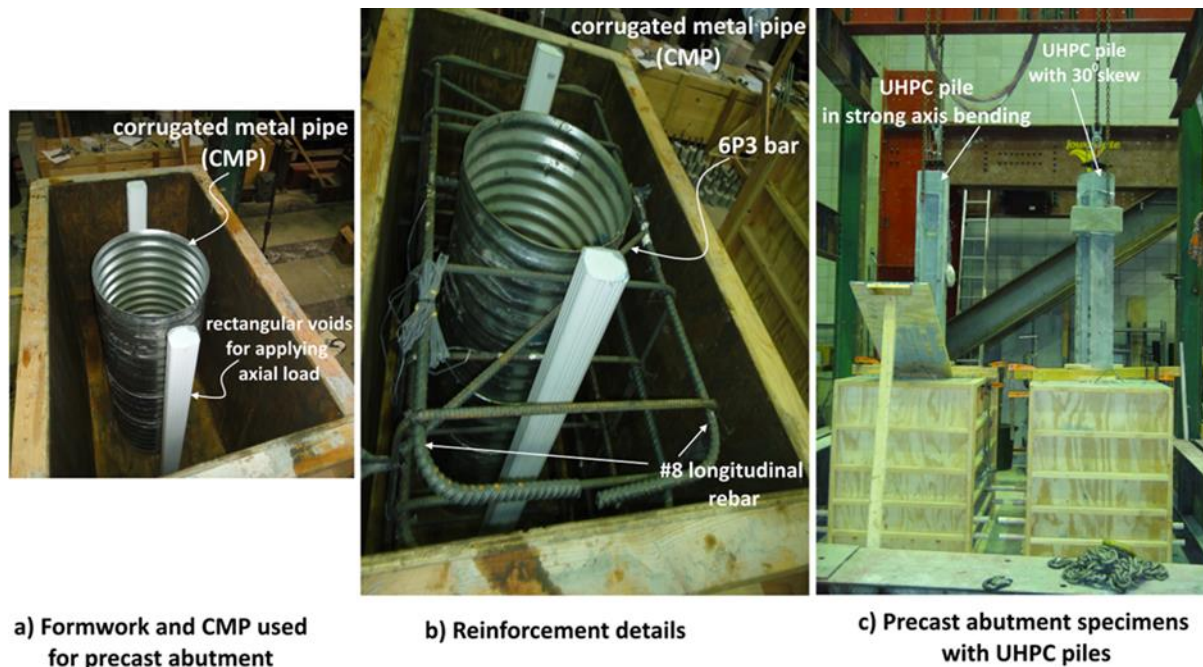
Figure 5-11. Reinforcement and construction of abutment specimens for UHPC piles in strong- and weak-axis bending

The full-depth void was created using a 21 in. diameter corrugated metal pile (CMP), which was used in several previous research projects and in the field by the Iowa DOT. The reinforcement details in the abutment were kept similar to previous cast-in-place abutments constructed in Phase I, with slight changes. The changes included the exclusion of the #2 spiral and removal of the 6P3 bar on one side. The intent of removing the 6P3 bar from one side was to evaluate the necessity of these bars in precast abutment designs. Similar to Phase I, 4 ksi ready mixed concrete was poured in the abutment caps. Three days after casting the abutments, UHPC piles were placed in the void with 2 ft of embedment. The void was filled with a 6 ksi concrete mix available at the local ready-mix concrete producer (see Figure 5-11).

5.2.5.   *Material Properties*

UHPC Material

Seven 3 in. diameter cylinders were cast and cured with the UHPC test piles and were tested in compression at the ISU structural laboratory using a universal compression machine. The measured strength of the seven cylinders was presented previously in Table 4-1.

The design strength of the UHPC mix was 26 ksi, and the results show an average strength of only 20.6 ksi was achieved for the UHPC material. Based on the failure mode, it was suspected that the measured strength was not achieved due to the end surface of the test cylinders not being perfectly horizontal. The elastic modulus for the test piles was calculated using equation (2-2) from Section 2.3 that was developed by Graybeal (2007). The resulting elastic modulus was 6,602 ksi as opposed to an expected value of 8,000 ksi.

Abutment Concrete

A total of twenty-four 6 in. diameter cylinders were cast for each concrete mix design used in the project. The concrete cylinders were cured along with the abutment cap in the same conditions until testing and then were tested in compression at the ISU structural laboratory. The measured concrete strengths at 3, 7, 14, and 28 days for the abutment cap and base block constructed in Phase I are given in Table 5-2 and Table 5-3, respectively.

Table 5-2. Measured concrete compressive strength for pile-to-abutment cap

Cylinder	Concrete compressive strength, psi			
	3-day	**7-day**	**14-day**	**28-day**
Test date	5/12/2011	5/16/2011	5/23/2011	6/6/2011
1	3,720	4,279	4,236	3,930
2	3,677	4,723	4,506	4,908
3	3,757	4,780	4,473	4,542
Average	3,118	4,594	4,405	4,460

Table 5-3. Measured concrete compressive strength of the base block

Cylinder	Concrete compressive strength, psi			
	3-day	**7-day**	**14-day**	**28-day**
Test date	5/12/2011	5/16/2011	5/23/2011	6/6/2011
1	4,051	4,939	4,439	5,491
2	3,656	4,148	5,051	4,983
3	3,857	4,649	4,768	5,331
Average	3,855	4,794	4,910	5,268

The design strength of the abutment cap concrete was 4 ksi, and the test measurements indicate that the 4 ksi average strength for this abutment block and the 5 ksi average strength for the base blocks were achieved before the age of 28 days. The elastic modulus for the test piles was calculated using equation (5-1).

$$E = 57,000\sqrt{f_c'} \text{ (psi)} \qquad \text{(ACI Committee 318 2005)} \qquad (5\text{-}1)$$

The resulting elastic modulus for the abutment cap was 3,807 ksi, and the elastic modulus for the base block was 4,137 ksi at 28-day strength. The measured concrete strengths at 3, 7, 14, and 28 days for the precast abutment cap and concrete used in the full-depth void in the abutments are given in Table 5-4 and Table 5-5, respectively.

Table 5-4. Measured concrete compressive strength for pile-to-precast abutment cap

Cylinder	Concrete compressive strength, psi				UPAC-2 test day	UPAC-3 test day
	3-day	7-day	14-day	28-day		
Test date	2/14/2012	2/17/2012	2/24/2012	03/09/2012	04/16/2012	05/16/2012
1	3,640	4,130	4,255	4,680	4,463	4,334
2	3,533	4,263	4,574	4,797	4,239	4,274
3	3,560	4,000	4,593	4,677	4,397	4,300
Average	3,578	4,131	4,474	4,718	4,366	4,302

Table 5-5. Measured compressive strength of concrete used in the voids

Cylinder	Concrete compressive strength, psi				UPAC-2 test day	UPAC-3 test day
	3-day	7-day	14-day	28-day		
Test date	2/27/2012	03/01/2012	03/08/2012	03/22/2012	04/16/2012	05/16/2012
1	4,730	5,513	5,795	6,168	6,321	6,033
2	4,802	5,474	5,706	6,206	6,273	6,020
3	4,834	5,082	5,878	5,486	6,288	5,869
Average	4,788	5,356	5,793	5,953	6,294	6,026

5.3. Analysis

Prior to testing the pile-to-abutment connection, a preliminary analysis was completed to develop the loading protocol for the tests. This section outlines this analysis while Section 5.4 presents the experimental results.

5.3.1. LPILE

LPILE^{PLUS} 5.0 was used to predict the response of abutment piles in weak-axis bending as installed in an integral bridge. The moment-curvature response for UHPC piles and steel HP 10 ×

57 piles calculated in Section 3.1 were used for the Type 5 analysis selected within LPILE. A fixed-pile head condition was assumed, which is not always the case in the field due to the potential vertical rotation of the abutment but was used because it would produce conservative results. Also, the 10 ft deep prebored hole filled with bentonite that is commonly required for piles in integral abutments was assumed to provide no lateral resistance to the pile.

Predicted Pile Response for Lateral Bridge Movements

Eight different scenarios with appropriate input were analyzed in LPILE to predict the response of the abutment piles for the two different pile types. Table 5-6 describes different cases, which uses different axial loads and lateral displacements.

Table 5-6. Eight cases used to predict the response of integral abutment piles

Case	Pile type	Axial load, kips	Lateral displacement, in.
1		100	1
2	UHPC		1.55
3		200	1
4			1.55
5		100	1
6	HP 10 × 57		1.55
7		200	1
8			1.55

The displacement response was calculated along the length of the pile and compared for each of the cases.

Figure 5-12a and Figure 5-12b illustrates the displacement response of the abutment piles for each of the eight scenarios.
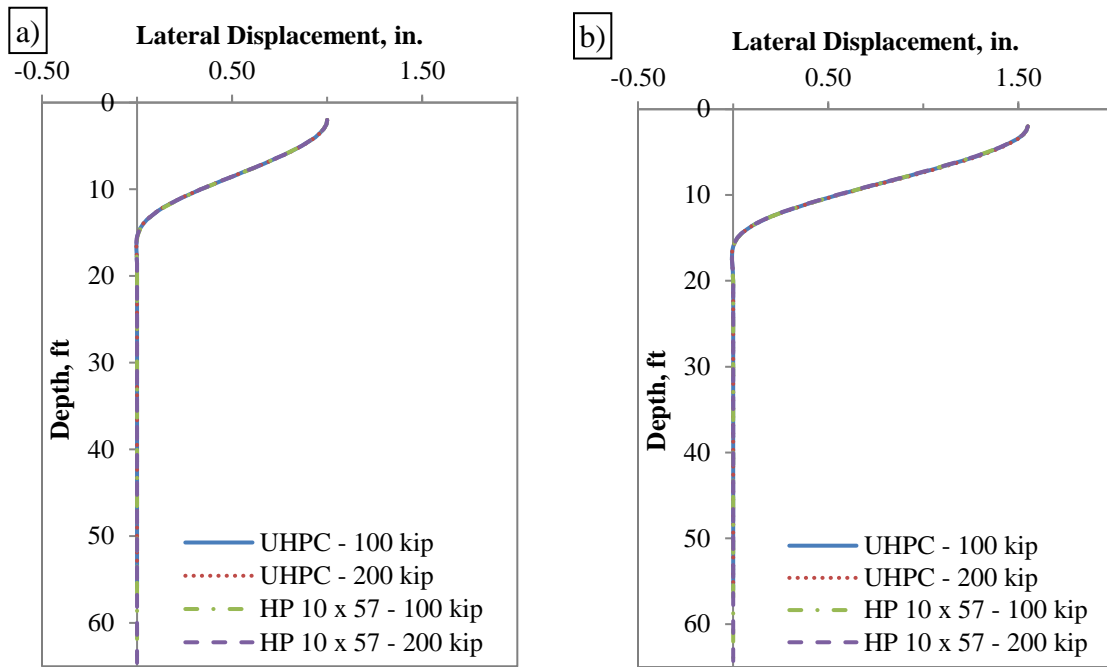
Figure 5-12. Displacement response of integral abutment piles subjected to (a) 1.00 in. and (b) 1.55 in. of lateral displacement

It is important to note that the displacements are almost identical when varying the axial load or pile type causing the lines to be on top of one another in Figure 5-12.

Target Laboratory Displacements

To relate the field conditions to the laboratory setup, the maximum displacement was scaled to produce an equivalent laboratory displacement, which is due to the consideration of the short length of the test piles. This was done by subtracting the translation displacement, Δ_t, from the total displacement, Δ_{total}, at a distance of 54 in. from the pile-to-abutment interface. Figure 5-13a and Figure 5-13b illustrates this process for 1 in. and 1.55 in. of lateral displacement.
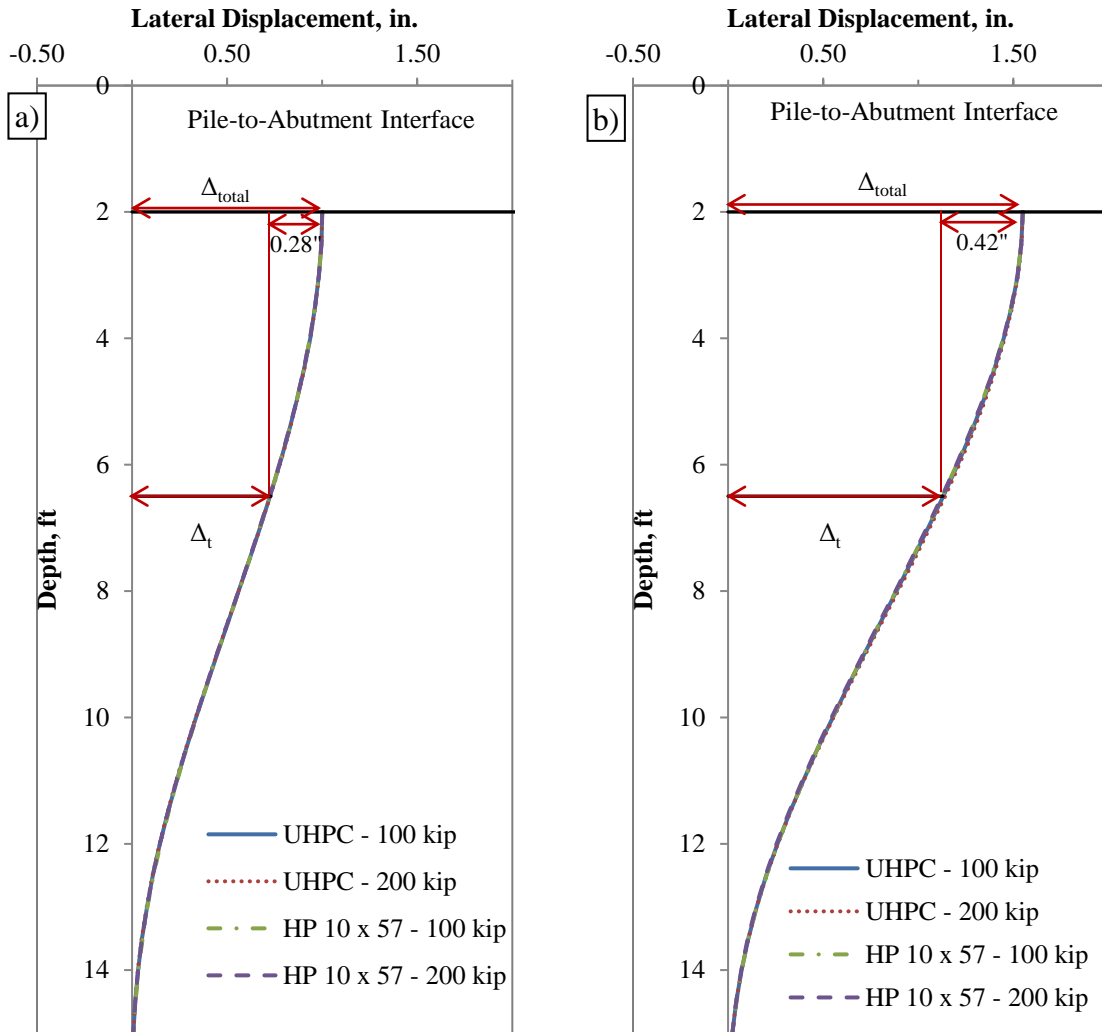
Figure 5-13. Displacement response of integral abutment piles subjected to (a) 1.00 in. and (b) 1.55 in. of lateral displacement

Based on this procedure for each of the scenarios, Table 5-7 lists the displacements for laboratory testing that correspond to the 1.0 in. and 1.55 in. of field displacements.

Table 5-7. Calculated laboratory displacement for each of the cases

Case	Laboratory displacements, in.
1	0.27
2	0.42
3	0.27
4	0.41
5	0.28
6	0.42
7	0.28
8	0.42

Since the target displacements are very similar, 0.28 in. was used to represent 1 in. of field displacement while 0.42 in. was used to represent 1.55 in. of field displacement.

5.3.2.   Cracking and Yielding Limits

From Section 3.2, the moments associated with micro-cracking, visible cracking, and maximum crack width were used to calculate the corresponding magnitude of lateral force required to examine these limits. They were calculated by dividing the moment given in Section 3.2 by the 54 in., where the 54 in. lever arm represented the distance from the applied lateral load to the pile-to-abutment interface. Additionally, the moment for yielding of the steel pile was used for a similar purpose. Table 5-8 lists the calculated lateral forces corresponding to these moments for the test setup described in Section 3.2.

Table 5-8. Lateral load corresponding to moment limits

Pile type	Axial load, kips	Corresponding strain to moment limits, kips			
		Micro-cracking	Visible cracking	> 0.012 in. crack width	Yielding
UHPC	100	9.9	17.6	21.2	-
	200	12.2	20.1	23.1	-
HP 10 × 57	100	-	-	-	20.5
	200	-	-	-	18.4

5.4.   Weak-Axis Pile-to-Abutment Connection Test for Steel HP 10 × 57 Pile

5.4.1.   Load Frame and Test Setup

Figure 5-14 shows the test set up in the laboratory.
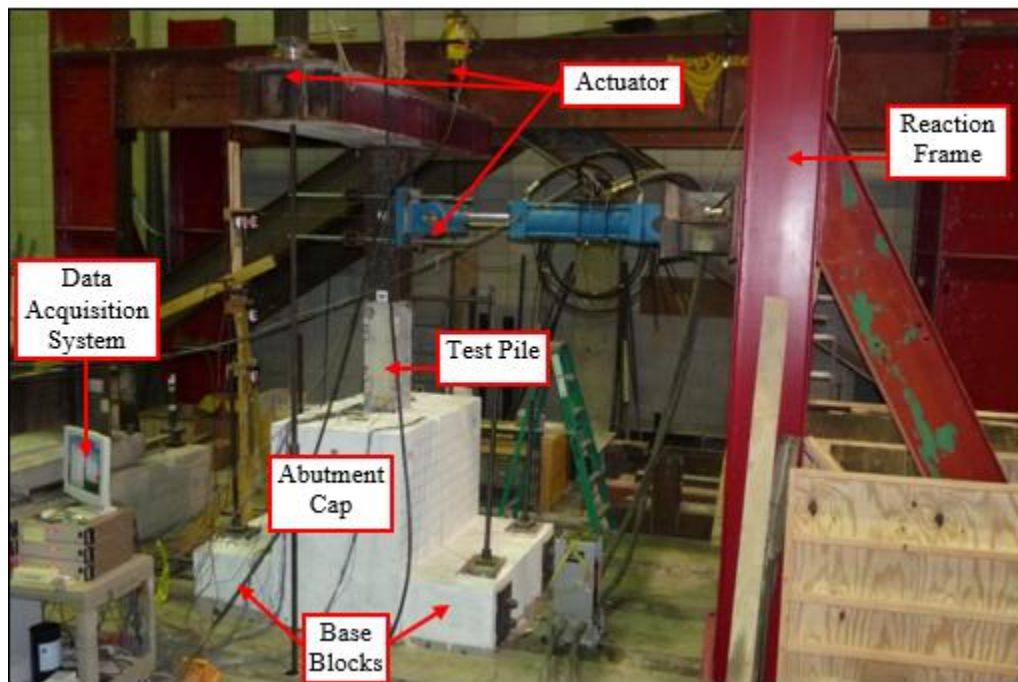
Figure 5-14. Pile-to-abutment connection test setup

The abutment cap was raised off of the strong floor by 2 in. to allow the punching of the pile through the cap to be evaluated during the testing. This arrangement was accomplished by using the two concrete base blocks on either side of the pile cap and post-tensioning them together through ducts that were cast into the concrete. An axial load was applied to the test unit by the two actuators shown at the top of Figure 5-14, and the lateral load was applied by a hydraulic actuator.

LVDTs, as shown in Figure 5-15, were used to measure the rotation and displacements at different location along the pile.

Figure 5-15. LVDTs used near the base of the test pile during laboratory testing

They were attached to the test unit using an epoxy. Rotation meters were also used to measure the rotation of the test unit at three locations on the pile and were also attached using epoxy. A rotation meter is shown in Figure 5-16.
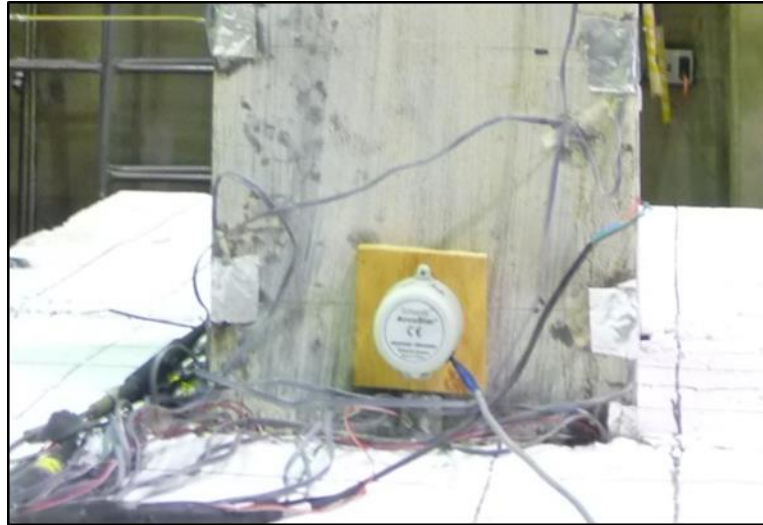
Figure 5-16. A rotation meter attached to the base of a test pile

For SPAC-1, TML strain gages were also used at the same locations specified as strain gages for the UHPC test units as shown in Figure 5-6.

5.4.2.   Test Protocol and Observations

The steel HP 10×57 test pile, SPAC-1, was tested in three phases. Phase I tested SPAC-1 with an axial load of 100 kips on August 8, 2011. The lateral load was initially applied in a force-controlled cyclic manner with two cycles per load step. Immediately following Phase I, Phase II increased the axial load on the test pile to 200 kips. Again, the lateral load was applied in a force-controlled cyclic manner with two cycles per load step. At the beginning of Phase III, the axial load was decreased to 100 kips and the lateral load was applied in a displacement controlled cyclic manner with three cycles at each displacement step. All three phases of testing with key forces and displacements are outlined in Table 5-9.

Table 5-9. Loading protocol used for SPAC-1

Phase	Axial load, kips	# cycles per load step	Controlling parameters	Load steps
I	100	2	Force, kips	±4, ±8, ±12, ±16
II	200	2	Force, kips	±3.5, ±7, ±10.5, ±12
III	100	3	Displacement, in.	±0.5, ±0.75, ±1.0, ±1.5, ±2.0, ±3.0, ±4.0

The cyclic force-displacement response of the HP 10×57 test unit during Phase III of SPAC-1 is given in Figure 5-17 along with the measured response envelope established from the first peak cycles.
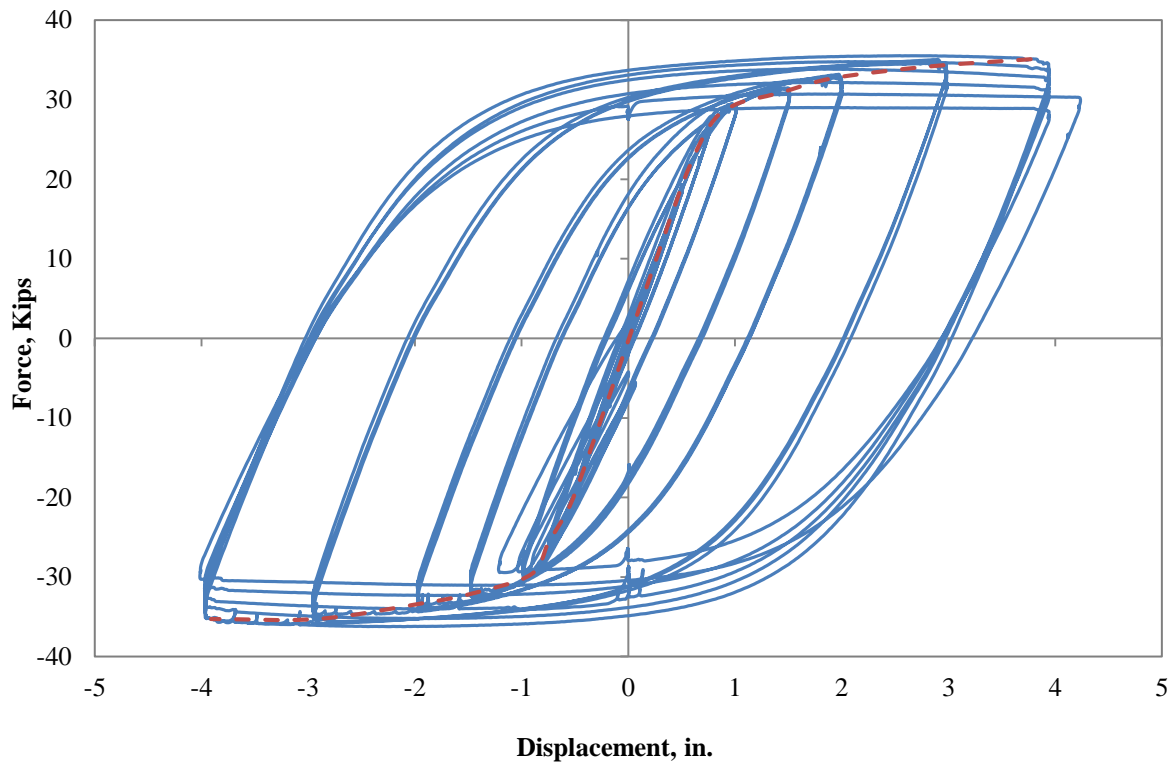
Figure 5-17. Force-displacement curve of SPAC-1 obtained from testing

The string potentiometers located at the point of load application were averaged to give the displacement of the test unit at a given load step. The maximum lateral load applied to S1 was 35.6 kips.

During SPAC-1, yielding was visible on the flanges of the HP 10×57 test piles at 26 kips of lateral load with a corresponding lateral displacement of 0.75 in. Figure 5-18 shows the yielding of the test pile flanges at a lateral load of 29 kips, which has a corresponding displacement of 1.0 in.
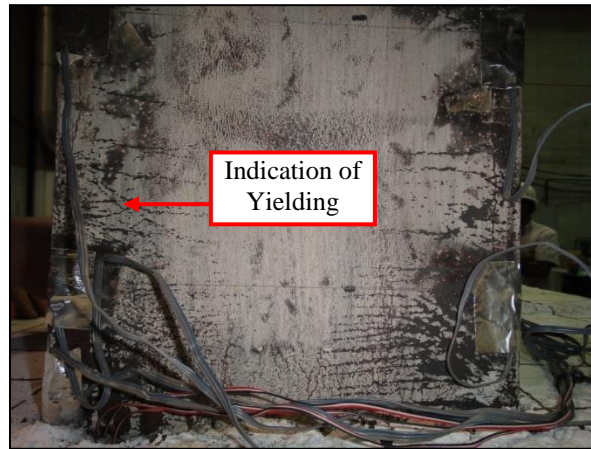
Figure 5-18. Yielding observed at the base of the steel HP 10 × 57 test pile during testing

A visible gap adjacent to the pile started to open up at the pile-to-abutment interface at 32 kips of lateral load corresponding to 2.0 in. of lateral displacement. Figure 5-19 shows the gap that was formed during the steel pile test.
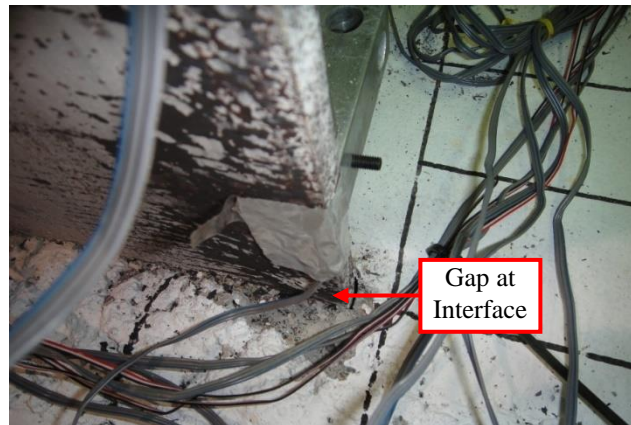
Figure 5-19. HP 10 × 57 test pile rotation at the pile-to-abutment interface

Also, at this same load step, cracking in the abutment cap was observed.

When the lateral displacement became large, buckling of the flanges near the pile-to-abutment interface was visible. Additionally, concrete adjacent to the pile on the top surface started to spall off the abutment cap when the pile was subjected to 4.0 in. of lateral displacement. Figure 5-20 shows the buckling and spalling of abutment cap concrete after the first cycle of 4 in. of lateral displacement.

Figure 5-20. Buckling of HP 10 × 57 steel pile and spalling at top surface of abutment cap

5.4.3.   Results

From Table 5-8, the lateral load that was expected to cause yielding at a 100 kip axial load is 20.5 kips. The service lateral displacement of 0.28 in. induced a lateral load of 11.3 kips in the push direction and 10.8 kips in the pull direction. Both of these values are well below the yield limit. The maximum displacement of 0.42 in. only induced a 16.9 kip lateral load in the push direction and a 16.4 kip lateral load in the pull direction, which were again below the expected yield limit of 20.5 kips for the HP 10 × 57 flanges.

5.5.   Weak-Axis Pile-to-Abutment Connection Test for UHPC Pile

5.5.1.   Load Frame and Test Setup

The test setup used for the testing of the UHPC pile in weak-axis bending was very similar to the setup used for the steel HP pile. Figure 5-21 shows the test set up in the laboratory.
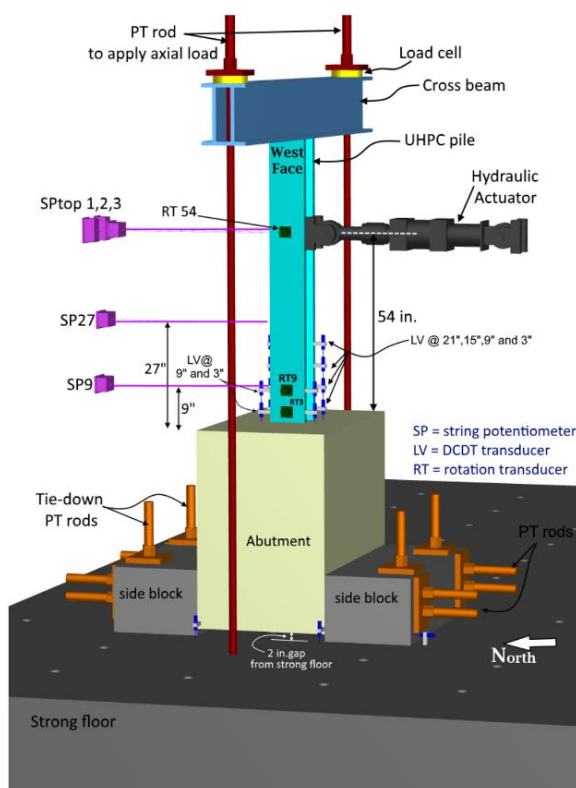
a) 3D Schematic of the test setup

b) Laboratory test setup

Figure 5-21. Test setup used for UHPC pile-to-abutment testing in weak-axis direction

Similar to the steel pile, the abutment cap was raised off of the strong floor by 2 in. to allow the punching of the pile through the cap to be evaluated during the testing. Axial load was applied to the test unit using a steel load beam with two center hole hydraulic jacks as shown in Figure 5-21b. The axial load applied during the testing was measured using two 200 kip load cells placed underneath the center hole jacks. The lateral load to the pile was applied using a 100 kip servo-controlled hydraulic actuator attached to the UHPC pile at 54 in. from the pile-to-abutment interface as shown in Figure 5-21. The test specimen was extensively instrumented with string potentiometers, LVDTs, and rotation devices as shown in Figure 5-21a. The string potentiometers and rotation devices were used to measure the lateral displacements and rotations of the pile at three different locations along the height of the pile. The LVDTs were attached on all four corners of the UHPC pile to capture average strains in the region close to the pile-abutment interface and any pull out of the pile during testing. The rotation meter RT3 was placed at 3 in. from the pile-to abutment interface to capture possible rotation in the pile-to-abutment connection. All the LVDTs and rotation meters were attached to the pile specimen using high-strength, quick-set epoxy. LVDTs were also placed at the bottom of the abutment to capture any horizontal and vertical movement during testing. The exact locations of the instrumentation and the nomenclature of the instrumentation is shown in Figure 5-21a.

111

A number of foil strain gages were placed on the shear, longitudinal and hoop reinforcement in the abutment to capture critical strains at different lateral displacements and axial load conditions. The details of the strain gages and the nomenclature are shown in Figure 5-22.
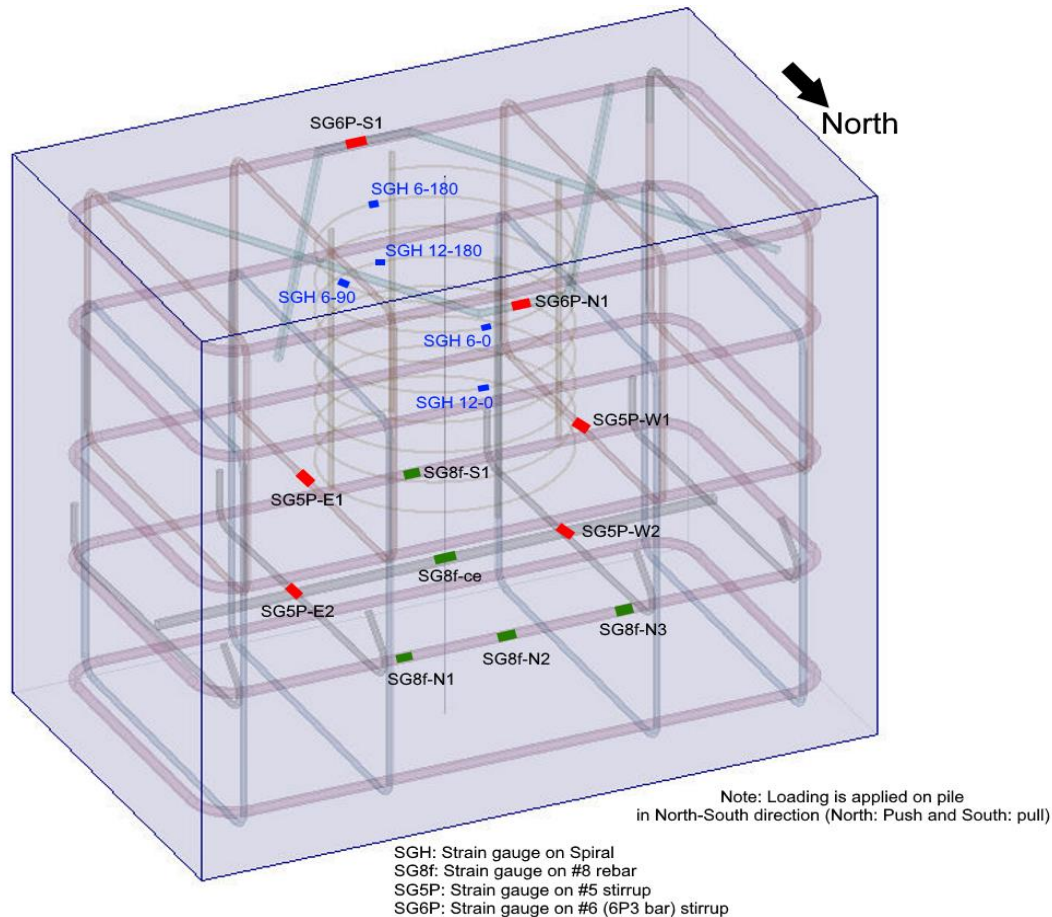
Figure 5-22. Details of strain gage on different reinforcement in pile abutment

5.5.2.   *Testing Sequence and Observations*

The first connection test completed for a UHPC pile was UPAC-1. UHPC test pile, L7, was tested in three phases similar to SPAC-1. In Phase I testing, UPAC-1 was subjected to lateral loading with an axial load of 100 kips on September 13, 2011. The lateral load was applied in a force-controlled cyclic manner with two cycles at each load step. This was followed by Phase II testing, in which the pile specimen was subjected to an axial load of 200 kips and force-controlled cyclic lateral loads with two cycles in each load step. The testing was completed with Phase III, where the axial load on the pile was decreased to 100 kips, and the cyclic lateral load was applied under displacement controlled with three cycles at each displacement. The loading protocol used for UPAC-1 is outlined in Table 5-10, and the applied displacement history to the pile specimen is shown in Figure 5-23a.

Table 5-10. Loading protocol chosen for UHPC pile connection test, UPAC-1

Phase	Axial load, kips	# cycles per step	Control	Load step
I	100	2	Force, kips	±4, ±8, ±12, ±16
II	200	2	Force, kips	±3.5, ±7, ±10.5, ±12
III	100	3	Displacement, in.	±0.5, ±0.75, ±1.0, ±1.5

a) Applied cyclic displacement history

b) Force vs. displacement (Phase I)   c) Force vs. displacement (Phase II)   d) Force vs. displacement (Phase III)
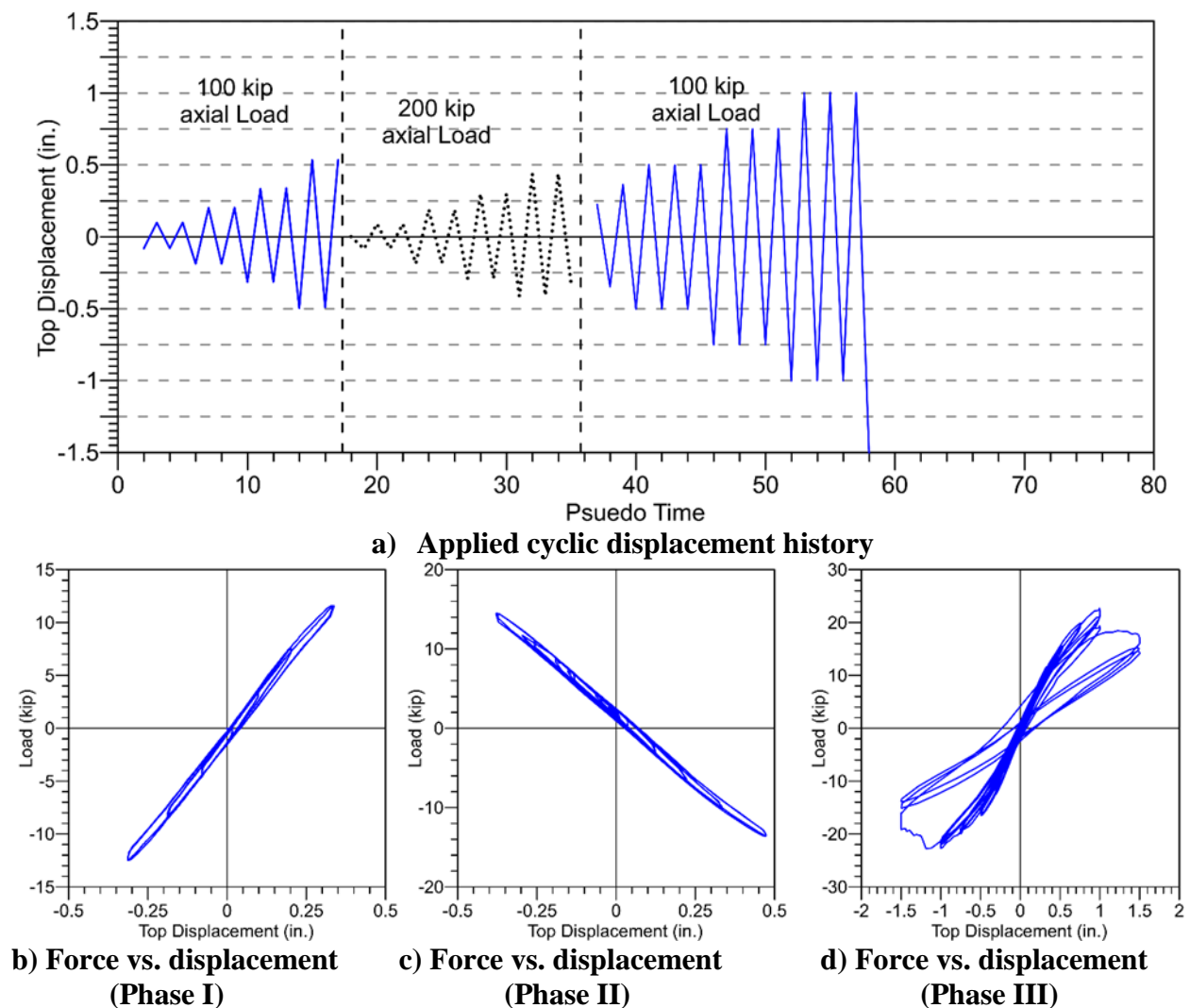
Figure 5-23. Loading history and measured force vs. displacement response of UPAC-1

The measured force-displacement responses of UPAC-1 in all three phases of testing are shown in Figure 5-23. The string potentiometers located at the point of load application were averaged to calculate the displacement of the test unit at a given load. The maximum lateral load applied to the specimen was 22.8 kips, which was 36% lower than the lateral load applied to the steel pile,

SPAC-1. It is important to note that these piles were not designed for any lateral force resistance; instead they were designed for target vertical load resistance. Hence, the reduced lateral load of the UHPC pile should not be of concern when used in the abutments.

Two hairline cracks as shown in Figure 5-24 developed on the UPAC-1 test pile near the pile-to-abutment interface at a lateral load of 12 kips during Phase I testing with an axial load of 100 kips.

Figure 5-24. Hairline tensile cracks on UHPC pile in UPAC-1 at 12 kip lateral load step with 100 kip axial load

Once Phase I testing was complete and the lateral load was returned to zero, all of the observed cracks were completely closed. No new cracks were developed during Phase II testing with the increased axial load. Also, the cracks from Phase I were not visible up to the lateral load of ±12 kips in the Phase II testing. During the Phase III testing, minor crushing of UHPC near the base of the pile became visible at 1.0 in. of lateral displacement. Figure 5-25 shows the minor crushing of UHPC after cycling through the three 1.0 in. cycles.

Figure 5-25. Spalled region of the UHPC pile due to crushing during the UPAC-1 test after completing of the 1.0 in. load displacement cycles

Throughout all three phases, no visible damage occurred to the abutment cap.

5.5.3.   Results

The predicted start of micro-cracking was induced at a lateral load of 9.9 kips and the predicted start of visible cracking was induced at 17.6 kips. A lateral load of 10.8 kips was required to move the UHPC test unit 0.28 in. in the push direction and 11.5 kips in the pull direction, which indicated micro-cracking should be present in the pile. Additionally, to achieve a lateral displacement of 0.42 in., a lateral load of 15.3 kips was applied in the push direction and 16.4 kips was applied in the pull direction, which was below the expected limit for visible cracking but increased the extent of micro-cracking.

During testing, two hairline tension cracks developed at 12 kips as shown in Figure 5-24, but were completely closed at 0 kip lateral load and 0 in. lateral displacement, and thus they can be considered in the range between micro-cracking and visible cracking. The Iowa DOT deems that hairline cracks are acceptable for UHPC members as long as the widths are negligibly small and are not expected to widen due to repeated loading under the most critical service load conditions (Aaleti et al. 2014). With a higher axial load in the pile, formation of hairline cracks will be delayed. Figure 5-26 compares the force-displacement response between UHPC and steel HP 10 $\times$ 57 piles up to ±0.5 in. of laboratory lateral displacement.
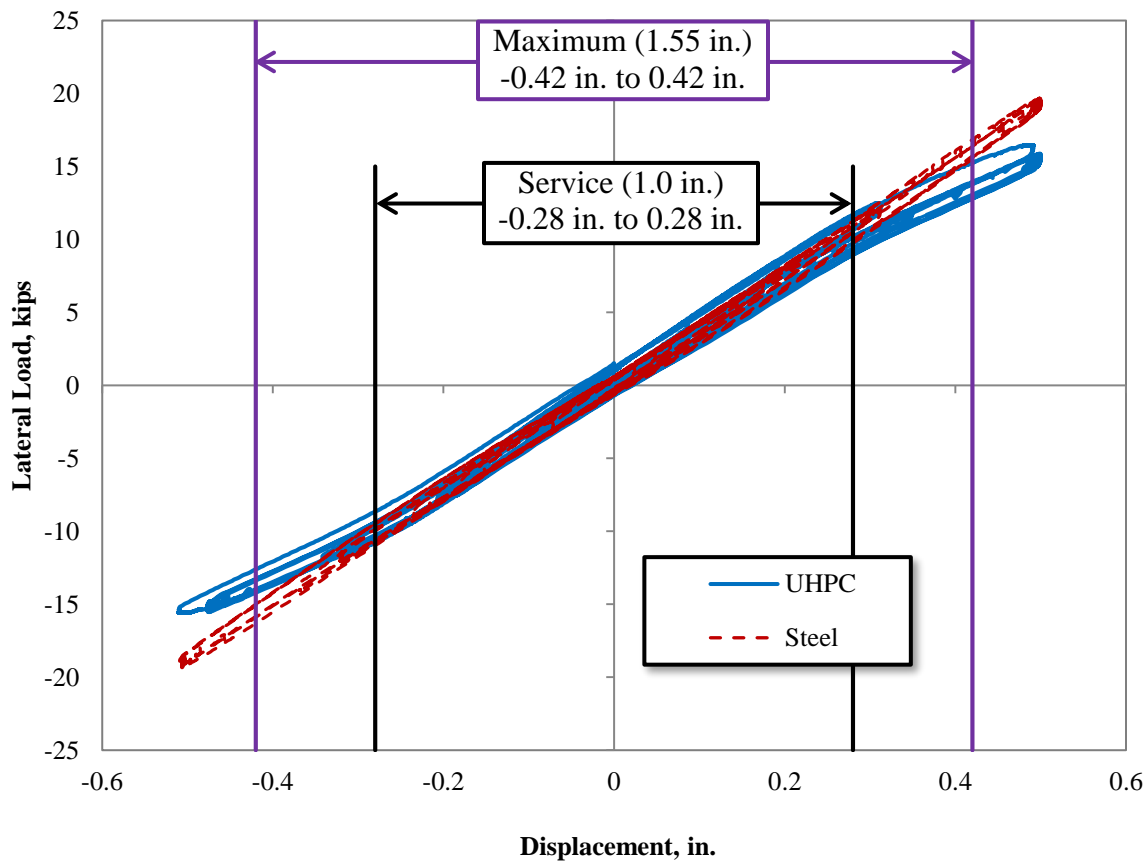
Figure 5-26. Comparison of UHPC and HP 10 × 57 force-displacement response up to 0.5 in. of lateral displacement

The correlation between the laboratory displacements and the full pile's service and maximum allowed abutment displacements of an integral bridge are noted in parenthesis in Figure 5-26.

As noted before, there was not much damage observed in the abutment. There were few hairline cracks observed on the abutment top face at 1 in. lateral displacement. This level of displacement is never expected in the field conditions. The measured strains in the spiral around the pile is shown in Figure 5-27.

a) **Phase I and Phase III testing**

b) **Phase II testing**
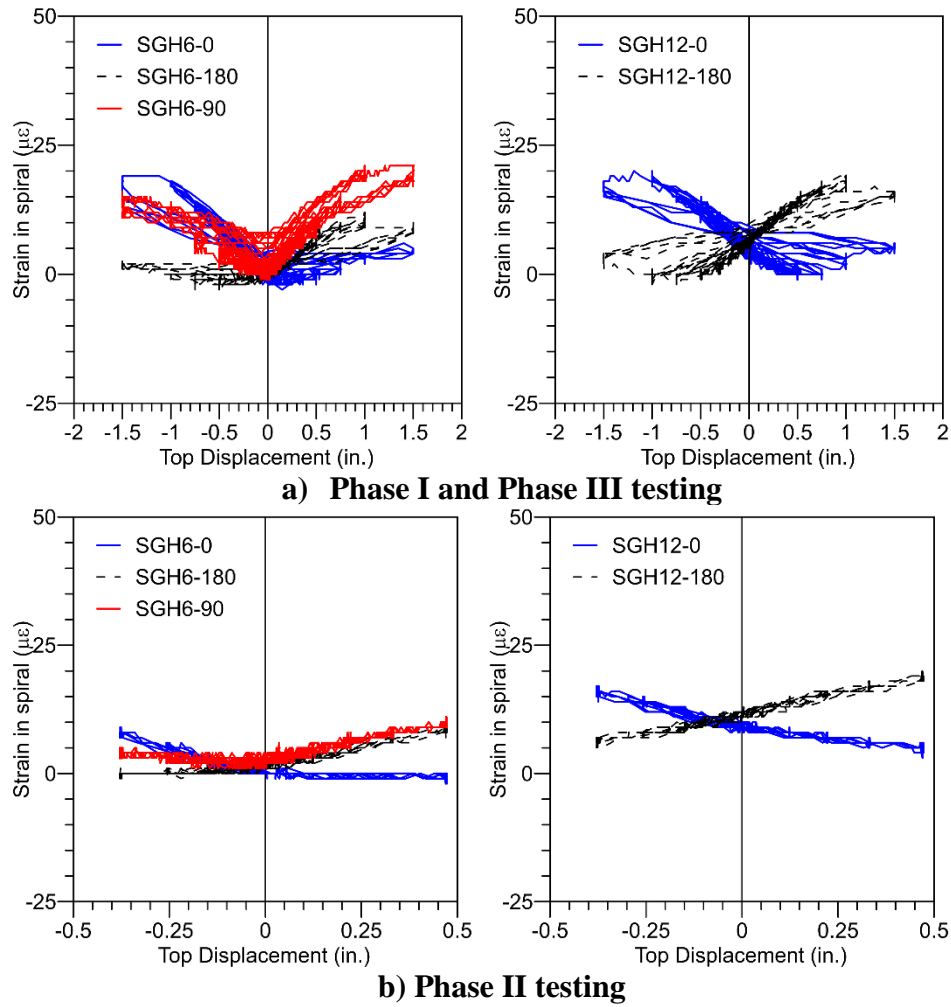
Figure 5-27. Measured strains in spiral around the pile in the abutment

Measured strains were less than 25 microstrains indicating no damage in the pile-to-abutment joint region.

The measured strains in the shear reinforcement, longitudinal reinforcement, and 6P3 bars in the abutment during Phase II and Phase III testing are shown in Figure 5-28.

a) Phase I and Phase III testing

b) Phase II testing
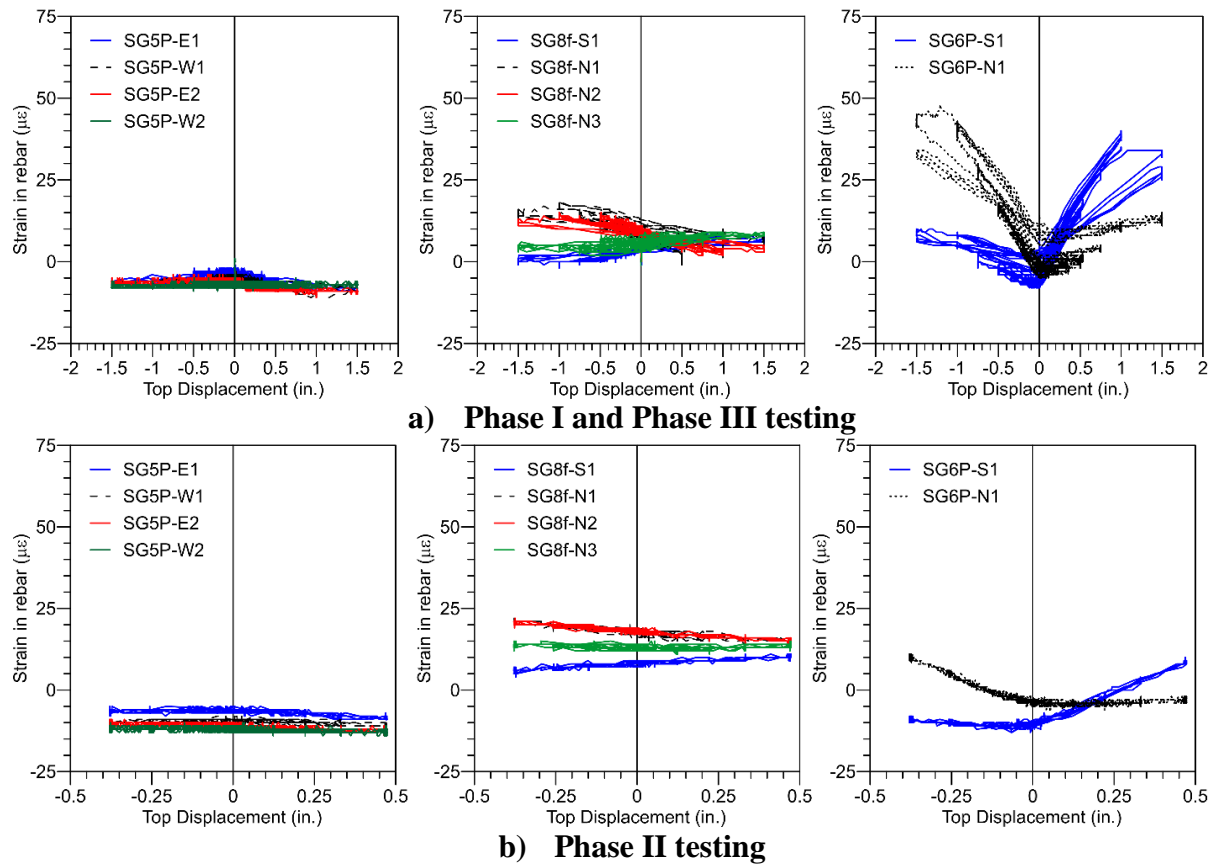
Figure 5-28. Measured strains in abutment reinforcement

It can be seen from the figure that the strains in all the reinforcement are less than 50 microstrains, which are well below the yield strain of the reinforcing steel bars. This observation indicates the current design and reinforcement detailing used for the abutment and pile-to-abutment connection are more than adequate for the UHPC pile in weak-axis bending direction. Based on the observations, a smaller reinforcing steel bar can be used, particularly those labeled 6P3 bars.

5.6. Strong Axis Pile-to-Abutment Connection Test

5.6.1. Load Frame and Test Setup

The same test setup used for the previous tests were used for evaluating the performance of the UHPC pile-to-abutment connection performance under strong-axis bending. Figure 5-29 shows the three dimensional (3D) schematic and actual picture of the test set up used in the laboratory.

(a) 3D schematic of the test setup　　　(b) Test setup in the laboratory
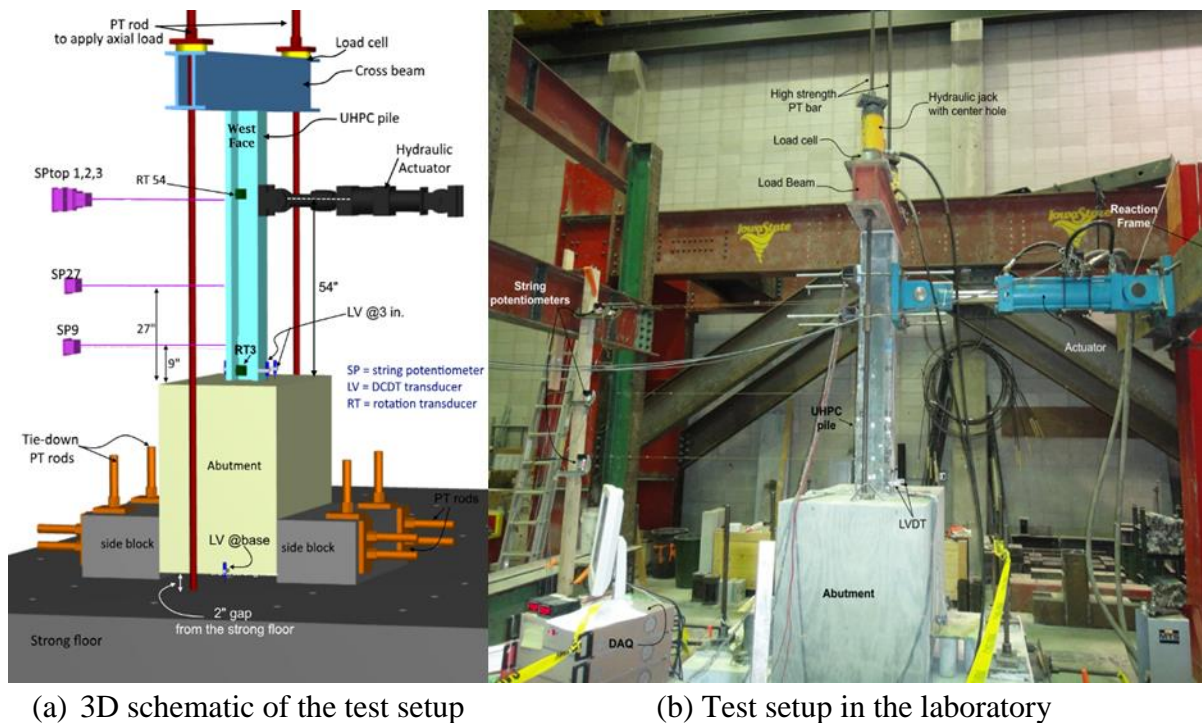
Figure 5-29. Test setup used for UHPC pile-to-abutment testing in strong-axis direction

Similar to previous tests, the abutment cap was raised off the strong floor by 2 in. to allow the punching of the pile through the cap to be evaluated during the testing. Axial load was applied to the test unit using a steel load beam with two center hole hydraulic jacks and was monitored using two 200 kip load cells during testing. The lateral load to the pile was applied using a 100 kip servo-controlled hydraulic actuator, attached to the UHPC pile at 54 in. from the pile-to-abutment interface as shown in Figure 5-29. The test specimen was instrumented with string potentiometers, LVDTs, rotation devices, and Optotrak LED sensors as shown in Figure 5-29.

The Optotrak LED sensors are part of a 3D non-contact displacement measure system, which captures the 3D location of a point on the structures with time and loading. The test specimen was instrumented with a total of 54 LED markers placed along the height and depth of the UHPC pile. The displacement data was captured at 5 Hz frequency. The string potentiometers and rotation devices were also used to measure the lateral displacements and rotations of the pile at three different locations along the height of the pile. Owing to the usage of the Optotrak system, a total of only three LVDTs were attached on the back corners of the UHPC pile to capture average strains in the region close to the pile-abutment interface and any pull out of the pile during testing. The rotation meter RT3 was placed at 3 in. from the pile-to abutment interface to capture possible rotation in the pile-to-abutment connection. All the LVDTs and rotation meters were attached to the pile specimen using high-strength, quick-set epoxy. LVDTs were also placed at the bottom of the abutment to capture any horizontal and vertical movement during testing. The exact locations of the instrumentation and the nomenclature of the instrumentation is shown in Figure 5-29a. A number of foil strain gages was placed on the shear, longitudinal, and CMP in the abutment to capture critical strains at different lateral displacements and axial load

119

conditions. The same nomenclature for strain gages as used in previous specimens were used for this specimen.

5.6.2. *Testing Sequence and Observations*

Like previous pile tests, UHPC test specimen UPAC-2 was subjected to combined axial and lateral loading causing bending about pile strong axis. In Phase I testing, UPAC-2 was subjected to lateral loading with an axial load of 100 kips. The lateral load was applied in a force-controlled cyclic manner with two cycles at each load step. This was followed by Phase II testing, in which the pile specimen was subjected to an axial load of 200 kips and force-controlled cyclic lateral loads with two cycles in each load step. The testing was completed with Phase III, where the axial load on the pile was decreased to 100 kips and the cyclic lateral load was applied under displacement controlled with three cycles at each displacement. The loading protocol used for UPAC-2 is outlined in Table 5-11, and the applied displacement history to the pile specimen is shown in Figure 5-30a.

Table 5-11. Loading protocol chosen for UHPC pile connection test, UPAC-2

Phase	Axial load, kips	# cycles per step	Control	Load step
I	100	2	Force, kips	±5, ±10, ±15, ±20
II	200	2	Force, kips	±6, ±12, ±18, ±24
III	100	3	Displacement, in.	±0.24, ±0.35, ±0.5, ±0.75, ±1.0, ±1.5
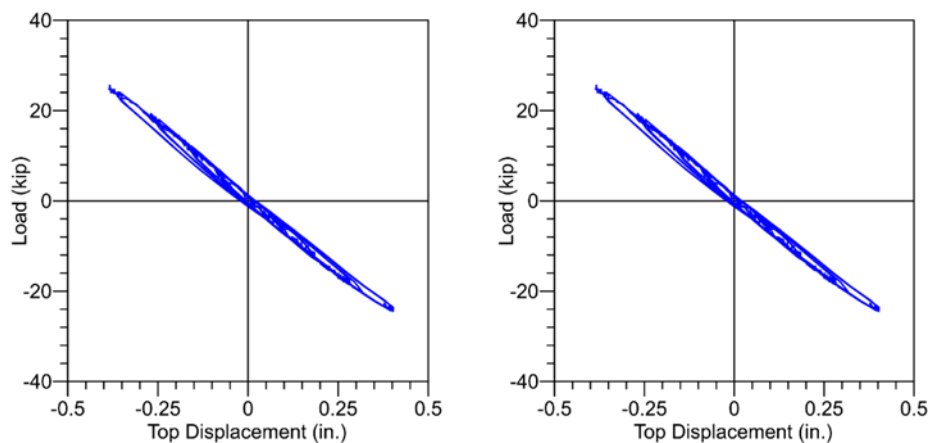
(a) Force vs. dispalcement (Phase I and III)
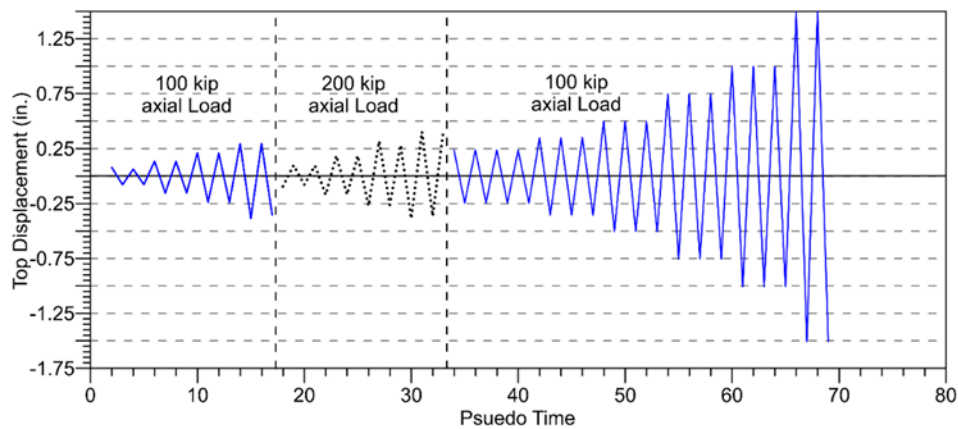
(b) Force vs. dispalcement (Phase II)

Figure 5-30. Loading history and measured force vs. displacement response of UPAC-2

The measured force-displacement responses of UPAC-2 in all three phases of testing are shown in Figure 5-30b and Figure 5-30c. The string potentiometers located at the point of load application were averaged to calculate the displacement of the test unit at a given load. The maximum lateral load applied to the specimen was 36.13 kips during the first 1 in. lateral displacement cycle. This load is 2 kips more than the maximum load of the steel pile in weak-axis bending. It is important to note that these piles were not designed for any lateral force resistance; instead they were designed for target vertical load resistance and lateral displacement.

In Phase I testing, at a lateral load of 10 kips, a hairline crack was observed at the pile-abutment interface, which further widened upon increase of the lateral load to 20 kips (Figure 5-31a).
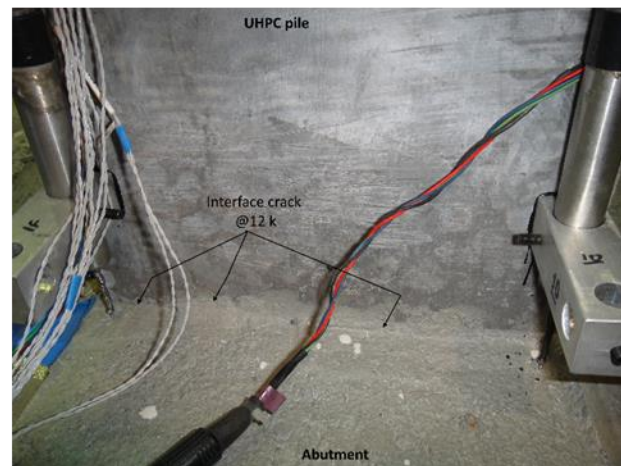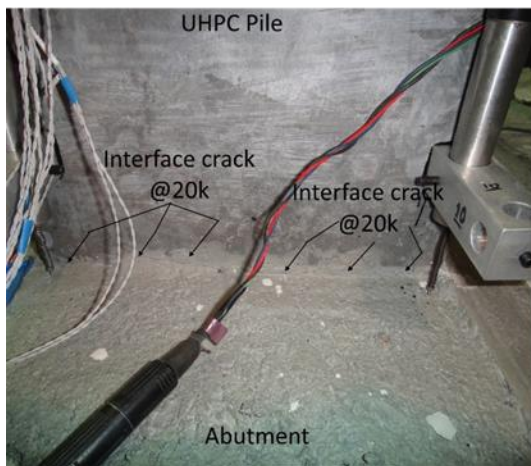
(a) Cracking at interface at 20 k load, Phase I   (b) Cracking at interface at 12 k load, Phase II

Figure 5-31. Observed damage in the UHPC pile specimen and abutment during Phase I and Phase II testing

121

It is important to note that the interface crack was not visible upon removal of the lateral load. No cracking was observed in the UHPC pile. In Phase II testing, where the axial load was increased to 200 kips, the same interface crack was visible at a lateral load of 12 kips (Figure 5-31b). No other cracks, either in the abutment or UHPC pile, were observed during the Phase II testing. In Phase III testing, during the 0.5 in. lateral displacement cycles, hairline cracking was observed in the UHPC pile at the base and in the concrete inside the CMP. The cracks are shown in Figure 5-32a.

(a)   Cracking at 0.5 in. lateral displacement during Phase III testing
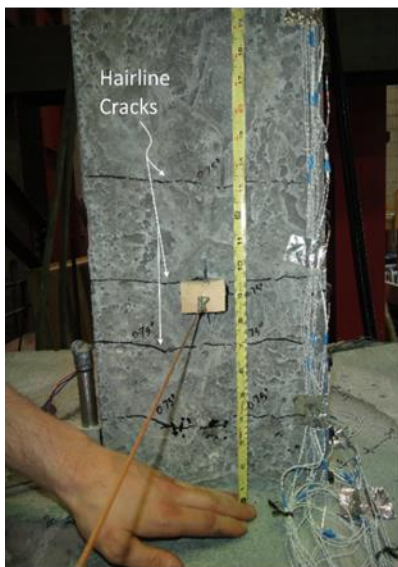
(b) Cracking at +0.5 in.   (c) Cracking at +1.0 in.   (d) Vertical crack at +1.0 in.
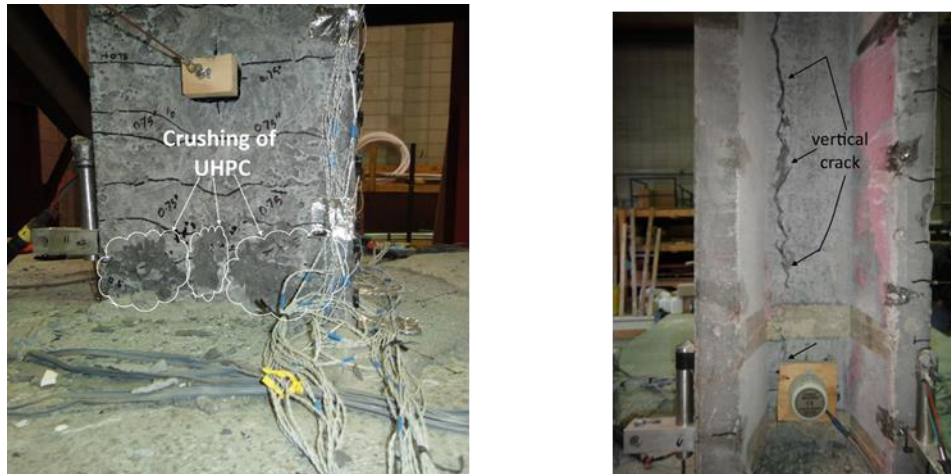
(e) Crushing of UHPC in flanges at 1.5 in. (f) Widened vertical crack in web at 1.5 in.

Figure 5-32. Observed damage in the UHPC pile and abutment during Phase III testing

All these cracks were closed upon unloading to zero lateral load. Four new cracks were formed in the UHPC pile over a 13 in. height at an average spacing of 3.25 in. during the first cycle of +0.75 in. displacement (pull), as shown in Figure 5-32b. No new cracks were observed in the abutment and the cracks from the previous displacement cycle did not extend. A number of new hairline cracks were formed in UHPC during the first +1.0 in. displacement cycle. The cracks were noticed over a 22 in. height from the top of the abutment (see Figure 5-32c). The cracks in the abutment were extended around 4 in. beyond the CMP, and no new cracks were formed.

During the second +1.0 in. displacement cycle, a lot of noise was heard coming from the UHPC pile, indicating cracking in the pile. There was a sudden drop in the load with the formation of a long, vertical crack in the web along the entire height of the pile. The crack was located closer to the web-to-tension flange interface and appeared to be at the location of a prestressing strand in web. The vertical crack along the height of the pile is shown in Figure 5-32d (shown by white arrows). The pile specimen was further subjected to 1.5 in. displacement cycles even after the vertical cracking was observed. The load capacity dropped by around 27% from the peak load, with the UHPC in the flanges near the base experiencing crushing. The crushing of the UHPC in the flanges is shown in Figure 5-32e. The testing was stopped after two cycles of 1.5 in. displacement due to significant widening of the vertical crack as shown in Figure 5-32f.

5.6.3.   Results

The measured strains in the shear reinforcement, longitudinal reinforcement, and 6P3 bars in the abutment during Phase I, Phase II, and Phase III testing are shown in Figure 5-33.

(a) Phase I and III testing
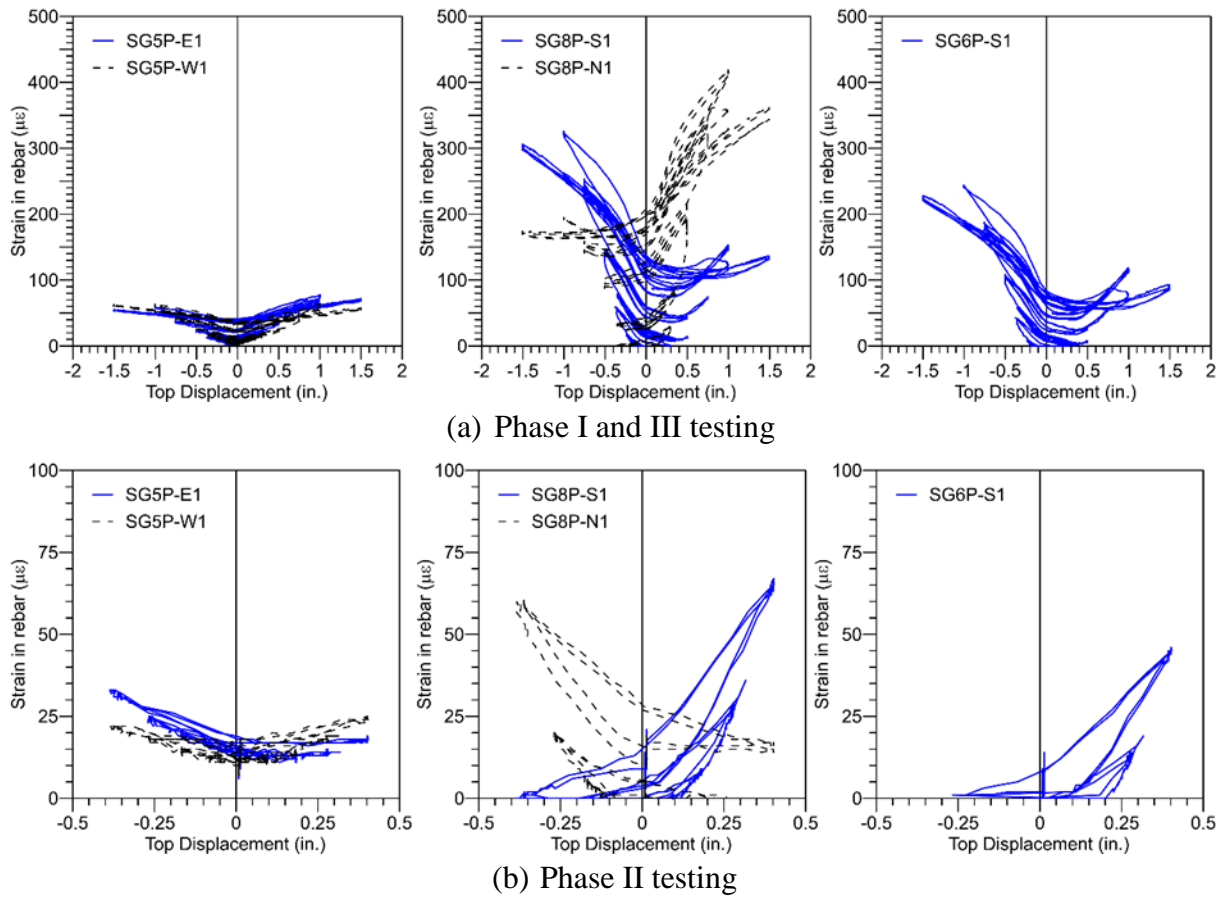
(b) Phase II testing

Figure 5-33. Measured strains in different types of reinforcement in abutment

It can be seen from the figure that the strains in all the shear and longitudinal reinforcement during Phase II testing are less than 75 microstrains, which are well below the yield strain of the rebars. Similarly, the measured maximum strains in the #8 longitudinal reinforcement during Phase III testing was around 400 microstrains, which is nearly 20% of the yield strains. The shear strains were around 80 microstrains, which is less than 5% of yield strains. This observation is consistent with the minimal cracking observed in the abutment during testing. The maximum strains recorded in the 6P3 bar at the abutment-to-pile interface was 250 microstrains, which is well below the yield strain of the bars. Based on the observations, a smaller reinforcing steel bar can be used, particularly those labeled as 6P3 bars. The measured strains in the CMP around the pile at different heights along the pile embedment depth is shown in Figure 5-34.

(a) Phase I and III testing

(b) Phase II testing
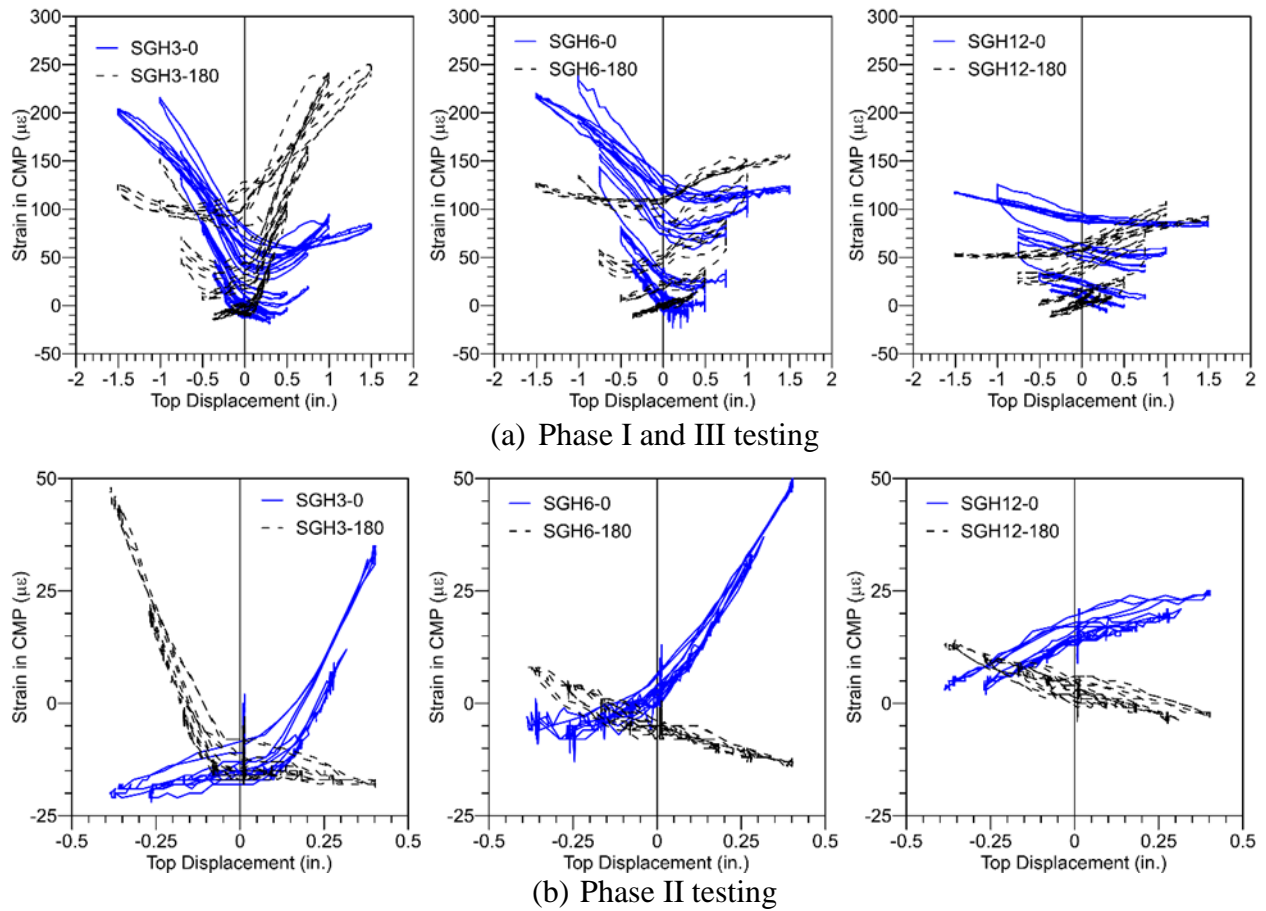
Figure 5-34. Measured hoop strains in CMP

The maximum measured hoop strains in the CMP were around 250 microstrains at 1.5 in. lateral displacement in the laboratory, which represents 5 in. field displacement. Even though this type of displacement is not expected in the field, the measured strains are still well below the yield capacity of the CMP. To optimize the design, one can further reduce the thickness of the CMP without causing any adverse effects on the connection behavior. However, this might not lead to economical design, as the current CMP is easily available in practice. The measured strain in the critical reinforcement supports that the current details used for the abutment and pile-to-abutment connection are more than adequate for the UHPC pile in strong-axis bending direction.

5.7. Skewed Pile-to-Abutment Connection Test

5.7.1. *Load Frame and Test Setup*

The same test setup used for the previous tests were used for evaluating the performance of the UHPC pile-to-abutment connection performance under bending about an axis, which is at 30º

125

skew with the weak-axis of the pile. Figure 5-35 shows the 3D schematic and actual picture of the test set up used in the laboratory.

a) 3D Schematic of the laboratory test setup   b) Laboratory test setup
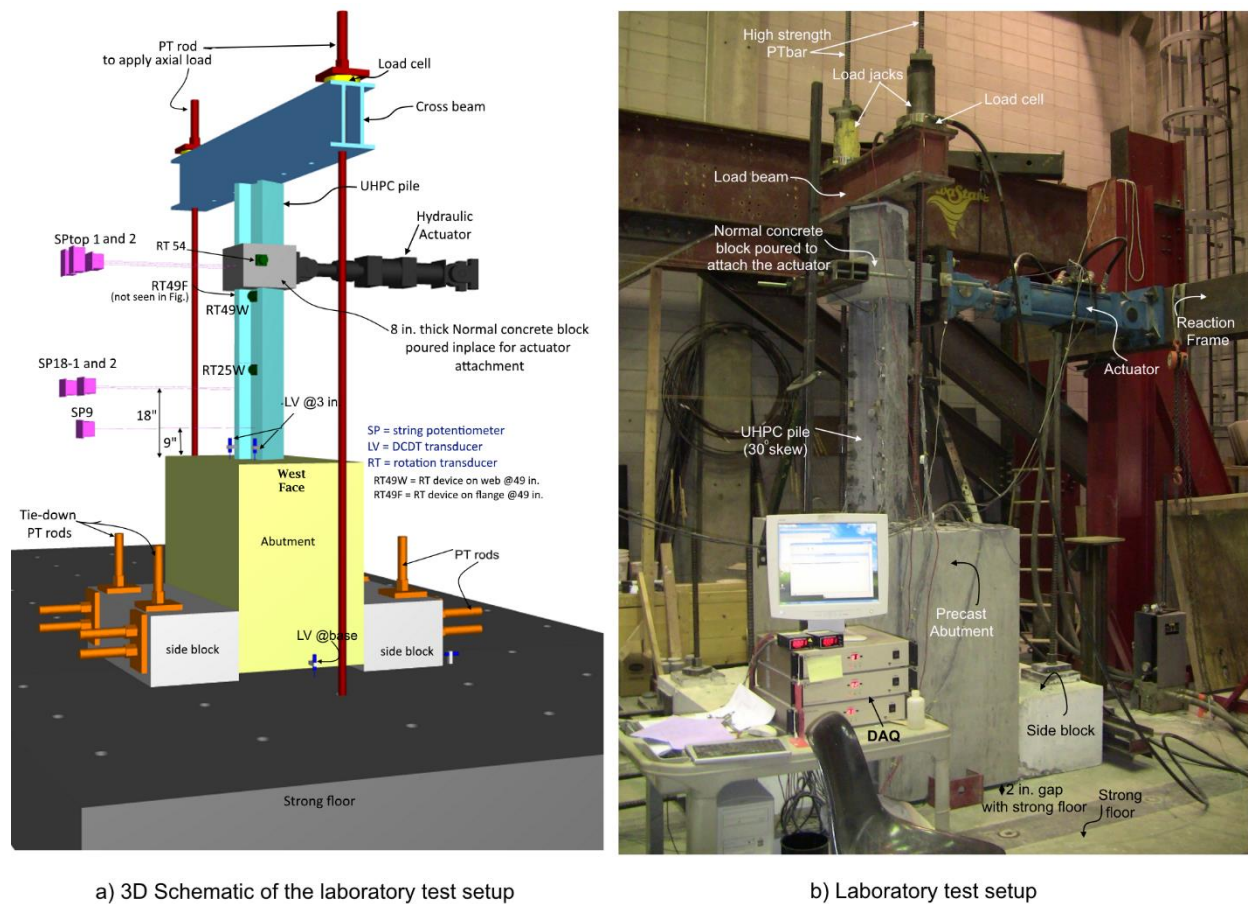
Figure 5-35. Test setup used for UHPC pile-to-abutment testing in skew axis direction

Like previous tests, the abutment cap was raised off the strong floor by 2 in. to allow the punching of the pile through the cap to be evaluated during the testing. Axial load was applied to the test unit using a steel load beam with two center hole hydraulic jacks and was monitored using two 200 kip load cells during testing. The lateral load to the pile was applied using a 100 kip servo-controlled hydraulic actuator attached to the UHPC pile at 54 in. from the pile-to-abutment interface as shown in Figure 5-35. To facilitate the attachment of the actuator to the skewed pile, an 8 in. thick, 16 in. x 16 in. concrete loading block was poured around the UHPC pile at the loading location. Similar to previous tests specimens, string potentiometers, LVDTs, rotation devices, and Optotrak LED sensors as shown in Figure 5-35, were used along the pile height, to capture critical displacements and rotations. The displacement data was captured at 5 Hz frequency. The string potentiometers and rotation devices were also used to measure the lateral displacements and rotations of the pile at three different locations along the height of the pile. Owing to the usage of the Optotrak system, a total of only three LVDTs were attached on the back corners of the UHPC pile to capture average strains in the region close to the pile-abutment interface and any pullout of the pile during testing. A total of three rotation meters

126

including two rotation meters on the pile web and one on the loading block were used to capture rotation of the pile under lateral loading. All the LVDTs and rotation meters were attached to the pile specimen using high-strength, quick-set epoxy. LVDTs were also placed at the bottom of the abutment to capture any horizontal and vertical movement during testing. The exact locations of the instrumentation and the nomenclature of the instrumentation is shown in Figure 5-35a. A number of foil strain gages were placed on the shear, longitudinal, and CMP in the abutment to capture critical strains at different lateral displacements and axial load conditions. The same nomenclature for strain gages as used in previous specimens were used for this specimen.

5.7.2.   *Testing Sequence and Observations*

Like previous pile tests, UHPC test specimen UPAC-3 was subjected to combined axial and lateral loading causing bending about a 30° skew axis. In Phase I testing, UPAC-3 was subjected to lateral loading with an axial load of 100 kips. The lateral load was applied in a force control manner in load increments of 4.25 kips up to a maximum load of 17 kips, with two cycles at each load step. This was followed by Phase II testing, in which the pile specimen was subjected to an axial load of 200 kips and lateral forces under force-control with two cycles in each load step. The load increments for this phase was 4.25 kips. The testing was completed with Phase III, where the axial load on the pile was decreased to 100 kips and the cyclic lateral load was applied under displacement controlled with three cycles at each displacement. The loading history applied on UPAC-3 in all three phases of testing is outlined in Table 5-12, and the applied displacement history of the pile specimen is shown in Figure 5-36a.

Table 5-12. Loading protocol chosen for skew UHPC pile connection test, UPAC-3

Phase	Axial load, kips	# cycles per step	Control	Load Step
I	100	2	Force, kips	±4.25, ±8.5, ±12.75, ±17
II	200	2	Force, kips	±4.25, ±8.5, ±12.75, ±17
III	100	3	Displacement, in.	±0.27, ±0.4, ±0.5, ±0.75, ±1.0, ±1.25
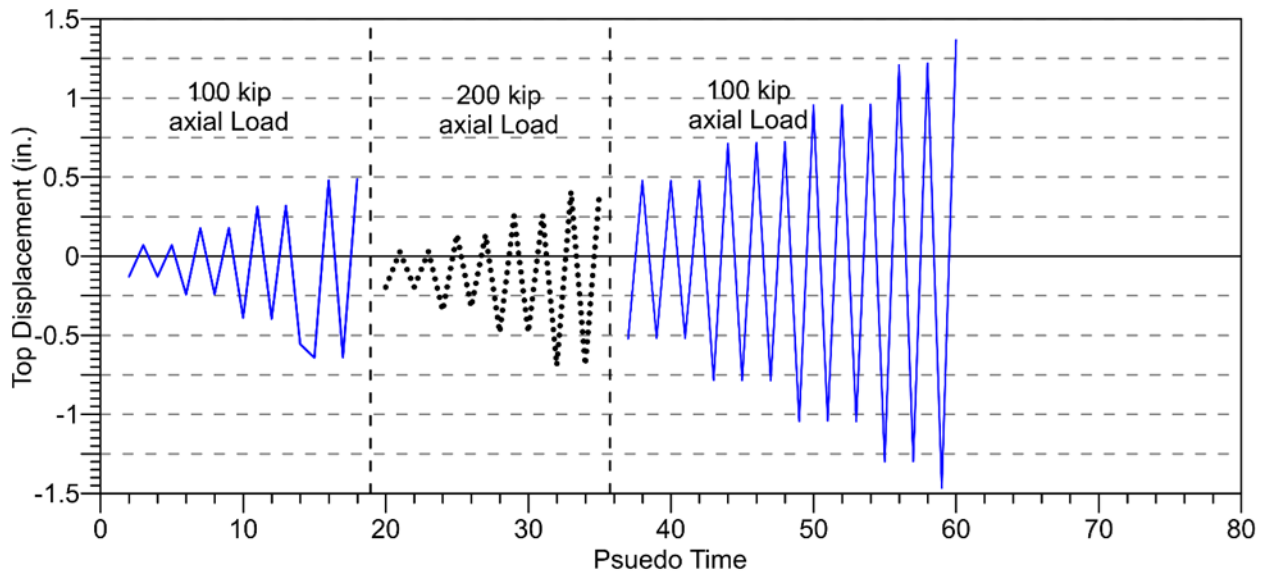
(a) Displacement history
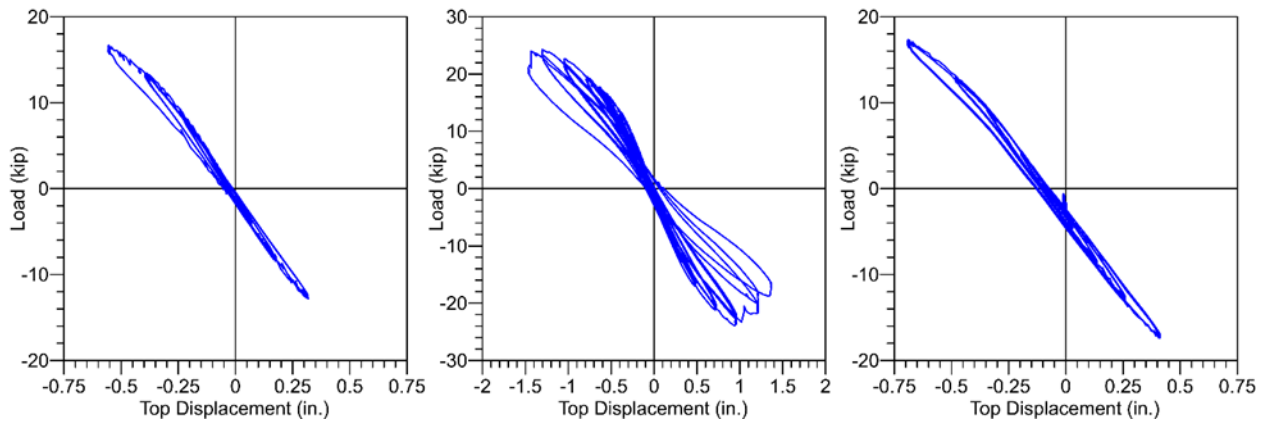
(b) Measured force-displacement response (Phase I, Phase III, and Phase II)

Figure 5-36. Loading history and measured force vs. displacement response of UPAC-3

The measured force-displacement responses of UPAC-3 in all three phases of testing are shown in Figure 5-36b. The string potentiometers located at the point of load application were averaged to calculate the displacement of the test unit at a given load.

In Phase I testing, at a lateral load of 8.5 kips, a hairline crack was observed in the abutment concrete in the region inside the CMP, starting at the top corner of the pile. At 12.75 kips of lateral load, hairline cracks were observed in UHPC pile, 1.5 in. from the pile-to-abutment interface (Figure 5-37a).

128
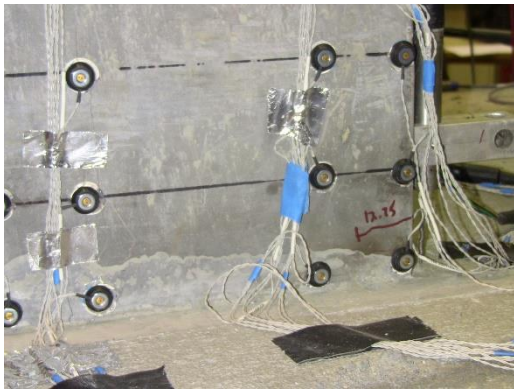
a) Hairline crack in pile at 12.75k (Phase I)
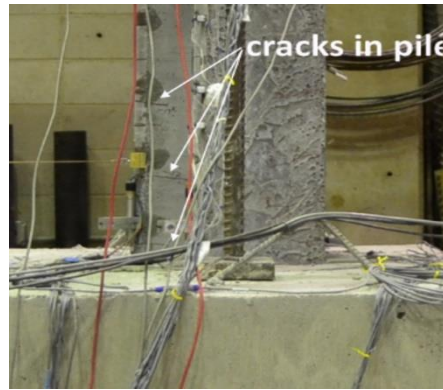
b) Hairline crack in pile at 17k (Phase I)
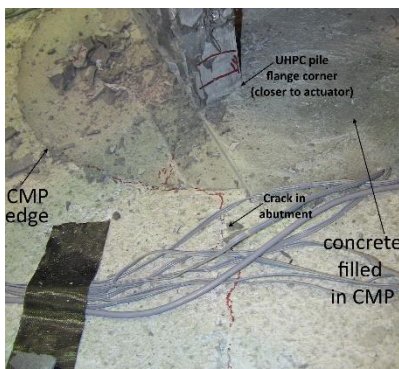
c) Cracking in abutment at 1 in. top displacement (Phase III

d) Cracking in pile flange at 1.25 in. top displacement (Phase III)
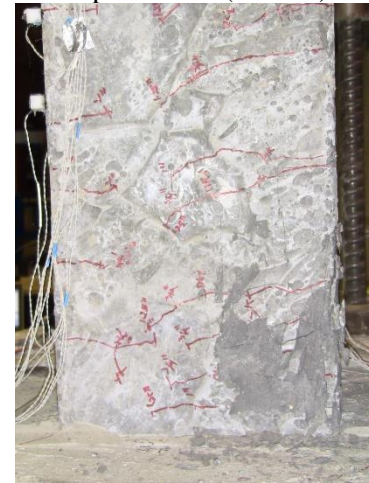
e) Crushing of UHPC in pile flange corner at 1.25 in. top displacement (Phase III)

f) Cracking in abutment at 1.25 in. top displacement (Phase III)
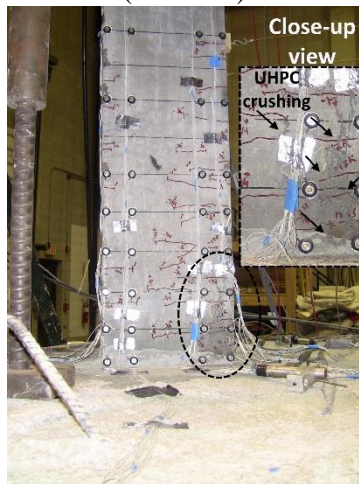
g) Cracking and crushing in pile flange at 1.4 in. top displacement (Phase III)
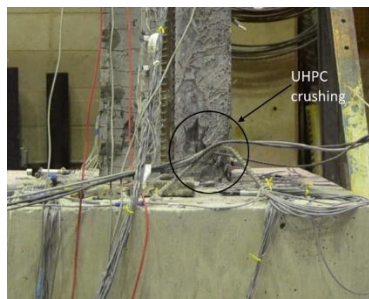
h) Crushing of UHPC in pile flange corner at 1.4 in. top displacement (Phase III)

Figure 5-37. Observed damage in the UHPC pile and abutment during testing

Also, a hairline crack formed along the pile-to-abutment interface over the length of the flange of the UHPC pile. During the 17 kips of lateral load cycle, noise was heard around 16 kips of lateral force. Hairline cracks were observed in the UHPC pile at 3 in., 8 in., and 15 in. from the top of the abutment (Figure 5-37b). It is important to note that the interface crack and cracks in the pile were not visible upon removal of the lateral load.

In Phase II testing, where the axial load was increased to 200 kips, no cracks were visible in the UHPC pile up to a lateral load of 12.75 kips. All the cracks from Phase I testing were closed at those loadings. At 17 kips of lateral loading, the cracks from Phase I testing became visible. Few new cracks formed during the 17 kips loading in the pull direction. No new cracks were observed in the abutment during Phase II testing. In Phase III testing, during the 0.5 in. lateral displacement cycles, hairline cracks from the previous phases opened and extended in length. All these cracks were closed upon unloading to zero lateral load. During the 0.75 in. lateral displacement cycles, a large number of cracks formed in the UHPC pile. A crack width in the UHPC pile at 6 in. from the abutment was measured to be 0.012 in. During the 0.75 in. displacement in the push direction, a few more new cracks were formed. The measured crack widths of the cracks were 0.01 in. During the 3rd cycle of this displacement, some spalling of UHPC was observed over a 3.5 in. height at the corner region of the flange. The maximum lateral load measured during this loading cycle was 19.3 kips in the pull direction and 21.3 kips in the push direction.

During the 1 in. displacement cycle in both push and pull directions, crushing and spalling of UHPC was observed in the corner region of the flanges of the UHPC pile. A long crack in the middle of the abutment, extending over half the width of the abutment that propagated from one of the pile flange corners, was also developed (Figure 5-37c). A horizontal crack was observed in the concrete loading block casted around the UHPC pile for load application. New cracks and more crushing and spalling of UHPC in the pile was observed during the 1.25 in. displacement cycles (Figure 5-37d and Figure 5-37e). The crack in the abutment extended up to the mid-depth of the abutment (Figure 5-37f). Even though it wasn't planned as part of the initial load protocol, the test specimen was subjected to one cycle of 1.4 in. displacement in each direction with the intent of failing the UHPC pile. A large number of cracks were formed with significant crushing in the flange corners (Figure 5-37g and Figure 5-37h). The pile resisted a lateral load around 16 kips at this displacement.

5.7.3.   Results

The measured strains in the CMP around the pile at different heights along the pile embedment depth is shown in Figure 5-38.
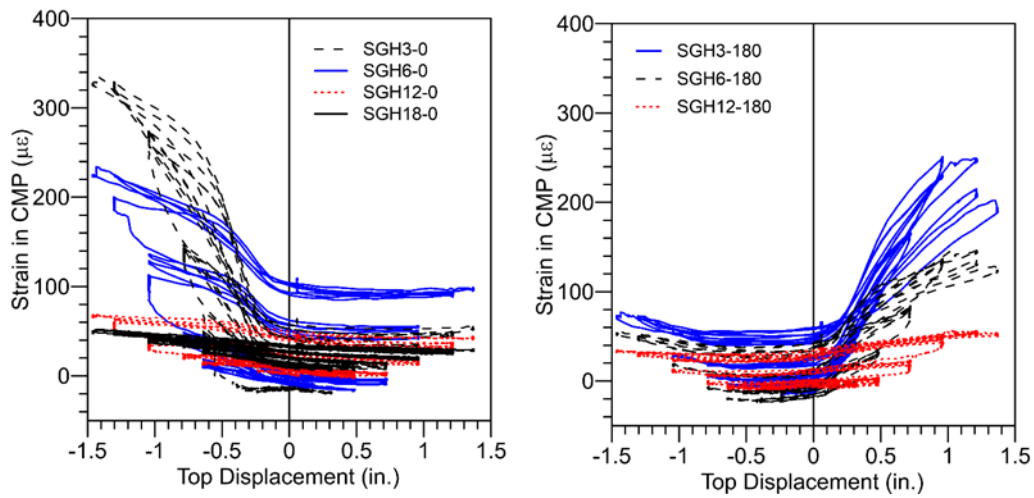
(a) Phase I and Phase III testing (100 kip axial load)
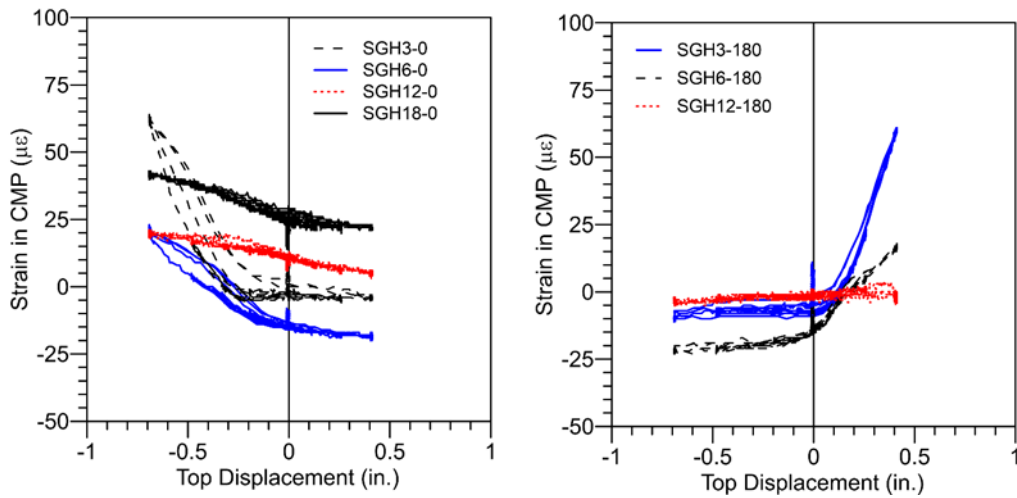
(b) Phase II testing (200k axial load)

Figure 5-38. Measured hoop strains in the CMP during testing

The measured hoop strains in the CMP reached 340 microstrains at 1.4 in. lateral displacement in the laboratory, which represents more than 5 in. of field lateral displacement. Even though this level of displacement is not expected in the field, the strains measured are still well below the yield strain of the CMP pipe. These strains are larger than the hoop strains measured in specimens testing under weak-axis and strong-axis bending.

The measured strains in the shear reinforcement, longitudinal reinforcement, and 6P3 bars in the abutment during Phase III testing are shown in Figure 5-39.
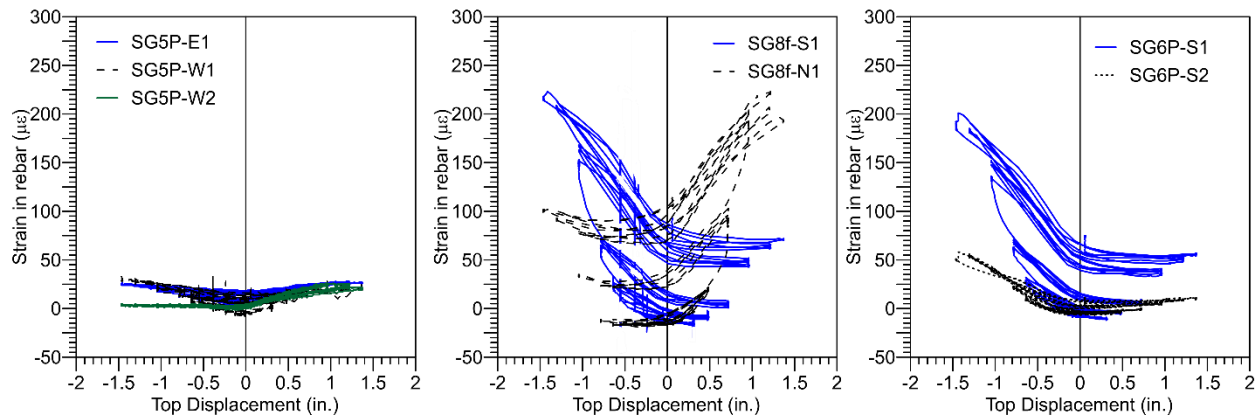
Figure 5-39. Measured strains in different types of reinforcement in abutment during Phase III

It can be seen from the figure that the strains in all the shear reinforcement are less than 50 microstrains, which are well below the yield strain of the rebars. Similarly, the measured maximum strains in the #8 longitudinal reinforcement were around 225 microstrains, which are nearly 10.7% of the yield strain of the rebar. This observation is consistent with the minimal cracking observed in the abutment during testing. The maximum strain recorded in the 6P3 bar at the abutment-to-pile interface was 210 microstrains, which is well below the yield strain of the bars. Based on the observations, a smaller reinforcing steel bar can be used, particularly those labeled as 6P3 bars.. The measured strain in the critical reinforcement supports the idea that the current details used for the abutment and pile-to-abutment connection are more than adequate for the UHPC pile in 30º skew.

CHAPTER 6: FIELD TESTING OF UHPC PILES

From the vertical load test in Phase I of the UHPC pile project, the UHPC pile was found to have an 86% higher capacity than HP 10×57 piles due to the increased toe area. The UHPC production pile for Phase II was designed to be 9 ft shorter than the 65 ft long HP 10×57 production pile and will be described in Section 7.2. To ensure that the 9 ft reduction in length would result in the UHPC production pile having the same capacity as the HP 10×57 production pile, a vertical load test was performed on a UHPC test pile with the estimated capacity of 200 kips. A second UHPC test pile was installed with a splice to confirm the performance of the UHPC pile splice during driving, which was followed by a lateral load test to verify the laboratory testing performed on the proposed splicing detail. This chapter describes the design, instrumentation, pouring, installation, and testing of the two UHPC test piles at the Sac County bridge project site.

6.1.   Design of Test Piles

The design length of the test piles, anchor piles, and production piles was calculated by following the current Iowa DOT Bridge Design Manual (2011). The predicted design capacity of each of the piles was calculated using DRIVEN (Matthias and Cribbs 1998), CAPWAP (Pile Dynamics, Inc. 2000), and one vertical load test. All of the design calculations are included in Appendix C, and Section 6.2 describes the instrumentation of the test piles in detail.

The vertical load test pile, P3, was designed for a 100 kip design load based on the Iowa DOT Blue Book. The soil profile at the location of the vertical load test is given in Section 6.4.2. The required length to achieve the design load of 100 kips using the Iowa DOT resistance factors available at the time of design is 45 ft, with 42 ft embedded in the ground. New resistance factors have been established for Iowa (Green et al. 2012), which would reduce the total length to 42 ft with 39 ft embedded into the ground. After the vertical load test was completed, P3 was then used for a lateral load test.

Two 15 ft UHPC pile sections were welded together end to end (P4) at the splice and were used to test the field performance of the splice in both driving and lateral loading. A push-over analysis check was performed using LPILE to make sure that the pile toe would not rotate. The estimated nominal capacity of the P4 using the Blue Book Method was 128 kips and is compared to the other methods in Section 2.5.

The reaction piles were given the names reaction pile south (RPS) and reaction pile north (RPN). The reaction piles were designed for axial tension by using the Iowa DOT Blue Book method. To give the load frame a capacity of 340 kips, the piles were 80 ft in length with 73 ft embedded into the soil. No instrumentation was installed along the length of the anchor piles, but PDA was run during driving and seven restrikes were performed on these piles. In axial compression, the current Iowa DOT design practices predicted the capacity of the anchor piles to be 331 kips.

6.2.   Instrumentation Scheme

The instrumentation used to measure the strains along the length of the UHPC test piles was chosen to be embedded concrete strain gages, as shown in Figure 6-1.

Figure 6-1. Embedded concrete strain gage

The gages were suspended between two prestressing strands at the specified gage locations by wires and installed using the procedure included in Appendix D. Because both P3 and P4 would have lateral loads applied during the lateral load test, the embedded strain gages, as shown in Figure 6-2, were placed on a diagonal at each level of instrumentation to measure the curvature of the piles.

Figure 6-2. Embedded concrete strain gage location in plan view

Additionally, steel plates were embedded into the web of the UHPC pile to provide a surface to weld a steel pipe that the ShapeAccelArray (SAA) could be inserted into after driving (Measurand Inc. 2011). A total of twelve 2 in. by 4 in. steel plates that are ¼ in. thick with shear studs welded in the center were embedded into the web of P4 on one side for a total length of 20 ft with a spacing of 18 in. except over the splice where 36 in. spacing was used. The Styrofoam inserts were cut at the location of the steel plates so that the plate would fit inside of the Styrofoam so not to reduce the area of the web too much as shown in Figure 6-3.

Figure 6-3. Locations of steel plates embedded into P4

The shear stud was the only part of the plate and shear stud combination that would be embedded in the UHPC.

During driving, the pile driving analyzer equipment was used to measure driving stresses on P3 and P4 and to predict the capacity of the pile using wave equation theory. In Figure 6-4, the conduits used to accommodate the PDA instrumentation is illustrated.
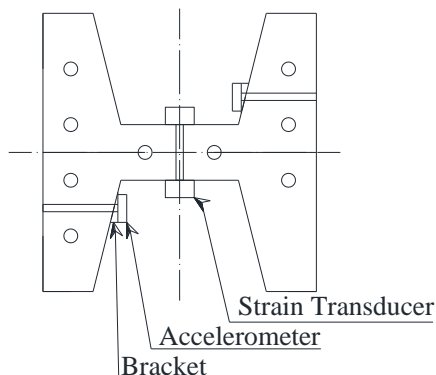
Figure 6-4. Illustration of PDA instrumentation in plan view

The strain gages and accelerometers were installed by inserting a bolt through the holes in the web and on the flange.

Notice that the accelerometers were located on the flanges of the pile. This was due to the limited space on the web of the UHPC pile resulting from the tapered flanges. In order to make sure the accelerometers remained flat and tight to the pile, inclined steel brackets were used between each accelerometer and pile. This setup worked very well, and valuable data was collected during

driving of the UHPC pile. The readings were wirelessly transmitted to the PDA unit provided by the Iowa DOT as shown in Figure 6-5.

Figure 6-5. PDA unit provided by the Iowa DOT

6.2.1.   Test Pile P3

The instrumentation for the vertical load test pile, P3, was installed on November 18, 2011 at Coreslab Structures, Inc. in Bellevue, Nebraska. When the forms were set up for P3, an extra foot was added making the total length of the pile 46 ft. Table 6-1 lists the adjusted location and label for each of the 20 embedded strain gages.

Table 6-1. Strain gage labels for test pile P3

Location from pile head, ft	Gage label	
4	ISU3-48-E	ISU3-48-W
7	ISU3-84-E	ISU3-84-W
9	ISU3-108-E	ISU3-108-W
11	ISU3-132-E	ISU3-132-W
13	ISU3-180-E	ISU3-180-W
20	ISU3-240-E	ISU3-240-W
28	ISU3-335-E	ISU3-335-W
36	ISU3-432-E	ISU3-432-W
43	ISU3-516-E	ISU3-516-W
45.25	ISU3-537-E	ISU3-537-W

An illustration of the vertical location of the gages is shown in Figure 6-6.
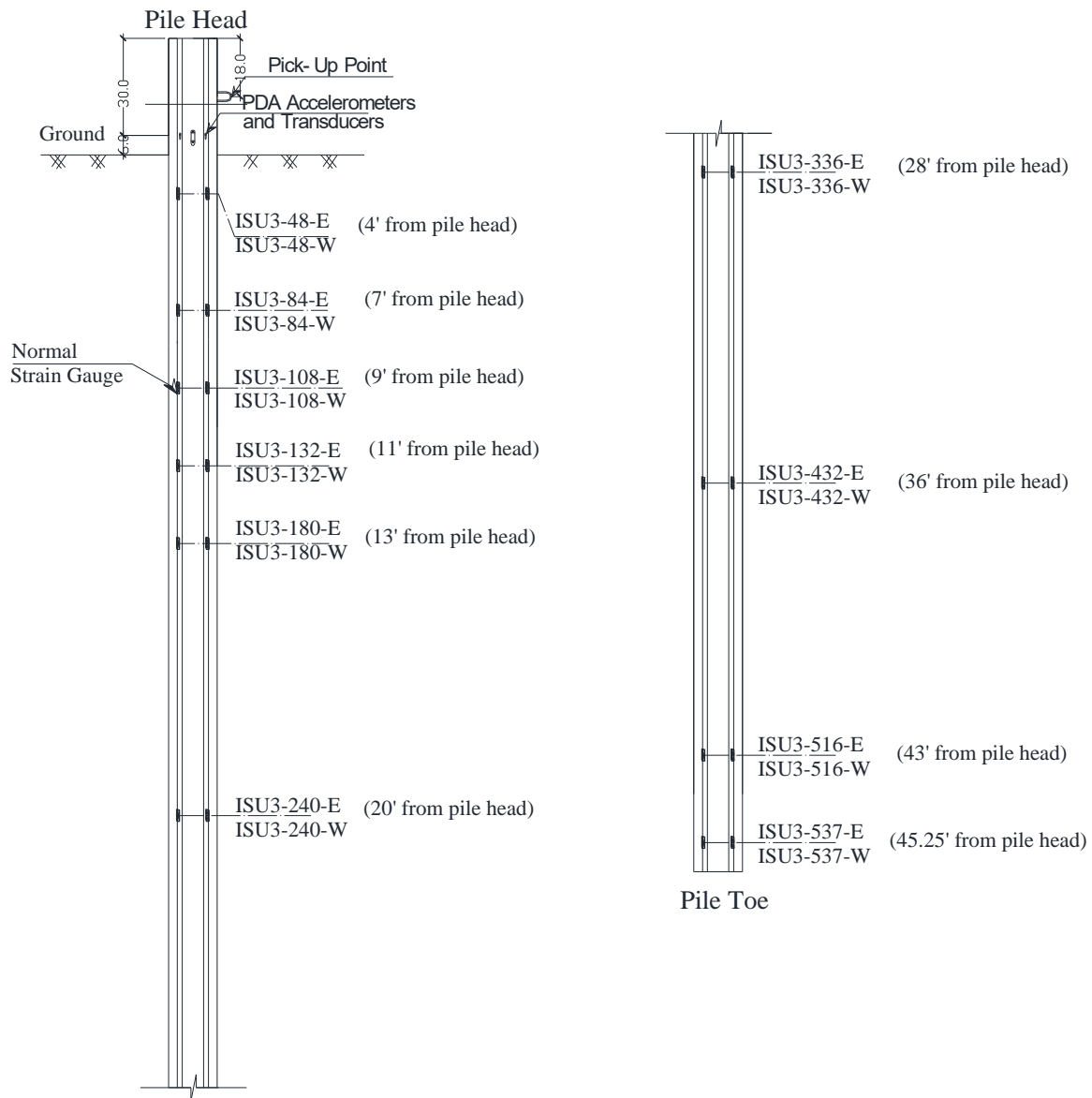
Figure 6-6. An elevation view of test pile P3 instrumentation

Strain gages ISU3-537-E and ISU3-537-W were included on the toe of the pile to measure the end bearing component of P3 during the load test.

6.2.2. Test Pile P4

The instrumentation for the lateral load test pile, P4, was also installed on November 18, 2011 at Coreslab Structures, Inc. in Bellevue, Nebraska. Table 6-2 lists the locations and labels for all six of the embedded strain gages.

Table 6-2. Strain gage labels for test pile P4

Location from pile head, ft	Gage label	
4	ISU4-48-E	ISU4-48-W
9	ISU4-108-E	ISU4-108-W
12.83	ISU4-168-E	ISU4-168-W

Figure 6-7 illustrates the locations of the strain gages as well as the splice in an elevation view of the pile.
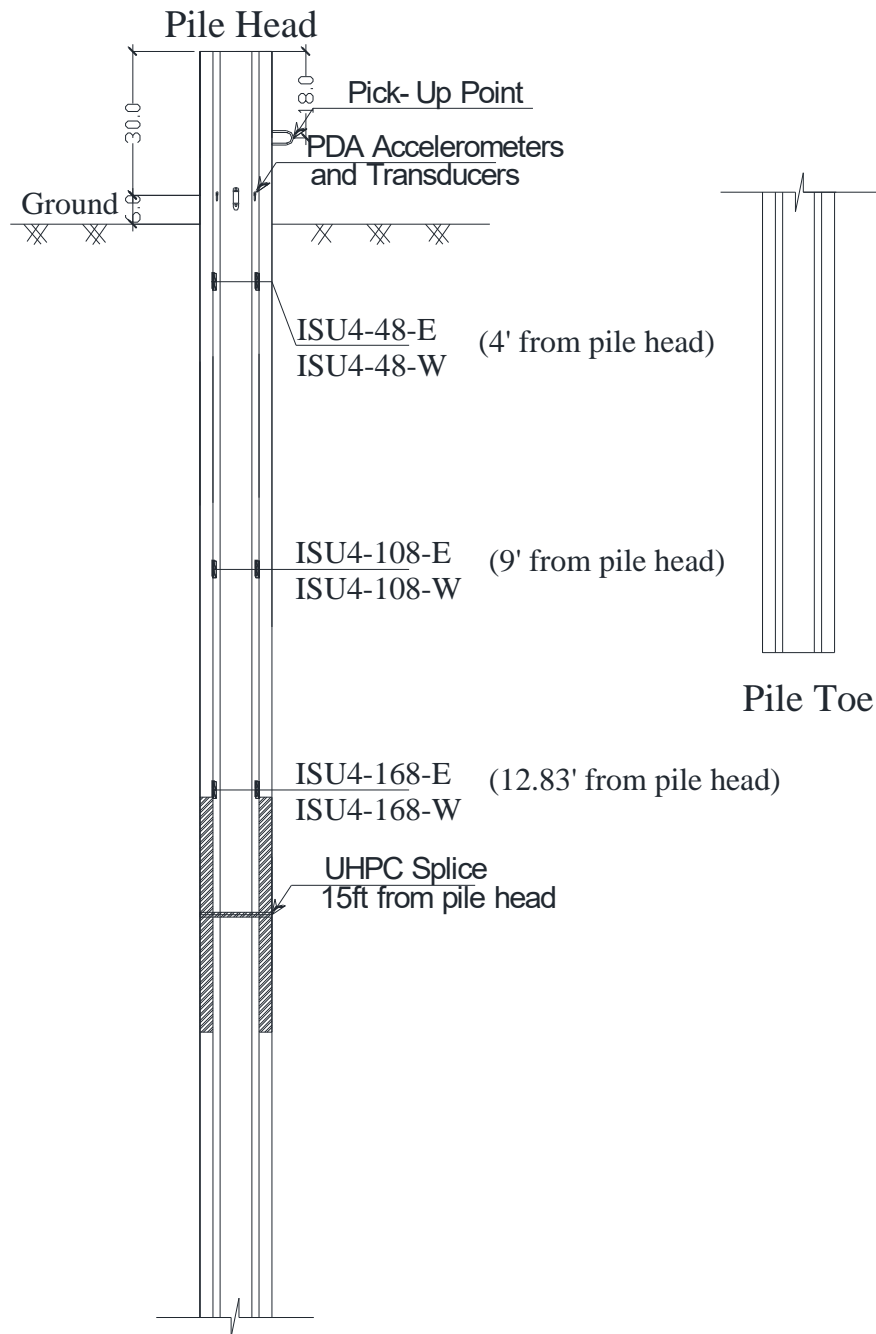
Figure 6-7. An elevation view of test pile P4

6.3. Precast Fabrication

By nature, UHPC induces much greater stresses on the concrete mixer and formwork. Therefore, when mixing UHPC, the mixer will be put under higher demand than that required for normal

concrete. The mixer must be able to accommodate higher amounts of shear, minimum blade clearances, and variable speeds (Wipf et al. 2009). As a result, there are limitations on the volume of UHPC that can be mixed at any one time using a typical concrete mixer, which is often only a percentage of the rated capacity. Additionally, when preparing the formwork for UHPC, precautions need to be taken to prevent leaking and lifting of the forms (Wipf et al. 2009). The leaking is prevented by sealing all of the joints and prestressing holes of the formwork, and lifting is prevented by fastening the forms to the precast bed.

6.3.1.   Splice Fabrication

The UHPC pile splices were fabricated by Howe Welding and Metal Fabrication in Ames, Iowa, by a certified welder. The ½ in. thick end plates were cut to the same dimensions as the tapered H-section of the UHPC pile, holes were cut into the end plates to accommodate the diameter and location of the prestressing strands, and the edges of the plate were chamfered to allow for welding in the field. Additionally, ¼ in. thick plates were bent to form the angles that were welded to each corner of the splice plate, and ½ in. diameter shear studs were welded to the bent plates at the specified locations. Figure 6-8 shows an actual splice and Figure 6-9 illustrates the details of the splice.
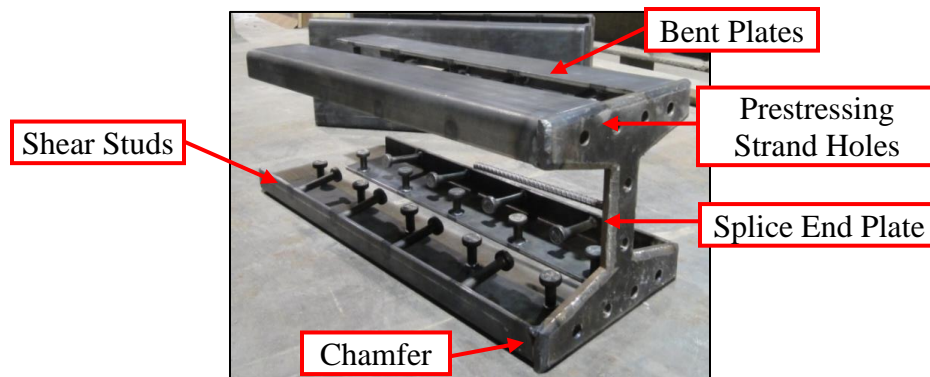
Figure 6-8. Components of UHPC pile splice attachment
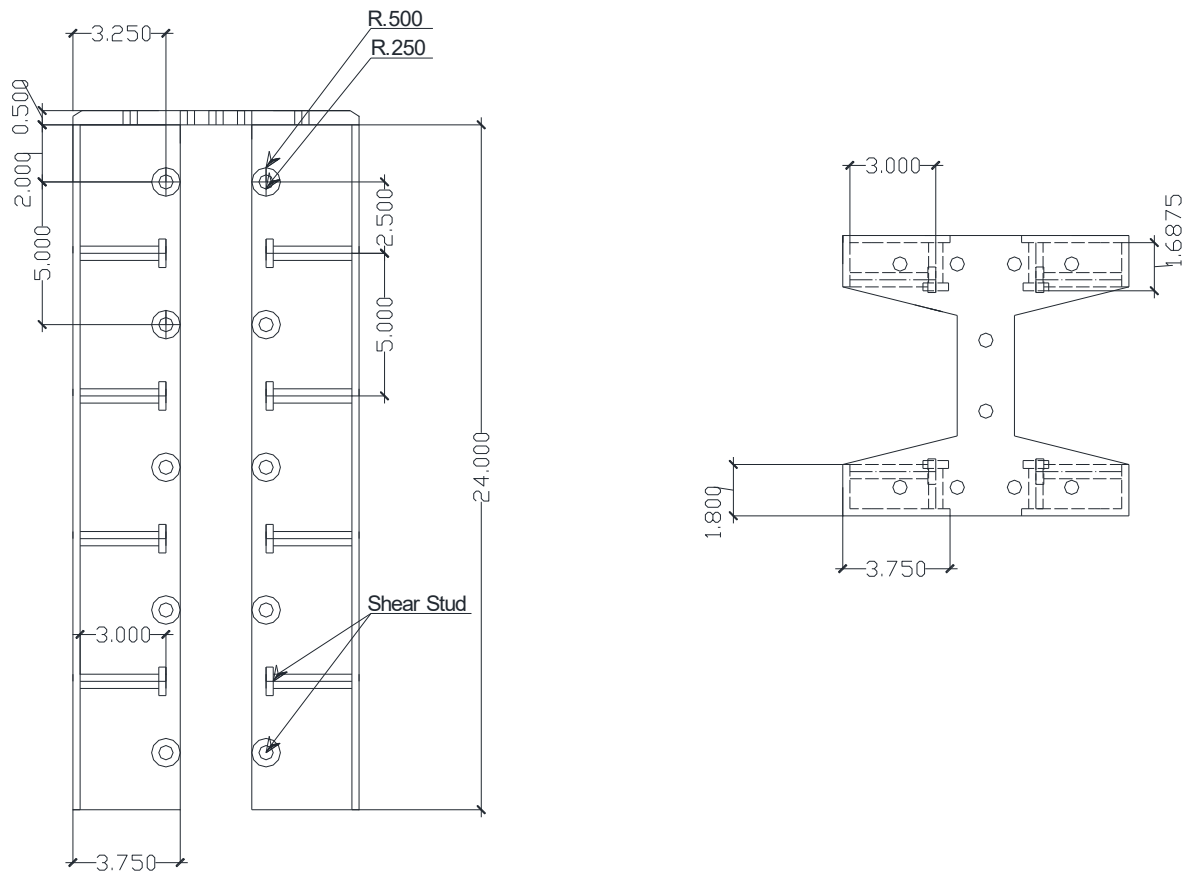
Figure 6-9. Splice design details

Note in Figure 6-9 that all units are in inches.

6.3.2.   Casting Process

The UHPC field test piles were cast in December of 2011 at Coreslab Structures, Inc. in Bellevue, Nebraska. For the two field test piles, half of the steel side forms with Styrofoam inserts were set up before the research team arrived. While the rest of the formwork was being set up, inserts to accommodate the PDA equipment were installed into the Styrofoam inserts as depicted in Figure 6-10.
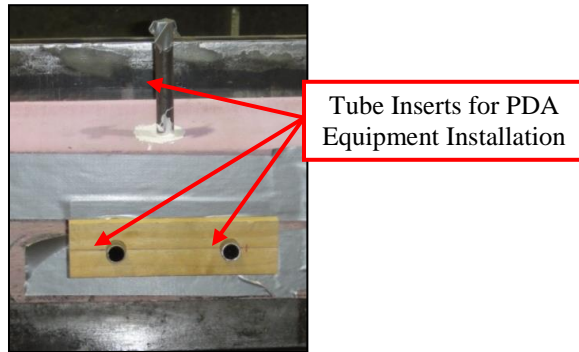
Figure 6-10. Tube inserts for the PDA equipment installed in ISU #3, ISU #4, and UW1-1

The two fabricated splices were installed as shown in Figure 6-11.

Figure 6-11. Splice at a UHPC pile end prior to placing the formwork

After the splices were installed, all 10 of the prestressing strands were arranged and stressed to their initial prestress of 202.5 ksi, which is approximately 75% of their ultimate strength. Strain gages were then installed on the field test piles, and the production pile is shown in Figure 6-12 following the instrumentation plan.
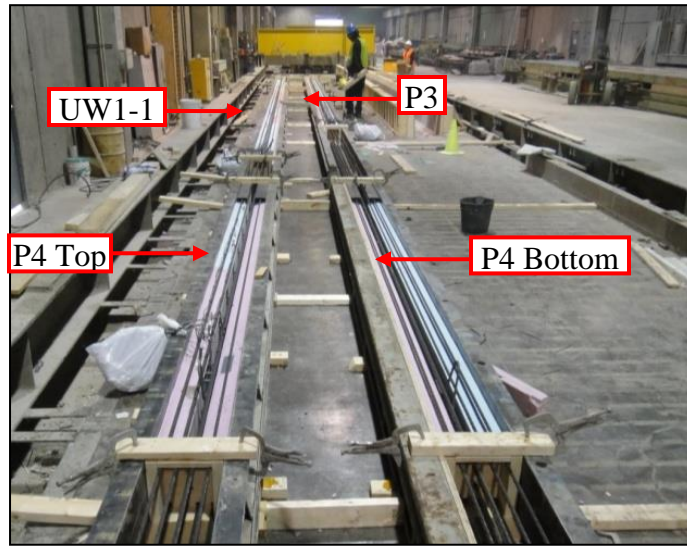
Figure 6-12. Layout of UHPC piles P3, P4, and UW1-1

The batching of the UHPC ensued at the precaster's batch plant in a 4.0 yd^3 mixer, and approximately 2.75 yd^3 of UHPC was produced for the pour. After completing the batching process the UHPC mix was transferred out of the mixer into a large bin (Figure 6-13) and subsequently transferred to the bed by the overhead crane.
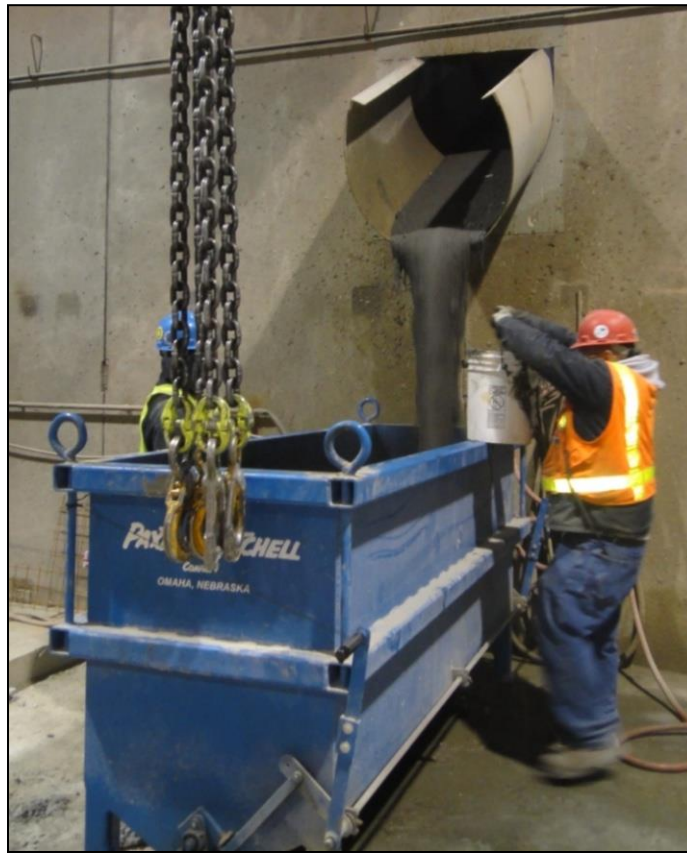
Figure 6-13. Transfer of UHPC from mixer to bin

The UHPC was poured into the forms for all of the field test units and production pile as depicted in Figure 6-14.

Figure 6-14. Pouring the UHPC from the bin into the forms

Immediately after the UHPC was poured in the forms, the top surface of the test units and production pile were covered with plastic wraps and traps to prevent moisture loss.

Propane heaters were used for the initial curing at 86°F. Along with the test units, twelve 3 in. diameter UHPC cylinders were cast with the pour. The precaster tested cylinders periodically during the initial curing of UHPC to determine the compressive strength of the mix. After reaching a compressive strength of 14 ksi, the prestressing strands were cut at the member ends.

6.3.3.   Details of Field Test Piles Pour

Test Pile P3

Test pile P3 was poured on November 21, 2011 at Coreslab Structures, Inc in Bellevue, Nebraska. The UHPC used for P3 had clumps of cement as shown Figure 6-15.
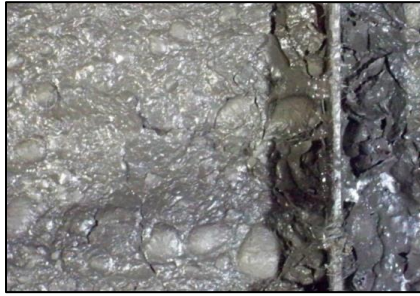
Figure 6-15. Clumps in UHPC after batching for the 11/21/2011 pour

The clumps are thought to have been caused by the age of the Ductal material, and the clumps came from the bags at the bottom of the pallet used to store the UHPC mix.

Once the concrete was batched and transported to the casting bed, the UHPC was poured into the forms. As the forms began to be filled with UHPC, the formwork shifted, and UHPC leaked out from underneath the formwork and caused the forms to start floating as shown in Figure 6-16.

Figure 6-16. Steel forms beginning to tilt causing UHPC to leak

The concreting was paused to reposition the forms and weigh them down, so they would stop floating. To weigh the forms down back into position, rolls of prestressing strands and large concrete blocks were lifted by the crane and placed on top of the formwork. There was a waiting time of about 55 minutes before pouring continued. The UHPC left inside of the forms was raked to join the two layers together.

After the forms were stripped, some noticeable defects were found. Figure 6-17 indicates that the Styrofoam portion of the form became detached and began to float for one of the form sections.

Figure 6-17. Change in the flange thickness of P3

No cracking from the prestressing was found on the top side where the flange was only 1 in. thick instead of the specified 1.8 in. It was decided to use P3 for field testing even with the identified defects.

UHPC Pile P4

Due to the complications that happened during the pour of P3, there was not enough UHPC to complete the pour of P4. Therefore, P4 was poured on November 22, 2011. The forms were reinforced to prevent shifting and floating.

The amount of UHPC needed to pour P4 was 0.6 yd^3 and was smaller than the minimum amount of concrete required for the 4 yd^3 mixer. Therefore, the small 1 yd^3 mixer was used at Coreslab. The mixer stopped due to the high demands of the UHPC on the mixer, as predicted by Wipf et al. (2009). To resolve the issue, 75% of the materials were removed from the mixer and stored in 5 gallon buckets so that the mixer could be restarted. When the material within the mixer became fluid, the removed mix was added back to the mixer one 5 gallon bucket at a time until all of the material was added and mixed.

6.3.4. Steam Curing

After the release of the prestressing strands in P3 and P4, the test piles were steam cured with UW1-1 at 194°F for 48 hours at the precasting plant. All 20 gages in P3 and 6 gages in P4 were working after the steam curing.

6.3.5. Handling of UHPC Test Piles

For the field test piles, lifting hooks were designed as shown in Figure 6-18 and Figure 6-19.
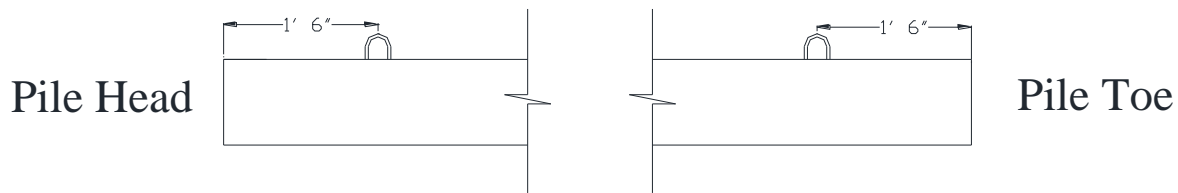
Figure 6-18. Locations of pickup points
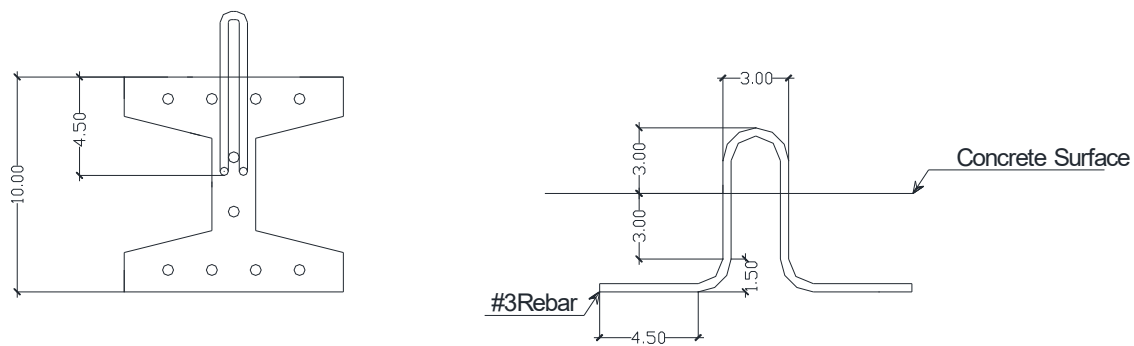
Figure 6-19. Original pickup point design for field installation

The lifting hook was placed 1.5 ft away from the pile head. Coreslab added an additional hook at the pile toe for easy storage and transportation out of the precast bed and to the construction site. Note that this pile handling detail required revision, which is presented in Section 7.4.6.

6.3.6. Material Properties

Prestressing Strands

Three 5 ft sections of the 270 ksi low-relaxation prestressing strands were cut from the prestressing strand roll used for the test piles and the first production pile. The three strand sections were tested in uniaxial tension at ISU until reaching the yield stress. Figure 6-20 shows the stress-strain response of the specimens.
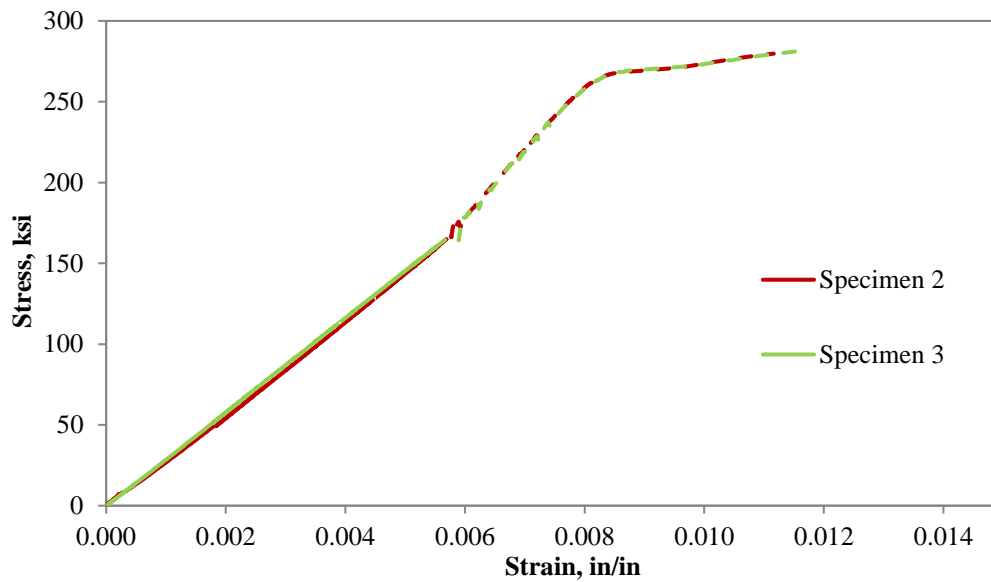
Figure 6-20. Stress-strain response of prestressing steel used in P3, P4, and UW1-1

The continuous lines are where the strain was directly measured and recorded by the data acquisition system, and the dashed lines are where the strain was calculated by taking the change in length of the specimen divided by the original length. The average yield stress was found to be 250.5 ksi, and the average modulus of elasticity is 29,449 ksi.

UHPC

The 3 in. diameter cylinders were cast and cured with the UHPC test piles and were tested in compression by Coreslab Structures, Inc. The measured strength of six of the cylinders is given in Table 6-3.

Table 6-3. UHPC compressive strength at 46 days for UHPC Piles P3, P4, and UW1-1

Cylinder #	f'_c, ksi
1	26.9
2	25.9
3	26.9
4	26.6
5	27.3
6	26.0
Average	**26.6**

The design strength of 26 ksi for the UHPC mix was achieved. The elastic modulus for the test piles was calculated using equation (2-2) from Section 2.3.4. The resulting elastic modulus was 7,502 ksi.

6.4. Driving of UHPC Test Piles

6.4.1. Test Site

The site for testing piles P3 and P4 was located on the same side of the bridge where the production UHPC pile would be installed to verify the capacity of the shortened UHPC production pile with respect to the production steel HP 10×57 piles. Figure 6-21 shows the approximate location relative to the Sac County bridge.
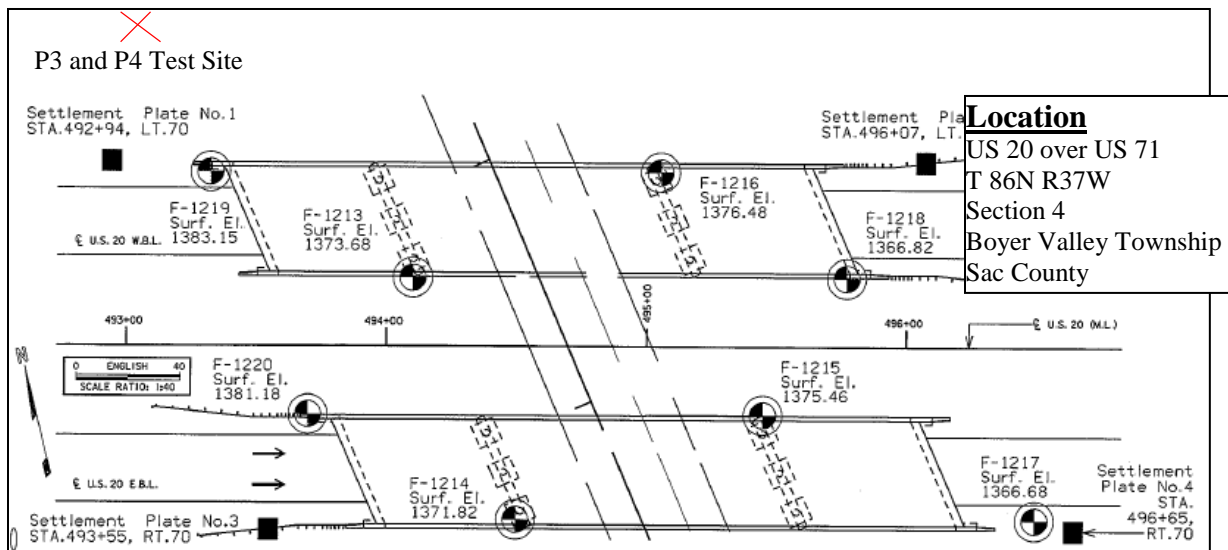
Figure 6-21. Location of test pile

6.4.2. Soil Profile

One standard penetration test (SPT) and one cone penetration test (CPT) were conducted by the Iowa State research team at the location of the test piles. The SPT was performed by TEAM Services on August 4, 2011, and the CPT was performed by Geotechnical Services, Inc. on August 10, 2011.

The soil at the Sac County bridge site consisted of cohesive clay and silty clay. The water table was located at a depth of approximately 20.50 ft according to the Iowa DOT soil report for borehole F-1219 near the west abutment of the westbound bridge. Figure 6-22 presents the toe resistance and side resistance from the CPT test while the soil classification reported by the Iowa DOT based on SPT and the classification by TEAM Services based on the CPT test and key soil properties are presented in Table 6-4.
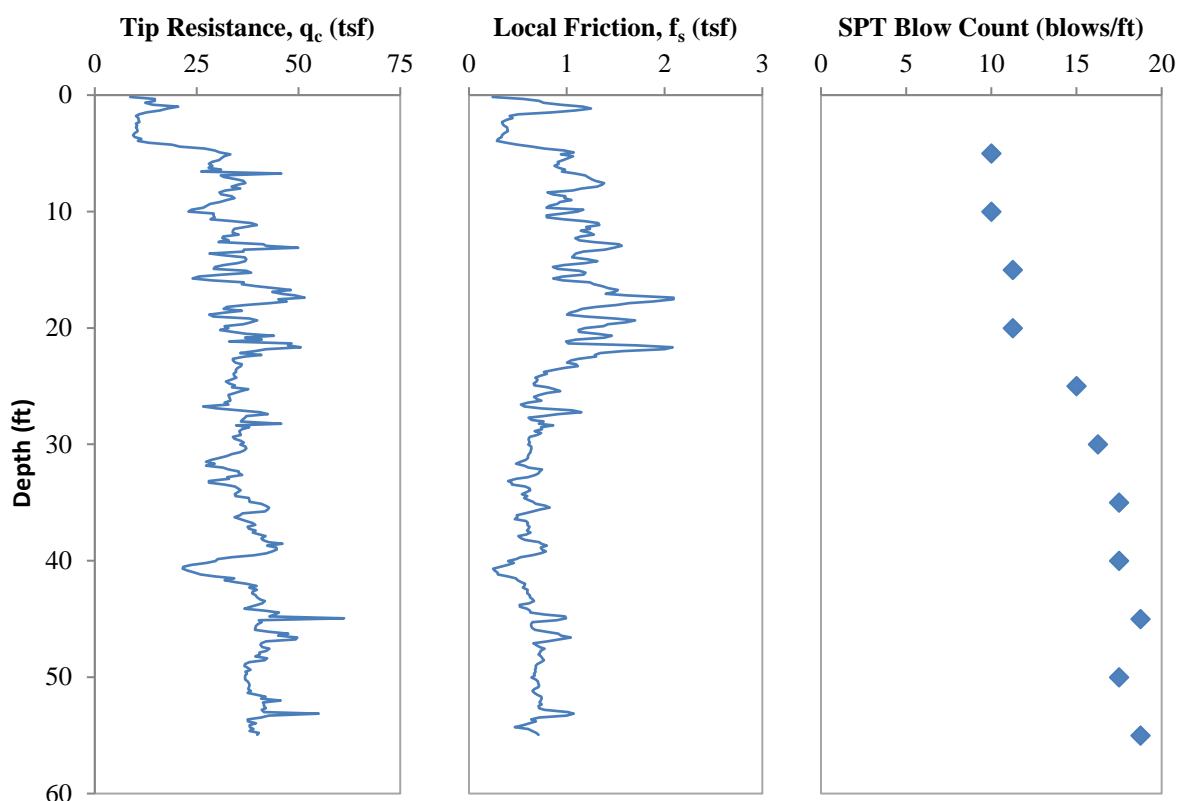
Figure 6-22. CPT and SPT data at the test pile location at the Sac County bridge site

Table 6-4. Undrained shear strengths and friction angles calculated from CPT data

Soil classification	Depth to bottom of layer, ft	Undrained shear strength, psi	Friction angle, degrees
Clay	4.43	11.52	34.9
Clayey silt to silty clay	10.66	28.02	35.8
Clayey silt to silty clay	16.4	31.07	34.9
Clayey silt to silty clay	17.88	41.66	35.8
Silty clay to clay	19.03	33.07	34.6
Sandy silt to clayey silt	55.12	31.45	32.9

Table 6-4 shows the undrained shear strength and friction angle for each soil layer, which was calculated from the CPT test results. The undrained shear strength and friction angle for each layer was calculated by using an empirically based approach described by Lunne et al. (1997).

6.4.3. Driving System

The HP 12×53 anchor piles were driven first, followed by P3, and then P4 at the locations indicated in Figure 6-23.

Total Pile Length = 80 ft
(with 73 ft driven into the ground)

Anchor Pile
HP 12x53

Total Pile Length = 45 ft
(with 42 ft driven into the ground)

Axial Load Test Pile P3
UHPC Pile

Total Pile Length = 80 ft
(with 73 ft driven into the ground)

Anchor Pile
HP 12x53

96.00''

96.00''

Splice Test Pile P4
UHPC Pile

48.00''

Total Pile Length = 30 ft
(with 27 ft driven into the ground)
Splice Location = 12 ft from ground surface

Figure 6-23. Locations of test piles P3 and P4 in plan view

A 4 in. thick plywood cushion with horizontal grain was used while driving P3 and P4. Even though the drivability analysis described in the following section indicated UHPC pile stresses during driving would be well within the allowable stress values with no pile cushion at the maximum hammer stroke, the pile cushion was used for the UHPC piles as a precautionary measure.

6.4.4. *Drivability Analysis*

In addition to the mentioned hammer properties in Section 6.4.3, an elastic modulus of 530 ksi and a coefficient of restitution of 0.8 were assumed for the hammer cushion. The elastic modulus and the coefficient of restitution for the plywood pile cushion used on the UHPC piles were assumed to be 30 ksi and 0.4, respectively, following Iowa DOT guidelines (Dirks and Kam 2003). The percent shaft resistance on the UHPC test piles and steel anchor piles was calculated using the undrained shear strength and friction angles calculated for the average CPT results using the FHWA computer program DRIVEN (Matthias and Cribbs 1998). The drivability analysis was conducted using GRLWEAP, and the maximum predicted stresses during driving for the UHPC and steel piles are shown in Table 6-5, which shows that both the tensile and compressive driving stresses for the test piles were well within the limits for UHPC.

Table 6-5. Predicted maximum stresses during driving of the UHPC test piles and steel anchor piles

	Pile	Maximum stress, ksi Predicted
RPS	Compressive stress	29.4
	Tensile stress	1.7
RPN	Compressive stress	29.4
	Tensile stress	1.7
P3	Compressive stress	7.2
	Tensile stress	0.1
P4	Compressive stress	5.9
	Tensile stress	0.0

6.4.5.   Driving Process

The first 40 ft of RPS was driven at the Sac County test site on December 6, 2011. The second 40 ft of RPS and both sections of RPN were driven on December 7, 2011. P3 and P4 were both driven on December 8, 2011. PDA equipment was used to monitor the driving of the HP 12×53 anchor piles, P3, and P4. Five restrikes were performed on the RPS, RPN, P3, and P4 at 5 minutes, 1 hour, 1 day, 3 days, and 7 days after the end of drive (EOD).

Steel Anchor Piles

The PDA equipment was bolted to the anchor piles while the pile was lying on the ground. In order to bolt the PDA equipment to the pile, five 3/8 in. diameter holes had to be drilled in the steel. Once completed, the steel piles were lifted into position by cutting a hole in the web and passing a crane hook through it. The pile was lifted to a vertical position while a second crane had the hammer leads. The steel piles were positioned inside the hammer leads at the correct location, and the helmet was placed on the top of the steel pile. When the leads, hammer, and pile were in place, the ram of the hammer was lifted manually by the crane and dropped.

Since the anchor piles were specified to be 80 ft in length, two 40 ft sections were spliced together for the anchor pile. After the first 40 ft section was installed, the second 40 ft section was picked up by the crane, and the two piles were spliced together by a butt-weld shown in Figure 6-24.

Figure 6-24. Steel HP 12 × 53 butt-weld splice

Once the welding was completed, the hammer was placed back on the pile and driving was resumed.

At the end of drive, both anchor piles, RPS and RPN, experienced minimal local buckling or bending of the flanges near the pile head. The top 12 in. were cut off as planned after the restrikes were performed to provide a level and even surface for the load frame to rest on.

UHPC Test Piles

Before P4 was installed, the two 15 ft long pieces were welded together horizontally on the ground as shown in Figure 6-25a.
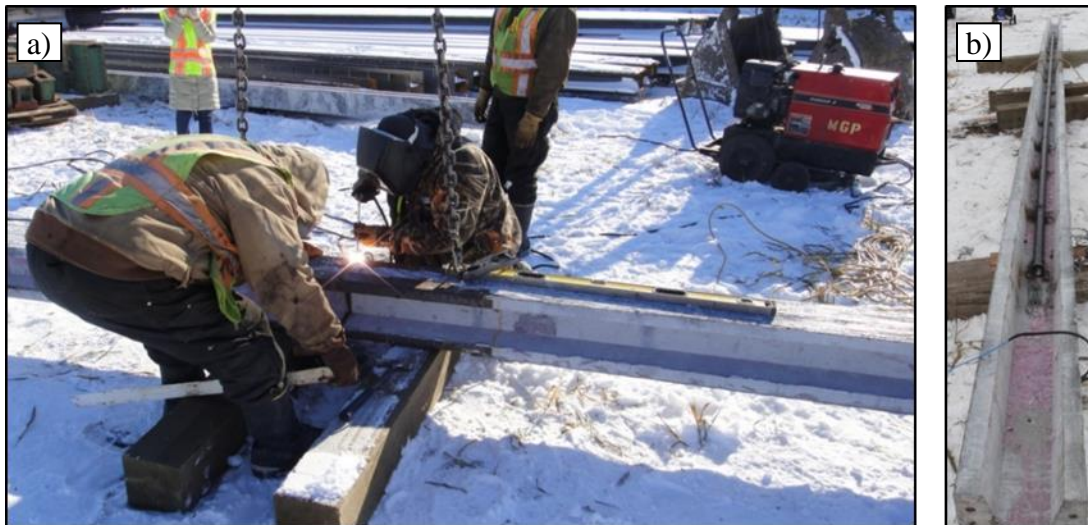
Figure 6-25. (a) Splicing of P4 horizontally on the ground and (b) after installing the steel pipe for the SAA equipment to P4

Once the splice was complete, the steel pipe for the SAA equipment was welded to the web of P4 so that it could be driven alongside the test pile as shown in Figure 6-25b.

The lifting hook cast into the UHPC piles to allow the piles to be raised into position with a lifting chain, similar to steel piles, was not used. Instead, a lifting strap was used to hold the head of the pile and insert the UHPC pile into the hammer leads lifted with the second crane.

The installation of the UHPC test piles was similar to that of the steel anchor piles. The low soil resistance at the beginning of driving required the ram to be raised manually several times before the hammer was able to develop enough combustion pressure to run continuously. PDA equipment monitored the driving of P3 and P4. During driving of P3, the bolt holding the accelerometer to the pile sheared off as the foot of the leads slid along the pile when the pile reached an embedment length of 38 ft. Driving was stopped temporarily to reattach the accelerometer with a new bolt. Precautions were taken from then on to ensure that the leads did not slide along the pile.

A 4 in. plywood pile cushion was used for the UHPC test piles, but both P3 and P4 punched through the pile cushion shortly after driving had begun. Instead of replacing the cushion with a new cushion, the pile was driven with essentially no cushion based on the experience in Phase I (Vande Voort et al. 2008). There was slight damage to P3 and no visible damage to P4 as shown in Figure 6-26 and Figure 6-27, respectively.

Figure 6-26. Slight damage observed to P3 pile head after driving the pile in place

Figure 6-27. No visible damage on P4 pile head after driving

The reason for the damage to P3 was the pile head was not perfectly centered under the helmet. It is also important to note that P3 tilted slightly during driving.

Strain readings were taken for each pile after driving. All of the strain gages in P3 and P4 were working after driving, giving an overall instrumentation success rate of 100%. Strains remained virtually unchanged from measurements taken shortly before driving, indicating minimal residual stresses in the piles. Overall, the UHPC test piles performed extremely well during driving.

6.4.6.   PDA Results

Steel Anchor Piles

The PDA confirmed that both anchor piles were not damaged during driving based on the shape of the force and velocity wave recorded at the pile head. The maximum compressive stress developed in RPS during driving was 28.5 ksi, and the maximum tensile stress was 1.2 ksi. The drivability analysis reported in Section 6.4.4, calculated the compressive stress with an error of 3.2%. The tension stress was underestimated by the drivability analysis but was still well below the allowable tensile stresses of 45 ksi for the south anchor pile. The CAPWAP results indicated the total capacity of RPS to be 369.3 kips with a Case damping factor of 0.242.

RPN had a maximum compressive stress during driving of 30.8 ksi, and the maximum tensile stress was 1.7 ksi. The drivability analysis reported in Section 6.4.4, calculated the compressive stress with an error of 4.5%. The drivability analysis predicted the maximum tensile stress with

0% error. The PDA results gave a total capacity of the RPN of 373 kips with a Case damping factor of 0.219.

UHPC Test Piles

P3 had a maximum measured compressive stress during driving of 5.4 ksi, and the maximum measured tensile stress was 0.2 ksi, which was measured by the PDA equipment attached near the pile head as shown in Figure 6-28.

Figure 6-28. Attached PDA equipment during the installation of P3

The drivability analysis reported in Section 6.4.4 over-predicted the compressive stress with an error of 33%. The tension stress was underestimated by the drivability analysis by 0.1 ksi and was still well below the pile's allowable tensile stress of 5.40 ksi. The PDA results gave a total capacity of 278.6 kips with a Case damping factor of 0.266.

P4 had a maximum compressive stress of 5.7 ksi, and the maximum tensile stress was 0.1 ksi during driving. The drivability analysis reported in Section 6.4.4, calculated the compressive stress with an error of 26.3%. The pile's tension stress was underestimated again only by 0.1 ksi and was still well below the allowable tensile stress of 5.4 ksi. The PDA results gave a total capacity of 170.1 kips with a Case damping factor of 0.083.

6.5. Vertical Load Test

6.5.1. Load Frame and Test Setup

The vertical load test was performed on P3 on December 16, 2011. Top and profile views of the test frame are shown in Figure 6-29 and Figure 6-30, respectively.
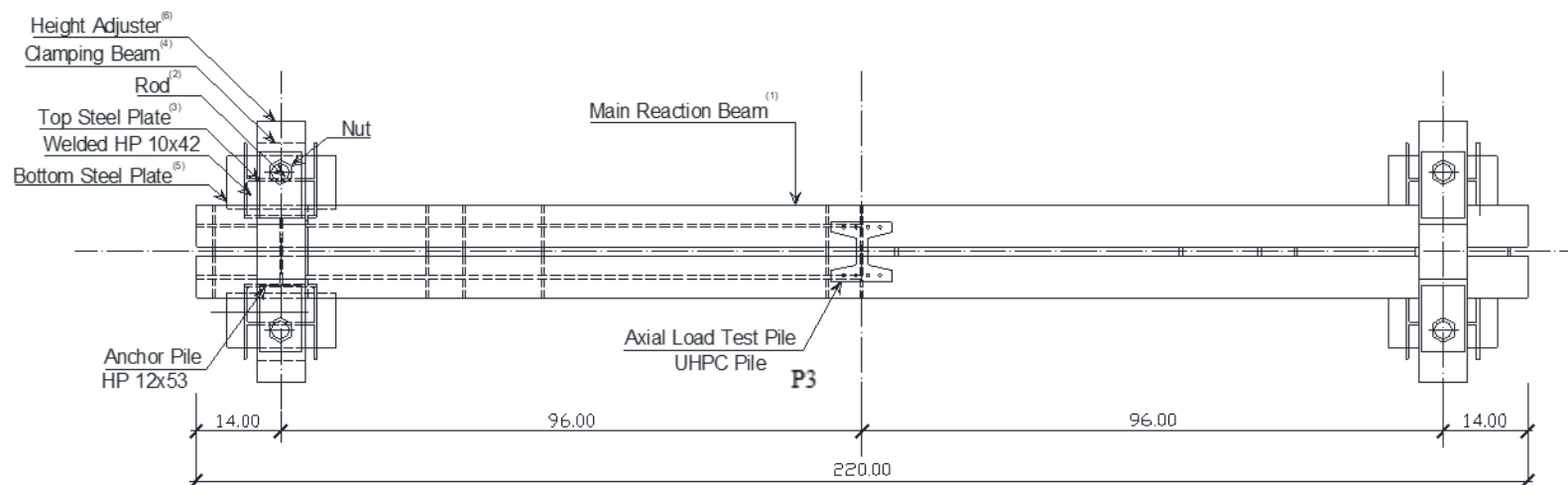
Figure 6-29. Top view of vertical load test setup

Note in the figure that all dimensions are in inches.
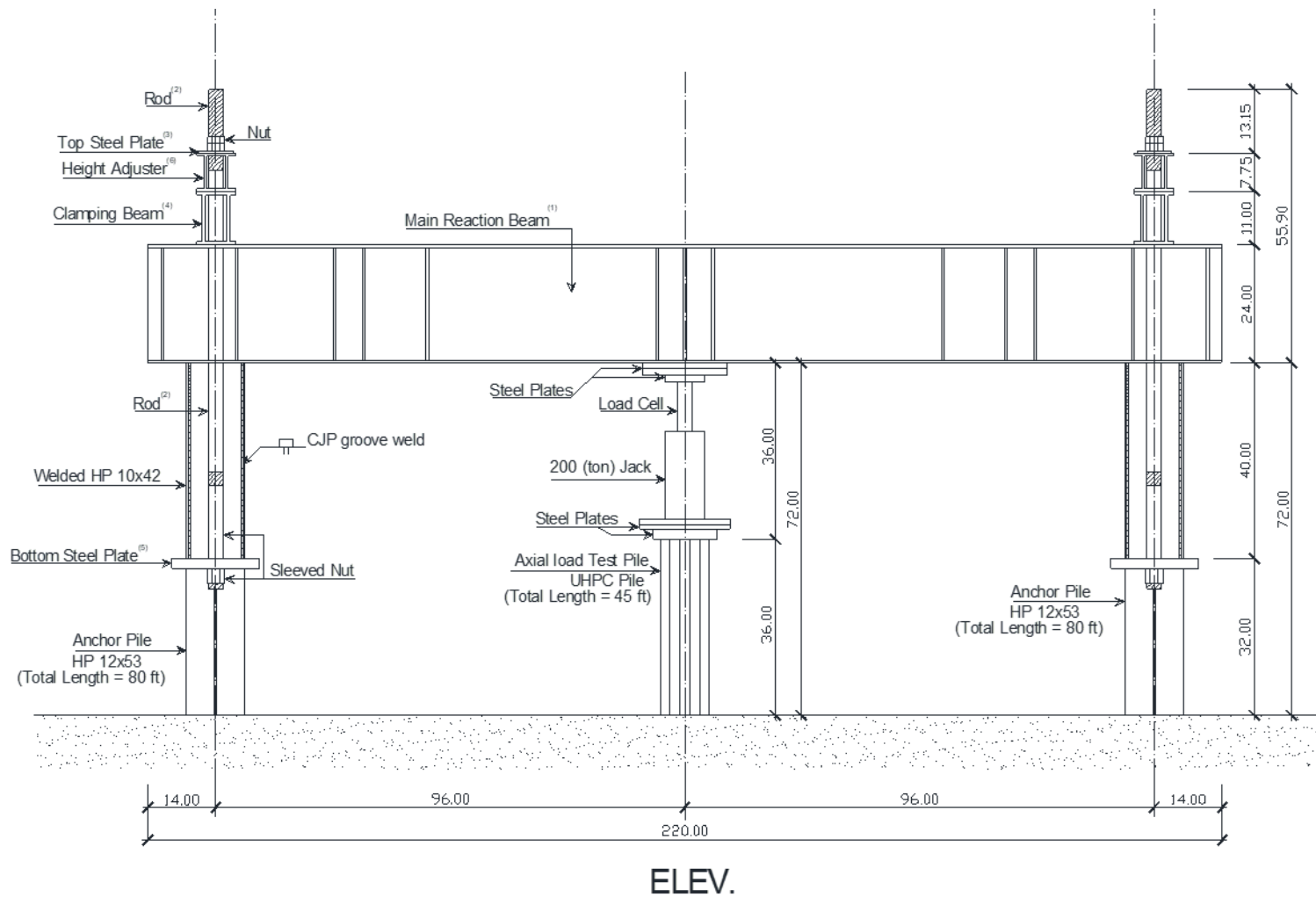
Figure 6-30. Elevation view of vertical load test reaction frame

After the seven-day restrike, the top 12 in. was cut off of the anchor piles and two shorter HP 10 × 57 pieces were welded to each of the anchor piles. The main reaction beam was lifted and placed on the protruding flanges of the pile's shorter side pieces. The 3 in. diameter rods were lowered through the holes in the height adjusters and clamping beams and through the spaces between each side pile piece web and each corresponding anchor pile web. Finally, sleeved rod nuts were tightened against the bottom plate directly underneath each side pile piece. The completed load frame is shown in Figure 6-31.

Figure 6-31. Completed axial load test setup

A hydraulic jack was used to apply a vertical load on P3 and imposed an equal and opposite load upward on the main reaction beam. The main reaction beam reacted upward against the clamping beams and transferred to the 3 in. diameter rods on either side of the main reaction beam. The rods reacted against the plates on the bottoms of each side pile piece, and the welds transferred the vertical load from the side pile pieces to the anchor piles and then to the soil. The anchor piles were subjected to axial tension throughout the test.

The load capacity of the test frame was controlled by the friction capacity of the anchor piles. Using a safety factor of two on the capacity of the anchor piles, the maximum load that could be applied to P3 was 340 kips. If the friction capacity of the anchor piles was not exceeded first, the load test frame could be used to apply a load of 680 kips to P3, which would be controlled by the tension capacity of the 3 in. diameter rods.

A 200 ton hydraulic jack was used to apply the vertical load on P3, and a 400 kip load cell was used to measure the applied load as shown in Figure 6-32.
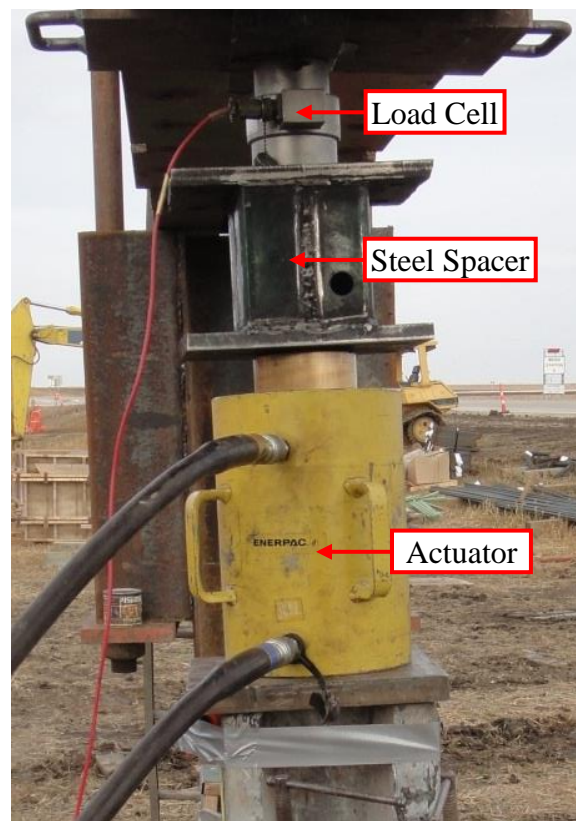
Figure 6-32. Vertical load testing equipment

Four 10 in. stroke displacement transducers were used to measure the vertical displacement at the top of P3 (Figure 6-33).
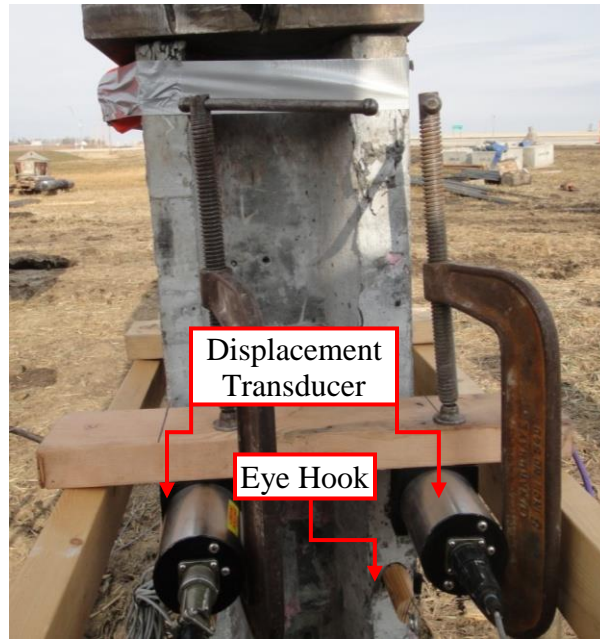
Figure 6-33. Displacement transducers

These transducers were mounted on 2 x 4 in. wooden reference beams, which were supported approximately 6 in. away from the pile on either side by attachment to short ladders. This set-up allowed for the pile displacement to be measured independent of the test load frame. The displacement transducers were attached to the top of the pile using eye hooks screwed into wooden pieces and glued with epoxy to the test pile in the field.

All embedded concrete strain gages in P3 were functioning and were zeroed before the load test began. The gages were used to calculate strains at various depths throughout the pile. Data from the load cell, deflection transducers, and strain gages were collected using a Megadac data acquisition system as shown in Figure 6-34.

Figure 6-34. Data acquisition system

6.5.2.   Test Procedure

The vertical load test was completed following "Procedure A: Quick Test" as outlined in ASTM D1143/D1143M-07. Accordingly, the test pile was loaded in 5% increments up to the anticipated failure load. The load was kept relatively constant during each load step until deflection readings had stabilized, which was specified as a minimum of 5 to 15 minutes for each step. Deflection, strain, and load measurements were recorded electronically every second. To estimate when failure occurred, the load-displacement behavior of P3 was monitored at each load step by hand. The Davisson failure criterion (1972) was used to determine the ultimate capacity of the pile and terminate the vertical load test. P3 was unloaded in five equal steps.

The vertical load test on P3 was performed on December 16, 2011 at the Sac County site near the west abutment of the westbound bridge. The calculated failure loads for P3 was approximately 200 kips according the Iowa DOT Blue Book Method and 216 kips from the DRIVEN computer software. The undrained shear strengths from averaged CPT results was used as input for the soil conditions within DRIVEN. A maximum load of 200 kips was planned for the test. The actual loading sequence of P3 is given in Table 6-6.

Table 6-6. Vertical load test step for P3

Approximate % of predicted failure load	Load applied, kips	Load duration, min
5	10	15
10	20	15
15	30	15
20	40	10
25	50	5
30	60	5
35	70	5
40	80	5
45	90	5
50	100	5
55	110	5
60	120	5
65	130	5
70	140	5
75	150	5
80	160	5
85	170	5
90	180	5
95	190	5
100	200	5
Overloading	210	5
Overloading	220	5
Overloading	230	5
Overloading	240	5
Overloading	250	5
Overloading	260	5
Overloading	270	5
Overloading	280	5
Overloading	290	5
Overloading	297	5
Unloading	270	5
Unloading	240	5
Unloading	210	5
Unloading	180	5
Unloading	150	5
Unloading	120	5
Unloading	90	5
Unloading	60	5
Unloading	30	5
Unloading	0	-

The anchor piles did not show noticeable movement at the planned maximum load of 200 kips, so the load on P3 was increased further using the same loading increments of 10 kips until a final load of 300 kips. After the final load was reached, the pile was unloaded in 30 kip increments.

6.5.3.   Observations and Test Results

Load-Displacement

The load-displacement behavior of P3 is given in Figure 6-35.
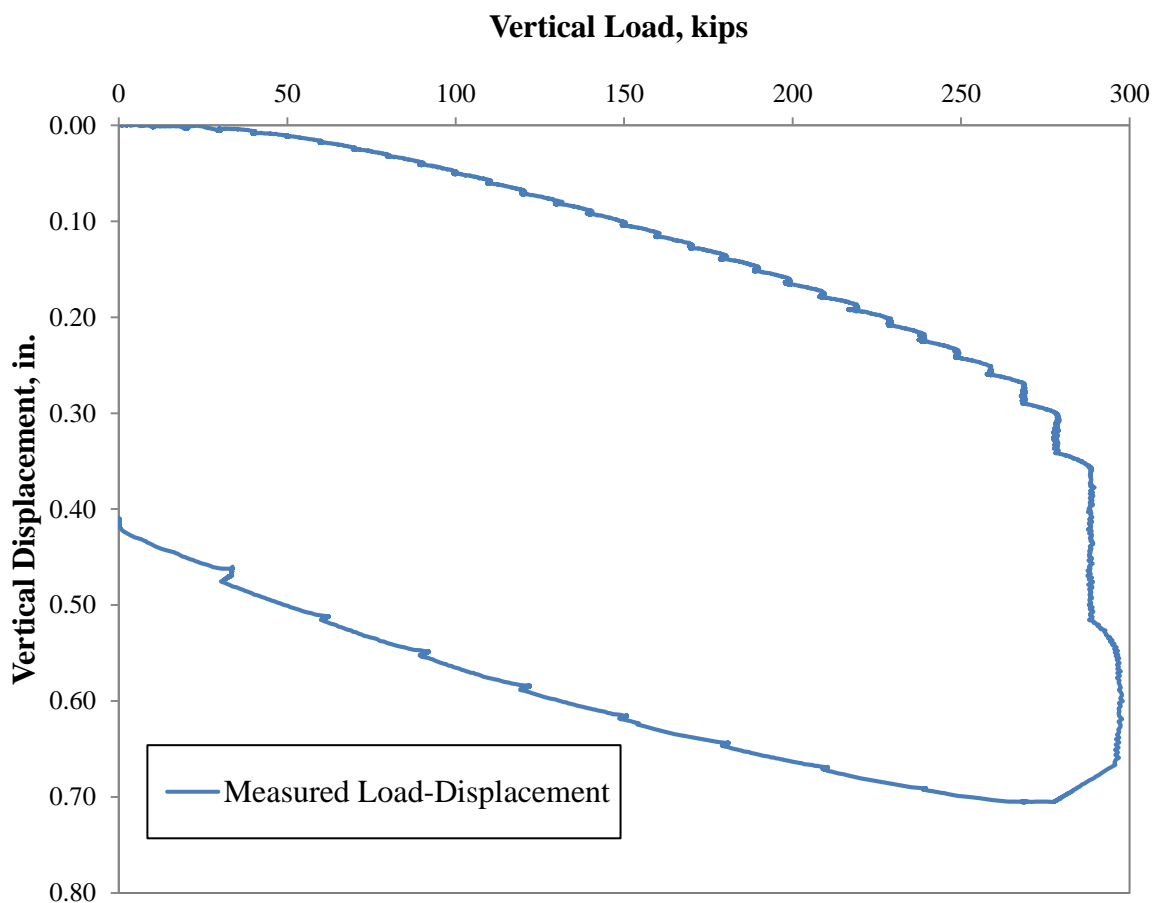
Vertical Load, kips

Figure 6-35. Observed load-displacement behavior for the vertical load test of P3

P3 was loaded to a maximum value of 297.25 kips and underwent a maximum downward displacement of 0.65 in. during this load step. The test pile continued its downward displacement for the first unloading step and reached a maximum downward displacement of 0.71 in.

A permanent vertical displacement of 0.42 in. of the test pile was recorded 3 minutes after the unloading procedure was completed. The relationship between load and displacement can be represented by connecting the average load and average displacement for each load step as illustrated in Figure 6-36.
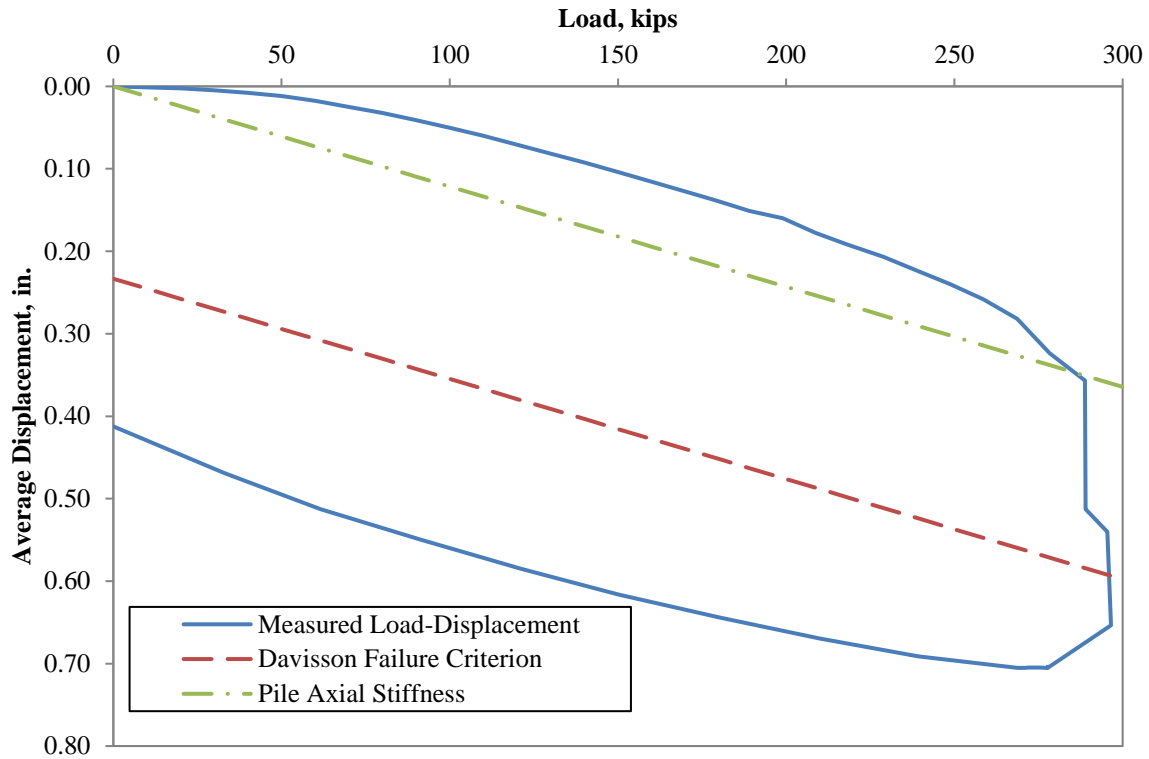
Figure 6-36. Load-displacement behavior established from the maximum load points and Davisson failure criterion for the vertical load test of P3

The pile axial stiffness was calculated using equation (6-1) and is shown in Figure 6-36, along with the Davisson failure criterion line, which was calculated using equation (6-2) (Davisson 1972). The load at the point where the Davisson failure criterion crosses the measured load-displacement curve is the capacity of the pile. The results from the vertical load test found the capacity of P3 to be 297 kips.

$$\Delta_k = \frac{PL}{AE} \tag{6-1}$$

where,
P = axial load, kips
L = length of pile, in.
A = cross-sectional area, in.^{2}
E = modulus of elasticity, ksi

$$\Delta_{Davisson} = \frac{PL}{AE} + 0.15 + \frac{D}{120} \tag{6-2}$$

where,
D = diameter of pile, in.

Load Transfer

The strain gages embedded along the length of P3 provided information about the skin friction along the pile. Figure 6-37 shows the average calculated load transfer along the length of the pile from the measured strains.
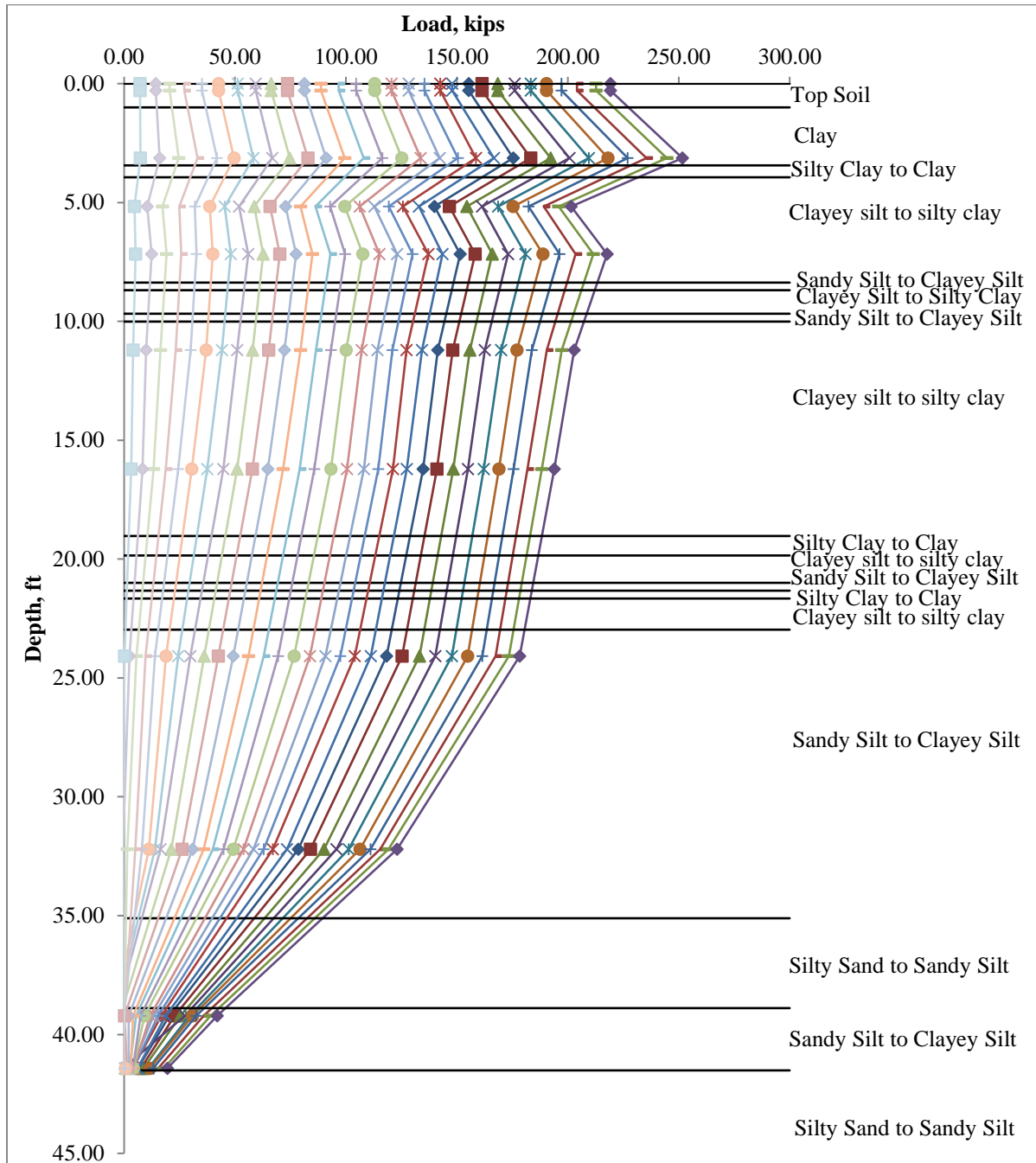
Figure 6-37. Measured force transfer response of P3 during the vertical load test

The maximum vertical load applied to P3 was 297.25 kips. In comparison, from the force transfer estimated from the strain gage data, a maximum load of 220 kips determined at the gage location 4 ft from the pile head, which is right at the ground surface.

There are some possible reasons that the load transfer obtained at the ground surface does not match the measured applied load. One such reason could be due to the prefabrication process. The embedded strain gages were hung between two prestressing strands as shown in Figure 6-38.

Figure 6-38. Suspended embedded strain gages

When UHPC was poured, the gages could have tilted in the y-direction or shifted in the x-direction, causing the gage to be subjected to bending. Also, when the gage shifts the distance from the gage to the neutral axis changes from the specified distance and could be different for every gage.

As mentioned in Section 6.4.4, there were some defects in the pile from the prefabrication process. One of the defects is an inconsistent flange thickness near the pile head, which could cause a change in stiffness and an unsymmetrical cross-section.

There was also an issue with the test set-up and installation of P3. The test pile was installed very close to two push-in pressure cells as shown in Figure 6-39.
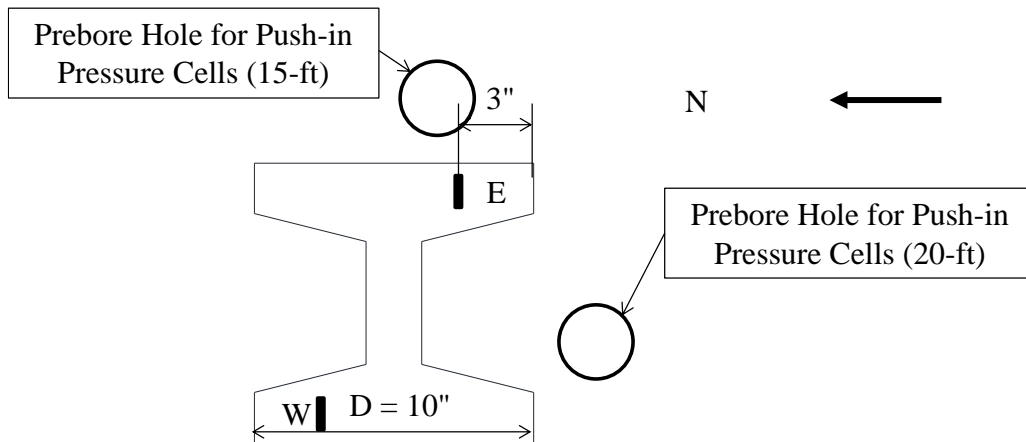
Figure 6-39. Locations of push-in pressure cells

To install the push-in pressure cells, 4 in. diameter holes were drilled, and the cells were pushed to the specified depth. The depth of one of the push-in pressure cells was 15 ft and the other was 20 ft from the ground surface. The proximity of these cells may have led to a reduction of the skin resistance along the pile, resulting in some eccentricity as a result of the non-uniform forces resisting the vertical load. In addition to the push-in pressure cells, it is worth noting that a void filled with water around P3 was formed due to driving as shown in Figure 6-40.

Figure 6-40. Void that formed from installation of P3

The depth of the void was measured to be 5 ft deep from the ground surface.

After the installation was complete, it was noticed that the pile was not installed vertically, but at an angle in both the x-axis and y-axis direction. Figure 6-41a and b show the tilt of P3 in the strong-axis and weak-axis direction, respectively.

Figure 6-41. Tilt of P3 after driving in the (a) weak-axis and (b) strong-axis direction

The angle causes load that is measured by the load cell to be the resultant force of two force components, vertical (P_v) and horizontal (P_h) as illustrated in Figure 6-42a and b. When testing to vertical loads, a moment is induced due to horizontal force P_h.
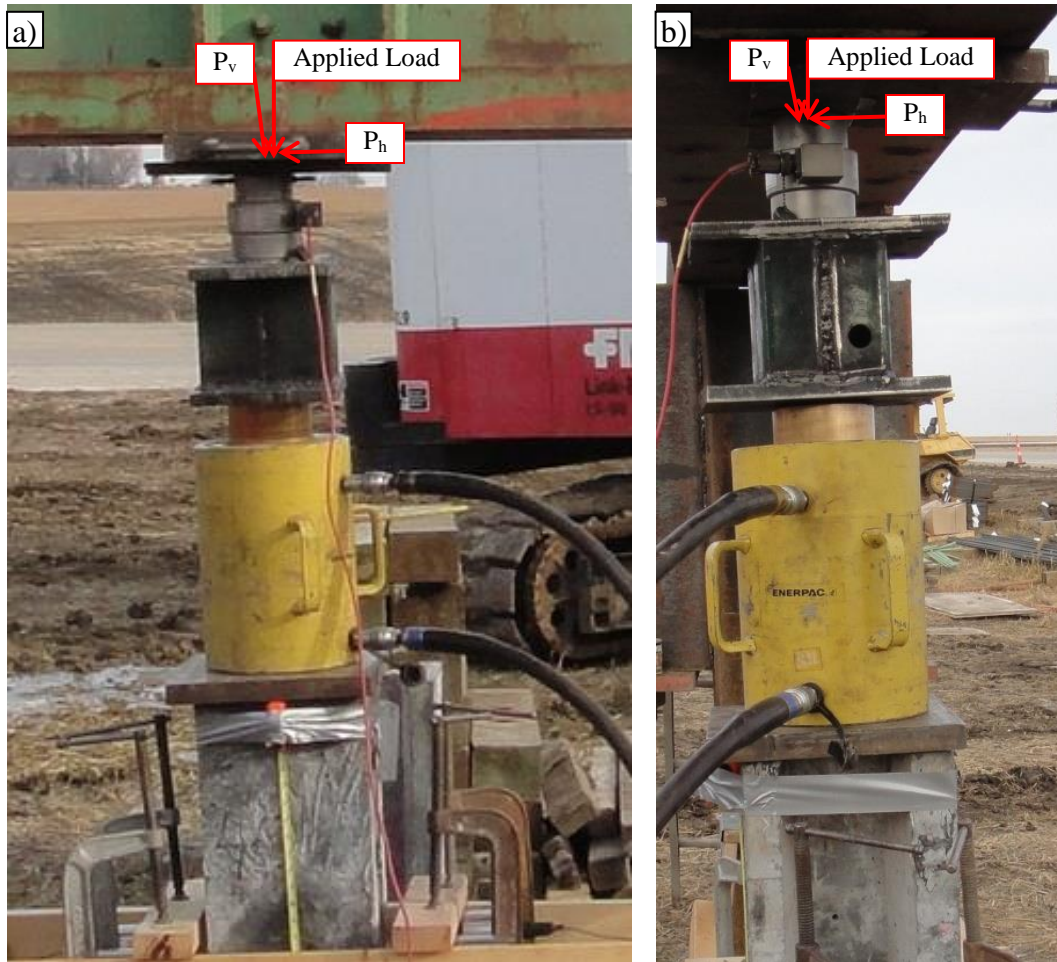
Figure 6-42. Components of applied load during vertical load test in the (a) weak-axis and (b) strong-axis direction

There was another issue during testing, which is due to the actuator being not positioned exactly on the center of the pile. This caused the vertical force to be applied with an eccentricity. There was an eccentricity in the x-axis and y-axis directions, which are also shown in Figure 6-41a and b, respectively.

To ensure that the measured applied load was accurate, the load cell was tested on April 23, 2012 with the universal compression machine in the ISU laboratory. The load cell had a 100 kip compression load applied to it and measured 99.9 kips, which resulted in an error of 0.1%.

Using estimated unit skin friction values, the load transfer curve was corrected to reflect the actual load that was applied to the pile head. Figure 6-43 shows the measured loads along the length of the pile as solid lines, and the corrected portions of the load transfer are shown as a dashed line.
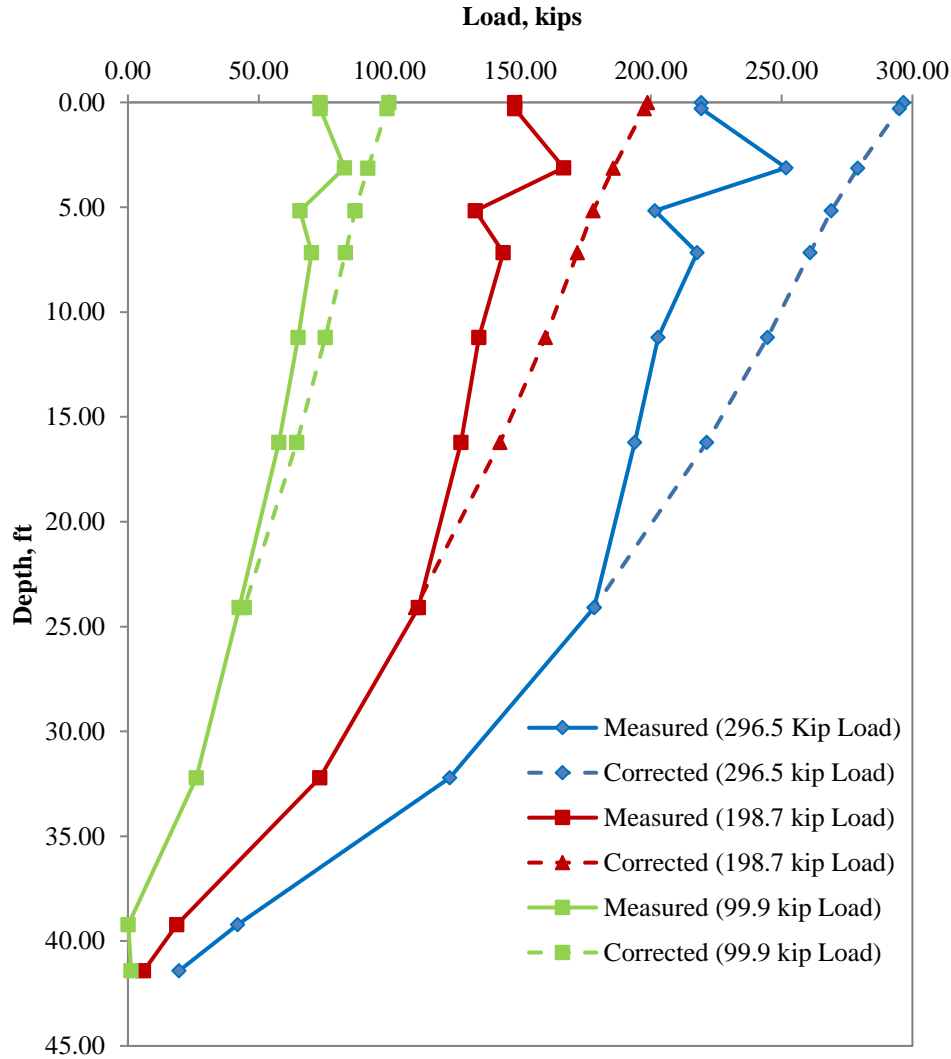
Figure 6-43. Measured and corrected load-transfer curves for three load steps

Only the 100, 200, and 300 kip load steps are shown in this figure.

6.6. Lateral Load Test

6.6.1. Test Setup

The UHPC test piles, P3 and P4, underwent a lateral load test on December 19, 2011. For the test, P3 was in strong-axis bending while P4 was in weak-axis bending and included a splice at 15 ft from the pile head. The elevation view of the setup for the designed lateral load test is shown in Figure 6-44.
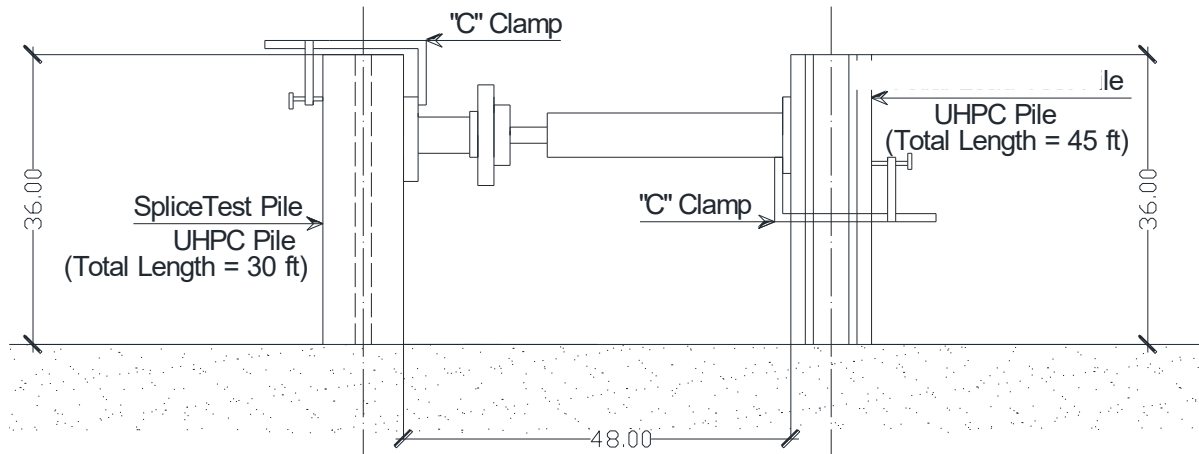
Figure 6-44. Elevation view of lateral load test setup

The field measurements identified that P3 had 3.83 ft exposed above the ground surface, and P4 had 2.98 ft exposed above the ground surface after driving and the specified restrikes.

A 100 kips actuator was used to apply the lateral load to P3 and P4 simultaneously. The actuator was clamped to P3 14.5 in. below the pile head and a steel spacer was clamped to P4 8 in. from the pile head. A 300 kips load cell was used to measure the applied load, which was positioned in line with the actuator and steel spacer. The actuator, load cell, and steel spacer are identified in Figure 6-45.
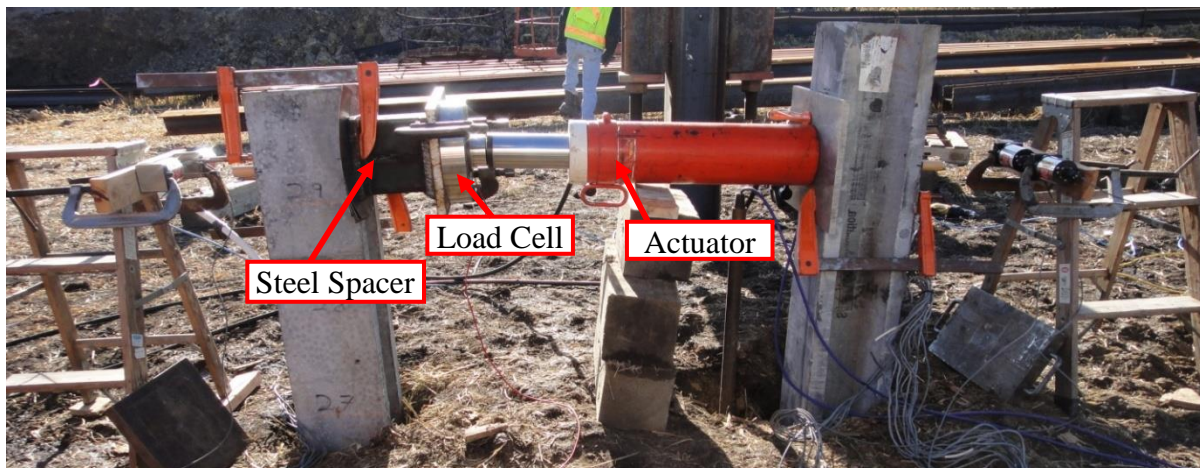
Figure 6-45. Setup used for the lateral load test

Two 10 in. displacement transducers were used to measure the lateral displacement at the top of each pile. The transducers were completely extended at the beginning of the test and were mounted to 2 x 4 in. wooden reference beams, which were supported approximately 1 ft from each of the piles on short ladders. The transducers were connected to the top of the pile using eye hooks screwed into wooden pieces glued to the pile head, as shown in Figure 6-46.
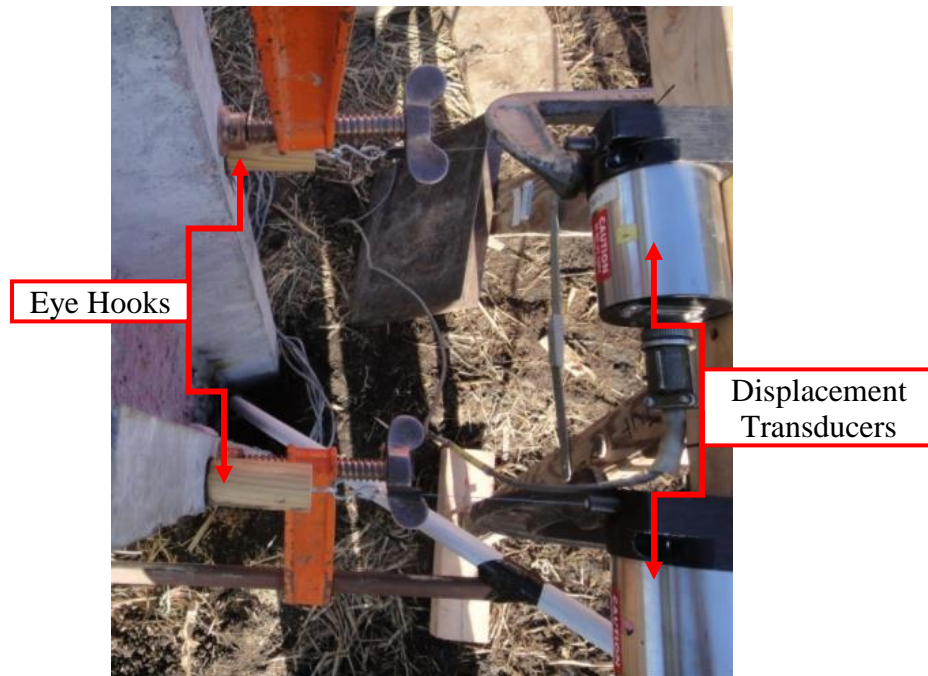
Figure 6-46. Displacement transducers and eye hooks mounted to P4

Test data on the UHPC piles were measured independently from each other as illustrated in Figure 6-47.

Figure 6-47. Illustration of eye hook and SAA Instrumentation location

A new piece of equipment was purchased to measure the displacement along the length of P4, which is called the SAA. The SAA was inserted into a steel tube that was welded to the embedded plates. The SAA ran along the east side of P4 as illustrated in Figure 6-47 for 20 ft. Three dimensional displacements and rotations were read starting 34.25 in. from the pile head. The x-axis of the SAA was lined up with the lateral force direction.

Throughout the length of pile P3, the top nine levels of embedded concrete gages had strain measurements recorded, while P4 had only three levels of gages providing strain measurements only along the upper portion of the P4. Data from the load cell, deflection transducers, and strain gages were collected using the Megadac data acquisition system, and the data from the SAA instrument was collected using the CR-1000 data logger.

6.6.2. Test Procedure

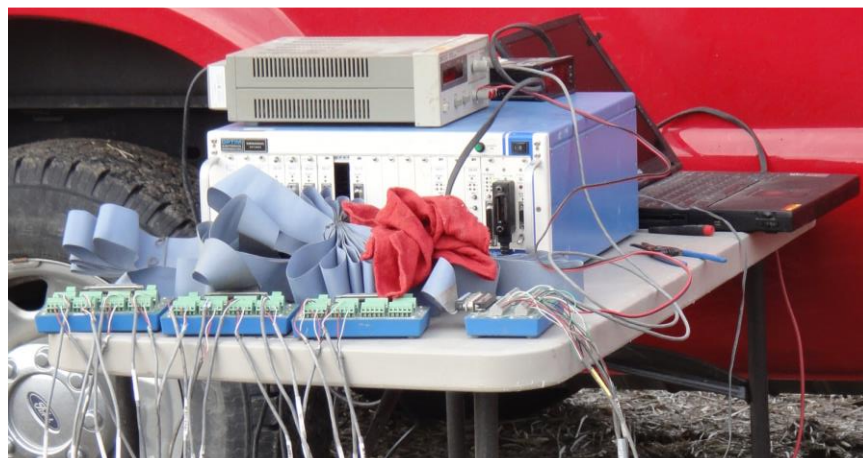The lateral load test was completed following "Procedure A: Standard Loading" of ASTM D3966-07. The procedure recommends applying a test load equal to 200% of the proposed pile lateral design load unless failure occurs first. Table 6-7 details the load steps used during the lateral load test.

Table 6-7. Lateral load sequence

% of design load	Load duration, min
0	10
25	10
50	15
75	20
100	20
125	20
150	20
170	20
180	20
190	20
200	60
150	10
100	10
50	10
0	-

A design load of 10 kips was used for the test.

To apply the lateral load to the UHPC test piles, a manual hydraulic jack was used for the test. During each load step, the load was kept relatively constant until deflection measurements had stabilized for a minimum duration of 10 minutes or a maximum duration of 20 minutes required by ASTM D3966-07. Deflection, strain, and load readings were electronically recorded once every second.

6.6.3. Observations and Test Results

The first part of the lateral load sequence used to test the UHPC piles is shown in Table 6-8, which consisted of force-controlled load steps.

Table 6-8. Force-control loading sequence during cycle 1 of the lateral load test

Lateral load, kips	Load duration, min
2.5	10
5.0	10
7.5	15
10.0	20
12.5	20
15.0	23
17.0	23
18.0	21
19.0	21
20.0	24
15.0	10
10.0	10
5.0	10
0.0	-

For the remaining cycles, the piles were displacement-controlled based on the measurements taken from test pile, P4, and is outlined in Table 6-9.

Table 6-9. Displacement-controlled loading sequence during load step 2 through 4 of the lateral load test

Load step	Lateral displacement, in.	Lateral load, kips
2	4	6.1
3	7	9.5
4	10	16.2

Between each cycle the UHPC test piles were unloaded to 0 kips of lateral load.

The actual applied loads varied slightly from those shown in Table 6-8. Since the manual hydraulic pump was used, the loads were applied very slowly. A combination of minor leakage in the hydraulic system and soil creep caused the applied load at each load step to drop slightly over the duration of each load step. The magnitude of the load reduction increased with increasing load step duration and applied load.

P3

P3 was tested in strong-axis bending during the lateral load test. The resulting force-displacement curve is given in Figure 6-48.
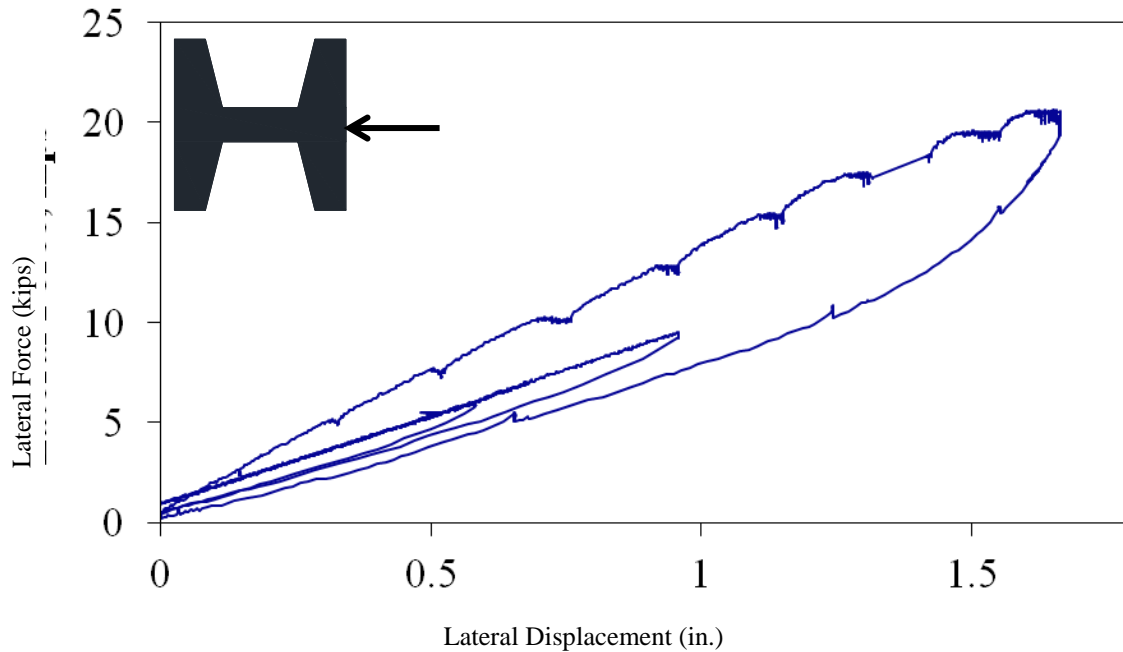
Figure 6-48. Force-displacement response of P3 during lateral load test

The pile was subjected to a maximum load of 20.6 kips with a lateral displacement of 1.7 in. A residual displacement of 0.08 in. was recorded after the pile was unloaded for the first cycle and a total residual displacement of 0.03 in. after all of the cycles were completed.

The tensile strain and compressive strain measurements along the length of the pile were obtained from the embedded strain gages. The information from the gages was used to calculate the bending moment resulting from the lateral loading on the pile. Two gages on the tension side of the pile stopped working during the test. Figure 6-49 shows the measured tensile strain compared to the measured compressive strain at the top six levels of strain gages in P3.
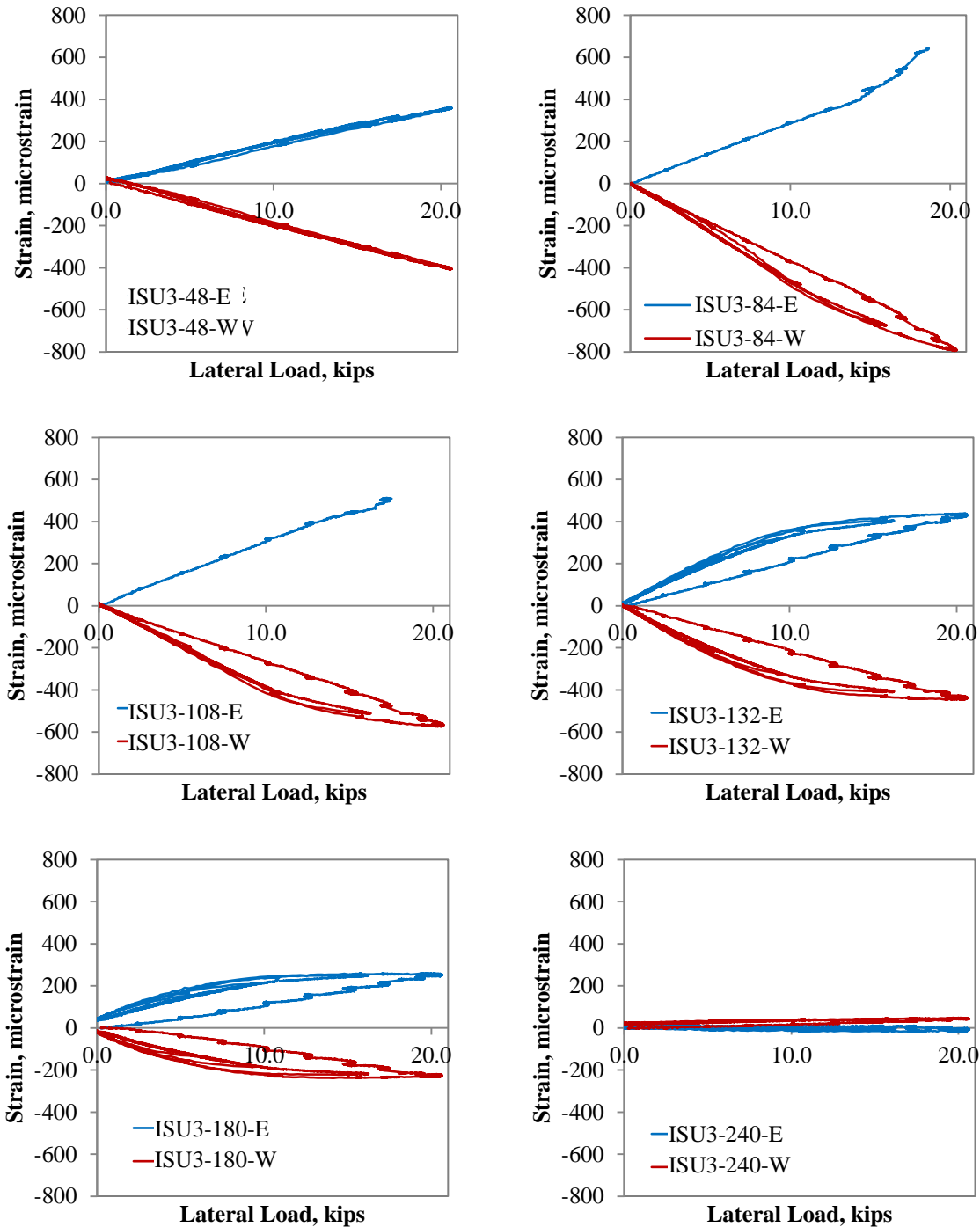
Figure 6-49. Measured compression strain compared to measured tensile strain for top six levels of strain gages from P3 during the lateral load test

As expected, the magnitude of strains in tension and compression are comparable, confirming the elastic response of the pile.

Table 6-10 identifies the lateral load and strain reading at which the embedded concrete gages stopped working.

Table 6-10. P3 gages that stopped working during lateral load test

Gage	Lateral load, kips	Strain, microstrain
P3-108-E	17.2	511
P3-84-E	18.7	643

The broken gages were identified by a large, sudden jump of two orders of magnitude in the strain value. The information collected after the gages stopped working was discarded.

P4

The test pile, P4, was tested in weak-axis bending, and exhibited a greatly reduced stiffness compared to P3 as expected. Figure 6-50 shows the pile's force-displacement curve.
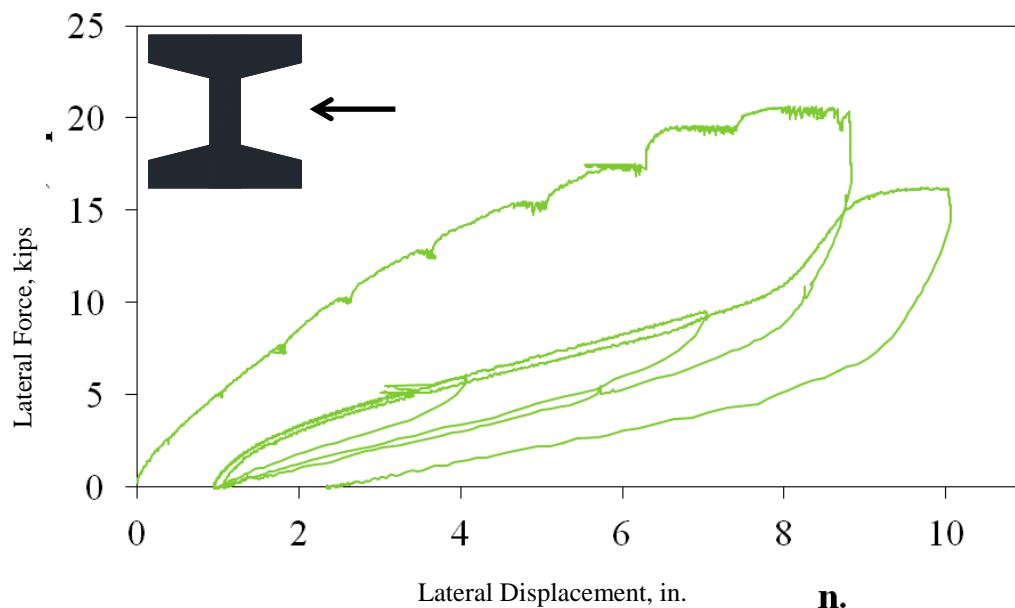
Figure 6-50. Force-displacement response of P4 during lateral load test

The pile was subjected to a maximum load of 20.6 kips with a corresponding lateral displacement of 8.3 in. during the first cycle. The maximum displacement achieved in the pile was 10 in. of lateral displacement. There was noticeable heaving of the soil on one side of the pile during the test, as shown in Figure 6-51.
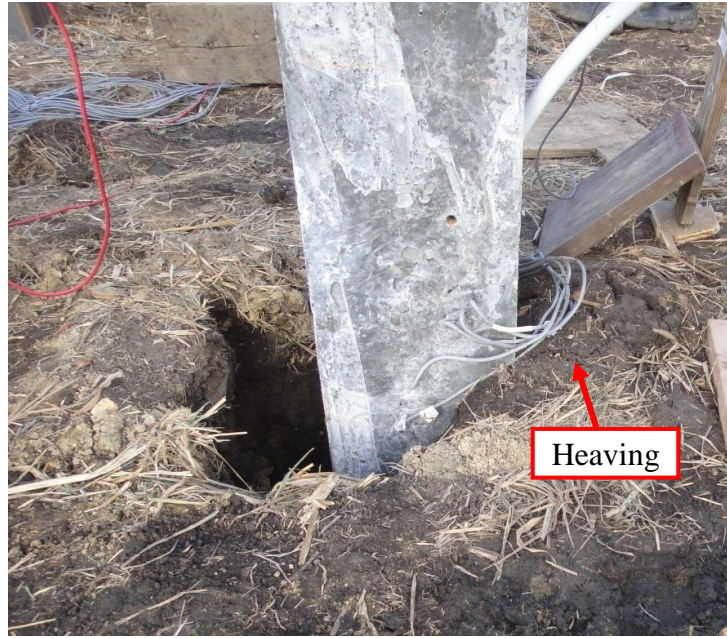
Figure 6-51. Heaving of soil during lateral load test of P4

P4 had a 0.95 in. residual displacement after the first cycle and a 2.35 in. residual displacement after the pile was unloaded for the final time.

The tensile strain and compressive strain measurements along the depth of the pile were obtained from the embedded concrete strain gages. The information from the gages was used to calculate the bending moment along the length of the pile resulting from the lateral loading. Figure 6-52 shows the tensile strain compared to the compressive strain at various strain gage levels.
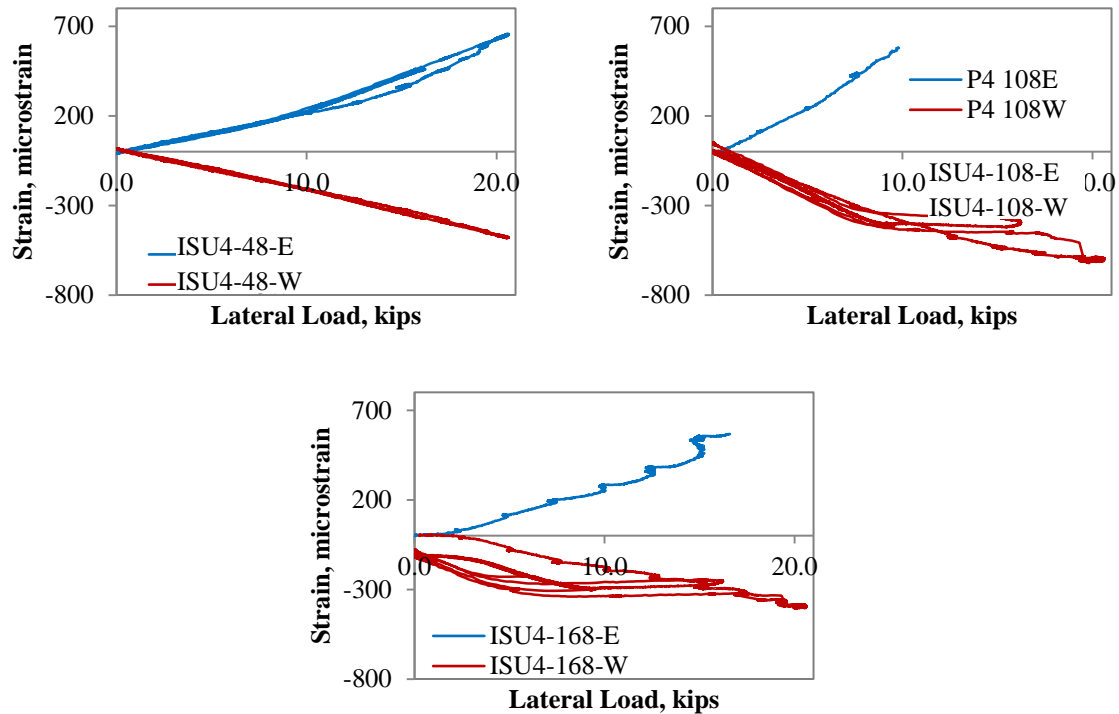
Figure 6-52. Measured compression strains compared to measured tension strains for all three levels of strain gages in P4 during the lateral load test

The gages embedded in P4 that stopped working during the lateral load test are identified in Table 6-11.

Table 6-11. P4 gages that stopped working during lateral load test

Gage	Lateral load, kips	Strain, microstrain
P4-108-E	9.8	581
P4-168-E	16.5	566

Again, the procedure to identify these gages was to identify the time when an unrealistically large sudden jump in strain was recorded. The range of data identified to be unreliable was disregarded during the analysis.

6.6.4. *Excavation of Test Pile P4*

The visual evaluation of the splice performance in P4 during the lateral load test was done by excavating the soil down to the location of the splice as shown in Figure 6-53.

182

Figure 6-53. Excavation of soil surrounding P4

The contractor tried to pull the pile out of the ground using a crane but had to terminate this plan because the crane was starting to tip. As a result, the excavation was completed on January 5, 2012 and only went 12 ft below the ground surface to the location of the splice.

A fairly large crack was discovered 9 ft from the pile head on the tension side of P4, which corresponded to the maximum moment location predicted in LPILE as described in Section 6.6.5. Figure 6-54 depicts the crack on the northwest corner of P4. No damage was observed in the splice.

Figure 6-54. Flexural crack found 9 ft from the ground surface on P4 due to the lateral load test

6.6.5.   *LPILE Analysis*

LPILEPLUS 5.0 was used to analyze the force-displacement behavior of P3 and P4 under lateral loading. The average undrained shear strengths calculated from the CPT test data and the

moment-curvature response calculated for strong-axis and weak-axis bending at 0 kips axial load were used as input values into LPILE. Figure 6-55 compares the measured force-displacement curve of P3 to the predicted and adjusted responses calculated in LPILE.
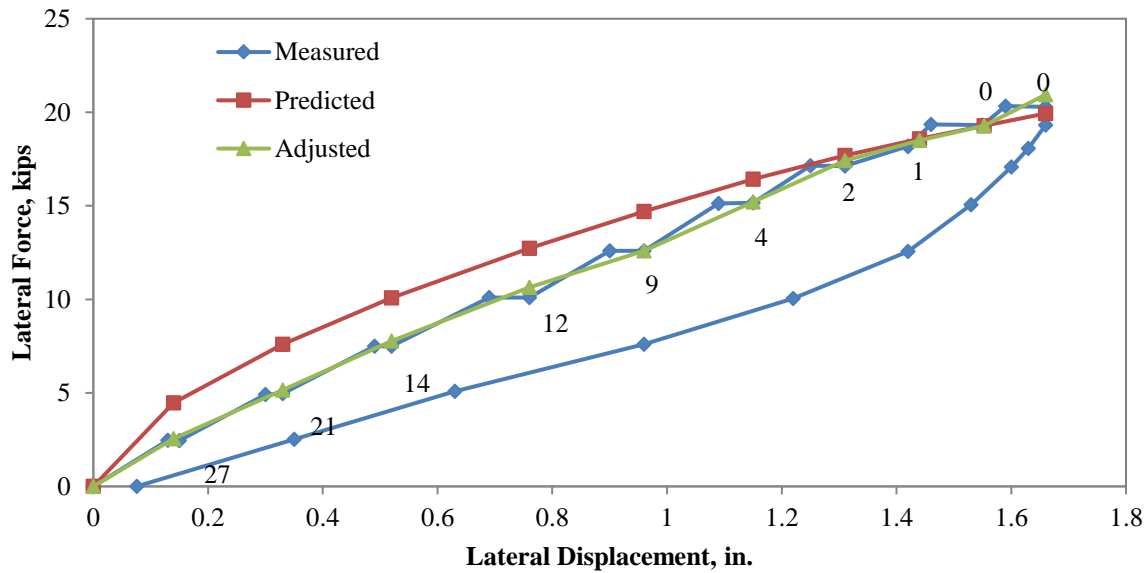
Figure 6-55. Predicted, adjusted, and measured force-displacement response of P3 during lateral load test

Additionally, the predicted, adjusted, and measured responses of P4 are shown in Figure 6-56.
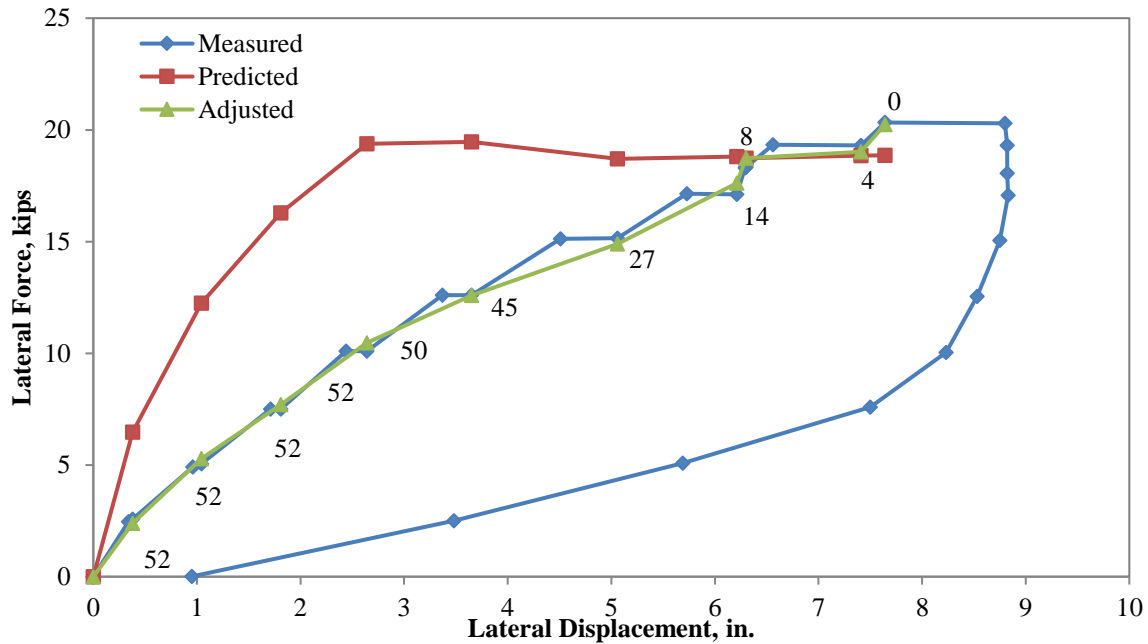
Figure 6-56. Predicted, adjusted, and measured force-displacement curve for P4 subjected to the lateral load test

The predicted curve was calculated using the CPT data from the test pile location as the soil input in LPILE. During driving, a noticeable gap was discovered around both UHPC test piles. An adjusted curve was calculated to take into account the changing gap as the pile displaces during the lateral load test. Figure 6-55 and Figure 6-56 include the gap depth for each load step in inches next to the force-displacement point.

The moment corresponding to the predicted and adjusted displacements were calculated so that they could be compared with the average measured moments for both P3 and P4. The average measured moments were calculated from the tension and compression strains, which were then averaged. Figure 6-57 and Figure 6-58 compare the moments calculated from the predicted and adjusted models for the 12.5 kips load step for P3 and P4, respectively.
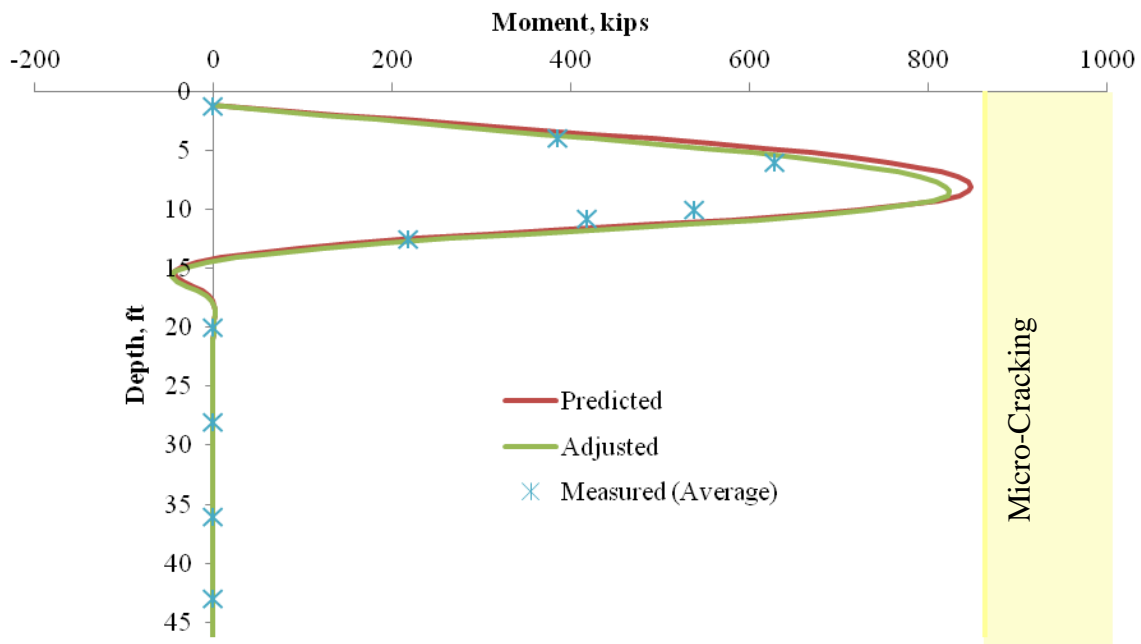
Figure 6-57. Predicted, adjusted, and average measured moments along the length of P3 at the 12.5 kip load step during the lateral load test
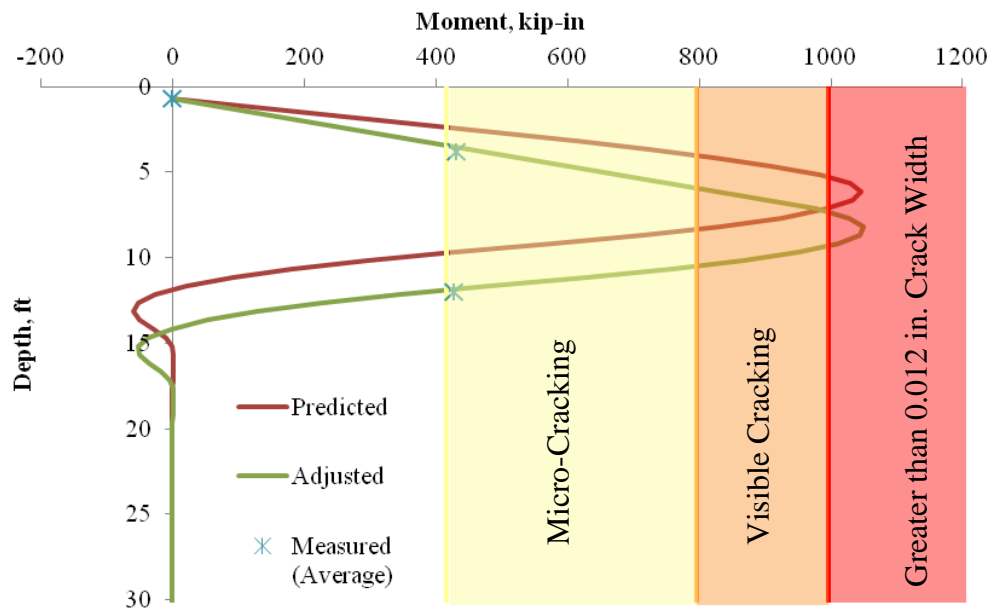
Figure 6-58. Predicted, adjusted, and average measured moments along the length of P4 at the 12.5 kip load step during the lateral load test

Appendix E include figures illustrating the predicted, adjusted, and average measured moments along the length of, both piles for all of the load steps.

186

Due to the small strains measured at the strain gage levels located 20 ft from the pile head and lower, drifts at these locations were significant. Figure 6-59 shows a strain gage located approximately 28 ft from the pile head as an example of the drift.
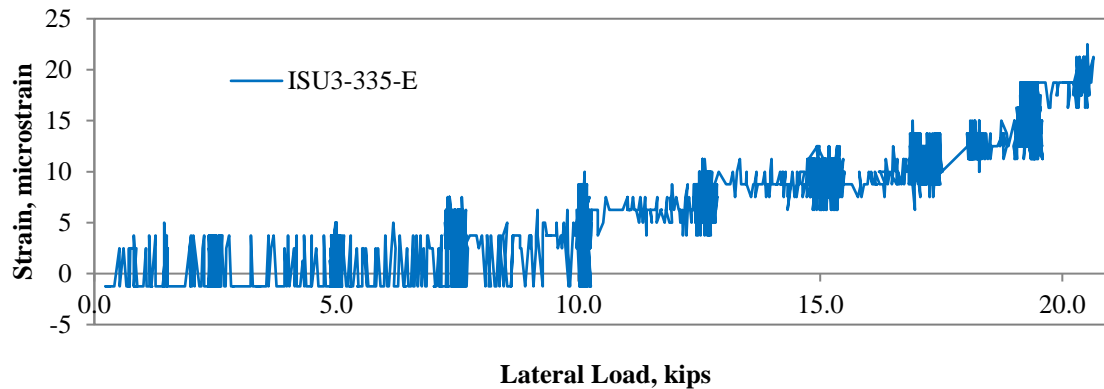
Figure 6-59. Drift in embedded concrete strain gage

In this particular case, the drift was taken into consideration and the average measured moment was corrected. P3 was predicted to perform well for a 12.5 kips lateral load, but P4 was predicted to have crack widths greater than 0.012 in. based on the moment calculated in Section 3.2.2.

For each of the load steps, the displacements measured by the SAA were compared to the displacements calculated in the adjusted LPILE model. Figure 6-60 compares the predicted, adjusted, and measured displacements during the 12.5 kip load step for P4; the figure shows that the adjusted LPILE model predicts the performance of P4 very well.
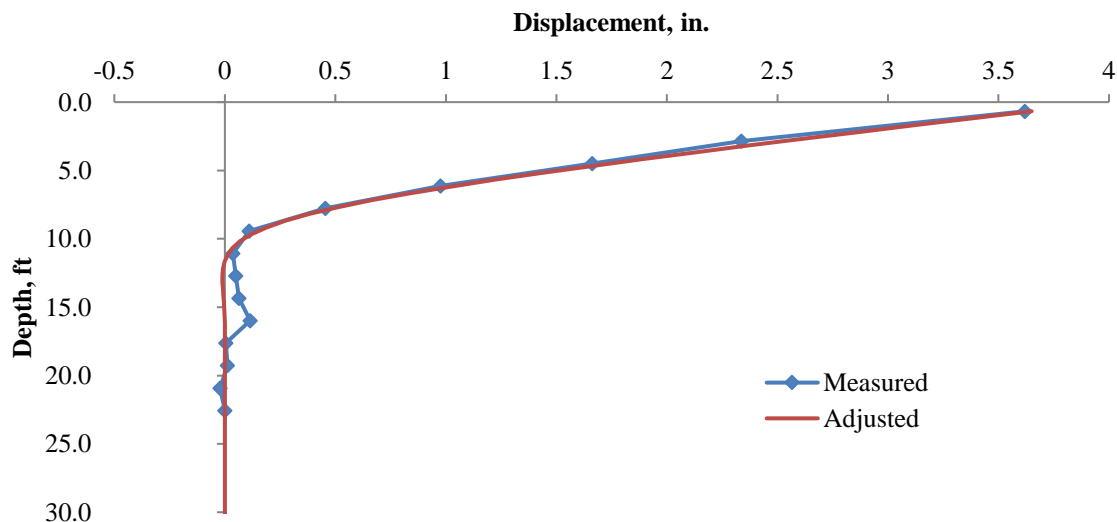
Figure 6-60. Measured displacements compared to adjusted displacements at the 12.5 kip load step during the lateral load test

All of the other displacement comparisons can be found in Appendix E.

6.6.6. Splice Performance

Since the splice was located 15 ft from the pile head on P4, it was subjected to a bending moment of 52.4 kip-in. and a lateral displacement of 0.08 in. as shown in Figure 6-58 and Figure 6-60, respectively. The predicted shear profile along the length of P4 for the 12.5 kip lateral load step is given in Figure 6-61, which indicates the splice would be subjected to a shear force of about 24 kips.

Shear Force, kip
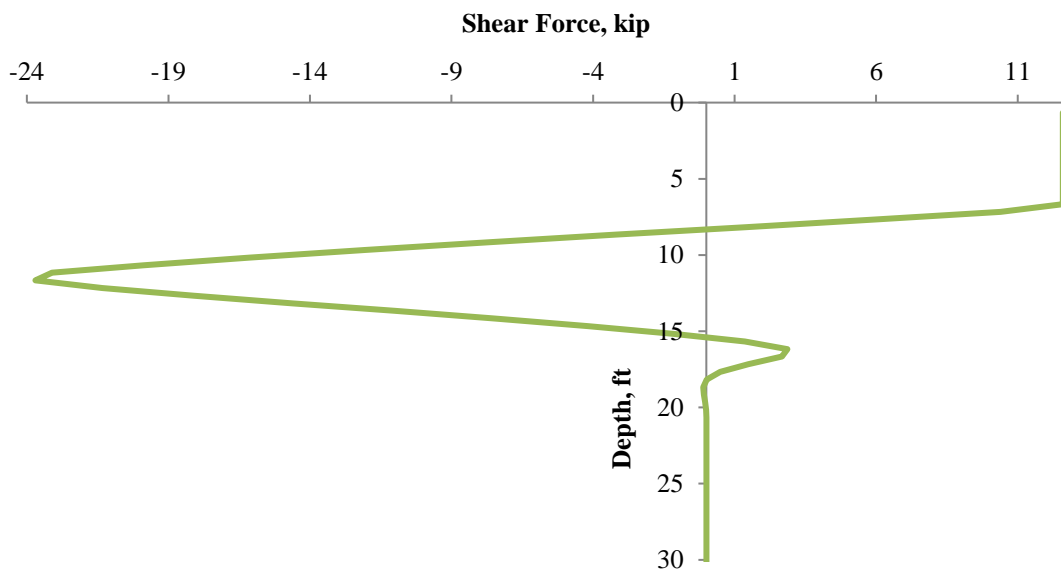
Figure 6-61. Adjusted shear along P4 during 12.5 kip load step of lateral load test

As mentioned in Section 6.6.4, no visible damage from driving or the lateral load test was found on or near the splice after excavation. The splice was subjected to compressive stresses of 5.7 ksi and tensile stress of 0.1 ksi during driving. Due to a mismatch between design and installation, the splice was driven to 12 ft below the ground surface instead of the required 9 ft embedment. The drawings in the chapter were changed to reflect the in-situ condition. As a result, the splice was only subjected to 2.6 kips of shear, 52.4 kip-in. of bending moment, and 0.1 in. of lateral displacement.

At the splice, P4 was subjected to a maximum shear force of 2.6 kips during the lateral load test. In the laboratory, a similar splice was subjected to additional shear and bending tests. The splice proved very robust with a shear capacity of 45 kips, which exceeds the maximum shear demand from the lateral load field test of 20.6 kips by 118% (Sritharan et al. 2012). When considering the field test with the laboratory results, the performance of the splice in the field can be expected to meet the required shear and moment demands even under extreme field conditions.

CHAPTER 7: FIELD IMPLEMENTATION AND MONITORING OF A UHPC PRODUCTION PILE

Following successful development of the UHPC pile and its connections, the evaluation of the performance of a UHPC production pile in a constructed bridge over a period of time was the next step. The overall goal of this exercise was to determine the suitability of UHPC piles in integral bridge foundations as well as the ability of these piles to sustain cyclic lateral movements resulting from time dependent movements including those due to thermal effects. This task was investigated as part of this project by replacing a steel HP 10×57 pile with an equivalent UHPC pile during construction of a new bridge.

7.1. Bridge Site

A suitable new or replacement bridge site for installing the UHPC production pile, identified as UW1, was selected using the following criteria: (1) the bridge must use an integral abutment, (2) the length should be in excess of 200 ft, and (3) the foundation soil type should be less favorable for pile movement. The Sac County bridge was chosen as the site for the UHPC production pile (UW1) because the bridge's geometry, soil conditions, and construction timeline met the criteria being sought. The site is just north of Early, Iowa, at the intersection of US 20 over US 71.

7.1.1. Bridge Geometry

The bridge is a 223 ft long and 40 ft wide with a 24° skew. The bridge consists of three spans, and the span lengths are 55 ft 9 in., 106 ft 6 in., and 60 ft 9 in. from west to east. HP 10×57 steel piles were designed to support the two abutments and the two bridge piers.

7.1.2. Soil Conditions

SPT information at the abutment with the UHPC production pile was obtained from the Iowa DOT. The identification (ID) number for the SPT borehole that was used for design of the HP 10 $\times$ 57 production piles was F-1219. A CPT was performed on the west abutment of the westbound bridge by Geotechnical Services, Inc., on August 10, 2011 at the request of the ISU research team to better classify the soil profile at the location of the UHPC production pile. The soil consisted of cohesive clay and silty clay with the water table located at a depth of approximately 20.50 ft according to the Iowa DOT soil report for borehole F-1219.

The variation of blow counts with respect to depth reported by Iowa DOT is shown in Figure 7-1 and is compared with the CPT results.
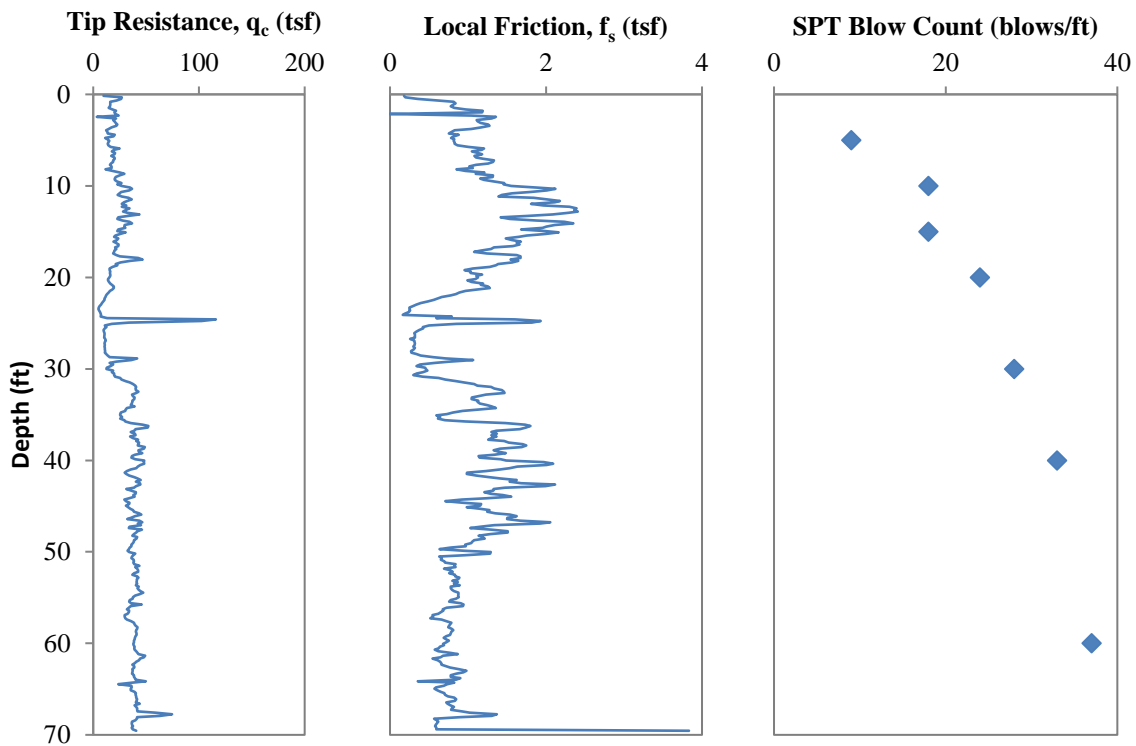
Figure 7-1. CPT and SPT results for the west abutment of the westbound bridge at the Sac County site

Table 7-1 summarizes the undrained shear strength and friction angle for each soil layer, which is calculated using an empirically based approach described by Lunne et al. (1997) and taking the average of properties for each soil layer.

Table 7-1. Undrained shear strengths and friction angles calculated from the CPT data for the west abutment

Soil classification	Depth to bottom of layer, ft	Undrained shear strength, psi	Friction angle, degrees
Clay	25.75	19.27	33.0
Silty clay to clay	28.54	8.87	27.9
Sandy silty to clayey silt	33.46	25.23	31.8
Clayey silt to silty clay	38.39	31.59	32.8
Clayey silt to silty clay	48.23	33.84	32.8
Sandy silt to clayey silt	69.72	32.18	31.9

7.2. Design of Production Piles

The steel HP 10×57 piles were designed for 100 kips of vertical load using the Iowa DOT Blue Book Method outlined in Section 2.5. The production pile, UW1, was to replace one of the HP

10×57 piles on the west abutment of the westbound bridge. As a result, UW1 was also designed for a 100 kip vertical load. The predicted design capacity of each of the piles was also calculated using DRIVEN 1.0 (Matthias and Cribbs 1998) and CAPWAP (PDI 2000). The location of all the instrumented piles in the bridge is given in Figure 7-2.
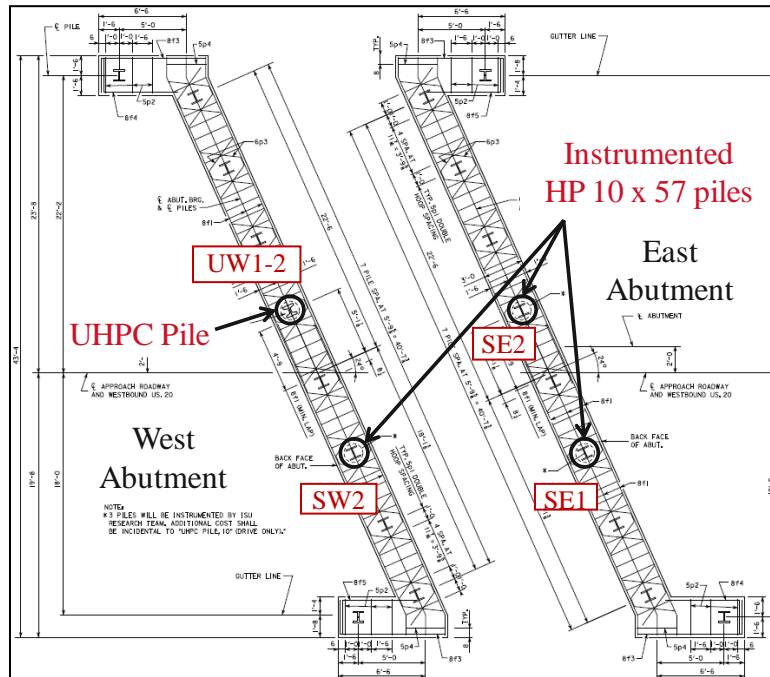
Figure 7-2. Locations of instrumented production piles

All design calculations based on the Blue Book Method are included in Appendix C.

7.2.1. *HP 10 × 57 Production Piles*

The HP 10×57 pile on the west abutment (SW2) was designed for a vertical load capacity of 100 kips, resulting in a total length of 65 ft with 62 ft embedded below the ground surface. Using the new LRFD resistance factors recommended by Green et al. (2012) to achieve the same design load, the total length of the pile would only need to be 60 ft. The amount the new resistance factors shorten the pile was 7.7%.

The two instrumented HP 10×57 piles on the east abutment, SE1 and SE2, had a design length of 85 ft with an embedment of 82 ft for the same 100 kip design load, but using the new LRFD resistance factors (Green et al. 2012) would shortened the piles by 5.9%, resulting in a total length of 80 ft.

7.2.2. *UHPC Production Pile*

UW1 was designed with a total length of 55 ft and a 53 ft embedment below ground surface for a 100 kip design load. Unlike steel HP 10 × 57 piles, the top 12 in. of UHPC piles does not need to be cut off because there is no buckling taking place, resulting in saved material. As a comparison, the new resistance factors calibrated by AbdelSalam et al. (2012) for H-piles were used to calculate the design length of UW1, which resulted in a total pile length of 52 ft with 50 ft embedded below the ground surface. The new resistance factors would only result in shortening the UHPC pile by 3 ft, or 5.5%.

To accommodate PDA equipment an extra foot was added to the design of UW1 to make the total length 56 ft. This resulted in an easier disassembly of the PDA equipment at the end of drive and reassembly for the restrikes because the PDA equipment was installed 30 in. from the pile head.

7.3. Instrumentation Scheme

The instrumentation used for the first UHPC production pile (UW1-1) was the same embedded concrete gages as described in Section 6.2 and shown in Figure 6-1. A second production pile (UW1-2) was needed because UW1-1 was dropped from the crane due to the use of inadequate hook and poor handling in the field and was deemed unusable as a production pile (Section 7.5). Due to the limited amount of time to gather instrumentation for the second production pile (UW1-2), two different types of concrete embedment gages were used along this pile. The two types of gages are shown in Figure 7-3.
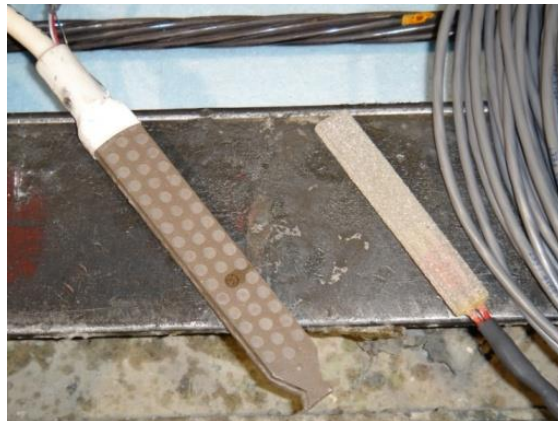
Figure 7-3. Embedded concrete strain gages for UW1-2

For the steel piles, weldable strain gages were used as shown in Figure 7-4.

Figure 7-4. Weldable steel strain gages used to monitor steel HP 10 × 57 production piles

All of the production piles had two gages at each level that were on the diagonal to measure the curvature of the pile during the expansion and contraction of the integral bridge due to thermal movements.

7.3.1.   First UHPC Production Pile

The concrete gages for UW1-1 were installed November 18, 2011 at Coreslab Structures, Inc. in Bellevue, Nebraska using the procedure given in Appendix C for embedded concrete strain gages. Table 7-2 lists the gage label and locations from the pile's head for each of the 12 gages.

Table 7-2. Location and labels of strain gages in UHPC production pile UW1

Location from pile head, ft	Gage label	
4	UW1-48-E	UW1-48-W
12	UW1-144-E	UW1-144-W
18	UW1-216-E	UW1-216-W
30	UW1-360-E	UW1-360-W
43	UW1-516-E	UW1-516-W
54.25	UW1-668-E	UW1-668-W

The gage locations are also illustrated in an elevation view in Figure 7-5.
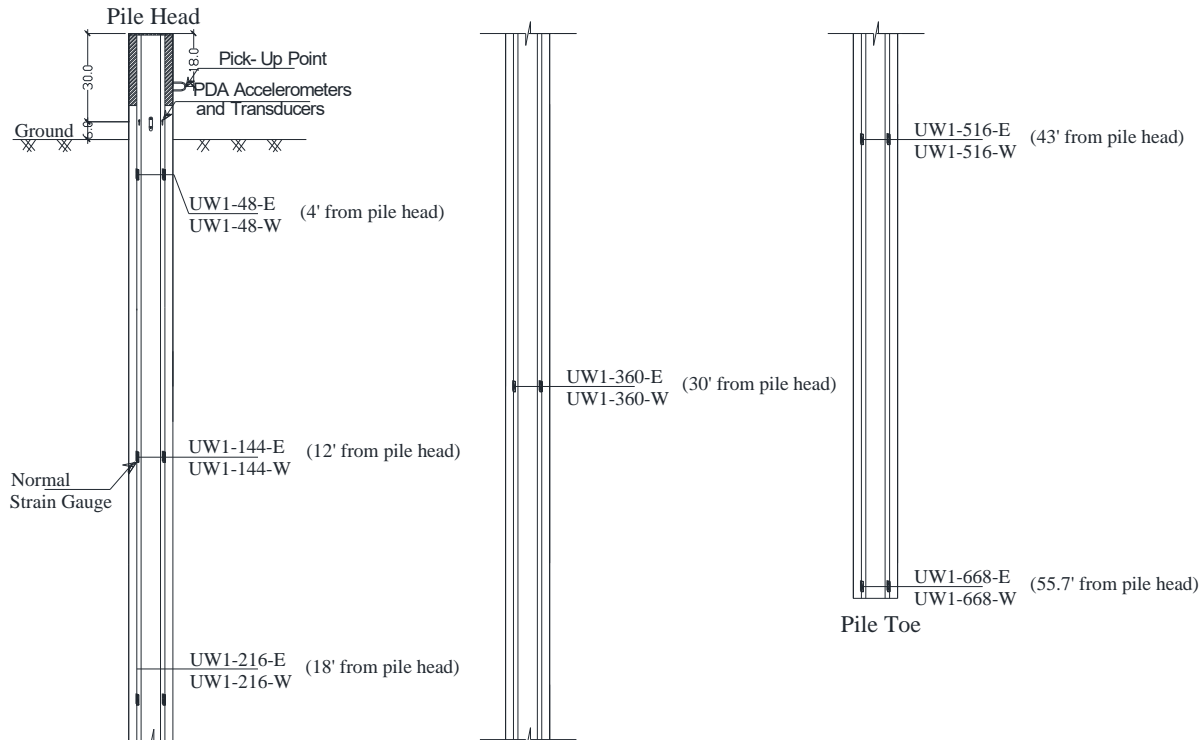
Figure 7-5. Elevation view of UW1 showing locations of instrumentation

7.3.2.   *Second UHPC Production Pile*

The instrumentation for UW1-2 was also installed at Coreslab Structures, Inc. in Bellevue, Nebraska but on February 13, 2012 with the same instrumentation scheme used for UW1-1. The only difference between the two piles was that UW1-2 did not include a splice at the pile head. There was no need to include the splice because the UHPC production pile capacity had been verified by the vertical load test described in Section 6.5 at the site near the west abutment, which was where UW1-2 would be located.

7.3.3.   *HP 10 × 57 Production Piles*

PDA was performed on all of the instrumented steel HP 10 × 57 production piles. The cross-section view of the location of the strain gages and accelerometers is given in Figure 7-6.
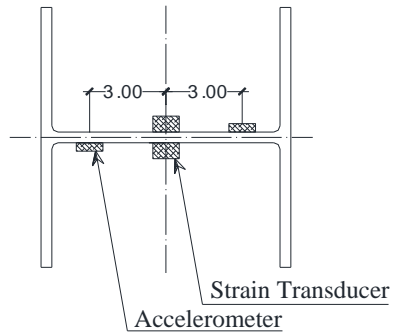
Figure 7-6. Location of PDA instrumentation on HP 10 × 57 piles at a cross-section 18 in. from the pile head

Notice that the accelerometers are on opposite sides of the web of the pile as was done by Ng et al. (2011). The data gathered by the PDA equipment was wirelessly transmitted to the PDA unit similar to the UHPC test piles.

To instrument the steel H-piles, weldable gages were used to measure the strain in the steel along the length of the pile. In order to secure the gages, a tack welder, shown in Figure 7-7, was used for gage installation.
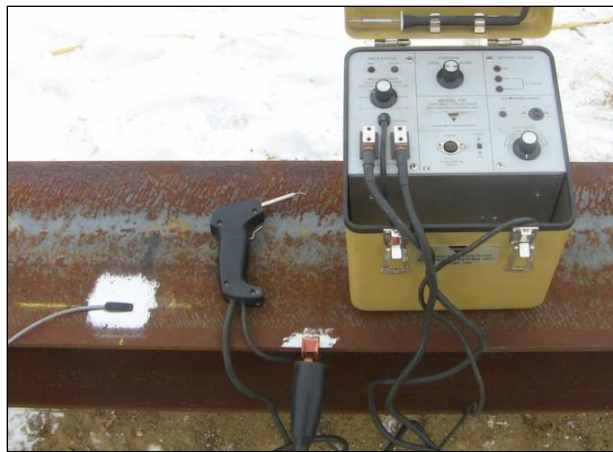
Figure 7-7. Tack welding machine

The procedure for installing the weldable strain gages is outlined in Appendix D. The cross-section of the instrumented steel HP 10 × 57 piles is shown in Figure 7-8, which also shows how the ends of the angle welded to the pile to protect the instrumentation was closed at the end.
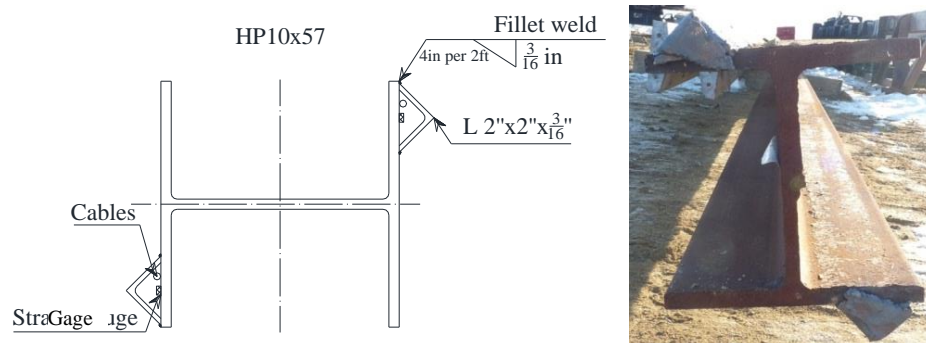
Figure 7-8. Cross-section view of HP 10 × 57 pile showing the strain gage location

SW2

SW2 was instrumented on January 23, 2012 using the procedure outlined in Appendix D for the weldable strain gages. Twelve gages were installed along the length of the pile at six levels with two gages at each level. Table 7-3 lists the strain gage label and location from the pile's head and Figure 7-9 illustrates the location of PDA and strain gages in elevation view.

Table 7-3. Location and labels of strain gages in steel production pile SW2

Location from pile head, ft	Gage label	
4	SW2-48-E	SW2-48-W
12	SW2-144-E	SW2-144-W
18	SW2-216-E	SW2-216-W
33	SW2-396-E	SW2-396-W
49	SW2-588-E	SW2-588-W
64.5	SW2-774-E	SW2-774-W
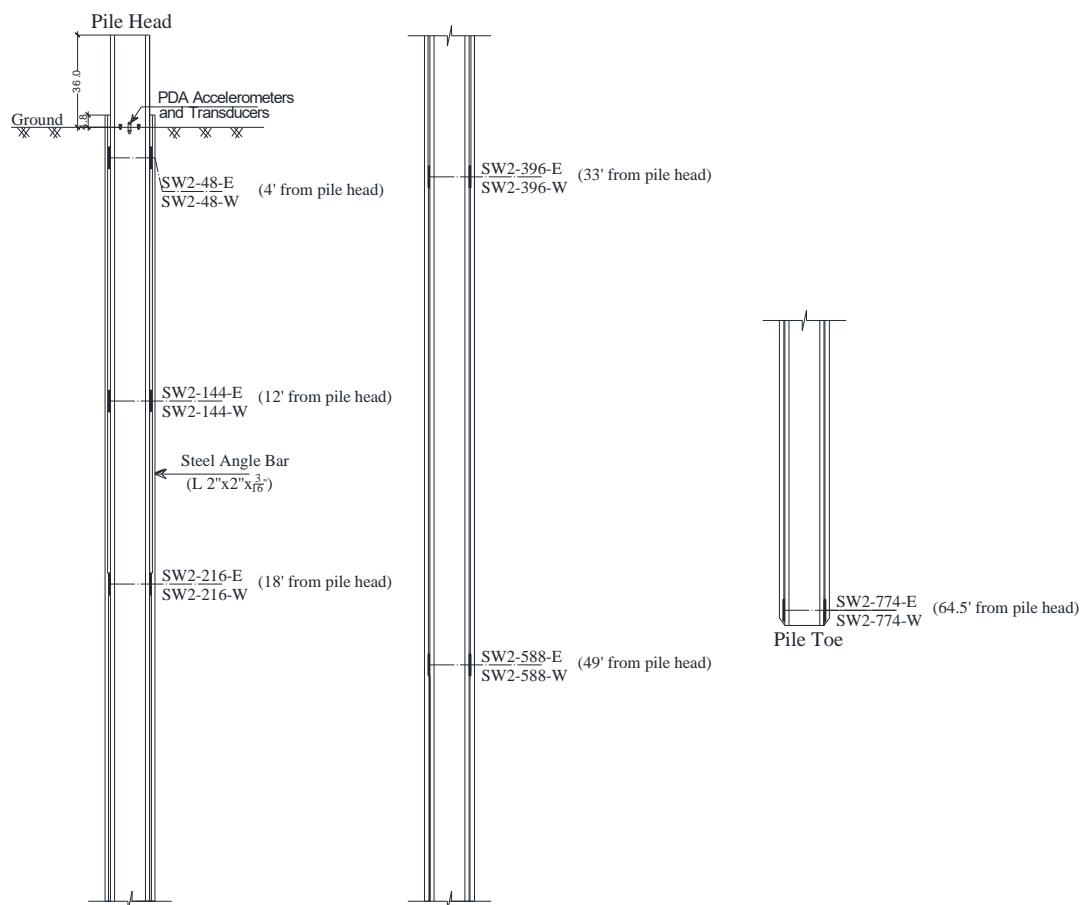
Figure 7-9. An elevation view of SW2 showing the locations of instrumentation

SE1 and SE2

SE1 and SE2 were instrumented on March 7, 2012 using the procedure outlined in Appendix D for the weldable strain gages. Six gages were installed along the length of the pile at three levels with two gages at each level. The reason for the reduced number of strain gages is that the piles on the east abutment were 85 ft in length. The east abutment piles were to be spliced at 40 ft from the pile's head, and it would have been difficult to run cables from the portion of HP 10×57 below the splice. Table 7-4 and Table 7-5 list the strain gage labels and locations from the pile's head for SE1 and SE2, respectively.

Table 7-4. Location and labels of strain gages in steel production pile SE1

Location from pile head, ft	Gage label	
4	SE1-48-E	SE1-48-W
12	SE1-144-E	SE1-144-W
16	SE1-192-E	SE1-192-W

197

Table 7-5. Location and labels of strain gages in steel production pile SE2

Location from pile head, ft	Gage label	
4	SE2-48-E	SE2-48-W
12	SE2-144-E	SE2-144-W
16	SE2-192-E	SE2-192-W

Figure 7-10 illustrates the location of PDA and strain gages in elevation view for SE1 and SE2.
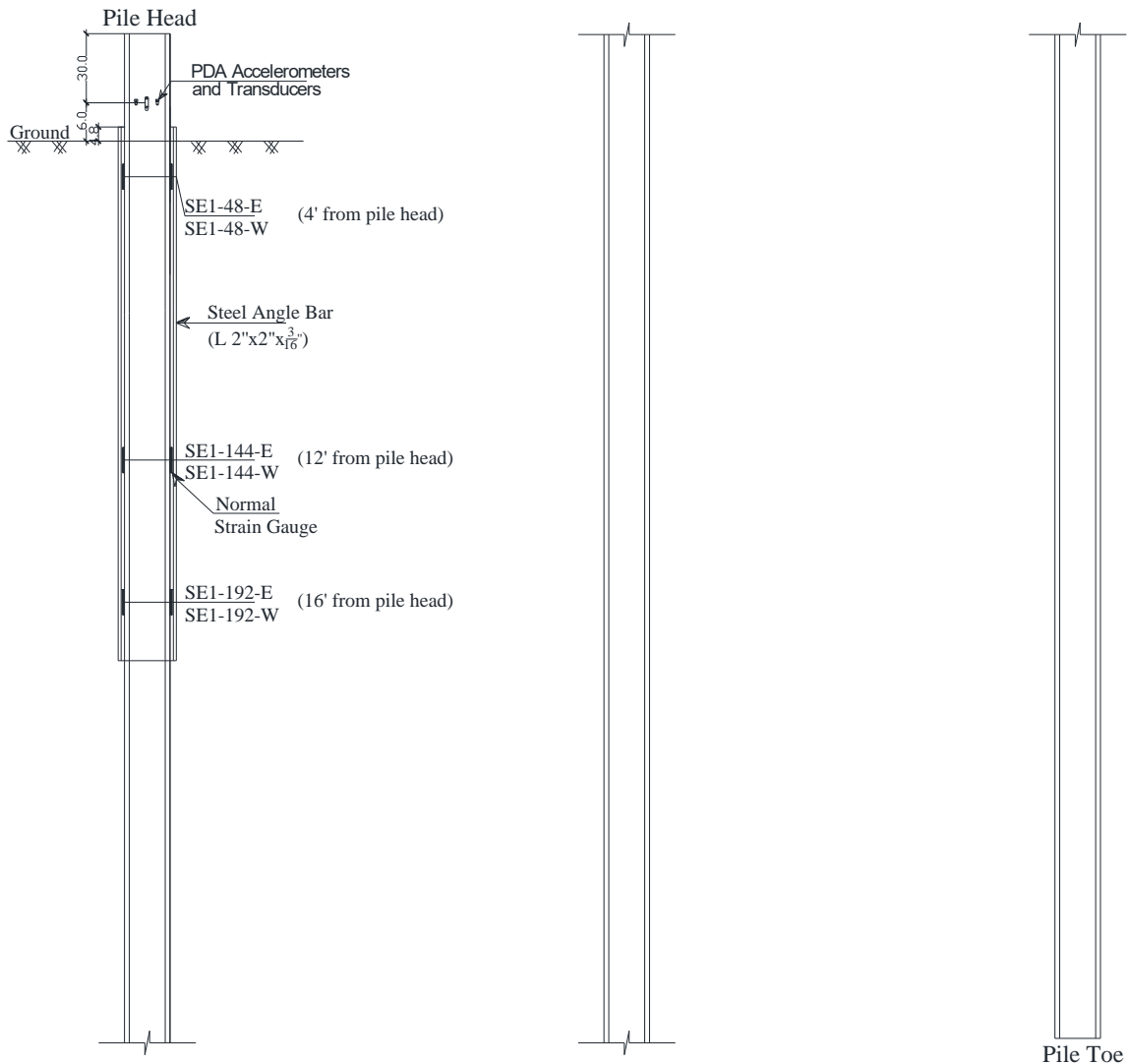
Figure 7-10. An elevation view of SE1 and SE2 showing the locations of instrumentation

7.4.   Fabrication of UHPC Piles

7.4.1.   Splice Fabrication

The splice for UW1-1 was fabricated at Howe Welding in Ames, Iowa by a certified welder along with the splices for the test piles. The fabrication is outlined in Section 6.3.1. No splice was fabricated for UW1-2 due to the verification of capacity through the vertical load test.

7.4.2.   Casting Process

The UHPC production piles were cast at Coreslab Structures, Inc. in Bellevue, Nebraska. UW1-1 was cast along with the test piles P3 and P4 in December of 2011.

UW1-1

The casting process, steam curing, and materials properties were the same for UW1-1 as for P3 as outlined in Section 6.3 because they were cast from the same batch. The layout of the production pile is shown in Figure 6-12.

UW1-2

The casting process and steam treatment were the same as outlined in Section 6.3 for UW1-2. One side of the steel forms was left off while all 10 prestressing strands were arranged and stressed to their initial prestress of 202.5 ksi. Because the side of the forms was left off, 12 strain gages could be installed along the pile's length. No inserts were added for the PDA equipment since it was just as easy to drill through the UHPC with a 3/8 in. diameter concrete drill. After the instrumentation was complete, the forms were closed as shown in Figure 7-11 by lifting the steel side with the overhead crane and then locked into place.
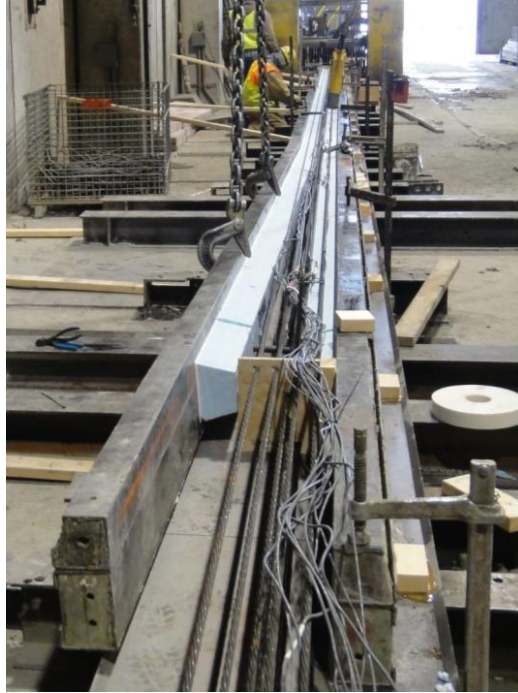
Figure 7-11. Closing the side forms before casting UW1-2

The UHPC was mixed using the precaster's 4.0 yd^3 mixer at the batch plant. A total of 1 yd^3 of Ductal was used for the pour. After completing the batching of the UHPC mix, it was poured into a large bin and transported by a fork lift to the building where the UHPC forms were located. The UHPC was then poured into the forms. Once the pour was complete, the top surface of UW1-2 was covered with plastic wrap to prevent moisture loss as shown in Figure 7-12.

Figure 7-12. Plastic wrap cover for UW1-2 at the end of casting

7.4.3.   *Details of First UHPC Production Pile Pour*

The pour of UW1-1 was on November 21, 2011, the same day as the pour for P3 and P4. The same batch of UHPC was used, and therefore the UHPC was lumpy. The formwork also moved, and concrete leaked out of the formwork as mentioned in Section 6.3.3. Concreting paused

halfway and resumed after a waiting time of about 55 minutes. After the forms were stripped, there were a few imperfections along the length of UW1-1, but the pile was deemed acceptable.

7.4.4. *Details of Second UHPC Production Pile Pour*

The pour of UW1-2 took place on February 14, 2012. The dry ingredients of the UHPC were broken up in the mixer before the liquids were added. Once the clumps were broken down, the water and admixtures were added to the mix in the proper order. The UHPC had a good consistency, and everything went well for the pour.

7.4.5. *Steam Curing and Instrumentation Performance*

After the release of the prestressing strands in UW1-1, it was steam cured with P3 and P4 at 194°F for 48 hours at the precasting plant. All 12 gages in UW1-1 were working after the steam curing. The same process for steam curing was used for UW1-2. All 12 gages in UW1-2 were also working after the steam curing was complete.

7.4.6. *Handling of UHPC Production Piles*

Due to the failure of the pickup point hook on UW1-1, a new pickup point detail was designed for UW1-2. A 1 in. diameter high-strength threaded rod was embedded into the web at the location of the previous pickup point hook by the pile head as shown in Figure 7-13.
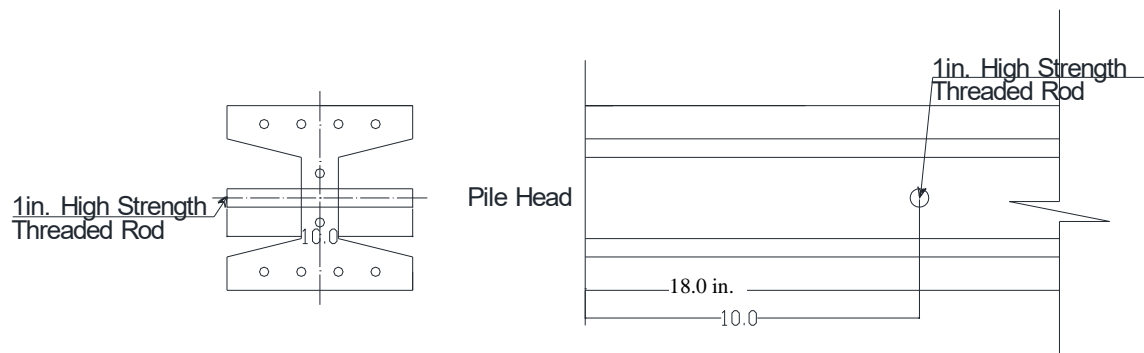
Figure 7-13. Revised pickup point design

Coreslab also inserted bent prestressing strands 1.5 ft away from the pile head and the pile toe, to provide easy transportation pickup points at the precast plant.

In order to lift the pile at the construction site, it was initially decided to slip a cable loop over the threaded rod and secure it in place using a washer and a nut as shown in Figure 7-14.

201

Figure 7-14. Proposed pickup point

However, this detail could not be constructed at the site because the thread size of the nut was much smaller than that of the threaded rod. Instead, an additional washer was welded to the threaded rod (Figure 7-15) to ensure that the cable loop would not slip off the threaded rod when picking up the pile.

(a)   (b)

Figure 7-15. (a) Welding the 2nd washer to the threaded rod and (b) pickup point after welding

7.4.7.   Material Properties

Prestressing Strands

The material properties for the prestressing strands of UW1-1 were the same as those for P3 and P4 because it was cast at the same time as the two test piles. As discussed in Section 6.3.6, the average yield strength and average modulus of elasticity of the strands were 250.5 ksi and 29,449 ksi, respectively.

Three 5 ft sections of the 270 ksi low-relaxation prestressing strands used in UW1-2 were cut and tested in uniaxial tension at ISU. The yield strength of the ½ in. strands was 256 ksi while the ultimate strength strands was 295 ksi.

UHPC

The 3 in. diameter cylinders that were cast out of the same batch as UW1-2 were tested in compression by Coreslab Structures, Inc. The average compressive strength of the UW1-2 was 28.1 ksi. The design strength of the mix was 26 ksi, and the results in Table 7-6 show that the 26 ksi average strength was achieved.

Table 7-6. Average compressive strength measured for the UW1-2 pile

Cylinder #	f′$_c$, ksi
1	27.5
2	28.4
3	28.5
Average	**28.1**

The elastic modulus for UW1-2 was calculated using equation (2-2) (Graybeal 2007) presented in Section 2.3.4 and was found to be 7,711 ksi.

7.5. Driving of Instrumented Production Piles

7.5.1. *Drivability Analysis*

A drivability analysis was conducted in GRLWEAP (PDI 2005) using the same hammer, cushion, and soil parameters used for the UHPC test piles, which are given in Section 6.4.4. The percent shaft resistance that UW1-2, SW2, SE1, and SE2 are subjected to during driving was calculated using the undrained shear strength and friction angles calculated from the average CPT results in the FHWA computer program DRIVEN (Matthias and Cribbs 1998). The maximum predicted and measured stresses during driving for the UHPC and steel production piles are shown in Table 7-7.

Table 7-7. Predicted and measured stresses in production piles during driving

	Pile	Maximum stress, ksi		% difference
		Predicted	Measured	
SW2	Compressive stress	27.0	25.9	+4.2
	Tensile stress	1.7	1.8	−5.6
SE1	Compressive stress	30.8	27.3	+12.8
	Tensile stress	1.8	1.3	+38.5
SE2	Compressive stress	30.8	28	+10.0
	Tensile stress	1.8	0.7	+157
UW1-2	Compressive stress	7.6	4.8	+58.3
	Tensile stress	0.2	0	N/A

The measured maximum stresses were calculated from the PDA analysis.

All predicted maximum stresses were over-predicted when compared to the measured maximum stresses from the PDA, except for the maximum tensile stress of SW2. The very large maximum tensile stress percent difference for SE1 and SE2 is due to the fact that the tensile stress were so low that a small change in stress resulted in a big percent difference. All of the compressive stresses and tensile stresses for all the production piles were well within the allowable driving stress limits given in Section 2.3.6.

7.5.2. *Driving Process*

The same driving system described in Section 6.4.3 was used to drive the steel HP 10×57 piles and UW1-2. Figure 7-16 illustrates the layout of the abutment piles within the abutment.

Figure 7-16. Layout of abutment piles

The installation details for each of the instrumented production piles are described in this section.

SW2 was driven into the west abutment of the westbound bridge on January 26, 2012. The only usable restrike for SW2 was the one performed on March 19, 2012, approximately 53 days after the EOD. The reason for the postponed restrike was that the PDA transmitters had to be replaced because it was damaged when UW1-1 fell.

Steel Production Piles

The PDA equipment was bolted to the HP 10×57 piles while lying on the ground as described in Section 6.4.5. Once completed, the steel piles were lifted into position using the pickup point shown in Figure 7-17.

Figure 7-17. Steel HP 10×57 production pile pickup point

The pile was lifted to a vertical position and set into the 10 ft deep prebored hole. The crane was unhooked from the steel pile in order to pick up the hammer leads and position them on the top of the steel pile. When the leads, hammer, and pile were in place, the ram of the hammer was lifted manually by the crane and dropped. SE1 and SE2 had a design length of 85 ft, and they were spliced 40 ft from the pile head using a similar method as described for the spliced anchor piles in Section 6.4.5.

UHPC Production Pile

PDA was performed during the installation of UW1-2. The strain gages and accelerometers were attached to the pile using the same procedure used for the test piles shown in Figure 6-4. The data gathered by the PDA equipment was wirelessly transmitted to the PDA unit by the same process as for the UHPC test piles.

The new pickup point designed for UW1-2 worked very well. To reduce the amount of stresses on the UHPC pile, the pile was picked up by the new pickup point at the pile head and the inserted prestressing strand hook at the pile toe. Once the pile was lifted off the ground, the crane operator rotated the pile to the vertical position in the air as shown in Figure 7-18.

Figure 7-18. Stages in lifting UW1-2

The installation was very similar to a steep H-pile, except that one of the crew's members had to be sent to the top of the UHPC pile to release the pile from the crane.

A 4 in. plywood pile cushion was used to protect the UHPC pile head, but UW1-2 punched through the pile cushion shortly after driving had begun. Instead of replacing the cushion with a new one, the pile was driven with essentially no cushion. There was slight damage to the pile head corners of UW1-2 as shown in Figure 7-19.

Figure 7-19. Damage to the pile head of UW1-2

The reason for the damage was that the pile head was not perfectly centered under the helmet. It is also important to note that the UW1-2 was slightly tilted after driving and on the back side of the prebored hole as shown in Figure 7-20, which might have reduced the effectiveness of the prebored hole.

Figure 7-20. UW1-2 after installed in the prebored hole

7.6. Estimated Capacity

7.6.1. UW1-2

As a comparison of the different methods used to design deep foundations, Table 7-8 lists the estimated nominal capacity of UW1-2 using the Iowa DOT current design procedures, DRIVEN and CAPWAP.

Table 7-8. UW1 nominal capacity calculated by various methods

Method	Estimated nominal capacity, kips
Iowa DOT current	200
DRIVEN	216
CAPWAP (3-day)*	212.9

Source: Ng et al. 2011
*Further gain is expected due to setup

The predicted capacity using DRIVEN was 8% higher than for the Iowa DOT current design method, and 6.5% higher than the Iowa DOT current design method when using CAPWAP. The CAPWAP analysis was completed using a Case damping factor of 0.166.

The vertical load test performed on P3, which was 10 ft shorter than UW1-2, produced a vertical capacity of 296.5 kips. P3 and UW1-2 are comparable in length, because the 10 ft reduction in length of P3 was to account for the prebored hole of UW1-2, which is often referred to as UW1

in the subsequent section. The vertical load test was performed eight days after the EOD, while the CAPWAP predicted capacity of UW1-2 was from a restrike three days after EOD. The difference in the amount of time after EOD for measuring or predicting the nominal capacity could account for a portion of the 39% difference in capacity due to the effect of setup in clays (Ng et al. 2011).

7.6.2.   SW2

The calculated nominal capacities using the three different types of design methods are given in Table 7-9.

Table 7-9. SW2 nominal capacity calculated by various methods

Method	Estimated nominal capacity, kips
Iowa DOT current	200
DRIVEN	212.3
CAPWAP (53-day)	318.6

DRIVEN calculates an estimated nominal capacity 6.2% higher than the current Iowa DOT method. Interestingly, CAPWAP estimated the nominal capacity of SW2 to be 318.6 kips by using a Case damping factor of 0.245, which was 59.3% higher than the current Iowa DOT method. One thing to note is that the final restrike, which was used to estimate the nominal capacity of SW2, took place 53 days after the end of drive instead of the specified 3 days. The reason for the delay was the two PDA transmitters were broken, and two new transmitters had to be ordered.

7.6.3.   SE1 and SE2

Using the Iowa DOT current design method, the predicted capacity of SE1 was 200 kips. The CAPWAP analysis estimated the nominal capacity of SE1 to be 286.9 kips using a Case damping factor of 0.335. The CAPWAP analysis predicted a value 43.5% higher than the capacity estimated by the Iowa DOT's current design method.

Like SE1, SE2 had a predicted nominal capacity of 200 kips from the Iowa DOT current design method, but the CAPWAP analysis estimated the capacity to be 271.2 kips using a Case damping factor of 0.277. This resulted in a 35.6% increase.

7.7. Results

7.7.1. Observations

For the data collected over 32 months, the average daily strain variations of the piles at different depths were first examined. Figure 7-21 shows the range of daily strain variation and corresponding frequencies for the UHPC pile at different levels.
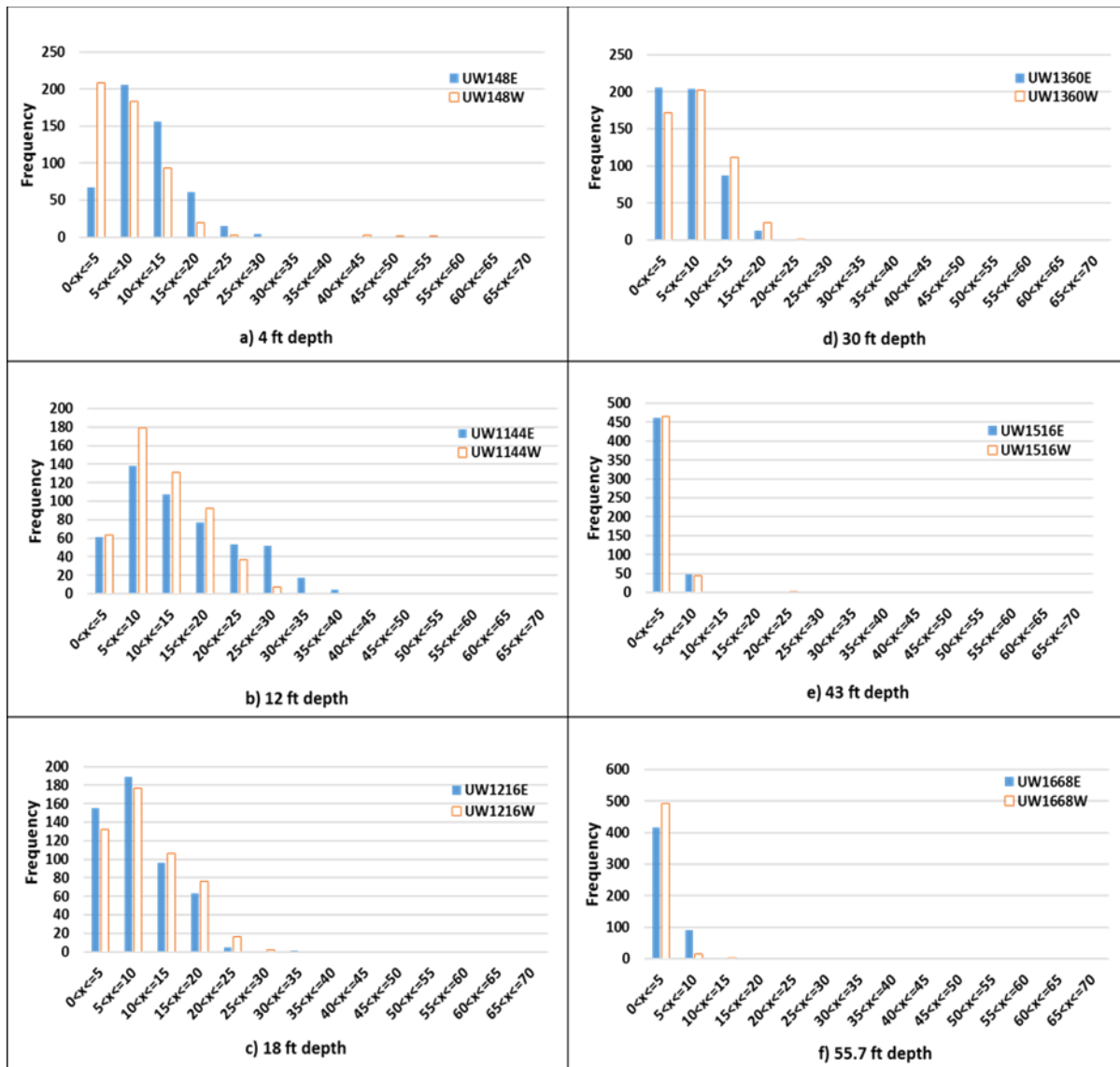
Figure 7-21. Daily strain variation observed in the UHPC pile

The vertical axis shows the frequency for each strain range while the horizontal stands for the strain ranges. For example, $5 < x \leq 10$ corresponds to strain less or equal to 10 microstrains but greater than 5 microstrains. It can be seen that the variations are in the range of 5 to 15 microstrains for the majority of the time. For gages located at 4, 12, 18, 30, 43, and 55.76 ft

below the pile head, the mean strain variations were found to be 8.8, 12.8, 9.0, 7.1, 6.2, and 3.1 microstrains, respectively. The largest daily strain variation occurred at a 12 ft depth. The daily strain variations seen in Figure 7-21 were generally found to be dependent on the ambient temperature and gage location. A large temperature change generally led to larger strain variation; this effect was more prominent in the top portion of the pile. This is consistent with the observation that gage UW1-144 (12 ft from the pile head) exhibited the largest strain variation in the UHPC pile. The information regarding average daily strain variation was subsequently used to estimate the long-term strain variation (see Figure 7-21 and Figure 7-22).
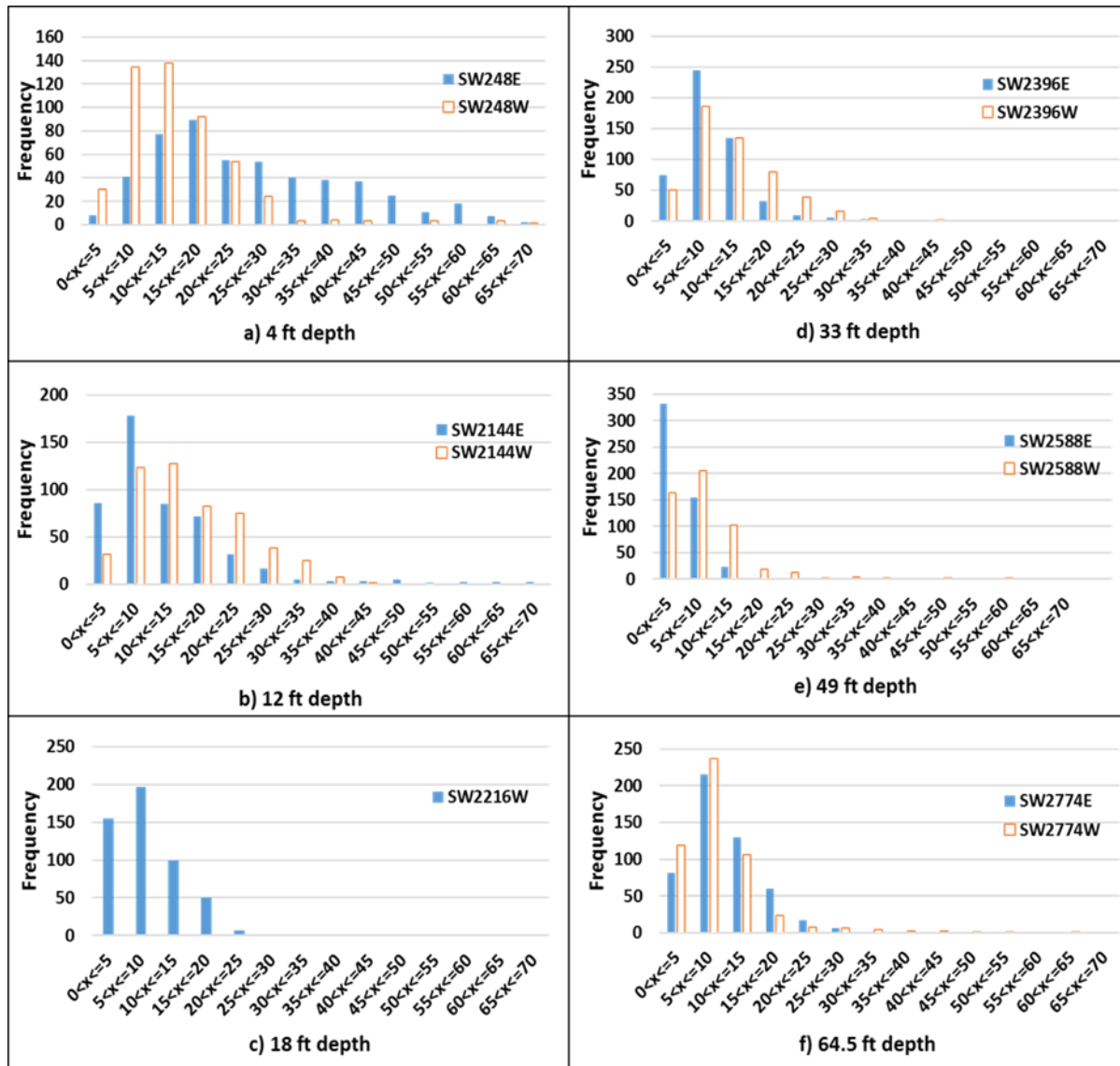
Figure 7-22. Daily strain variation frequency for steel pile

Strain data from the steel piles showed similar trends to those observed for the UHPC pile. Figure 7-22 summarizes the frequency of different daily strain range at different depths for SW2, with mean daily strain variations at 4, 12, 18, 33, 49, and 64.5 ft depths of 28.4, 17.5, 8.2, 12.2,

6.5, and 9.5 microstrains, respectively. Based on the calculated values, the largest daily strain variation occurred at 4 ft from the top of the pile. For SE1, the mean daily variations at 4, 12, and 16 ft depth were 26.7, 18.0, and 10.7 microstrains, respectively. For SE2, the corresponding average daily variation at depths of 12 and 16 ft were 15.69 and 13.52 microstrains, respectively.

Long-term strain variations were influenced by bridge deck movement, so in addition to the temperature change, these variations were examined using two different methods. The first method used all data from the beginning to the end of the monitored period and estimated the largest long-term strain change and its corresponding time. In the second method, only the data obtained each day at 3 p.m. were used, and the largest strain values were estimated. The latter approach was intended to minimize the influence of daily temperature variation on the long-term change in strain.

Figure 7-23 compares the two methods of measurements from gage UW1-48-E in the UHPC pile along with the ambient temperature over a period of more than two years.
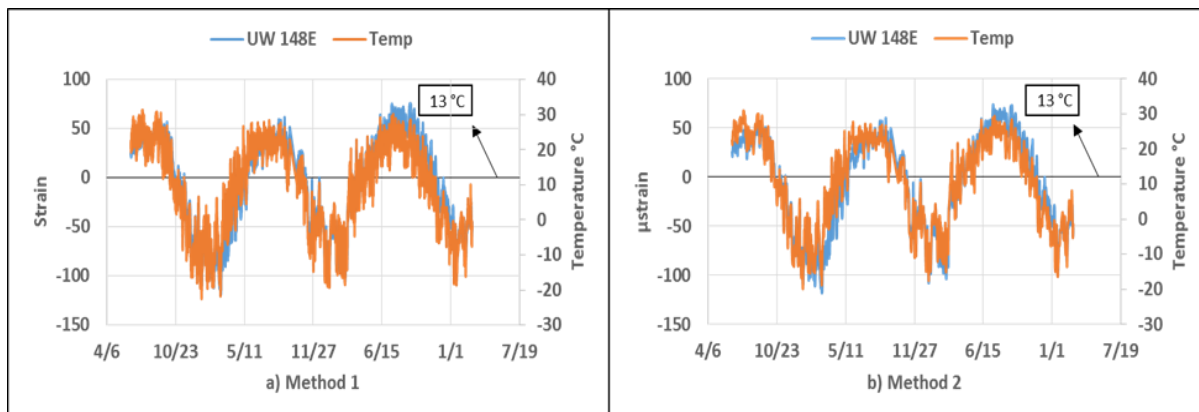
Figure 7-23. Comparison of strain using Method 1 and Method 2

As shown in this figure, all strains, including UW1-48-E, were taken as zero at an ambient reference temperature of 13°C. This temperature represents the average ambient temperature for the month of May 2013, when the bridge construction was completed. Consequently, the positive strains shown in Figure 7-23 correspond to strain build-up during extension of the bridge in warmer temperatures, and the negative values reflected the strains corresponding to contraction of the bridge during winter months. It was found that the maximum long-term temperature and the corresponding strain changes were 34°C (i.e., from +27°C to –7°C) and 150 microstrains (i.e., from +50 to –100 microstrains), respectively, using the first method in Figure 7-23a. Similarly, variations were found to be 35°C and 150 microstrains in Figure 7-23b using the second method. Since these values are similar, Method 1 was used for the remainder of this study. In Figure 7-23, both graphs show that temperature values peaked near mid-August while the lowest value was recorded toward the end of January. This pattern is also reflected in the data obtained from the other strain gages and displacement transducers.

211

In addition to recording strains, the movements of the bridge abutments were measured from March 22, 2014 to March 3, 2016. Figure 7-24 compares the readings of UW 1-48-E with the rest of the gages for the same period.
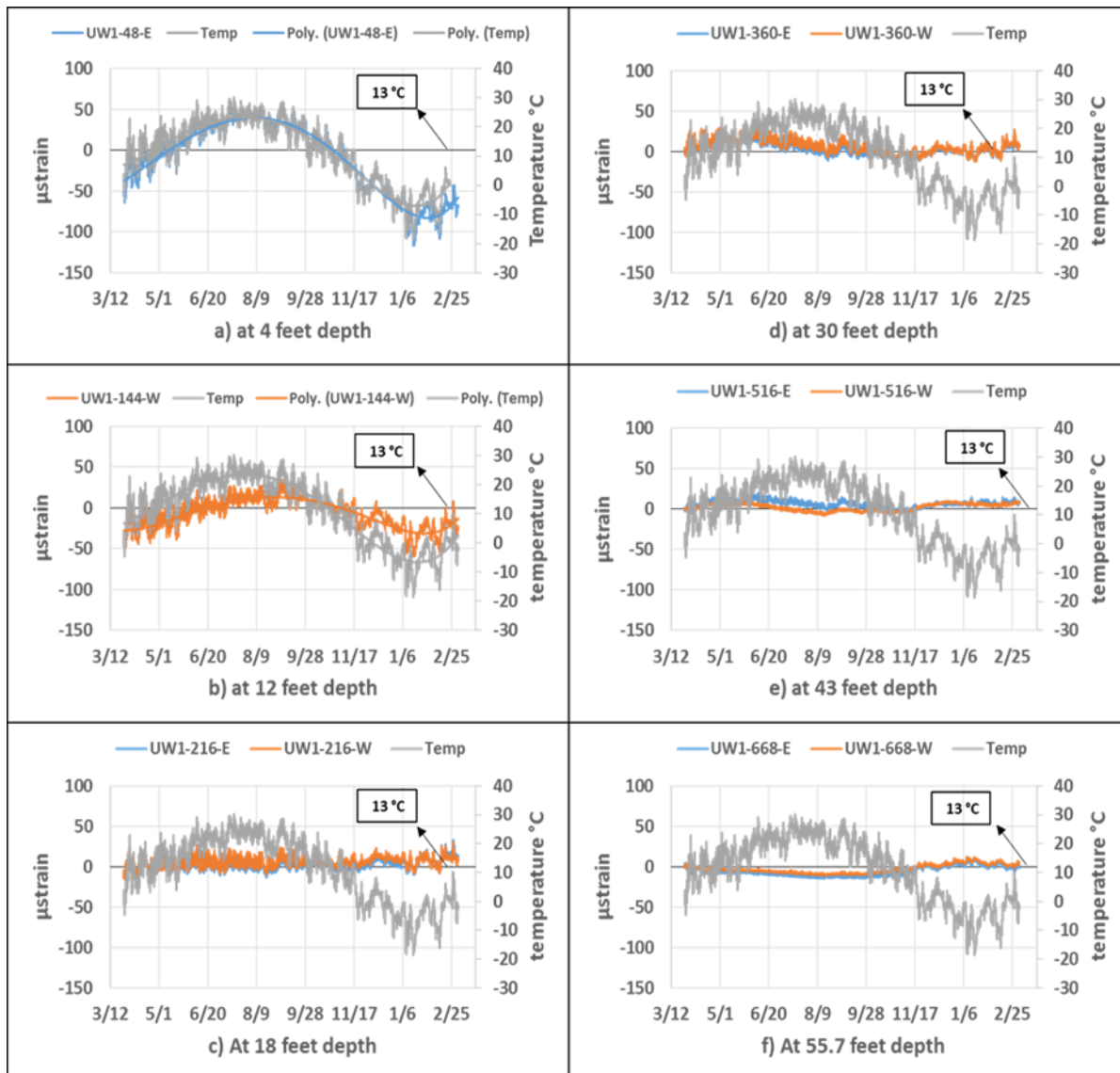
Figure 7-24. UHPC pile (UW1) long-term strain change at different depth (3/22/2015–3/3/2016)

Polynomial best-fit lines were added for the first two charts in Figure 7-24. Due to malfunction, reading from gages UW1-48-W and UW1-144-E are not shown in Figure 7-24a and b. Over this 12-month period, during which the largest temperature change was 34°C, long-term strain variations at different depths of the UHPC pile were found to be 120 (i.e., from +40 to –80 microstrains), 50 (i.e., from +15 to –35 microstrains), 20 (i.e., from +10 to –10 microstrains), 20 (i.e., from +10 to -10 microstrains), 10 (i.e., from +5 to -5 microstrains) and 10 (i.e., from +5 to –5 microstrains) at depth of 4, 12, 18, 30, 43, and 55.7 ft from the pile head, respectively. From

these values, and from reported daily strain variation (Figure 7-21), it can be concluded that the changes in strain at 18 ft depth and below were insignificant. This implies that the UHPC pile is not subjected to significant flexural actions below an 18 ft depth.

Figure 7-25 presents the data from all the working strain gages in the SW2 pile, along with the ambient temperature.
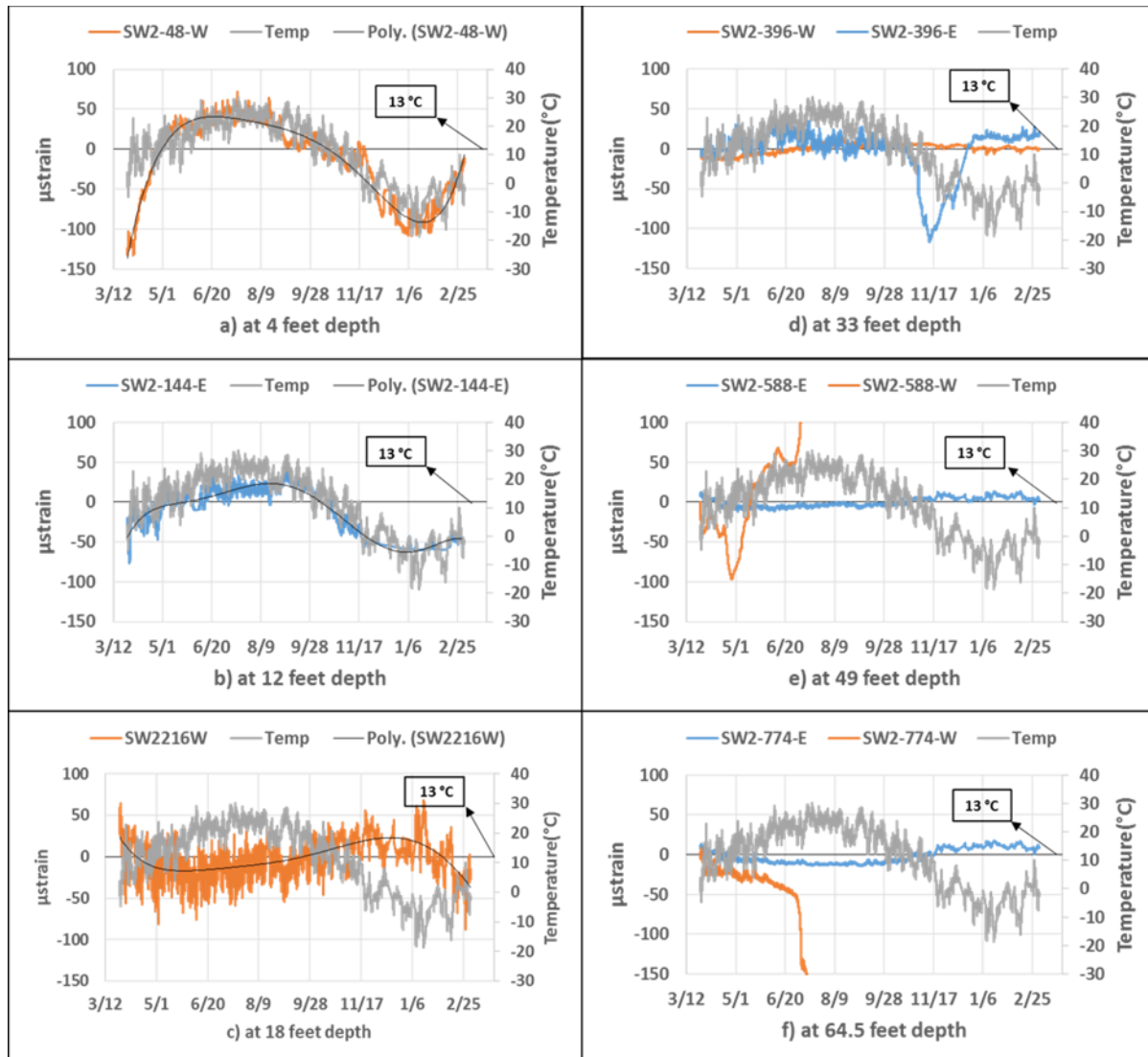
Figure 7-25. Steel pile (SW2) long-term strain change at different depth (3/22/2015– 3/3/2016)

Readings from gages SW2-48-E, SW2-144-W, and SW2-216-E were not included in this figure, since they appeared to have been damaged during pile construction. Gages SW2-396-E, SW2-588-W, and SW2-774-W shown in Figure 7-25 experienced significant drift and therefore were not used in the analysis. Using Method 1, the selected gages of SW2 were used to determine the maximum long-term strain variation and corresponding temperature change. Because UW1 and

213

SW2 shared the same temperature gage, the temperature readings in Figure 7-24 and Figure 7-25 are the same. During the monitored period, the maximum long-term strain variations at 4, 12, 18, 33, 49, and 64.5 ft below the pile head were 175 (i.e., from +60 to –115 microstrains), 125 (i.e., from +40 to –85 microstrains), 40 (i.e., from +15 to –25 microstrains), 20 (i.e., from +10 to –10 microstrains), 20 (i.e., from +10 to –10 microstrains), and 20 (i.e., from +10 to –10 microstrains), respectively, with respect to the selected reference temperature. When the SW2 daily strain variations were considered (Figure 7-22), a similar conclusion could be drawn, i.e., that the strains at 18 ft and below from the pile head were insignificant. The long-term strain variations were primarily caused by daily strain variation, when the depth was equal to or greater than 18 ft. No significant flexural actions by the SW2 pile head were expected below 18 ft.

To complement the strain data and analytical evaluation of the pile's response, displacement transducers and rotation gages were added. The data from these devices were collected at the same frequency used for the strain gages, starting on October 10, 2014.

Figure 7-26 shows the frequencies of abutment daily horizontal displacement variations over a 12-month period, influenced primarily by temperature.
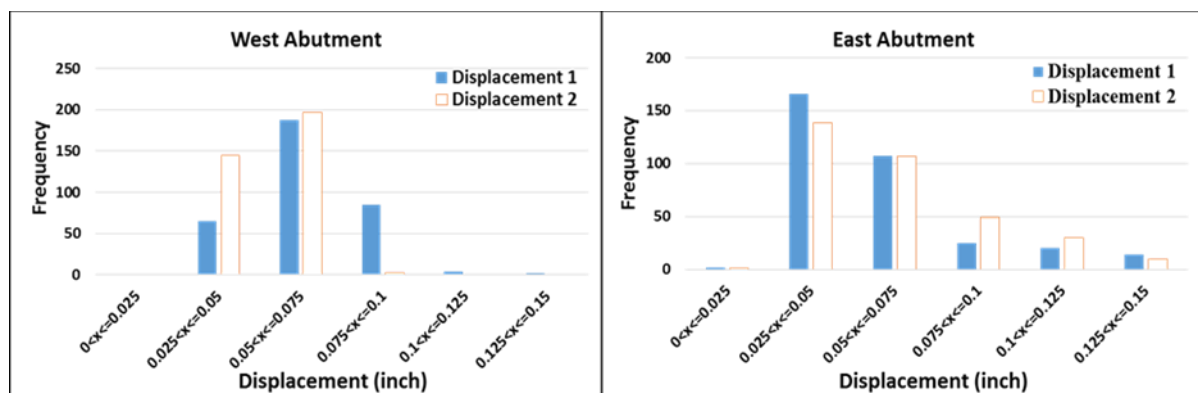
Figure 7-26. Maximum daily movement of the abutment

For both cases, the most common daily variations were in a range from 0.025 in. to 0.075 in. It was observed that large daily displacement variations corresponded to large daily temperature changes, as expected.

Using Method 1, Figure 7-27 compares the change in abutment displacement and ambient temperature as a function of time over a period of about 12 months.
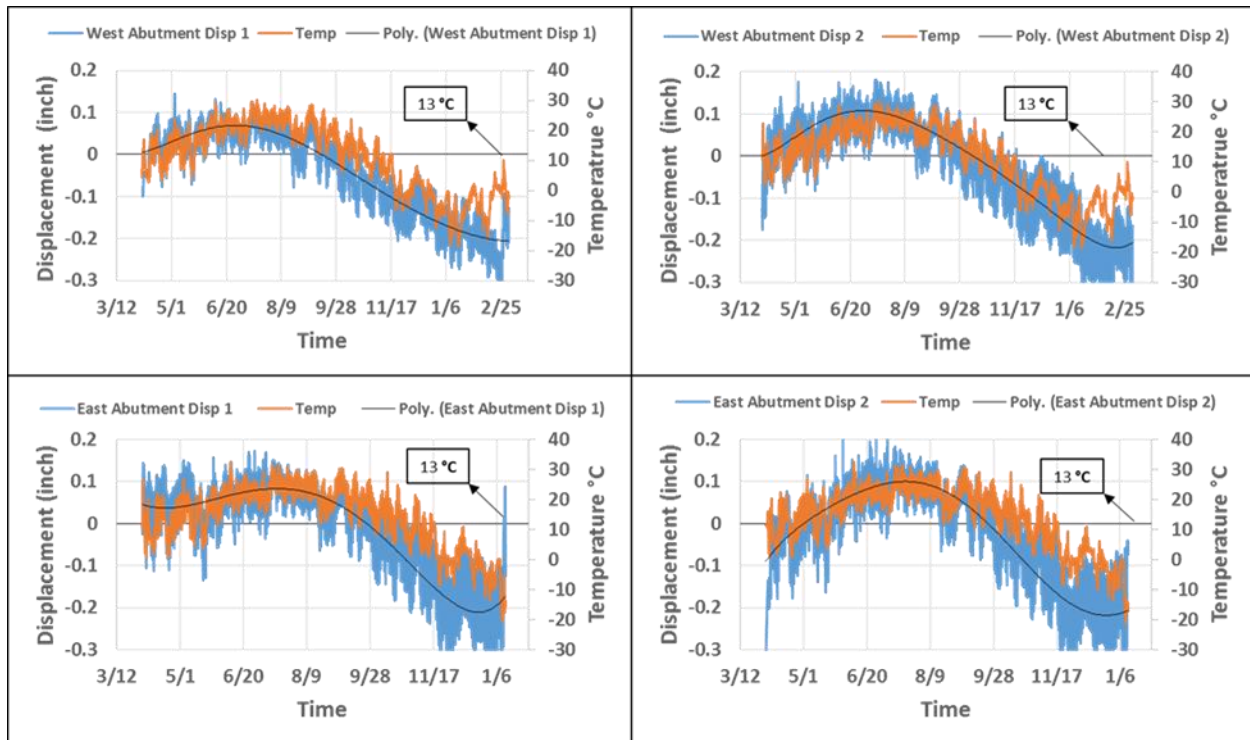
Figure 7-27. Abutments long-term displacement

All displacement values were taken as zero at the reference ambient temperature of 13°C. Polynomial best-fit lines are also included in Figure 7-27, where negative values indicate shortening of the bridge at temperatures lower than 13°C and positive values suggest the bridge lengthening in warmer temperatures. As shown in Figure 7-27, the maximum long-term displacements from West-Abutment-Disp 1, West-Abutment-Disp 2, East-Abutment-Disp 1, and East-Abutment-Disp 2 were 0.28 in. (i.e., 0.08 in. to –0.2 in.), 0.32 in. (i.e., 0.11 in. to –0.21 in.), 0.29 in. (i.e., 0.09 in. to –0.2 in.), and 0.32 in. (i.e., 0.10 in. to -0.22 in.), respectively. It was found that the maximum long-term temperature change and the corresponding abutment displacement were 35°C (i.e., from 20°C to –15°C) and 0.35 in (i.e., 0.1 in. to –0.21 in.), respectively. Since there is insignificant difference between Disp 1 and Disp 2 in both cases, the displacement value was taken as the average value from these four gages.

Figure 7-28 compares the abutment displacement and strain as a function of time over a 12-month period, with data from the top two gages from UW1 and SW2 chosen for this figure.
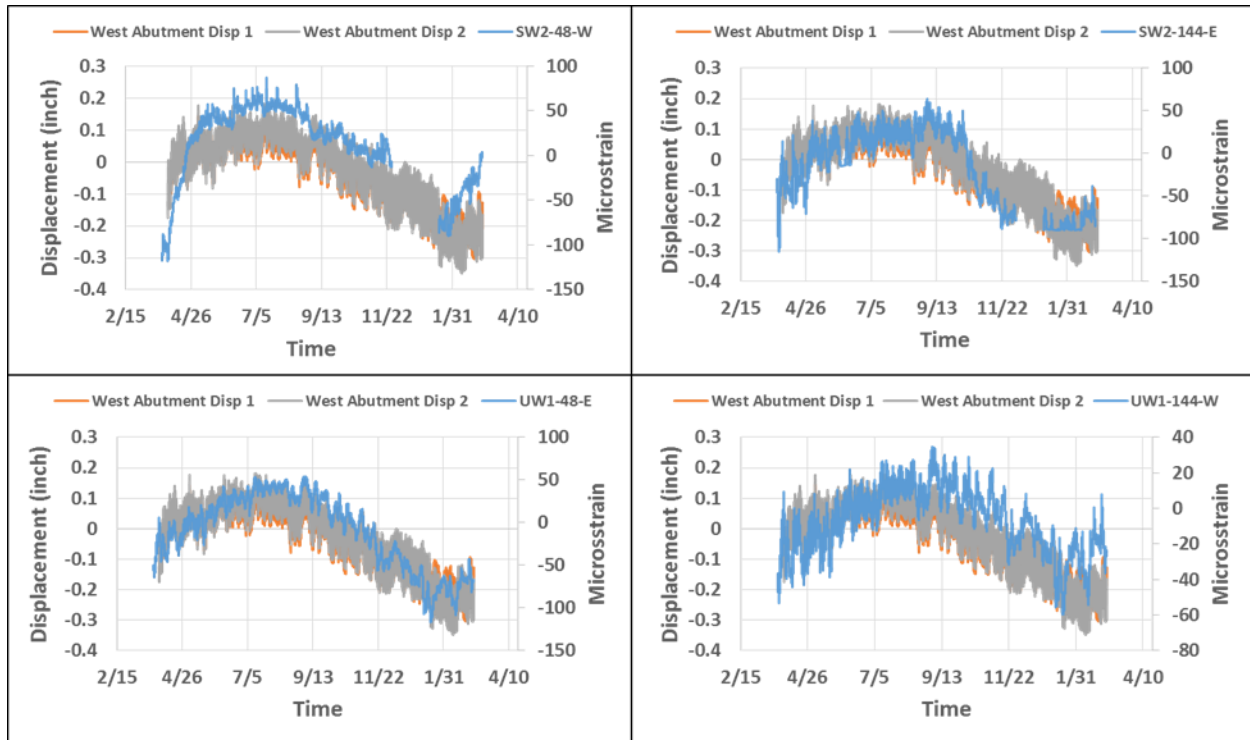
Figure 7-28. Displacement vs. strain for west abutment

Overall, the strain variation follows the displacement change pattern. In Figure 7-27, it can be observed that the abutment displacements reached their peak values around mid-July and their lowest values toward the end of January, consistent with previous observation.

7.7.2. *Data Interpretation and Analysis*

The bridge deck coefficient of thermal expansion (CTE) was evaluated using data from Figure 7-28. Given that recorded data from all four displacement gages were comparable, an average value was established using equation (7-1).

$$C = \frac{(R_h - R_c)}{\Delta T} \tag{7-1}$$

where,
C = Coefficient of linear thermal expansion of the concrete 10^-6/°F (°C)
Rh = Max extension at high temperatures, in. or mm
Rc = Max contraction at lower temperatures, in. or mm
ΔT = Difference in temperature of specimens between the two length readings, °F or °C

The calculated average CTE value for this bridge is 6.32*10^-6/°C. According to AASHTO LRFD Bridge Design Specification (2007), the CTE for normal concrete is 10.8*10^-6/°C (6*10^-6/°F), and is slightly larger than the calculated value in this report, possibly because of the restraints provided by bridge abutment and granular backfill placed behind the abutments.

The steel rebars in the bridge deck could have also played a positive role in reducing the bridge deck CTE value. Because of these restraints, the bridge deck exhibited a lower CTE value than that of unreinforced normal concrete.

The skewness of the bridge causes its longitudinal direction not to align with the pile strong axis, as shown in Figure 7-29.
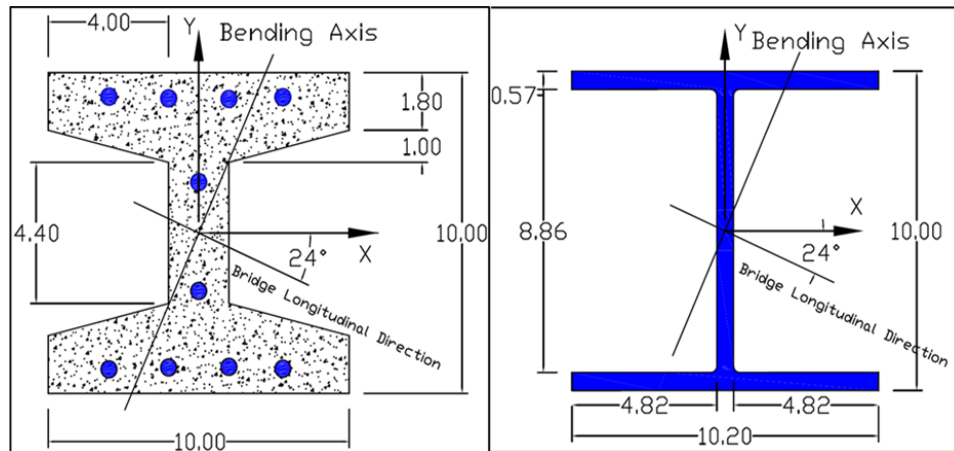
Figure 7-29. UHPC and steel piles cross-section and corresponding bending axes

Determination of the moment of inertia along the bridge longitudinal direction was required. The moments of inertia of the UHPC pile, and HP 10 × 57 sections were first determined. Then, the moments of inertia along the bridge's longitudinal direction was determined using equation (7-2).

$$I_{B,long} = I_x * Sin^2 24 + I_y * Cos^2 24 \qquad (7\text{-}2)$$

$$M = \frac{\sigma * I}{y} \qquad (7\text{-}3)$$

The following tables (Table 7-10, Table 7-11, Table 7-12, and Table 7-13) summarize the largest long-term strain change for the four production piles and the corresponding estimated moments at different levels.

Table 7-10. UW2 strain variation and calculated moment

Depth (ft)	4	12	18	33	49	64.5
Strain (µstrain)	115	–35	–20	0	0	0
Moment (kip-in.)	82.2	–46.4	–28.6	0	0	0

Table 7-11. UW1/UW1-2 strain variation and calculated moment

Depth (ft)	4	12	18	30	43	55.67
Strain (µstrain)	80	–35	–20	0	0	0
Moment (kip-in.)	41.5	–18.2	–10.4	0	0	0

Table 7-12. SE1 strain variation and calculated moment

Depth (ft)	4	12	16
Strain (µstrain)	N/A	N/A	–35
Moment (kip-in.)	N/A	N/A	–46.4

N/A = Not available data from strain gages

Table 7-13. SE2 strain variation and calculated moment

Depth (ft)	4	12	16
Strain (µstrain)	N/A	–80	–45
Moment (kip-in.)	N/A	–106.1	–59.7

N/A = Not available data from strain gages

As described in Subsection 7.7.1, the strain change was insignificant at depths equal or greater than 18 ft from the pile head. Given the fact that the long-term strain variation was close to the daily strain variation at depths of 18 ft and greater, it is reasonable to assume zero long-term strain change at those depths.

Figure 7-30 presents the moment profiles along piles SW2 and UW1 obtained from LPILE analysis after subjecting them to 0.2 in. head lateral displacement.
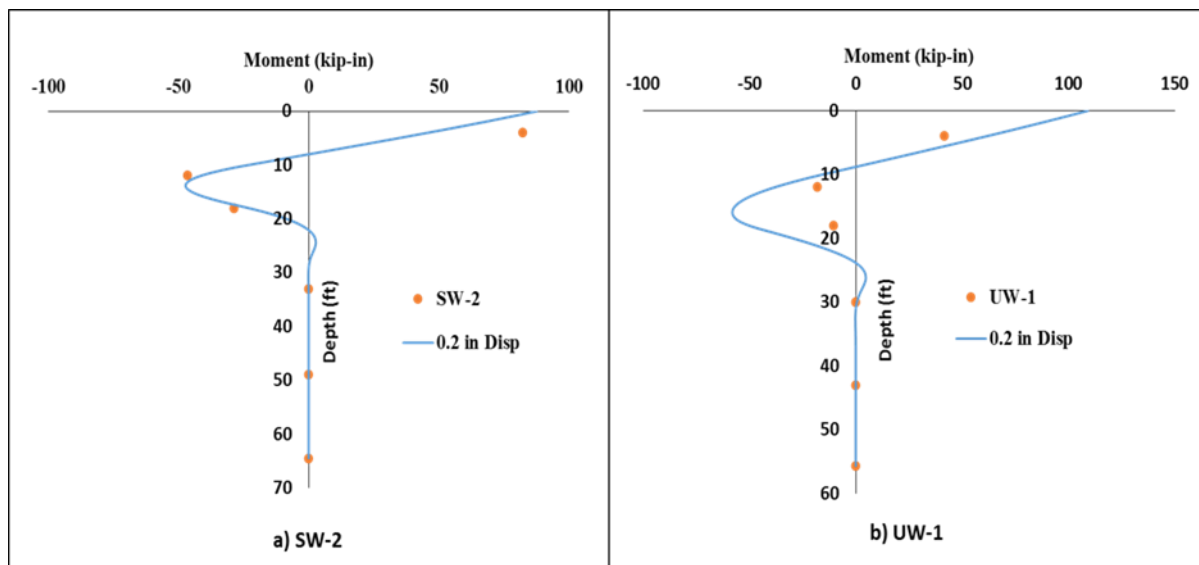
Figure 7-30. Model moment vs. strain moment for SW2 and UW1

The moments estimated from the measured strains at the corresponding depths are also included in this figure. For the SW2 pile, the experimental and theoretical values were in good agreement. For the UW1 pile, the experimental values were close to the analytical values, but the comparison was not as good as that observed for SW2. The deviation at a depth of 12 ft is less than half of the theoretical value. At a depth of 18 ft below the pile head, the experimental moment value is about one-third of the theoretical value. These variations are not unexpected for the following reasons: (1) the measured strains are relatively small and could be affected by daily temperature, and (2) soil profiles used for the analysis were not taken at these pile locations.

In Figure 7-31, the experimental moment values from SE1 and SE2 are shown along with theoretical curves. They too provide a satisfactory comparison.
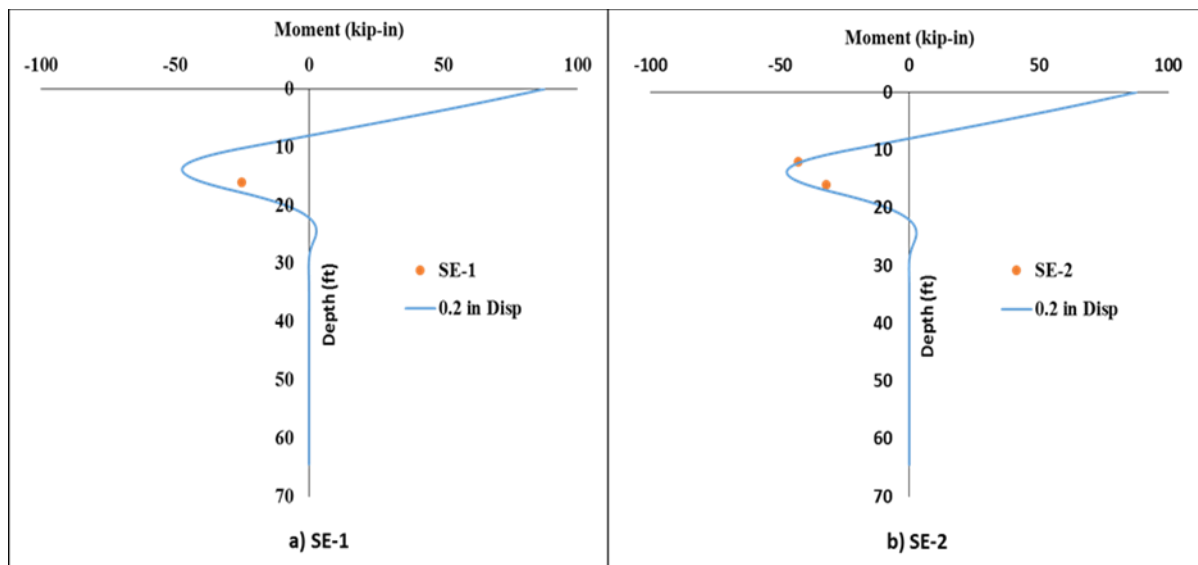
Figure 7-31. Steel pile model verification

Given that the UHPC pile experienced only a 0.2 in. head lateral displacement and the maximum corresponding estimated moment is 114 kip-in., it can be concluded that the performance of the UHPC pile meets expectations. Since no micro-cracking is expected on this pile until a moment of 536 kip-in., the UHPC pile in Sac County is not expected to experience any cracking during its service life. The performance of the steel pile also meets expectations. According to the analysis, the maximum estimated moment for the steel pile is 91 kip-in., only 11% of its yield moment.

7.7.3.   Pile Responses under Large Displacements

Since no cracking formed in the UHPC pile and no yielding was expected in the steel pile, this subsection explores permissible pile head lateral displacements at different damage stages and the impact of prebored holes. According to the Iowa DOT, all abutment piles for bridges longer than 130 ft are placed in prebored holes at a 10 ft depth (Iowa DOT 2019).

Figure 7-32 depicts the expected UHPC pile response corresponding to various damage stages in two different cases: (a) with prebored holes and (b) without prebored holes.
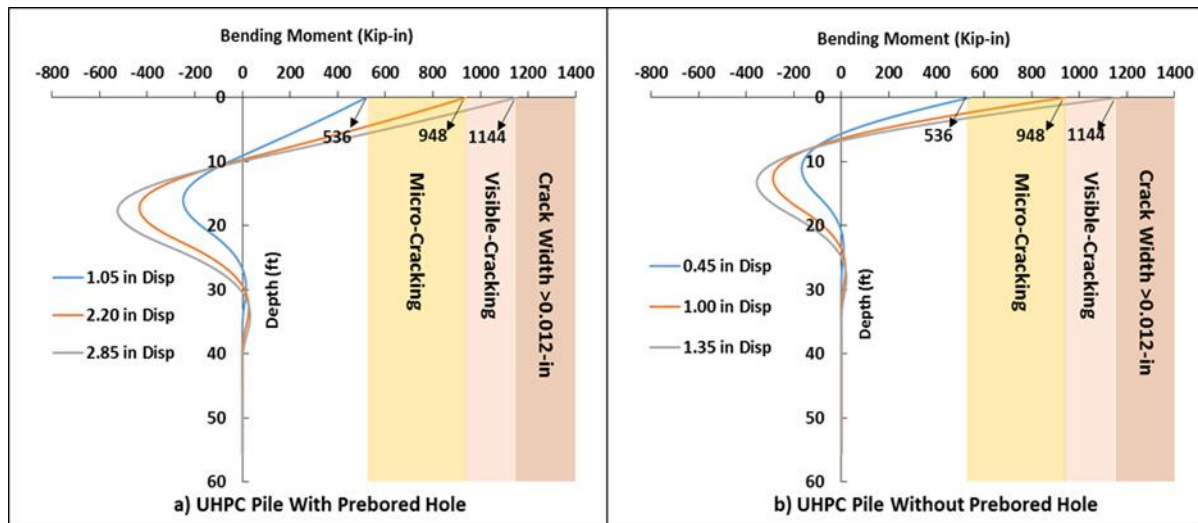
Figure 7-32. UHPC pile top displacement at different damage stage

Table 7-14 summarizes the UHPC pile head lateral displacement values when micro-cracking, visible cracking, and cracking with widths more than 0.012 in. are anticipated.

Table 7-14. UHPC pile head displacement for different damage case

	Acceptable range, in.		Unacceptable range, in.
	Micro-cracking	Visible cracking	Crack width > 0.012 in.
With prebored hole	1.05	2.20	2.85
Without prebored hole	0.45	1.00	1.35

Similarly, Figure 7-32 shows steel pile performance when the pile head reaches its maximum permissible displacement for two different scenarios: (a) with prebored holes and (b) without prebored holes.
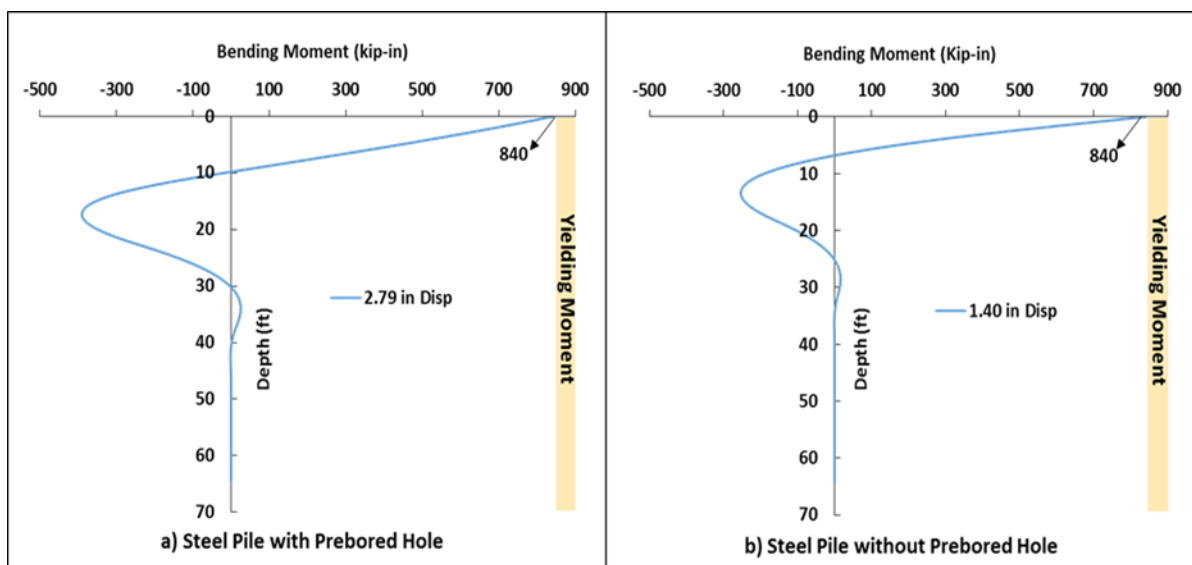
Figure 7-33. Steel pile general application

Table 7-15 summarizes the pile head lateral displacements for steel piles.

Table 7-15. Steel pile head displacement at yielding

	Max permissible displacement, in.
With prebored hole	2.79
Without prebored hole	1.40

With the prebored hole, the UHPC pile head lateral displacements for micro-cracking, visible-cracking, and crack widths wider than 0.012 in. were 1.05, 2.20, and 2.85 in., respectively. These values were 5, 11, and 14 times greater than the largest measured displacement values found throughout the project. Similarly, for the steel pile with a prebored hole, the maximum permissible displacement is 2.79 in., almost 14 times greater than the measured largest pile head lateral displacement. With no prebored hole, the UHPC pile head lateral displacements for micro-cracking, visible-cracking, and crack widths wider than 0.012 in. were 0.45, 1.00, and 1.35 in., equivalent to 2, 5, and 7 times greater than the largest measured values. For the steel pile, the maximum permissible displacement was 1.40 in., which was seven times greater than the measured values.

The piles with prebored holes exhibited twice as great a lateral displacement as the corresponding piles without prebored holes at the same damage stage, showing that the pile's flexibility was increased by the holes. For the same head lateral displacement, the piles with prebored holes produced a smaller bending moment at the critical sections, which is one of the purposes of a prebored hole. The analysis also reflects that, in the presence of a prebored hole, the magnitude of the second largest moment at depths below 10 ft increases by about 30% in both piles, although this should not cause any concern. According to the Iowa DOT, another purpose of the prebored hole is to reduce and/or eliminate additional load on the pile as a new

221

grade settles, which is referred to as "negative skin friction." However, since the prebored holes were filled with bentonite after the completion of pile installation, the second purpose was insignificant in this project.

For this project, the expected pile service displacement and maximum pile displacements were initially chosen to be 1.0 in. and 1.55 in. The 1.00 in. value was estimated to be the potential average displacement, from previous long-term monitoring of integral abutments, while the values of 1.55 in. was chosen based on the Iowa DOT LRFD Bridge Design Manual commentary, with both values designed for piles with prebored holes. Figure 7-34 summarizes pile performance for both UW1 and SW2 when the pile head experiences 1.0 in. and 1.55 in. displacement.
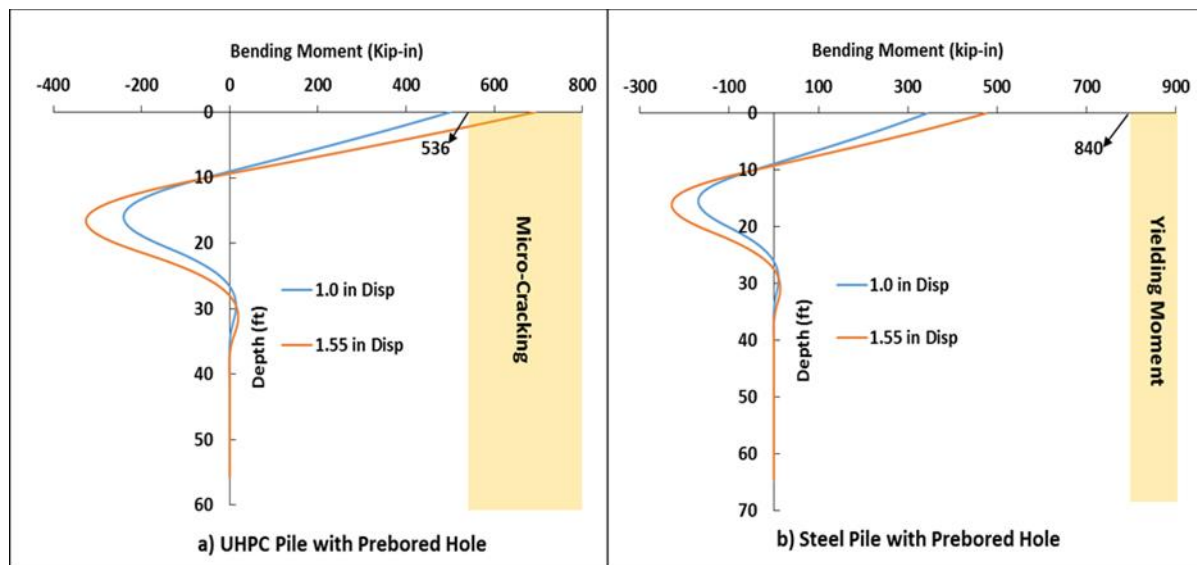
Figure 7-34. UW1 and SW2 extreme case performance analysis

For UW1, only the top 2 ft exhibited a micro-cracking issue when the displacement value was 1.55 in., an acceptable result according to Iowa DOT. For the steel pile, no yielding issue is expected in either case. Both piles performed well under expected service displacement and maximum allowable displacement, and no unacceptable damage was observed.

Given the fact that both piles performed well under both service and maximum displacements when there was a prebored hole, the following paragraphs will discuss how those two values are likely to change when there is no prebored hole.

Figure 7-35 compares UHPC pile head displacement for the similar moment profile in two different cases: (a) with a prebored hole and (b) without a prebored hole.

222
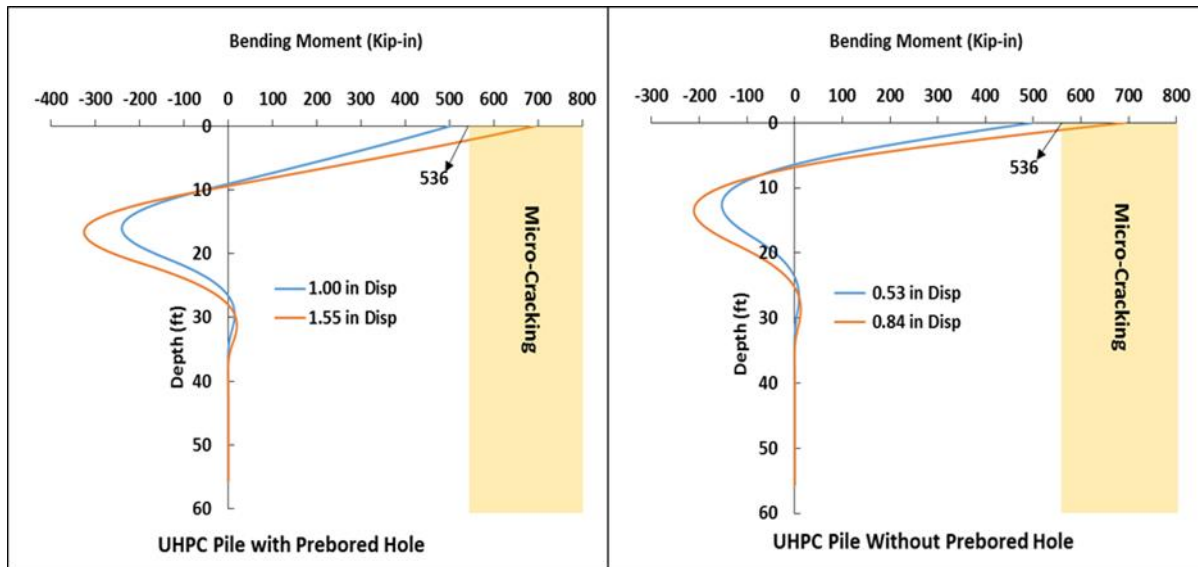
Figure 7-35. UHPC pile head displacement change for difference cases

From this figure, it can be observed that when no prebored hole exists, the service displacement and maximum displacement change from 1.00 and 1.55 in. to 0.53 and 0.84 in., respectively. The corresponding displacement ratio between the pile with prebored hole and the pile without prebored hole is approximately 2, matching the previous analysis results.

Figure 7-36 depicts the service displacement and maximum displacement change for a steel pile.
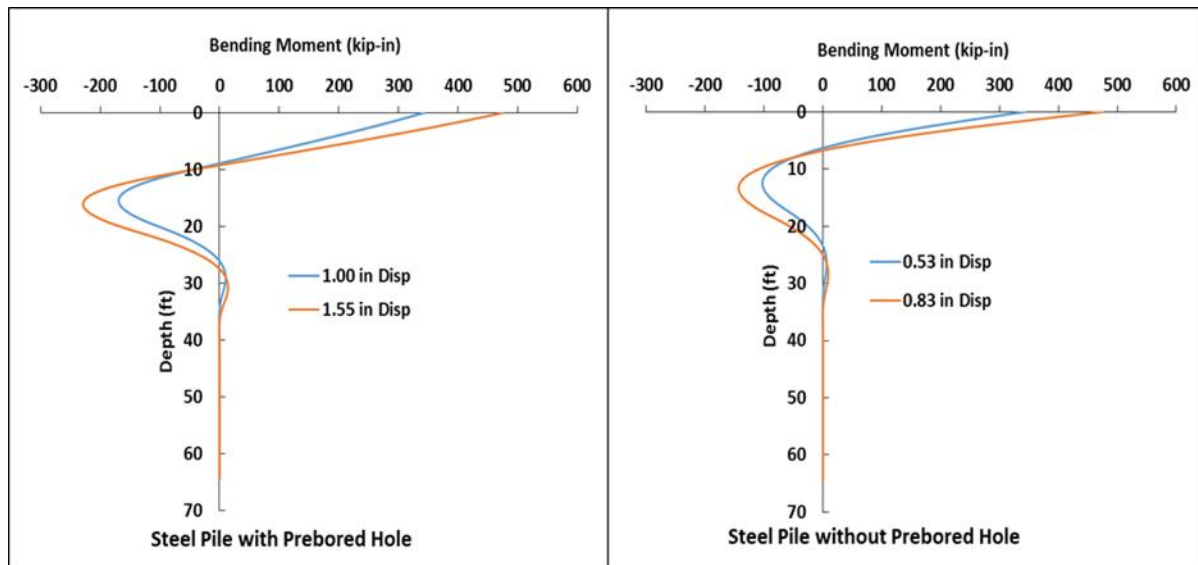
Figure 7-36. Steel pile head displacement change for difference cases

Similarly, there are two cases: (a) with prebored hole and (b) without prebored hole. When there is no prebored hole, the service displacement and maximum displacements diminish from 1.00 and 1.55 in. to 0.53 and 0.834 in., respectively. The corresponding displacement ratio between

223

these two different cases is also approximately 2, consistent with the values obtained for the UHPC pile.

Figure 7-37 shows the shear profile for UHPC and steel when their heads are subjected to a 0.2 in. lateral displacement.
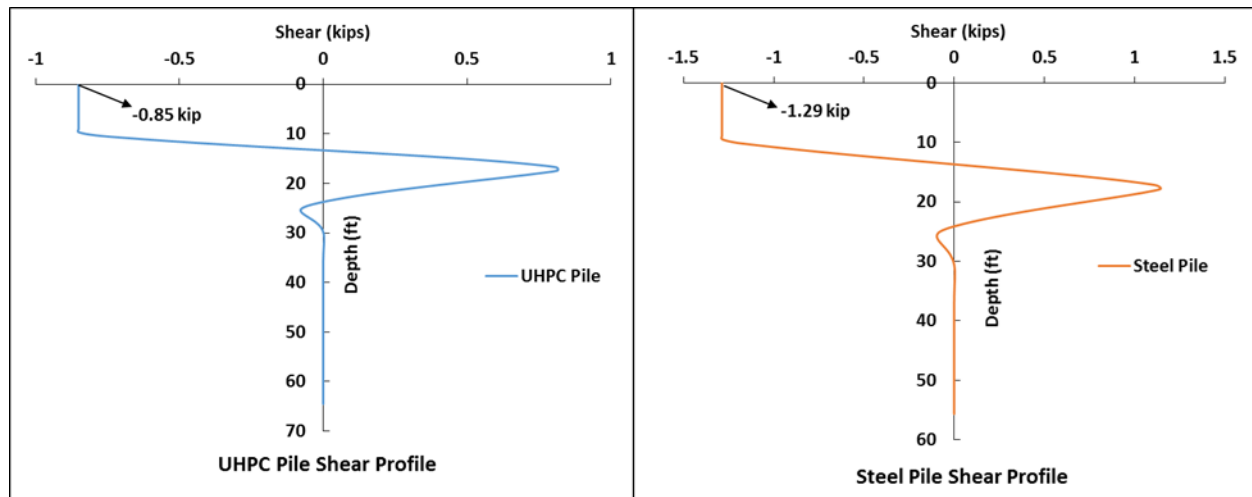
Figure 7-37. Pile shear profile under 0.2 in. displacement

There are two reasons for small values to be chosen for the stiffness calculation. First, the piles fall under the category of elastic criteria under small deformation. Second, small displacements match the field monitoring result. Equation (7-4) is used in the stiffness calculation.

$$k = \frac{F}{X}$$
(7-4)

where,
k= pile stiffness, kip/in.
F = applied force, kips
X = pile displacement, in.

In Figure 7-37, the shear forces remain constant over the first 10 ft below the pile head, due to the presence of a prebored hole. According to the calculation, the stiffness values for the UHPC pile and the steel pile are 4.25 and 6.45 kip/in., respectively, indicating that the UHPC pile is more flexible than the steel pile.

Based on the analysis of the pile performance in this section, the following conclusions can be drawn:

- The presence of a prebored hole could improve pile flexibility and increase the displacement by a factor of two

224

- With a prebored hole, both UHPC pile and steel pile perform well both under full service displacement and at maximum allowable displacement
- When there is no prebored hole, the allowable displacements recommended by the Iowa DOT should be reduced to half their original values
- Given that the observed performance of the pile being similar to that obtained from the analysis, it would be possible to replace all the steel piles with UHPC piles in this project

7.8. Estimated Initial Cost Comparison

For the Sac County bridge replacement project, it was suggested by the Iowa DOT to use an average price of $35 per linear foot for the material and installation. The fabrication cost of UHPC piles, as recommended by industry, is $2,500 per yd^3. There are 0.015 yd^3 of UHPC in every linear foot of the pile. This would give a material and fabrication cost of $37.50 per linear foot. From RS Means (2009), the labor and equipment cost in Iowa for pile installation is $7.47 per linear foot with an additional $5.50 per linear foot for overhead and profit costs for the crew and equipment given in Table 7-16.

Table 7-16. Crew and equipment for labor cost estimate

Crew	Equipment
1 pile driver foreman	1 crawler crane
4 pile drivers	1 90 ft lead
2 equipment operators (crane)	1 diesel hammer
1 equipment operator (oiler)	

The total price per linear foot of UHPC is estimated to be approximately $50.47.

Clearly, UHPC piles are more expensive per linear foot than the HP 10×57 piles used for the Sac County bridge project. Table 7-17 lists the number and length HP 10×57 piles used in both the westbound and eastbound bridges.

Table 7-17. Total length of HP 10×57 piles needed for Sac County bridge project

Bridge	Location	# of piles	Length/Pile, ft	Total length, ft
Westbound	West abutment	10	65	650
	Pier 1	27	50	1,350
	Pier 2	27	55	1,485
	East abutment	10	85	850
Eastbound	West abutment	10	65	650
	Pier 1	27	50	1,350
	Pier 2	27	55	1,485
	East abutment	10	85	850
			Sum	8,670

Similarly, Table 7-18 lists the number and corresponding length of UHPC piles needed to support the two bridges based on the current Iowa DOT Blue Book Method.

Table 7-18. Total length of UHPC piles needed for Sac County bridge project

Bridge	Location	# of piles	Length/Pile, ft	Total length, ft
Westbound	West abutment	10	55	550
	Pier 1	27	40	1,080
	Pier 2	27	45	1,215
	East abutment	10	85	850
Eastbound	West abutment	10	55	550
	Pier 1	27	40	1,080
	Pier 2	27	45	1,215
	East abutment	10	80	800
			Sum	7,290

Based on the total length of HP 10×57 piles, the cost of the foundation at $35 per linear foot would be $303,450. The UHPC pile foundation would cost a total of $367,926. Based on the initial cost estimate, UHPC piles are approximately 21% more expensive. For the Sac County bridge project, the price for UHPC material and prefabrication costs needs to be reduced to $1,910 per yd^3 to have the same total foundation cost as for the steel HP 10×57 piles, which is a reduction of 31%. One thing to note is that this estimate does not take into account the increased durability and reduced maintenance costs associated with UHPC piles. For a more accurate cost comparison, a total life-cycle cost analysis should be done with due consideration of the increased life span of the UHPC piles.

CHAPTER 8:SUMMARY, CONCLUSIONS, AND FUTURE RESEARCH

8.1.   Summary of Research

The research presented herein is part of the second phase of an extensive study on the development and field installation of UHPC piles, which focused on the design, precast fabrication, installation, and performance verification in the field.

During Phase I of the project, the design of the UHPC pile cross-section was optimized, and the section behavior in strong-axis bending was predicted and verified through laboratory testing, followed by a vertical and a lateral load test in the field. Specifically, this study (1) investigated the performance of a UHPC pile as part of an integral bridge using analytical models, (2) tested the typical pile-to-abutment connection detail in the laboratory by subjecting the connection to a combination of axial and lateral cyclic loading, (3) conducted a field vertical load test to failure, (4) performed a lateral load test in the field on a spliced UHPC pile, and (5) instrumented and installed a production UHPC pile as part of a bridge foundation to compare its driving behavior and performance to a comparable steel H-pile.

A brief introduction to the history and background of the challenges associated with traditional concrete and steel piles in the US, along with an introduction to Phase I of the UHPC pile project, was provided in Chapter 1, which focused on the way UHPC members with enhanced engineering and durability properties could be used to extend bridge foundation service life.

A review of published studies describing the composition, microstructure, durability, material properties, applications, practice for splicing piles in the field, pile-to-abutment connection details, integral abutment issues relevant to this study, and analysis procedures for evaluating drivability and lateral load performance of piles was given in Chapter 2.

Chapter 3 focused on an analysis of UHPC piles in integral abutments by describing the section behavior of UHPC and HP 10×57 piles in weak-axis bending and strong-axis bending, and a parametric study on the lateral load behavior of UHPC piles with the appropriate axial load using the calculated section behavior.

Splice design and relevant testing were presented in Chapter 4, while the fabrication and casting of the UHPC test units and abutment cap were described in Chapter 5. Chapter 5 also presented the lateral load tests of the HP 10×57 and UHPC test piles connected to the abutment blocks and the findings.

A description of the fabrication and casting process, installation, vertical load test, and lateral load test for the UHPC test piles in the field is provided in Chapter 6.

Chapter 7 describes the fabrication and casting process of the UHPC production pile, the installation and instrumentation of three instrumented HP 10×57 piles and the UHPC production pile, and the results from long-term monitoring of the four plies.

8.2.   Conclusions

This study provided a complete analysis of the design, fabrication, and installation of UHPC piles in comparison to steel HP 10×57 piles. The conclusions drawn from the pile analysis, production, handling, installation, feasibility, and performance of the pile in the laboratory and field are described in this section.

8.2.1.   Pile Analysis

The parametric study of the UHPC pile in comparison with the HP 10×57 pile proved that the UHPC pile could be a viable option for supporting integral abutment bridges. At higher axial loads, such as 200 kips, it was found that the UHPC pile resisted cracking even at large target lateral displacements of 1.0 in. and 1.55 in. compared to a 100 kip axial load, as previously specified in Section 3.2 In comparison, HP 10×57 piles resisted yielding at the same target displacements. The strength benefits associated with increasing axial loads on UHPC piles supported their use in integral abutments.

The lateral load analysis conducted in LPILE supported the use of prebored holes for both UHPC piles and HP 10×57 piles, which is currently required by the Iowa DOT for bridges over 130 ft in length. The benefit of prebored holes was that they were found to minimize or prevent cracking of the UHPC piles and yielding of H-piles to an acceptable level during the cyclic expansion and contraction of the bridge due to thermal movements.

8.2.2.   Production, Handling, and Installation of UHPC Piles

The newly design pickup point for UHPC piles described in Section 6.4.6, which used a 1 in. diameter high-strength threaded rod, washers, and a nut, proved to be successful but somewhat labor intensive since a crew member had to be lifted by the crane to unhook the pile from the crane head before driving could begin. A release mechanism similar to that used for steel H-piles needs to be established as it will increase the efficiency during installation of UHPC piles in the field. After the pile was positioned to be vertical, the UHPC pile could be set in the prebored hole in the same way as an HP 10×57 pile. The benefit of the new pickup point was to have the pile hang in the vertical position as straight as possible to provide easy insertion into the prebored hole, which was successful in the field.

During installation, a void in the soil opened up near the web on both sides of the UHPC piles. The void at the 46 ft long test pile had a depth of approximately 5 ft, while the void at the 30 ft long test pile was 3 ft deep. This possibly indicates the occurrence and depth of the void to be related to the embedment length of the pile. Another likely parameter that may affect the size and occurrence of the void could be the soil condition at the site of installation. Analysis of UHPC piles should take this void into account when establishing the vertical load capacity and lateral load performance as the void can have some limited influence on the pile performance.

228

In some cases, minimal damage to the UHPC pile head was seen in the field after driving. The 30 ft test pile did not have any visible damage to the pile head after installation. The longer 46 ft and 56 ft UHPC piles sustained minor damage to the corners of the pile head. This was believed to be due to not placing the hammer at the center of the pile head during installation, which should be given attention in the field.

8.2.3.   *Feasibility of using UHPC Piles in Integral Abutments*

The test of the pile-to-abutment connection confirmed that the current Iowa DOT design of integral abutments with steel piles was robust and would accommodate UHPC piles as well. Even though two hairline tension cracks with negligibly small widths developed at 12 kips of lateral load during testing in the laboratory with an axial load of 100 kips, they were considered acceptable based on previous experience with testing and use of UHPC members.

During the UHPC vertical load test in the field, the UHPC test pile reached an ultimate capacity of 297 kips, which was 49% greater than the estimated nominal capacity of 200 kips. The capacity measured during the field testing confirmed that a 16% shorter UHPC production pile compared to the HP 10×57 piles was appropriate for the Sac County bridge.

The UHPC lateral load piles were tested to a maximum lateral load of 20.6 kips with a corresponding lateral displacement of 8.3 in. for the weak-axis pile. The weak-axis pile failed 3 ft above the splice. The soil was excavated around the 30 ft long test pile where a significant tension crack was discovered at approximately the location of expected maximum moment. Within the design lateral movements of 1.55 in., the UHPC piles performed well and indicated no damage.

In this project, the design of the UHPC piles followed the Iowa DOT design practice (summarized in Section 2.5 with sample calculations in Appendix C) with due consideration to the skin friction and end bearing components. In these calculations, UHPC piles were treated with the resistance recommended for prestressed concrete. While further refinements to the design procedure are possible, the study supports the notion that H-shaped tapered UHPC piles can be designed with the existing design provisions developed for prestressed concrete piles.

8.2.4.   *Performance of Pile Splice*

The splice located on P4, 15 ft from the pile head, performed very well during installation. No visible damage from driving or the lateral load test was found on or near the splice after excavation. Based on the field testing and additional laboratory tests, the performance of the splice in the field can be expected to meet the required shear, moment demands, and tensile demands.

8.3.   Future Research

To ensure quality production of UHPC piles without any defects, consistent tolerances and procedures need to be developed. The tolerances for imperfections should include limits on shrinkage cracking along the pile, air voids within the web of the pile, and inconsistent dimensions of the flanges and other applicable quality issues that are used today for precast concrete piles.

Prebored holes may not be as effective as intended during design. Future research with regard to lateral load tests on UHPC piles installed in prebored holes filled with bentonite may be used to verify their performance. For a reference, a similar pile test without a prebored hole may be used.

It is common to have battered piles in bridge piers. To increase the broad use of the UHPC piles, the use of battered UHPC piles as well as their connections to pile caps and abutments should be investigated and their performance should be evaluated in the field.

Additional sizes of the tapered H-section UHPC pile should be investigated to make the product feasible for various soil and structural conditions. Having a variety of sizes would increase the efficiency and frequency of use of UHPC piles. Steel piles are increasing in size to meet the demands for efficient, higher capacity foundations, and in order to provide a comparable solution, a larger sized UHPC pile might be necessary. With increased web and flange dimensions in larger UHPC sections, the production efficiency of UHPC piles will likely increase.

To reduce the relatively high cost of UHPC piles, the UHPC material, design, fabrication, installation, and increased life cycle need to be investigated or improved from current knowledge. Integrating the life-cycle cost and expected maintenance cost reduction for the UHPC members into the analysis will help realize the true costs of the UHPC piles. In order to improve the design procedures for UHPC piles, additional vertical load tests need to be performed to more accurately predict the ultimate pile capacity. In doing so, the length of UHPC piles can be optimized, and overall foundation costs may be reduced. At the fabrication stage, it is essential to develop easier to use steel forms to cast multiple UHPC piles and shorten the time the piles need to be on the precast bed to gain strength in order to streamline the production process. Improved installation procedures and an improved pickup point also need to be developed.

REFERENCES

Aaleti, S., S. Sritharan, D. Bierwagen, and B. Moore. 2011. Precast UHPC Waffle Bridge Deck Panels and Connections for Accelerated Bridge Construction. *Proceedings of the National Bridge Conference / PCI Annual Convention and Exhibition*, October 22–26, Salt Lake City, UT.

Aaleti, S., E. Honarvar, S. Sritharan, M. Rouse, and T. Wipf. 2014. *Structural Characterization of UHPC Waffle Deck and Connections*. Bridge Engineering Center, Iowa State University, Ames, IA. https://intrans.iastate.edu/app/uploads/2018/03/uhpc_waffle_deck_w_cvr.pdf.

AbdelSalam, S. S., K. W. Ng, S. Sritharan, M. T. Suleiman, and M. Roling. 2012. *Development of LRFD Procedures for Bridge Pile Foundations in Iowa—Volume III: Recommended Resistance Factors with Consideration of Construction Control and Setup*. Bridge Engineering Center, Iowa State University, Ames, IA. https://intrans.iastate.edu/app/uploads/2018/03/tr-584_lrfd_vol_iii_w_cvr1.pdf.

Abendroth, R. E. and L. F. Greimann. 2005. *Field Testing of Integral Abutments*. Center for Transportation Research and Education, Iowa State University, Ames, IA. https://intrans.iastate.edu/app/uploads/2018/03/hr399.pdf.

Abendroth, R. E., L. F. Greimann, and M. D. LaViolette. 2007. A*n Integral Abutment Bridge with Precast Concrete Pile*s. Center for Transportation Research and Education, Iowa State University, Ames, IA. https://intrans.iastate.edu/app/uploads/2018/03/tama-integral-abutment-bridge.pdf.

AASHTO. 2007. *LRFD Bridge Design Specifications, 4th Edition*. American Association of State Highway and Transportation Officials, Washington, DC.

AASHTO Highway Subcommittee on Bridges and Structures. 2005. *Grand Challenges: A Strategic Plan for Bridge Engineering*. American Association of State Highway and Transportation Officials, Washington, DC.

ACI Committee 318. 2005. *Building Code Requirements for Structural Concrete (ACI 318-05)*. American Concrete Institute, Farmington Hills, MI.

API. 1993. *Recommended Practice on Planning, Designing, and Constructing Fixed Offshore Platforms – Load and Resistance Factor Design – 1st Edition*. API RP 2A-LRFD. American Petroleum Institute, Dallas, TX.

Arsoy, S., R. M. Barker, and J. M. Duncan. 2002. *Experimental and Analytical Investigations of Piles and Abutments of Integral Bridges*. Virginia Transportation Research Council, Charlottesville, VA.

AFGC. 2002. *Ultra High Performance Fibre-Reinforced Concretes – Interim Recommendations*. AFGC Scientific and Technical Documents. Association Française de Génie Civil, Paris, France.

ASTM D3966-07: Standard Test Methods for Deep Foundations under Lateral Load. ASTM International, West Conshohocken, PA.

ASTM D1143/D1143M-07: Standard Test Methods for Deep Foundations under Static Axial Compressive Load. ASTM International, West Conshohocken, PA.

Behloul, M., O. Bayard, and J. Resplendino. 2006. Ductal Prestressed Girders for a Traffic Bridge in Mayenne, France. *7th International Conference on Short and Medium Span Bridges*. August 23–25, Montreal, Quebec, Canada.

Behloul, M., R. Ricciotti, R. F. Ricciotti, P. Pallot, and J. Leboeuf. 2008. Chapter 48. Ductal Pont du Diable Footbridge, France. In *Tailor Made Concrete Structures.* Taylor & Francis Group, London, UK.

Blais, P. Y. and M. Couture. 1999. Precast, Prestressed Pedestrian Bridge — World's First Reactive Powder Concrete Structure. *PCI Journal*, Vol. 44, No. 5, pp. 60–71. https://www.pci.org/PCI_Docs/Publications/PCI%20Journal/1999/Sept-Oct/Precast%20Prestressed%20Pedestrian%20Bridge%20-%20World%27s%20First%20Reactice%20Poweder%20Concrete%20Structure.pdf.

Bonczar, C., S. F. Breña, S. Civjan, J. DeJong, B. Crellin, and D. Crovo. 2005. Field Data and FEM Modeling of the Orange-Wendell Bridge. *FHWA Conference – Integral Abutment and Jointless Bridges (IAJB 2005)*, March 16–18, Baltimore, MD.

Brown, D. A., M. W. O'Neill, M. Hoit, M. McVay, M. H. El Naggar, and S. Chakraborty. 2001. *NCHRP Report 461: Static and Dynamic Lateral Loading of Pile Groups*. National Cooperative Highway Research Program, Washington, DC.

Bustamante, M. and L. Gianeselli, L. 1982. Pile Bearing Capacity Prediction by Means of Static Penetrometer CPT. *Proceedings of the Second European Symposium on Penetration Testing*, pp. 493–500. May 24–27, Amsterdam, Netherlands.

CDOT. 2009. *CDOT Bridge Design Manual*. Colorado Department of Transportation, Denver, CO. http://www.coloradodot.info/library/bridge/bridge-manuals.

Chanvillard, G. and S. Rigaud. 2003. Complete Characterization of Tensile Properties of Ductal UHPFRC According to the French Recommendations. *Workshop on High Performance Fiber Reinforced Cement Composites, Proceedings of the International RILEM Conference,* pp. 21–34. Ann Arbor, Michigan.

Cheyrezy, M. and M. Behloul. 2001. Creek and Shrinkage of Ultra-High Performance Concrete. *Proceedings of the 6th International Conference CONCREEP-6@MIT: Creep, Shrinkage, and Durability Mechanics of Concrete and Other Quasi-Brittle Materials,* pp. 526–538. August 20–22, Cambridge, MA.

Davisson, M. T. 1972. High Capacity Piles. *Proceedings of Lecture Series on Innovations in Foundation Construction*, American Society of Civil Engineers, Illinois Section, Chicago, IL.

Decker, J. B., K. M. Rollins, and J. C. Ellsworth. 2008. Corrosion Rate Evaluation and Prediction for Piles Based on Long-Term Field Performance. *Journal of Geotechnical and Geoenvironmental Engineering,* Vol. 134, No. 3, pp. 341–351.

Dicleli, M. and S. M. Albhaisi. 2004 Effect of Cyclic Thermal Loading on the Performance of Steel H-Piles in Integral Bridges with Stub-Abutments. *Journal of Constructional Steel Research*, Vol. 60, No. 2, pp. 161–182.

DiMillio, A. 1999. *A Quarter Century of Geotechnical Research*. FHWA-RD-98-139. Federal Highway Administration, McLean, VA. https://www.fhwa.dot.gov/publications/research/infrastructure/geotechnical/98139/.

Dirks, K. and P. Kam. 2003. *Foundation Soils Information Chart, Pile Foundation*. Office of Road Design, Iowa Department of Transportation, Ames, IA.

Dugat, J., N. Roux, and G. Bernier. 1996. Mechanical Properties of Reactive Powder Concretes. *Materials and Structures,* Vol. 29, No. 4, pp. 233–240.

Ductal. 2012. Structural. LafargeHolcim, Jona, Switzerland. Accessed March 2012. http://www.ductal-lafarge.com/wps/portal/ductal/2-Structural.

Duncan, J. M. and S. Arsoy. 2003. Effect of Bridge-Soil Interaction on Behavior of Piles Supporting Integral Bridges, *Transportation Research Record*, Vol. 1849, pp. 91–97.

Ehsani, M., M. Farahani, and E. Raatz. 2012. Product Watch: Repair of Columns with FRP Laminates. *STRUCTURE magazine*. https://www.structuremag.org/wp-content/uploads/2014/08/D-ProductWatch-Eshani-Jan121.pdf.

FHWA. 2010. *Focus – Ultra High Performance Concrete: Taking Concrete to New Levels*. FHWA-HRT-10-015. Federal Highway Administration, McLean, VA. www.fhwa.dot.gov/publications/focus/10jul/05.cfm.

Freyermuth, C. 2009. Service Life and Sustainability of Concrete Bridges. *Aspire*, pp. 12–15.

Frosch, R. J., M. Wenning, and V. Chovichien. 2005. The In-Service Behavior of Integral Abutment Bridges: Abutment Pile Response. *FHWA Conference – Integral Abutment and Jointless Bridges (IAJB 2005)*, March 16–18, Baltimore, MD.

Girton, D. D., T. R. Hawkinson, and L. F. Greimann. 1991. Validation of Design Recommendations for Integral-Abutment Piles, *Journal of Structural Engineering*, Vol. 117, No. 7, pp. 2117–2134.

Gowripalan, N. and R. I. Gilbert. 2000. Design Guidelines for Ductal Prestressed Concrete Beams. *VSL (Aust) Pty Ltd*, Thornleigh, Australia.

Graff, C. R. 1965. The Wave Equation and Pile Driving. *Foundation Facts*, Vol. 1, No. 2, pp. 8–9, 18.

Graybeal, B. A. 2005. Characterization of the Behavior of Ultra-High Performance Concrete. PhD dissertation. University of Maryland, College Park, MD.

Graybeal, B. 2006. *Material Property Characterization of Ultra-High Performance Concrete*. FHWA-HRT-06-103. Federal Highway Administration, McLean, VA.

Graybeal, B. A. 2007. Compressive Behavior of Ultra-High-Performance Fiber-Reinforced Concrete. *ACI Materials Journal,* Vol. 104, No. 2, pp. 146–152.

Graybeal, B. 2009. *Structural Behavior of a 2nd Generation UHPC Pi-Girder*. FHWA-HRT-09-068. Federal Highway Administration. McLean, VA.

Green D., K. W. Ng, K. F. Dunker, S. Sirtharan, and M. Nop. 2012. *Development of LRFD Design Procedures for Bridge Pile Foundations in Iowa – Volume IV: Design Guide and Track Examples*. Bridge Engineering Center, Iowa State University, Ames, IA. https://intrans.iastate.edu/app/uploads/2018/03/lrfd_vol_iv_final_w_cvr.pdf.

GRL Engineers. 2001. *Pile Driving Wave Equation Workshop – Course Notes*. March 21, Iowa State University, Ames, IA.

Grünewald, S. 2004. *Performance-Based Design of Self-Compacting Fibre Reinforced Concrete*. Delft University Press, Delft, The Netherlands.

Hannigan, P. J., G. G. Goble, G. E. Likins, and F. Rausche. 2006a. *Design and Construction of Driven Piles Foundations: Reference Manual – Volume I*. FHWA-NHI-05-042. Federal Highway Administration, Washington, DC. http://faculty.uml.edu/ehajduk/Teaching/14.528/documents/FHWANHI-05-042DesignandConstructionofDrivenPileFoundations-VolumeI.pdf.

Hannigan, P. J., G. G. Goble, G. E. Likins, and F. Rausche. 2006b. *Design and Construction of Driven Piles Foundations: Reference Manual – Volume II*. FHWA-NHI-05-043. Federal Highway Administration, Washington, DC. http://faculty.uml.edu/ehajduk/Teaching/14.528/documents/FHWANHI-05-043DesignandConstructionofDrivenPileFoundations-VolumeII.pdf.

Hetényi, M. 1946. *Beams on Elastic Foundation: Theory with Application in the Fields of Civil and Mechanical Engineering*. University of Michigan Press, Ann Arbor, MI. https://ia601609.us.archive.org/7/items/in.ernet.dli.2015.73919/2015.73919.Beams-On-Elastic-Foundation-Theory-With-Applications-In-The-Fields-Of-Civil-And-Mechanical-Engineering.pdf.

Hassiotis, S. 2007. Data Gathering and Design Details of an Integral Abutment Bridge. *Proceedings of 18th Engineering Mechanics Division Conference (EMD 2007)*, Blacksburg, VA.

Hoffmann, S. and H. Weiher. 2012. Innovative Design of Bridge Bearings by the Use of UHPFRC. *Proceedings of the 3rd International Symposium on UHPC and Nanotechnology for High Performance Construction Materials,* pp. 973–980. March 7–9, Kassel, Germany.

Huang, J., C. E. French, and C. K. Shield. 2004. *Behavior of Concrete Integral Abutment Bridges*. Minnesota Department of Transportation, St. Paul, MN.

Iowa DOT. 2019. C6.5*LRFD Bridge Design Manual Commentary*. Iowa Department of Transportation, Ames, IA. https://iowadot.gov/bridge/policy/06-05-00AbutLRFDC.pdf.

Iowa DOT. 2011. *LRFD Bridge Design Manual*. Iowa Department of Transportation, Ames, IA. https://iowadot.gov/bridge/policy/LRFDBridgeDesignManual.pdf.

JSCE. 2008*. Recommendations for Design and Construction of High Performance Fiber Reinforced Cement Composites with Multiple Fine Cracks (HPFRCC)*. Japan Society of Civil Engineers, Tokyo, Japan.

Jungwirth, J. and A. Muttoni. 2004. Structural Behavior of Tension Members in UHPC. *Proceedings of the International Symposium on Ultra High Performance Concrete*, pp. 533–544. September 13–15, Kassel, Germany. http://ibeton.epfl.ch/Publications/2004/Jungwirth04b.pdf.

Kamel, M. R., J. V. Benak, M. K. Tadros, and M. Jamshidi. 1996. Prestressed Concrete Piles in Jointless Bridges. *PCI Journal*, Vol. 41, No. 2, pp. 56–67.

Kim, B. S., S. Kim, Y. J. Kim, S. Y. Park, K. T. Koh, and C. Joh. 2012. R&D Activities and Application of Ultra High Performance Concrete to Cable Stayed Bridges. *Proceedings of the Hipermat 2012 3rd International Symposium on UHPC and Nanotechnology for High Performance Construction Materials,* pp.865–872. March 7–9, Kassel, Germany.

Lunne, T., P. K. Robertson, and J. J. M. Powell. 1997. *Cone Penetration Testing in Geotechnical Practice*. CRC Press, Boca Raton, FL.

Ma, J. and H. Schneider. 2002. Properties of Ultra-High-Performance Concrete. *Zeipzig Annual Civil Engineering Report (LACER),* No. 7, pp. 25–32.

Ma, J., M. Orgass, F. Dehn, D. Schmidt, and N. V. Tue. 2004. Comparative Investigations on Ultra-High Performance Concrete with and without Coarse Aggregates. *Proceedings of the International Symposium on Ultra-High Performance Concrete*, pp. 205–212. September 13–15, Kassel, Germany.

MaineDOT. 2003. *Bridge Design Guide*. Maine Department of Transportation, Augusta, ME. https://www.maine.gov/mdot/bdg/docs/Complete2003BDG.pdf.

MassDOT. 2009. *LRFD Bridge Manual*, Highway Division, Massachusetts Department of Transportation, Boston, MA. https://www.mass.gov/manual/lrfd-bridge-manual-2013-edition.

Matthias, D. and M. Cribbs. 1998. *Driven 1.0: A Microsoft Windows Based Program for Determining Ultimate Vertical Static Pile Capacity (User's Manual)*. FHWA-SA-98-074. Federal Highway Administration, Washington, DC.

McKenna, F., G. L. Fenves, F. C. Filippou, S. Mazzoni, M. Scott, B. Jeremic, A. Elgamal, P. Arduino, P. McKenzie, G. G. Deierlein, and K. Law. 2006. *OpenSees 2.3.2*. Pacific Earthquake Engineering Research Center, University of California, Berkeley, CA. http://opensees.berkeley.edu/index.php.

Measurand Inc. 2011. *ShapeAccelArray (SAA) Installation Guide*. Measurand Inc., Fredericton, NB, Canada.

Menn, C. 1990. *Prestressed Concrete Bridges*. Birkhäuser Verlag AG Basel, Basel, Switzerland.

Meyerhof, G. G. 1976. Bearing Capacity and Settlement of Pile Foundations. *Journal of the Geotechnical Engineering Division*, Vol. 102, No. 3, pp. 195–228.

MnDOT. 2011. *LRFD Bridge Design Manual*, Minnesota Department of Transportation, Oakdale, MN. https://www.dot.state.mn.us/bridge/lrfd.html

Moser, R., B. Holland, L. Kahn, P. Singh, and K. Kurtis. 2011. *Durability of Precast Prestressed Concrete Piles in Marine Environment: Reinforcement Corrosion and Mitigation – Part 1*. Georgia Department of Transportation, Atlanta, GA. http://www.dot.ga.gov/BuildSmart/research/Documents/07-30.pdf.

Naaman, A. E. and K. Wille. 2012. The Path to Ultra-High Performance Fiber Reinforced Concrete (UHP-FRC): Five Decades of Progress. *Proceedings of the Hipermat 2012 3rd International Symposium on UHPC and Nanotechnology for High Performance Construction Materials,* pp. 3–15. March 7–9, Kassel, Germany.

Naval Facilities Engineering Command. 1982. *NAVFAC Design Manual DM 7.2: Foundations and Earth Structures*. Department of the Navy, Alexandria, VA. https://www.scribd.com/document/267563167/Design-Manual-7-2-Foundations-and-Earth-Structures.

Ng, K. W., M. T. Suleiman, M. Roling, S. S. AbdelSalam, and S. Sritharan. 2011. *Development of LRFD Design Procedures for Bridge Piles in Iowa – Volume II: Field Testing of Steel H-Piles in Clay, Sand, and Mixed Soils and Data Analysis*. Bridge Engineering Center, Iowa State University, Ames, IA. https://intrans.iastate.edu/app/uploads/2018/03/TR-583_LRFD_Volume_II_Final_Report.pdf.

Nordlund, R. L. 1963. Bearing Capacity of Piles in Cohesionless Soils. *Journal of the Soil Mechanics and Foundations Division*, Vol. 89, No. 3, pp. 1–36.

Nottingham, L. C. and J. H. Schmertmann. 1975. *An Investigation of Pile Capacity Design Procedures*. University of Florida, Gainesville, FL.

NYSDOT. 2011. *Bridge Manual – 1st Edition with Addendum #2*, New York State Department of Transportation, Albany, NY. www.dot.ny.gov/divisions/engineering/structures/manuals/bridge-manual-usc.

Oesterle R. G. and H. R. Lotfi. 2005. Transverse Movement in Skewed Integral Abutment Bridges. *FHWA Conference – Integral Abutment and Jointless Bridges (IAJB 2005)*, March 16–18, Baltimore, MD.

Ozyildirim, C. 2011. *Evaluation of Ultra-High-Performance Fiber-Reinforced Concrete*. Virginia Center for Transportation Innovation & Research, Charlottesville, VA.

Perry, V. H. and P. J. Seibert. 2011. Working with Ductal Ultra-High Performance Concrete. *Concrete Plant International*, No. 1.

PDI. 2005. *GRLWEAP – Wave Equation Analysis of Pile Driving, Procedures and Models*. Pile Dynamics, Inc., Cleveland, OH.

PDI. 2000. *CAPWAP for Windows Manual*. Pile Dynamics, Inc. Cleveland, OH.

PileBuck. 2013. *Concrete Pile Splices*. https://www.pilebuck.com/education/pile-points/concrete-pile-splices/.

PCA. 2012. *Ultra High-Performance Concrete Case Study*. Portland Cement Association, Skokie, IL. Accessed March 2012. http://www.cement.org/bridges/br_case_jakway.asp.

PCI. 2010. *PCI Design Handbook: Precast and Prestressed Concrete, 7th Edition*. Precast/Prestressed Concrete Institute, Chicago, IL.

Reese, L. C., S. T. Wang, W. M. Isenhower, and J. A. Arréllaga. 2004. *Computer Program LPILE Plus Version 5.0 Technical Manual: A Program for the Analysis of Piles and Drilled Shafts under Lateral Loads*. Ensoft, Inc., Austin, TX. https://www.ensoftinc.com/products/lpile/.

Reese, L. C., W. R. Cox, and F. D. Koop. 1974. Analysis of Laterally Loaded Piles in Sand, Paper No. OTC 2080-MS. *Offshore Technical Conference*. May 6–8, Houston, TX.

Reese, L. C. and H. Matlock. 1956. Non-Dimensional Solutions for Laterally Loaded Piles with Soil Modulus Proportional to Depth. *Proceedings of the 8th Texas Conference on Soil Mechanics and Foundation Engineering*, Austin, TX.

Resplendino, J. 2012. State of the Art of Design and Construction of UHPFRC Structures in France. *Proceedings of the 3rd International Symposium on UHPC and Nanotechnology for High Performance Construction Materials,* pp. 27–41. March 7–9, Kassel, Germany.

Rhode Island DOT. 2007. *Rhode Island LRFD Bridge Design Manual*. Rhode Island Department of Transportation, Providence, RI. http://www.dot.ri.gov/documents/doingbusiness/RILRFDBridgeManual.pdf.

Richard, P. and M. Cheyrezy. 1995. Composition of Reactive Powder Concretes. *Cement and Concrete Research*, Vol. 25, No. 7, pp. 1501–1511.

Romanoff, M. 1962. Corrosion of Steel Pilings in Soils. *NBS Monograph No. 58,* National Bureau of Standards, U.S. Department of Commerce, Washington, DC.

RS Means. 2009. *Heavy Construction Costs*. RS Means, Rockland, MA.

Scheydt, J. C. and H. S. Müller. 2012. Microstructure of Ultra High Performance Concrete (UHPC) and Its Impact on Durability. *Proceedings of the 3rd International Symposium on UHPC and Nanotechnology for High Performance Construction Materials* pp. 349–356. March 7–9, Kassel, Germany.

Schmertmann, J. 1978. *Guidelines for Cone Penetration Test, Performance and Design*. FHWA-TS-78-209. Federal Highway Administration, Washington, DC.

Smith, E. A. L. 1960. Pile-Driving Analysis by the Wave Equation. *Journal of the Soil Mechanics and Foundations Division,* Vol. 86, No. 4, pp. 35–64.

Smith, E. A. 1962. Pile-Driving Analysis by the Wave Equation. *Transactions*, Vol. 127, pp. 1145–1171.

Sritharan, S. 2015. Design of UHPC Structural Members: Lessons Learned and ASTM Test Requirements. *Advances in Civil Engineering Materials, An ASTM International Journal*, Vol. 4, No. 2, pp. 113–131.

Sritharan, S., B. J. Bristow, and V. H. Perry. 2003. Characterizing an Ultra-High Performance Material for Bridge Applications under Extreme Loads. *Proceedings of the 3rd International Symposium on High Performance Concrete,* Orlando, FL, October.

Sritharan, S., S. Aaleti, D. Bierwagen, J. Garder, and A. Abu-Hawash. 2012. Current Research on Ultra High Performance Concrete (UHPC) for Bridge Applications in Iowa. *Proceedings of the 3rd International Symposium on UHPC and Nanotechnology for High Performance Construction Materials,* pp. 857–864. March 7–9, Kassel, Germany.

Tang, M.-C. 2004. High Performance Concrete – Past, Present, and Future. *Proceedings of the International Symposium on Ultra High Performance Concrete,* pp. 3–9. September 13–15, Kassel, Germany.

Tomlinson, M. J. 1994. *Pile Design and Construction Practice, Fourth Edition*. Taylor & Francis Group, London, UK.

TRIP. 2008. *Iowa's Deficient Bridges: Strategies to Improve and Maintain the Condition of Iowa's Bridges*. The Road Information Program (TRIP), Washington, DC. https://www.lombardilaw.com/library/Iowa_Bridge_Report_Feb_2008.pdf.

Vande Voort, T. L., M. T. Suleiman, and S. Sritharan. 2008. *Design and Performance Verification of UHPC Piles for Deep Foundations*. Center for Transportation Research and Education, Iowa State University, Ames, IA. https://intrans.iastate.edu/app/uploads/2018/03/tr-558_uhpc_piles.pdf.

VTrans. 2008. *Integral Abutment Bridge Design Guidelines*, Vermont Agency of Transportation, Montpelier, VT. https://vtrans.vermont.gov/sites/aot/files/highway/documents/structures/SEI-08-004-1.pdf.

Walraven J. C. 2002. From Design of Structures to Design of Materials. *Proceedings of the International Conference for Innovations and Developments in Concrete Materials and Construction.* pp. 281–294. September 9–11, Dundee, Scotland, UK.

Wang, S.-T. and L. C. Reese. 1993. *COM624P-Laterally Loaded Pile Analysis Program for Microcomputer, Version 2.0*. FHWA-SA-91-048. Federal Highway Administration, Washington, DC.

Wipf, T. J., B. M. Phares, S. Sritharan, B. E. Degen, and M. T. Giesmann. 2009. *Design and Evaluation of Single-Span Bridge Using Ultra-High Performance Concrete*. Bridge Engineering Center, Iowa State University, Ames, IA. https://intrans.iastate.edu/app/uploads/2018/03/UHPC_Wappello_Co_Report.pdf.

Wong, I. H. and K. H. Law. 1999. Corrosion of Steel H Piles in Decomposed Granite. *Journal of Geotechnical and Geoenvironmental Engineering*, Vol. 126, No. 6, pp. 529–532.

Young, W. F., J. Boparai, V. Perry, B. I. Archibald, and S. Salib. 2012. Whiteman Creek Bridge – A Synthesis of Ultra High Performance Concrete and Fibre Reinforced Polymers for Accelerated Bridge Construction. *Proceedings of the 3rd International Symposium on UHPC and Nanotechnology for High Performance Construction Materials*, pp. 849–856. March 7–9, Kassel, Germany.

APPENDIX A. OPENSEES SCRIPT EXAMPLES

OpenSees script used to calculate the moment-curvature response of steel HP × 57 piles in strong-axis and weak-axis bending for various axial loads are given in this appendix.

```
### UHPC PILE PROJECT_PHASE 2
### ------------------------------------------------------------------------------------------------------------------
##--------- Written by Sriram Aaleti date: 26th August 2010 -------------------------------------------------------
#-------------------------------------------------------------------------------------------------------------------
wipe;

##--------------- Simulation Parameters-------------------------------------------------------------------------------
set specimen HP10by57;
set orientation weakaxis; # other option is weakaxis/strongaxis
##set orientation strongaxis; # other option is weakaxis/strongaxis
#### CHANGE ORIENTATION TO STRONGAXIS OR WEAKAXIS FOR ANALYSIS IN BOTH DIRECTIONS

#--------------- unit definition------------------------------------------------------------------------------------
set in 1.; # define basic units
set sec 1.; # define basic units
set kip 1.; # define basic units
set ft [expr 12.*$in]; # define engineering units
set ksi [expr $kip/pow($in,2)];
set psi [expr $ksi*1000.];
set in2 [expr $in*$in]; # inch^2
set in4 [expr $in*$in*$in*$in]; # inch^4
set PI [expr 2*asin(1.0)]; # define constants
set g [expr 32.2*$ft/pow($sec,2)]; # gravitational acceleration
set Ubig 1.e10; # a really large number
set Usmall [expr 1/$Ubig]; # a really small number
set cm [expr $in/2.54]; # SI centimeter unit
# --------- end of unit definition ----------------------------------------------------------------------------------

##################----------------------------------------------------------------------------------------------------
# ## -------------------------- Defining the procedures for the cross section (steel pile) --------------------------------
################----------------------------------------------------------------------------------------------------

# input parameters
# secID - section ID number
# matID - material ID number
# d = nominal depth
# tw = web thickness
# bf = flange width
# tf = flange thickness
# nfdw = number of fibers along web depth
# nftw = number of fibers along web thickness
# nfbf = number of fibers along flange width
# nftf = number of fibers along flange thickness

####----------------------Weak axis bending definition----------------------------------------------------------------
proc Wsection_weak {secID matID d tw bf tf nfdw nftw nfbf nftf} {
set dw [expr $d - 2 * $tf]
set z1 [expr -$d/2]
set z2 [expr -$dw/2]
```

```
set z3 [expr $dw/2]
set z4 [expr $d/2]
set y1 [expr $bf/2]
set y2 [expr $tw/2]
set y3 [expr -$tw/2]
set y4 [expr -$bf/2]
#
section Fiber $secID {
patch quad $matID $nftf $nfbf $y1 $z3 $y1 $z4 $y4 $z4 $y4 $z3
patch quad $matID $nfdw $nftw $y2 $z2 $y2 $z3 $y3 $z3 $y3 $z2
patch quad $matID $nftf $nfbf $y1 $z1 $y1 $z2 $y4 $z2 $y4 $z1

# # # patch quad $matID $nfbf $nftf $y1 $z3 $y4 $z3 $y4 $z4 $y1 $z4
# # # patch quad $matID $nftw $nfdw $y2 $z2 $y3 $z2 $y3 $z3 $y2 $z3
# # # patch quad $matID $nfbf $nftf $y1 $z1 $y4 $z1 $y4 $z2 $y1 $z2
}
}


####----------------------Strong axis bending definition-------------------------------------------------------------
proc Wsection_strong {secID matID d tw bf tf nfdw nftw nfbf nftf} {
set dw [expr $d - 2 * $tf]
set y1 [expr -$d/2]
set y2 [expr -$dw/2]
set y3 [expr $dw/2]
set y4 [expr $d/2]
set z1 [expr -$bf/2]
set z2 [expr -$tw/2]
set z3 [expr $tw/2]
set z4 [expr $bf/2]
#
section Fiber $secID {
patch quad $matID $nftf $nfbf $y1 $z1 $y2 $z1 $y2 $z4 $y1 $z4
patch quad $matID $nfdw $nftw $y2 $z2 $y3 $z2 $y3 $z3 $y2 $z3
patch quad $matID $nftf $nfbf $y3 $z1 $y4 $z1 $y4 $z4 $y3 $z4

# # # # patch quad $matID $nfbf $nftf $y1 $z1 $y1 $z4 $y2 $z4 $y2 $z1
# # # # patch quad $matID $nftw $nfdw $y2 $z2 $y2 $z3 $y3 $z3 $y3 $z2
# # # # patch quad $matID $nfbf $nftf $y3 $z1 $y3 $z4 $y4 $z4 $y4 $z1
}
}

####---------------------------------------------------------------------------------------------------------------------

set ndm 2; # 2-D problem
set ndf 3;
model basic -ndm $ndm -ndf $ndf
logFile screendump.dat


#########----------------------------------------------------------------------------------------------------------
###-------------------------- defining the dimensions of the section HP 10×57 ------------------------------------
#########----------------------------------------------------------------------------------------------------------

set tflange [expr 0.57*$in]; #flange thickness
set tweb [expr 0.57*$in]; # web thickness
set bflange [expr 10.2*$in];#flange width
set dpile [expr 9.99*$in];#depth of the section
```

```
######## ---------------------------------------------------------------------------------------------------------
## --------------------------------- Defining the material properties ----------------------------------------------
######## ---------------------------------------------------------------------------------------------------------
set Grade50 1
set Fy [expr 50.*$ksi];
set Es [expr 29000.*$ksi];
set bratio 0.004;
uniaxialMaterial Steel01 $Grade50 $Fy $Es $bratio
##uniaxialMaterial Steel02 $Grade50 $Fy $Es $bratio 15 0.925 0.15 0 5 0 5;

## Defining the nodes
node 1 0 0
node 2 0 0

## boundary conditions
fix 1 1 1 1
fix 2 0 1 0

######-----------------------------------------------------------------------------------------------######## 
######-------------------------DEFINING THE FIBER SECTION-----------------------------------------######
-------------------------------------------------------------------------------------------------- ---------

set HP_10b57 1;
 if {$orientation == "strongaxis"} {
        puts " Strong axis cross section in section defination"
        Wsection_strong 1 1 $dpile $tweb $bflange $tflange 80 8 24 8
}

 if {$orientation == "weakaxis"} {
        puts " Weak axis cross section in section defination"
        Wsection_weak 1 1 $dpile $tweb $bflange $tflange 15 8 80 8
}
##################### ---------------------------------------------------------------------------------------

geomTransf PDelta 1;
# Define element
element zeroLengthSection 1 1 2 1;

########------------------------------------------------------------------------------------------------#####
###-------------------------------- Create recorder ------------------------------------------------------
###############--------------OUTPUT DATA -------------------------------------------------------

set kword $orientation;
recorder Node -file momcurv_$kword.out -time -node 2 -dof 3 disp

if {$orientation == "strongaxis"} {
puts " recoreders for stronf axis bending"
recorder Element -file flangeComp_$kword.out -time -ele 1 section fiber [expr 0.5*$dpile] 0 $Grade50
stressStrain;##strain in the compression flange
recorder Element -file flangeTension_$kword.out -time -ele 1 section fiber -[expr 0.5*$dpile] 0 $Grade50
stressStrain;##strain in the tension flange
}

if {$orientation == "weakaxis"} {
puts "recorder for weak axis bending"
```

recorder Element -file flangeComp_$kword.out -time -ele 1 section fiber [expr 0.5*$bflange] [expr 0.5*$dpile] $Grade50 stressStrain;##strain in the compression flange
recorder Element -file flangeTension_$kword.out -time -ele 1 section fiber -[expr 0.5*$bflange] [expr 0.5*$dpile] $Grade50 stressStrain;##strain in the tension flange
}

########---##
#####-- --
Define constant axial load
set P 300; ##p is the axial load
pattern Plain 1 "Constant" {
 load 2 $P 0.0 0.0
 }
# Define analysis parameters
integrator LoadControl 0 1 0 0
set tolerence 1.0e-8;
set nItr 1000;
system SparseGeneral -piv
test NormDispIncr $tolerence $nItr 1
##test NormUnbalance $tolerence $nItr 1
numberer Plain
constraints Plain
algorithm KrylovNewton
analysis Static

analyze 1

Define reference load
pattern Plain 2 "Linear" {
 load 2 0.0 0.0 1.0
}

Maximum curvature from Anndrianna
set maxK 0.15246063
set numIncr 800
set dK [expr $maxK/$numIncr]

Use displacement control at node 2 for section analysis
integrator DisplacementControl 2 3 $dK

Perform the section analysis
analyze $numIncr

APPENDIX B. MAXIMUM MOMENT AND SHEAR CHARTS

The maximum moment and shear predicted along the length of a pile and the second maximum moment and shear along the length of the same pile are given with their corresponding locations in this appendix.

Table B-1. Maximum moment and maximum shear for trials 1a through 64a

Axial load, kips	Soil type	Pile head boundary condition	Maximum moment, kip-in.	Maximum shear, kips
	— Parameters: (1) HP 10 × 57, (2) weak-axis bending, (3) 1.00 in. of lateral displacement, and (4) no prebored hole			
0	Loose sand	Fixed	1215.9	27.7
		Pinned	491.5	11.7
	Dense sand	Fixed	1579.3	45.8
		Pinned	726.6	20.4
	Soft clay	Fixed	768.2	14.2
		Pinned	303.0	6.9
	Very firm glacial clay	Fixed	1902.5	80.3
		Pinned	973.4	44.9
100	Loose sand	Fixed	1211.0	26.8
		Pinned	502.8	10.6
	Dense sand	Fixed	1569.7	44.5
		Pinned	736.0	19.0
	Soft clay	Fixed	767.3	13.6
		Pinned	317.8	6.1
	Very firm glacial clay	Fixed	1889.6	78.8
		Pinned	984.0	43.2
200	Loose sand	Fixed	1201.4	25.8
		Pinned	514.8	9.5
	Dense sand	Fixed	1548.0	43.1
		Pinned	744.4	17.6
	Soft clay	Fixed	766.0	13.0
		Pinned	333.3	5.2
	Very firm glacial clay	Fixed	1860.1	77.1
		Pinned	989.8	41.3
300	Loose sand	Fixed	1186.3	24.7
		Pinned	527.3	8.4
	Dense sand	Fixed	1513.3	41.4
		Pinned	751.6	16.2
	Soft clay	Fixed	764.8	12.3
		Pinned	349.4	4.3
	Very firm glacial clay	Fixed	1815.0	75.0
		Pinned	993.5	39.4

Table B-2. Maximum moment and maximum shear for trials 65a through 128a

Axial load, kips	Soil type	Pile head boundary condition	Maximum moment, kip-in.	Maximum shear, kips
Parameters: (1) HP 10 × 57, (2) weak-axis bending, (3) 1.55 in. of lateral displacement, and (4) no prebored hole				
0	Loose sand	Fixed	1515.5	33.7
		Pinned	700.5	15.1
	Dense sand	Fixed	1772.4	52.2
		Pinned	965.7	25.1
	Soft clay	Fixed	997.0	17.6
		Pinned	410.6	8.8
	Very firm glacial clay	Fixed	2000.4	89.7
		Pinned	1199.3	52.9
100	Loose sand	Fixed	1505.7	32.2
		Pinned	715.8	13.4
	Dense sand	Fixed	1758.3	50.3
		Pinned	978.7	23.0
	Soft clay	Fixed	995.5	16.7
		Pinned	433.7	7.6
	Very firm glacial clay	Fixed	1988.1	87.5
		Pinned	1215.6	50.3
200	Loose sand	Fixed	1484.9	30.7
		Pinned	730.2	11.7
	Dense sand	Fixed	1731.3	48.1
		Pinned	987.9	20.8
	Soft clay	Fixed	991.7	15.8
		Pinned	457.9	6.3
	Very firm glacial clay	Fixed	1966.4	85.1
		Pinned	1227.1	47.5
300	Loose sand	Fixed	1452.3	28.9
		Pinned	743.9	9.9
	Dense sand	Fixed	1691.1	45.7
		Pinned	993.1	18.4
	Soft clay	Fixed	984.6	14.8
		Pinned	483.2	5.0
	Very firm glacial clay	Fixed	1934.0	82.4
		Pinned	1227.8	44.4

Table B-3. Maximum moment and maximum shear for trials 129a through 192a

Axial load, kips	Soil type	Pile head boundary condition	Maximum moment, kip-in.	Maximum shear, kips
Parameters: (1) HP 10 × 57, (2) strong-axis bending, (3) 1.00 in. of lateral displacement, and (4) no prebored hole			
0	Loose sand	Fixed	2490.7	45.4
0	Loose sand	Pinned	953.0	18.6
0	Dense sand	Fixed	3240.9	76.4
0	Dense sand	Pinned	1496.1	33.6
0	Soft clay	Fixed	1376.5	19.7
0	Soft clay	Pinned	533.9	9.7
0	Very firm glacial clay	Fixed	3663.7	115.7
0	Very firm glacial clay	Pinned	1862.0	64.0
100	Loose sand	Fixed	2507.0	44.8
100	Loose sand	Pinned	963.6	17.7
100	Dense sand	Fixed	3301.6	76.2
100	Dense sand	Pinned	1506.6	32.5
100	Soft clay	Fixed	1385.3	19.2
100	Soft clay	Pinned	566.9	9.1
100	Very firm glacial clay	Fixed	3728.1	115.5
100	Very firm glacial clay	Pinned	1877.3	62.8
200	Loose sand	Fixed	2478.2	43.8
200	Loose sand	Pinned	974.4	16.8
200	Dense sand	Fixed	3216.4	74.3
200	Dense sand	Pinned	1517.3	31.4
200	Soft clay	Fixed	1375.9	18.8
200	Soft clay	Pinned	563.3	8.4
200	Very firm glacial clay	Fixed	3502.6	111.8
200	Very firm glacial clay	Pinned	1885.4	61.5
300	Loose sand	Fixed	2356.2	41.9
300	Loose sand	Pinned	985.7	15.8
300	Dense sand	Fixed	2830.9	68.7
300	Dense sand	Pinned	1528.1	30.3
300	Soft clay	Fixed	1376.0	18.3
300	Soft clay	Pinned	579.3	7.7
300	Very firm glacial clay	Fixed	3083.7	105.5
300	Very firm glacial clay	Pinned	1870.6	59.6

Table B-4. Maximum moment and maximum shear for trials 193a through 256a

Axial load, kips	Soil type	Pile head boundary condition	Maximum moment, kip-in.	Maximum shear, kips
Parameters: (1) HP 10 × 57, (2) strong-axis bending, (3) 1.55 in. of lateral displacement, and (4) no prebored hole
0	Loose sand	Fixed	3095.9	55.7
		Pinned	1395.0	24.5
	Dense sand	Fixed	3802.9	89.8
		Pinned	2041.1	42.3
	Soft clay	Fixed	1842.6	24.8
		Pinned	720.2	12.2
	Very firm glacial clay	Fixed	4072.1	132.0
		Pinned	2322.6	75.9
100	Loose sand	Fixed	3144.6	55.0
		Pinned	1411.7	23.1
	Dense sand	Fixed	3730.1	87.7
		Pinned	2060.8	40.7
	Soft clay	Fixed	1825.3	23.4
		Pinned	754.9	11.1
	Very firm glacial clay	Fixed	3980.4	129.6
		Pinned	2354.5	74.3
200	Loose sand	Fixed	3076.9	53.3
		Pinned	1429.6	21.8
	Dense sand	Fixed	3435.9	82.7
		Pinned	2063.0	38.8
	Soft clay	Fixed	1842.2	23.5
		Pinned	766.4	10.3
	Very firm glacial clay	Fixed	3701.6	124.6
		Pinned	2350.3	72.0
300	Loose sand	Fixed	2718.7	48.8
		Pinned	1448.1	20.4
	Dense sand	Fixed	2985.3	75.3
		Pinned	2010.2	36.0
	Soft clay	Fixed	1832.9	22.7
		Pinned	790.8	9.3
	Very firm glacial clay	Fixed	3240.8	116.3
		Pinned	2241.0	67.5

Table B-5. Maximum moment and maximum shear for trials 1b through 64b

Axial load, kips	Soil type	Pile head boundary condition	Maximum moment, kip-in.	Maximum shear, kips
Parameters: (1) UHPC, (2) weak-axis bending, (3) 1.00 in. of lateral displacement, and (4) no prebored hole				
0	Loose sand	Fixed	1140.8	26.6
		Pinned	475.5	11.4
	Dense sand	Fixed	1418.8	42.9
		Pinned	690.3	19.7
	Soft clay	Fixed	738.0	13.9
		Pinned	294.8	6.8
	Very firm glacial clay	Fixed	1575.2	74.2
		Pinned	919.1	43.5
100	Loose sand	Fixed	1212.5	26.6
		Pinned	488.1	10.4
	Dense sand	Fixed	1509	43.5
		Pinned	728.2	18.9
	Soft clay	Fixed	757.3	13.4
		Pinned	309.4	6.0
	Very firm glacial clay	Fixed	1526.9	72.9
		Pinned	986.6	43.3
200	Loose sand	Fixed	1258.6	26.3
		Pinned	500.1	9.2
	Dense sand	Fixed	1530.8	42.9
		Pinned	749.1	17.7
	Soft clay	Fixed	762.1	12.9
		Pinned	324.5	5.1
	Very firm glacial clay	Fixed	1430.7	70.5
		Pinned	1034.8	42.5
300	Loose sand	Fixed	1279.9	25.7
		Pinned	512.6	8.1
	Dense sand	Fixed	1448.4	40.6
		Pinned	762.4	16.4
	Soft clay	Fixed	761.9	12.2
		Pinned	340.3	4.2
	Very firm glacial clay	Fixed	1416.5	69.2
		Pinned	1065.9	41.4

Table B-6. Maximum moment and maximum shear for trials 65b through 128b

Axial load, kips	Soil type	Pile head boundary condition	Maximum moment, kip-in.	Maximum shear, kips
Parameters: (1) UHPC, (2) weak-axis bending, (3) 1.55 in. of lateral displacement, and (4) no prebored hole				
0	Loose sand	Fixed	1359.2	31.6
		Pinned	668.6	14.6
	Dense sand	Fixed	1247.4	44.1
		Pinned	907.7	24.0
	Soft clay	Fixed	947.0	17.2
		Pinned	400.0	8.7
	Very firm glacial clay	Fixed	1440.7	79.5
		Pinned	1123.6	51.0
100	Loose sand	Fixed	1438.8	31.4
		Pinned	706.8	13.3
	Dense sand	Fixed	1270.4	43.6
		Pinned	976.4	23.1
	Soft clay	Fixed	991.1	16.6
		Pinned	423.0	7.4
	Very firm glacial clay	Fixed	1466.5	79.2
		Pinned	1093.8	46.7
200	Loose sand	Fixed	1442.8	30.1
		Pinned	731.1	11.7
	Dense sand	Fixed	1280.9	42.6
		Pinned	1037.4	21.8
	Soft clay	Fixed	1015.6	15.9
		Pinned	446.3	6.2
	Very firm glacial clay	Fixed	1478.7	78.2
		Pinned	1020.0	41.3
300	Loose sand	Fixed	1169.4	25.6
		Pinned	750.3	10.0
	Dense sand	Fixed	1264.9	40.9
		Pinned	1075.1	20.1
	Soft clay	Fixed	1026.8	15.1
		Pinned	471.7	4.8
	Very firm glacial clay	Fixed	1447.8	73.6
		Pinned	1010.4	36.9

Table B-7. Maximum moment and maximum shear for trials 129b through 192b

Axial load, kips	Soil type	Pile head boundary condition	Maximum moment, kip-in.	Maximum shear, kips
Parameters: (1) UHPC, (2) strong-axis bending, (3) 1.00 in. of lateral displacement, and (4) no prebored hole			

Axial load, kips	Soil type	Pile head boundary condition	Maximum moment, kip-in.	Maximum shear, kips
0	Loose sand	Fixed	1767.6	36.4
		Pinned	761.2	15.9
	Dense sand	Fixed	2080.4	57.8
		Pinned	1135.0	27.8
	Soft clay	Fixed	1119.7	17.6
		Pinned	440.1	8.6
	Very firm glacial clay	Fixed	2329.7	93.1
		Pinned	1400.3	54.7
100	Loose sand	Fixed	2003.9	38.3
		Pinned	798.7	15.3
	Dense sand	Fixed	2434.8	62.4
		Pinned	1226.4	28.0
	Soft clay	Fixed	1169.0	17.5
		Pinned	467.7	8.1
	Very firm glacial clay	Fixed	2677.4	98.4
		Pinned	1566.8	56.7
200	Loose sand	Fixed	2141.8	39.0
		Pinned	809.7	14.3
	Dense sand	Fixed	2702.8	64.9
		Pinned	1243.3	26.9
	Soft clay	Fixed	1168.9	17.0
		Pinned	482.6	7.4
	Very firm glacial clay	Fixed	2978.7	101.6
		Pinned	1624.2	56.3
300	Loose sand	Fixed	2205.1	39.0
		Pinned	820.9	13.3
	Dense sand	Fixed	2856.4	65.9
		Pinned	1254.8	25.7
	Soft clay	Fixed	1168.6	16.5
		Pinned	499.0	6.6
	Very firm glacial clay	Fixed	29327	100
		Pinned	1645.8	55.2

Table B-8. Maximum moment and maximum shear for trials 193b through 256b

Axial load, kips	Soil type	Pile head boundary condition	Maximum moment, kip-in.	Maximum shear, kips
Parameters: (1) UHPC, (2) strong-axis bending, (3) 1.55 in. of lateral displacement, and (4) no prebored hole				
0	Loose sand	Fixed	2000.2	42.5
		Pinned	1083.1	20.4
	Dense sand	Fixed	2205.0	64.1
		Pinned	1452.8	33.3
	Soft clay	Fixed	1434.1	21.7
		Pinned	594.4	10.9
	Very firm glacial clay	Fixed	2434.6	103.3
		Pinned	1661.7	63.2
100	Loose sand	Fixed	2339.4	45.2
		Pinned	116.3	19.9
	Dense sand	Fixed	2513.5	68.9
		Pinned	1670.2	34.7
	Soft clay	Fixed	1557.5	21.9
		Pinned	635.1	10.1
	Very firm glacial clay	Fixed	2722.6	108.6
		Pinned	1916.7	65.8
200	Loose sand	Fixed	2593.9	46.6
		Pinned	1185.7	18.5
	Dense sand	Fixed	2815.1	72.1
		Pinned	1770.2	34.3
	Soft clay	Fixed	1577.2	21.3
		Pinned	659.0	9.1
	Very firm glacial clay	Fixed	2973.1	111.8
		Pinned	2073.0	66.6
300	Loose sand	Fixed	2735.0	46.9
		Pinned	1202.8	17.1
	Dense sand	Fixed	2774.5	70.5
		Pinned	1812.0	33.0
	Soft clay	Fixed	1577.8	20.5
		Pinned	684.1	8.0
	Very firm glacial clay	Fixed	3001.5	111.1
		Pinned	2169.5	66.2

Table B-9. Maximum moment and maximum shear for trials 257 through 264

Parameters: (1) weak-axis bending, (2) 1.00 in. of lateral displacement, (3) fixed-pile head, and (4) 10 ft prebored hole				
Pile type	**Axial load, kips**	**Soil type**	**Maximum moment, kip-in.**	**Maximum shear, kips**
UHPC	100	Soft clay	363.6	3.1
		Very stiff clay	686.9	13.2
	200	Soft clay	358.2	2.9
		Very stiff clay	682.7	13.3
HP10 x 57	100	Soft clay	377.6	3.2
		Very stiff clay	705.6	13.5
	200	Soft clay	371.9	2.9
		Very stiff clay	698.1	13.7

Table B-10. Maximum moment and maximum shear for trials 265 through 272

Parameters: (1) weak-axis bending, (2) 1.55 in. of lateral displacement, (3) fixed-pile head, and (4) 10 ft prebored hole				
Pile type	**Axial load, kips**	**Soil type**	**Maximum moment, kip-in.**	**Maximum shear, kips**
UHPC	100	Soft clay	520.2	4.3
		Very stiff clay	956.8	17.1
	200	Soft clay	511.9	3.8
		Very stiff clay	979.2	10.7
HP10 x 57	100	Soft clay	539.6	4.4
		Very stiff clay	963.7	17.3
	200	Soft clay	531.5	3.9
		Very stiff clay	950.8	17.5

Table B-11. Depth to 2nd maximum bending moment and shear forces and depth of fixity for trials 1a through 64a

| Axial load, kips | Boundary condition | Soil type | Location from GS of 2nd maximum, ft | | Depth of fixity, ft |
			Bending moment	Shear	
0	Pinned	Loose sand	17.0	9.0	17.5
		Dense sand	12.5	7.5	12.0
		Soft clay	20.0	11.5	19.5
		Very stiff clay	9.5	6.0	9.0
	Fixed	Loose sand	7.5	11.0	19.0
		Dense sand	6.5	8.5	13.5
		Soft clay	11.0	15.5	22.5
		Very stiff clay	5.5	8.0	10.0
100	Pinned	Loose sand	16.5	8.5	17.5
		Dense sand	12.5	7.5	12.0
		Soft clay	20.0	11.0	19.5
		Very stiff clay	9.5	6.0	9.0
	Fixed	Loose sand	7.5	10.5	19.0
		Dense sand	6.5	8.5	13.5
		Soft clay	11.0	15.5	22.5
		Very stiff clay	5.5	8.0	10.0
200	Pinned	Loose sand	16.5	8.5	17.5
		Dense sand	12.0	7.5	12.0
		Soft clay	19.5	10.5	19.5
		Very stiff clay	9.5	6.0	9.0
	Fixed	Loose sand	7.5	10.5	19.0
		Dense sand	6.5	8.5	13.5
		Soft clay	11.0	15.0	23.0
		Very stiff clay	5.5	7.5	10.0
300	Pinned	Loose sand	16.5	8.0	17.0
		Dense sand	12.0	7.0	12.0
		Soft clay	19.5	10.0	20.0
		Very stiff clay	9.5	6.0	9.0
	Fixed	Loose sand	7.5	10.5	19.0
		Dense sand	6.0	8.5	13.0
		Soft clay	11.0	14.5	23.0
		Very stiff clay	5.5	7.5	10.0

Parameters: (1) HP 10 × 57 pile, (2) weak-axis bending, (3) 1.00 in. of lateral displacement, and (4) no prebored hole

Table B12. Depth to 2nd maximum bending moment and shear forces and depth of fixity for trials 65a through 128a

Axial load, kips	Boundary condition	Soil type	Location from GS of 2nd maximum, ft		Depth of fixity, ft
			Bending moment	Shear	
0	Pinned	Loose sand	17.0	9.0	18.0
		Dense sand	12.5	7.5	12.5
		Soft clay	21.5	12.5	21.5
		Very stiff clay	10.0	6.5	9.5
	Fixed	Loose sand	8.0	11.0	19.5
		Dense sand	6.5	9.0	13.5
		Soft clay	12.0	16.5	25.0
		Very stiff clay	5.5	8.0	11.0
100	Pinned	Loose sand	17.0	9.0	18.0
		Dense sand	12.5	7.5	12.5
		Soft clay	21.5	11.5	21.5
		Very stiff clay	10.0	6.5	9.5
	Fixed	Loose sand	8.0	11.0	19.5
		Dense sand	6.5	8.5	13.5
		Soft clay	11.5	16.5	25.0
		Very stiff clay	5.5	8.0	10.5
200	Pinned	Loose sand	16.5	8.5	18.0
		Dense sand	12.5	7.5	12.5
		Soft clay	21.0	11.0	22.0
		Very stiff clay	10.0	6.0	9.5
	Fixed	Loose sand	7.5	10.5	19.5
		Dense sand	6.5	8.5	13.5
		Soft clay	11.5	16.0	25.0
		Very stiff clay	5.5	8.0	10.5
300	Pinned	Loose sand	16.5	8.5	18.0
		Dense sand	12.0	7.0	12.5
		Soft clay	21.0	10.5	22.0
		Very stiff clay	10.0	6.0	9.5
	Fixed	Loose sand	7.5	10.5	19.5
		Dense sand	6.0	8.5	13.5
		Soft clay	11.5	15.5	25.0
		Very stiff clay	5.5	7.5	10.5

Parameters: (1) HP 10 × 57 pile, (2) weak-axis bending, (3) 1.55 in. of lateral displacement, and (4) no prebored hole

Table B-13. Depth to 2nd maximum bending moment and shear forces and depth of fixity for trials 129a through 192a

Axial load, kips	Boundary condition	Soil type	Location from GS of 2nd maximum, ft		Depth of fixity, ft
			Bending moment	Shear	
0	Pinned	Loose sand	20.5	11.0	21.5
		Dense sand	15.0	9.0	15.0
		Soft clay	26.0	14.5	25.5
		Very stiff clay	12.5	8.0	11.5
	Fixed	Loose sand	9.5	13.5	23.0
		Dense sand	7.5	10.5	16.5
		Soft clay	14.5	20.5	29.5
		Very stiff clay	7.0	10.0	13.5
100	Pinned	Loose sand	20.5	10.5	21.5
		Dense sand	15.0	9.0	15.0
		Soft clay	24.5	14.5	23.5
		Very stiff clay	12.5	8.0	11.5
	Fixed	Loose sand	9.5	13.5	23.5
		Dense sand	7.5	10.5	16.5
		Soft clay	14.5	20.0	27.5
		Very stiff clay	7.0	10.0	13.5
200	Pinned	Loose sand	20.5	10.5	21.5
		Dense sand	15.0	9.0	15.0
		Soft clay	25.5	14.0	25.5
		Very stiff clay	12.5	8.0	11.5
	Fixed	Loose sand	9.5	13.0	23.5
		Dense sand	7.5	10.5	16.0
		Soft clay	14.5	20.0	29.5
		Very stiff clay	7.0	10.5	13.5
300	Pinned	Loose sand	20.5	10.5	21.5
		Dense sand	15.0	8.5	15.0
		Soft clay	25.5	13.5	25.5
		Very stiff clay	12.5	8.0	11.5
	Fixed	Loose sand	9.0	13.0	23.5
		Dense sand	7.5	9.5	16.0
		Soft clay	14.5	19.5	29.5
		Very stiff clay	7.0	9.5	13.0

Parameters: (1) HP 10 × 57 pile, (2) strong-axis bending, (3) 1.00 in. of lateral displacement, and (4) no prebored hole

Table B-14. Depth to 2nd maximum bending moment and shear forces and depth of fixity for trials 193a through 256a

Axial load, kips	Boundary condition	Soil type	Location from GS of 2nd maximum, ft		Depth of fixity, ft
			Bending moment	Shear	
0	Pinned	Loose sand	21.0	11.0	22.5
		Dense sand	15.5	8.5	15.5
		Soft clay	28.0	16.0	28.5
		Very stiff clay	13.0	8.5	12.5
	Fixed	Loose sand	9.5	13.5	24.5
		Dense sand	7.5	10.5	17.0
		Soft clay	15.5	22.0	32.5
		Very stiff clay	7.5	10.5	14.5
100	Pinned	Loose sand	21.0	11.0	22.5
		Dense sand	15.5	9.0	15.5
		Soft clay	26.5	15.5	26.5
		Very stiff clay	13.0	8.5	12.5
	Fixed	Loose sand	9.5	13.5	24.5
		Dense sand	7.5	10.5	17.0
		Soft clay	15.5	21.5	31.0
		Very stiff clay	7.5	10.5	14.5
200	Pinned	Loose sand	21.0	11.0	22.0
		Dense sand	15.0	9.0	15.5
		Soft clay	27.5	15.0	28.0
		Very stiff clay	13.0	8.5	12.5
	Fixed	Loose sand	9.5	13.0	24.5
		Dense sand	7.5	10.5	16.5
		Soft clay	15.5	21.0	32.5
		Very stiff clay	7.0	10.0	14.5
300	Pinned	Loose sand	20.5	10.5	22.0
		Dense sand	15.0	8.5	15.5
		Soft clay	27.5	14.5	28.0
		Very stiff clay	13.0	8.0	12.5
	Fixed	Loose sand	9.5	13.0	24.0
		Dense sand	7.5	10.0	16.5
		Soft clay	15.5	21.0	32.5
		Very stiff clay	7.0	10.0	14.0

Parameters: (1) HP 10 × 57 pile, (2) strong-axis bending, (3) 1.55 in. of lateral displacement, and (4) no prebored hole

Table B-15. Depth to 2nd maximum bending moment and shear forces and depth of fixity for trials 1b through 64b

Axial load, kips	Boundary condition	Soil type	Location from GS of 2nd maximum, ft		Depth of fixity, ft
Parameters: (1) UHPC pile, (2) weak-axis bending, (3) 1.00 in. of lateral displacement, and (4) no prebored hole					
			Bending moment	Shear	
0	Pinned	Loose sand	16.5	8.5	17.5
		Dense sand	12.0	7.5	12.0
		Soft clay	20.0	11.5	19.5
		Very stiff clay	9.5	6.0	8.5
	Fixed	Loose sand	7.5	10.5	19.0
		Dense sand	6.0	8.5	13.0
		Soft clay	11.0	15.5	22.5
		Very stiff clay	5.0	7.5	9.5
100	Pinned	Loose sand	16.5	8.5	17.0
		Dense sand	12.0	7.5	12.0
		Soft clay	19.5	11.0	19.5
		Very stiff clay	6.0	9.5	9.0
	Fixed	Loose sand	7.5	10.5	19.0
		Dense sand	6.0	8.5	13.0
		Soft clay	11.0	15.0	22.5
		Very stiff clay	5.0	7.5	10.0
200	Pinned	Loose sand	16.5	8.5	17.0
		Dense sand	12.0	7.0	12.0
		Soft clay	19.5	10.5	19.5
		Very stiff clay	9.5	6.0	9.0
	Fixed	Loose sand	7.5	10.5	19.0
		Dense sand	6.0	8.5	13.5
		Soft clay	11.0	15.0	22.5
		Very stiff clay	5.0	7.5	10.0
300	Pinned	Loose sand	16.0	8.0	17.0
		Dense sand	12.0	7.0	12.0
		Soft clay	19.0	10.0	19.5
		Very stiff clay	9.5	6.0	9.0
	Fixed	Loose sand	7.5	10.5	19.0
		Dense sand	6.0	8.5	13.0
		Soft clay	11.0	14.5	22.5
		Very stiff clay	5.0	7.5	10.0

Table B-16. Depth to 2nd maximum bending moment and shear forces and depth of fixity for trials 65b through 128b

Axial load, kips	Boundary condition	Soil type	Location from GS of 2nd maximum, ft		Depth of fixity, ft
			Bending moment	Shear	
0	Pinned	Loose sand	17.0	9.5	18.0
		Dense sand	12.5	7.5	12.5
		Soft clay	21.5	12.0	21.5
		Very stiff clay	10.0	6.5	9.5
	Fixed	Loose sand	7.5	11.0	19.5
		Dense sand	6.0	8.5	13.5
		Soft clay	11.5	16.5	24.5
		Very stiff clay	5.0	7.5	10.5
100	Pinned	Loose sand	17.0	9.0	18.0
		Dense sand	12.5	7.5	12.5
		Soft clay	21.0	11.5	21.5
		Very stiff clay	9.5	6.0	9.0
	Fixed	Loose sand	7.5	11.0	19.5
		Dense sand	6.0	8.5	13.5
		Soft clay	11.5	16.0	25.0
		Very stiff clay	5.0	7.5	10.5
200	Pinned	Loose sand	16.5	8.5	18.0
		Dense sand	12.5	7.5	12.5
		Soft clay	21.0	11.0	21.5
		Very stiff clay	9.5	6.0	9.5
	Fixed	Loose sand	7.5	10.5	19.5
		Dense sand	6.0	8.5	13.5
		Soft clay	11.5	15.5	25.0
		Very stiff clay	5.0	7.5	11.0
300	Pinned	Loose sand	16.5	8.5	17.5
		Dense sand	12.5	7.5	12.5
		Soft clay	20.5	10.5	21.5
		Very stiff clay	9.0	5.5	8.5
	Fixed	Loose sand	7.5	10.0	19.0
		Dense sand	6.0	8.5	13.5
		Soft clay	11.5	15.5	25.0
		Very stiff clay	5.0	7.5	10.5

Parameters: (1) UHPC pile, (2) weak-axis bending, (3) 1.55 in. of lateral displacement, and (4) no prebored hole

Table B-17. Depth to 2nd maximum bending moment and shear forces and depth of fixity for trials 129b through 192b

| Axial load, kips | Boundary condition | Soil type | Location from GS of 2nd maximum, ft | | Depth of fixity, ft |
			Bending moment	Shear	

Parameters: (1) UHPC pile, (2) strong-axis bending, (3) 1.00 in. of lateral displacement, and (4) no prebored hole

Axial load, kips	Boundary condition	Soil type	Bending moment	Shear	Depth of fixity, ft
0	Pinned	Loose sand	19.5	10.0	20.0
		Dense sand	14.0	8.5	14.0
		Soft clay	23.5	13.5	23.0
		Very stiff clay	11.0	7.0	10.5
	Fixed	Loose sand	8.5	12.5	21.5
		Dense sand	7.0	9.5	15.0
		Soft clay	13.0	18.5	27.0
		Very stiff clay	6.0	9.0	11.5
100	Pinned	Loose sand	19.5	10.0	20.0
		Dense sand	14.0	8.5	14.0
		Soft clay	24.0	13.5	23.5
		Very stiff clay	11.5	7.5	10.5
	Fixed	Loose sand	9.0	12.5	22.0
		Dense sand	7.0	9.5	15.0
		Soft clay	13.5	18.5	27.5
		Very stiff clay	6.5	9.0	12.5
200	Pinned	Loose sand	19.5	10.0	20.0
		Dense sand	14.0	8.5	14.0
		Soft clay	23.5	13.0	23.5
		Very stiff clay	11.5	7.5	11.0
	Fixed	Loose sand	9.0	12.5	22.0
		Dense sand	7.0	10.0	15.5
		Soft clay	13.5	18.5	27.5
		Very stiff clay	6.5	9.5	12.5
300	Pinned	Loose sand	19.0	9.5	20.0
		Dense sand	14.0	8.5	14.0
		Soft clay	23.5	12.5	23.5
		Very stiff clay	11.5	7.5	11.0
	Fixed	Loose sand	9.0	12.5	22.0
		Dense sand	7.5	10.0	15.5
		Soft clay	13.5	18.0	27.5
		Very stiff clay	6.5	9.5	12.5

Table B-18. Depth to 2nd maximum bending moment and shear forces and depth of fixity for trials 193b through 256b

Axial load, kips	Boundary condition	Soil type	Location from GS of 2nd maximum, ft		Depth of fixity, ft
			Bending moment	Shear	
0	Pinned	Loose sand	19.5	10.5	21.0
		Dense sand	14.0	8.5	14.5
		Soft clay	25.5	14.5	25.5
		Very stiff clay	11.5	7.5	11.0
	Fixed	Loose sand	8.5	12.5	22.5
		Dense sand	7.0	9.5	15.5
		Soft clay	14.0	20.0	29.5
		Very stiff clay	6.0	9.0	12.5
100	Pinned	Loose sand	19.5	10.5	21.0
		Dense sand	14.5	8.5	14.5
		Soft clay	25.5	14.0	26.0
		Very stiff clay	12.0	7.5	11.5
	Fixed	Loose sand	9.0	12.5	22.5
		Dense sand	7.0	10.0	15.5
		Soft clay	14.5	20.0	30.0
		Very stiff clay	6.5	9.5	13.0
200	Pinned	Loose sand	19.5	10.0	21.0
		Dense sand	14.5	8.5	14.5
		Soft clay	25.5	13.5	26.0
		Very stiff clay	12.5	8.0	12.0
	Fixed	Loose sand	9.0	12.5	23.0
		Dense sand	7.0	10.0	16.0
		Soft clay	14.5	19.5	30.5
		Very stiff clay	6.5	9.5	13.5
300	Pinned	Loose sand	19.5	10.0	21.0
		Dense sand	14.5	8.5	14.5
		Soft clay	25.0	13.0	26.0
		Very stiff clay	12.5	8.0	12.0
	Fixed	Loose sand	9.0	12.5	23.0
		Dense sand	7.0	10.0	16.0
		Soft clay	14.5	19.0	30.5
		Very stiff clay	6.5	9.5	13.5

Parameters: (1) UHPC pile, (2) strong-axis bending, (3) 1.55 in. of lateral displacement, and (4) no prebored hole

Table B-19. Depth to 2nd maximum bending moment and shear forces and depth of fixity for trials 257 through 264

Pile type	Axial load, kips	Soil type	Location from GS of 2nd maximum, ft		Depth of fixity, ft
			Bending moment	Shear	
UHPC	100	Soft clay	15.0	19.0	25.0
		Very soft clay	11.0	13.5*	13.5
	200	Soft clay	15.0	18.5*	25.0
		Very soft clay	11.0	13.5*	13.0
HP 10 × 57	100	Soft clay	15.0	19.0	25.5
		Very soft clay	11.0	13.5*	13.5
	200	Soft clay	15.0	19.0*	25.5
		Very soft clay	11.0	13.5*	13.5

*The depth of the maximum shear force

Table B-20. Depth to 2nd maximum bending moment and shear forces and depth of fixity for trials 265 through 272

Axial load, kips	Boundary condition	Soil type	Location from GS of 2nd maximum, ft		Depth of fixity, ft
			Bending moment	Shear	
UHPC	100	Soft clay	15.5	20.0	28.0
		Very soft clay	11.5	14.0*	15.5
	200	Soft clay	15.5	19.5*	27.5
		Very soft clay	11.0	14.0*	16.0
HP 10 × 57	100	Soft clay	15.5	20.0	27.5
		Very soft clay	11.5	14.0*	15.5
	200	Ls	15.5	19.5*	27.5
		Ds	11.5	17.0*	16.0

*The depth of the maximum shear force

APPENDIX C. TEST PILE CALCULATIONS

Test pile and production pile design calculations are included in this appendix using the procedures from Section 2.5.Pile Design Method.

C.1. Design Calculations for UHPC Test Pile P3

C.1.1. Current Iowa DOT Practice to Determine Pile Design Length

Step 1: Idealize the Soil Layers

Table C-1. Idealized soil layers for P3

Layer	N-Value	Thickness	fs, kip/ft (Iowa DOT 2011)
Above ground	-	3	0
Firm glacial clay	9	6	3.2
Very firm glacial clay	24	24	3.2
Very firm glacial clay	34	L	4.8

Step 2: Calculate the Nominal Capacity
  A nominal capacity of 200 kips is used to calculate the design length of P3 to verify the piles design for the integral abutments.

Step 3: Calculate End Bearing
$$Q_p = 60kip \times \frac{100in^2}{144in^2} = 41.7kips$$

Step 4: Calculate Side Friction
$$Q_s = 6ft \times 3.2\frac{kip}{ft} + 24ft \times 3.2\frac{kip}{ft} + L \times 4.8\frac{kip}{ft} = 96 + 4.8L$$

Step 5: Calculate L
  $200kips = 41.7 + 96 + 4.8L$
  $L = 13ft$

Step 6: Calculated Required Depth of Pile
$$Design\ Length = 3ft + 6ft + 24ft + 13ft = 46 \approx 45ft$$

C.1.2. New Resistance Factors to Predict Nominal Capacity

Step 1: Idealize the Soil Layers
  Use Table B-1 for the idealized soil layers.

Step 2: Calculate the Nominal Capacity
$$P_n = \frac{1.45 \times 100kip}{0.8} = 183 \; kips$$

Step 3: Calculate End Bearing
$$Q_p = 60kip \times \frac{100in^2}{144in^2} = 41.7kips$$

Step 4: Calculate Side Friction
$$Q_s = 6ft \times 3.2\frac{kip}{ft} + 24ft \times 3.2\frac{kip}{ft} + L \times 4.8\frac{kip}{ft} = 96 + 4.8L$$

Step 5: Calculate L
$$183kips = 41.7 + 96 + 4.8L$$
$$L = 9.4ft$$

Step 6: Calculated Required Depth of Pile
$$Design\; Length = 3ft + 6ft + 24ft + 9.4ft = 42ft$$

C.2. Design Calculations for UHPC Test Pile P4

C.2.1. Current Iowa DOT Practice

Step 1: Idealize the Soil Layers

Table C-2. Idealized soil layers for P4

Layer	N-Value	Thickness	fs, kip/ft (Iowa DOT 2011)
Above ground	-	3	0
Firm glacial clay	9	6	3.2
Very firm glacial clay	24	21	3.2

Step 2: Calculate End Bearing
$$Q_p = 60kip \times \frac{100in^2}{144in^2} = 41.7kips$$

Step 3: Calculate Side Friction
$$Q_s = 6ft \times 3.2\frac{kip}{ft} + 21ft \times 3.2\frac{kip}{ft} = 86.4kips$$

Step 4: Calculate Nominal Capacity
$$P_n = 41.7kips + 86.4kips = 128kips$$

C.3. Design Calculations for Steel HP 12×53 Anchor Piles RPS and RPN

C.3.1. Current Iowa DOT Practice for Uplift

Step 1: Idealize the Soil Layers

Table C-3. Idealized soil layers for RPS and RPN

Layer	N-Value	Thickness	fs, kip/ft (Iowa DOT 2011)
Cutoff	-	1	0
Above ground	-	6	0
Fill	-	0.4	0
Firm glacial clay	9	6	3.2
Very firm glacial clay	24	24	3.2
Very firm glacial clay	34	L	4.8

Step 2: Calculate Factored Uplift

$$Uplift = \frac{1.7 \times 100 kips}{0.6} = 283 kips$$

Step 3: Calculated Side Friction

$$Q_s = 6ft \times 3.2\frac{kip}{ft} + 24ft \times 3.2\frac{kip}{ft} + L \times 4.8\frac{kip}{ft} = 96 + 4.8L$$

Step 5: Calculate L

$$283 kips = 96 + 4.8L$$
$$L = 40ft$$

Step 6: Calculated Required Depth of Pile

$$Design\ Length = 1ft + 6ft + 0.4ft + 6ft + 24ft + 40ft = 77 = 80ft$$

C.3.2. Current Iowa DOT Practice for Downward Load

Step 1: Idealize the Soil Layers
Table B-3 is used to idealize the soil layers.

Step 2: Calculate End Bearing

$$Q_p = 2ksi \times 15.5in^2 = 31 kips$$

Step 3: Calculate Side Friction

$$Q_s = 6ft \times 3.2\frac{kip}{ft} + 24ft \times 3.2\frac{kip}{ft} + 42.6 \times 4.8\frac{kip}{ft} = 300 kips$$

Step 4: Calculate Nominal Capacity
$$P_n = 31kips + 300kips = 331kips$$

C.4. Design of UHPC Production Pile UW1

C.4.1. Current Iowa DOT Practice

Step 1: Idealize the Soil Layers

Table C-4. Idealized soil layers for UW1

Layer	N-Value	Thickness	fs, kip/ft (Iowa DOT 2011)
Abutment	-	2	0
Prebored hole	-	10	0
Fill	-	0.4	0
Firm glacial clay	9	6	3.2
Very firm glacial clay	24	24	3.2
Very firm glacial clay	34	L	4.8

Step 2: Calculate the Nominal Capacity
A nominal capacity of 200 kips is used to calculate the design length of P3 to verify the piles design for the integral abutments.

Step 3: Calculate End Bearing
$$Q_p = 60kip \times \frac{100in^2}{144in^2} = 41.7kips$$

Step 4: Calculate Side Friction
$$Q_s = 7ft \times 3.2\frac{kip}{ft} + 22ft \times 3.2\frac{kip}{ft} + L \times 4.8\frac{kip}{ft} = 92.8 + 4.8L$$

Step 5: Calculate L
$$200kips = 41.7 + 92.8 + 4.8L$$
$$L = 13.6ft$$

Step 6: Calculated Required Depth of Pile
$$Design\ Length = 2ft + 10ft + 0.4ft + 7ft + 22ft + 13.6ft = 55ft$$

C.4.2. New Resistance Factors

Step 1: Idealize the Soil Layers
Use Table B-4 for the idealized soil layers.

Step 2: Calculate the Nominal Capacity

$$P_n = \frac{1.45 \times 100 kips}{0.8} = 183 \ kips$$

Step 3: Calculate End Bearing
$$Q_p = 60 kip \times \frac{100 in^2}{144 in^2} = 41.7 kips$$

Step 4: Calculate Side Friction
$$Q_s = 6ft \times 3.2 \frac{kip}{ft} + 24ft \times 3.2 \frac{kip}{ft} + L \times 4.8 \frac{kip}{ft} = 96 + 4.8L$$

Step 5: Calculate L
$$183 kips = 41.7 + 96 + 4.8L$$
$$L = 9.4 ft$$

Step 6: Calculated Required Depth of Pile
$$Design \ Length = 2ft + 10 + 0.4ft + 6ft + 24ft + 9.4ft = 52ft$$

C.5. Design of Steel HP 10 × 57 Production Pile SW2

C.5.1. Current Iowa DOT Practice

Step 1: Idealize the Soil Layers

Table C-5. Idealized soil layers for SW2

Layer	N-Value	Thickness	fs, kip/ft (Iowa DOT 2011)
Cutoff	-	1	0
Abutment	-	2	0
Prebored hole	-	10	0
Fill	-	0.4	0
Firm glacial clay	9	6	2.8
Very firm glacial clay	24	24	2.8
Very firm glacial clay	34	L	4.0

Step 2: Calculate the Nominal Capacity
$$P_n = \frac{1.45 \times 6 ksi \times 16.8 in^2}{0.725} = 201.6 = 200 kips$$

Step 3: Calculate End Bearing
$$Q_p = 2ksi \times 16.8 in^2 = 33.6 kips$$

Step 4: Calculate Side Friction

$$Q_s = 7ft \times 2.8\frac{kip}{ft} + 22ft \times 2.8\frac{kip}{ft} + L \times 4.0\frac{kip}{ft} = 81.2 + 4.0L$$

Step 5: Calculate L
$$200 kips = 33.6 + 81.2 + 4.0L$$
$$L = 21.3ft$$

Step 6: Calculated Required Depth of Pile
$$Design\ Length = 1ft + 2ft + 10ft + 0.4ft + 7ft + 22ft + 21.3ft = 63.7$$
$$Design\ Length = 65ft$$

C.5.2. New Resistance Factors

Step 1: Idealize the Soil Layers
Use Table B-5 for the idealized soil layers.

Step 2: Calculate the Nominal Capacity
$$P_n = \frac{1.45 \times 6ksi \times 16.8in^2}{0.8} = 183\ kips$$

Step 3: Calculate End Bearing
$$Q_p = 2ksi \times 16.8in^2 = 33.6kips$$

Step 4: Calculate Side Friction
$$Q_s = 6ft \times 2.8\frac{kip}{ft} + 24ft \times 2.8\frac{kip}{ft} + L \times 4.0\frac{kip}{ft} = 84 + 4.0L$$

Step 5: Calculate L
$$183 kips = 33.6 + 84 + 4.0L$$
$$L = 16.4ft$$

Step 6: Calculated Required Depth of Pile
$$Design\ Length = 1ft + 2ft + 10ft + 0.4ft + 6ft + 24ft + 16.4ft = 60ft$$

C.6. Design of Steel HP 10×57 Production Pile SE1 and SE2

C.6.1. Current Iowa DOT Practice

Step 1: Idealize the Soil Layers

Table C-6. Idealized Soil Layers for SE1 and SE2

Layer	N-Value	Thickness	fs, kip/ft (Iowa DOT 2011)
Cutoff	-	1	0
Abutment	-	2	0
Prebored hole	-	10	0
Fill	-	17	0
Soft sand silty clay	4	7	0.8
Firm glacial clay	17	23	2.8
Firm glacial clay	24	L	4.0

Step 2: Calculate the Nominal Capacity

$$P_n = \frac{1.45 \times 6ksi \times 16.8in^2}{0.725} = 201.6 = 200kips$$

Step 3: Calculate End Bearing

$$Q_p = 2ksi \times 16.8in^2 = 33.6kips$$

Step 4: Calculate Side Friction

$$Q_s = 7ft \times 0.8\frac{kip}{ft} + 23ft \times 2.8\frac{kip}{ft} + L \times 4.0\frac{kip}{ft} = 70 + 4.0L$$

Step 5: Calculate L

$$200kips = 33.6 + 70 + 4.0L$$
$$L = 24.1ft$$

Step 6: Calculated Required Depth of Pile

$$Design\ Length = 1ft + 2ft + 10ft + 17ft + 7ft + 23ft + 24.1ft = 84.1$$
$$Design\ Length = 85ft$$

C.6.2. New Resistance Factors

Step 1: Idealize the Soil Layers

Use Table B-6 for the idealized soil layers.

Step 2: Calculate the Nominal Capacity

$$P_n = \frac{1.45 \times 6ksi \times 16.8in^2}{0.8} = 183\ kips$$

Step 3: Calculate End Bearing

$$Q_p = 2ksi \times 16.8in^2 = 33.6kips$$

Step 4: Calculate Side Friction

$$Q_s = 7ft \times 0.8\frac{kip}{ft} + 23ft \times 2.8\frac{kip}{ft} + L \times 4.0\frac{kip}{ft} = 70 + 4.0L$$

Step 5: Calculate L

$$183kips = 33.6 + 70 + 4.0L$$
$$L = 19.9ft$$

Step 6: Calculated Required Depth of Pile

$$Design\ Length = 1ft + 2ft + 10ft + 17ft + 7ft + 23ft + 20ft = 80ft$$

APPENDIX D. INSTRUMENTATION INSTALLATION PROCEDURES

The instrumentation installation procedure are given for the test units, test piles, and production piles in this appendix.

D.1. Procedure for Installing TML Strain Gages

1. Grind down the surface of the prestressing strand at the desired location of installation with sand paper
2. Clean the bonding surface with a clean cloth and acetone
3. Apply the bonding adhesive to the back of the gage base. Place the gage on the guide mark and then place on the polyethylene sheet. Press down on the gage constantly
4. After curing is complete, remove the polyethylene sheet, and raise the gage leads with a pair of tweezers
5. Protect the gage by covering it with a water proofing agent, followed by Butyl rubber, and finally aluminum tape (See Figure D-1)
6. Attach the cable to the prestressing strand close to the gage making sure to leave some slack in case the cable is pulled
7. Continue to attach the cable periodically along the prestressing strand until the point where the cable will exit. Make sure to spread the cables throughout the cross-section to ensure no weak points such as bonding problems between the UHPC and prestressing strands

Figure D-1. TML strain gage after aluminum foil was applied

D.2. Procedure for Installing Weldable Strain Gages

1. Grind down the surface of the H-pile at the specified gage locations
2. Align the strain gage with the transition end pointing toward the pile head
3. Tack the gage with 1 weld at each side of the align marks on the strain gage
4. Continue welding the gage in place. The first line of welds should be adjacent to the hermetic sealant 1/6 in. on center. The sequence of welds should be:
5. Vertically down from the right side alignment mark looking at the gage from transition end
6. Vertically up from the right side alignment mark
7. Vertically down from the left side alignment mark
8. Vertically up from the left side alignment mark
9. Horizontally across the top of the gage
10. Complete the tack welding by adding a second row of tack welds between and 1/32 in. outboard of the first row
11. Cover with butyl rubber
12. Cover with aluminum tape
13. Weld 3/8 in. nuts at various locations along the pile
14. Tie the strain gage cables together
15. Wrap the cable with aluminum foil to protect the cables during welding of the protective angle (See Figure D-2)
16. Secure the cables to the nuts welded onto the pile with zip ties
17. Weld the steel angle over the cables 4 in. every 24 in., but adjusting the location of the weld when near the location of a gage

Figure D-2. Installed weldable strain gage

D.3. Procedure for Installing Embedded Concrete Strain Gages

1. Twist wire around the bottom of the strain gage, which is nearest to the attached cable, leaving excess wire on both sides
2. Twist wire around the top of the strain gages, leaving excess wire on both sides
3. Align the strain gages with the transition end pointing toward the head of the pile
4. Twist the excess wire from steps 1 and 2 around the adjacent prestressing strands (see Figure D-3)
5. String the cables along the prestressing strands using zip ties, until at the pile head. Make sure to spread the cables out so a weak point does not develop in the cross-section of the pile

Figure D-3. Strung embedded concrete strain gage

APPENDIX E. LATERAL TEST LOAD RESULTS

The comprehensive results from the lateral load tests are given in this appendix, which includes: 1) the predicted, adjusted and average measured moments along P3 and P4; 2) the adjusted and measured displacements along the length of P4; and 3) the adjusted shear force along the length of P4.

## E.1. Predicted, Adjusted, and Average Measured Moments along the Length of P3
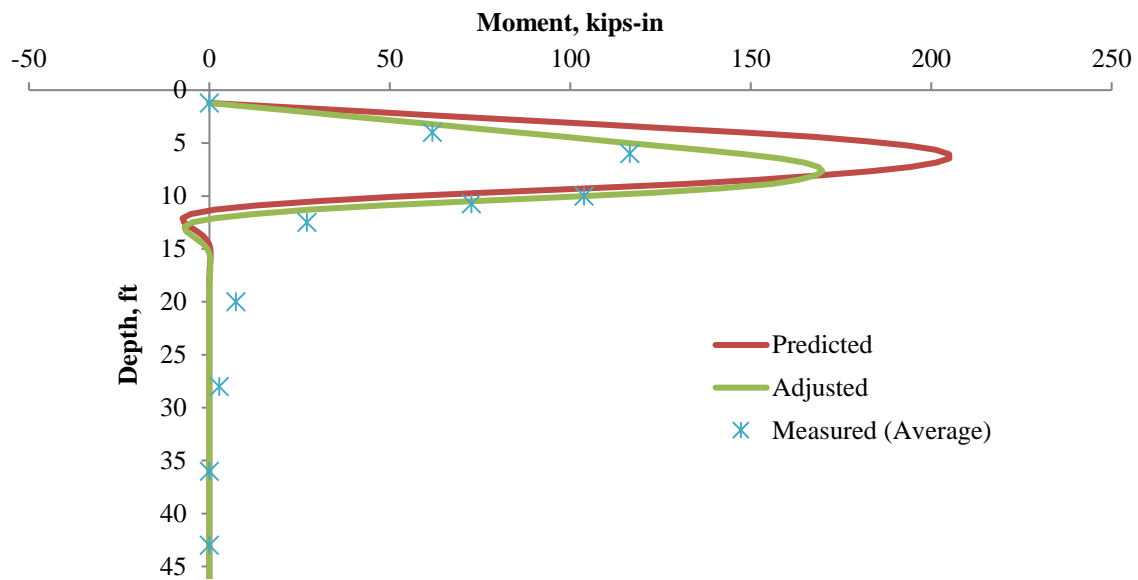
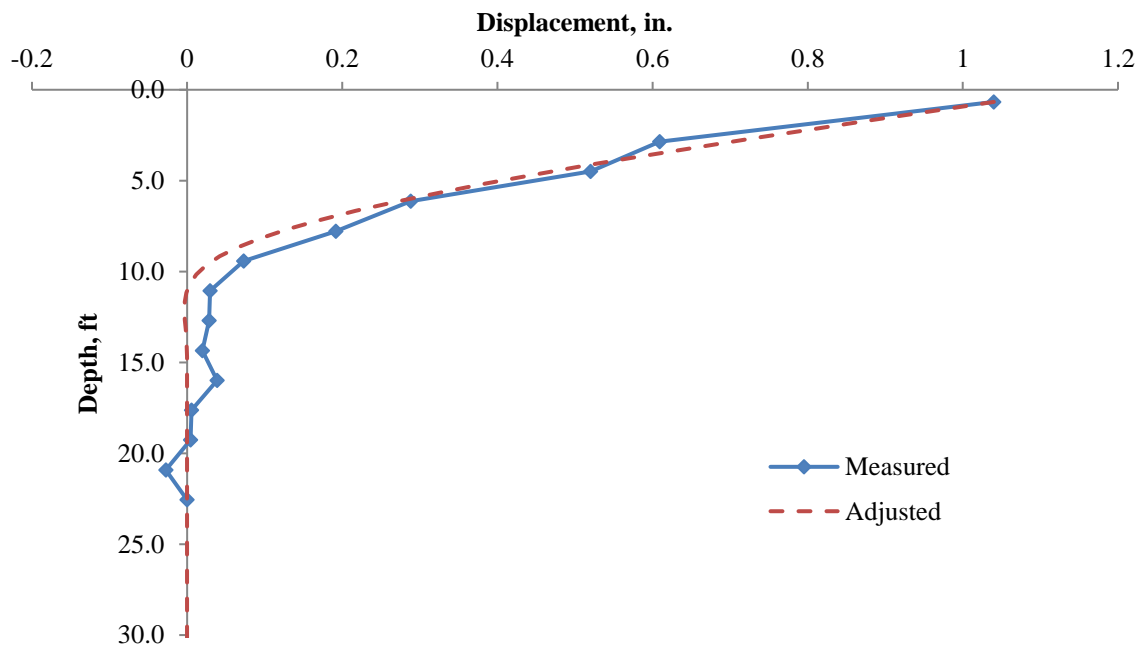**Figure E-1. Moments along length of P3 at 2.5 kip load step during lateral load test**
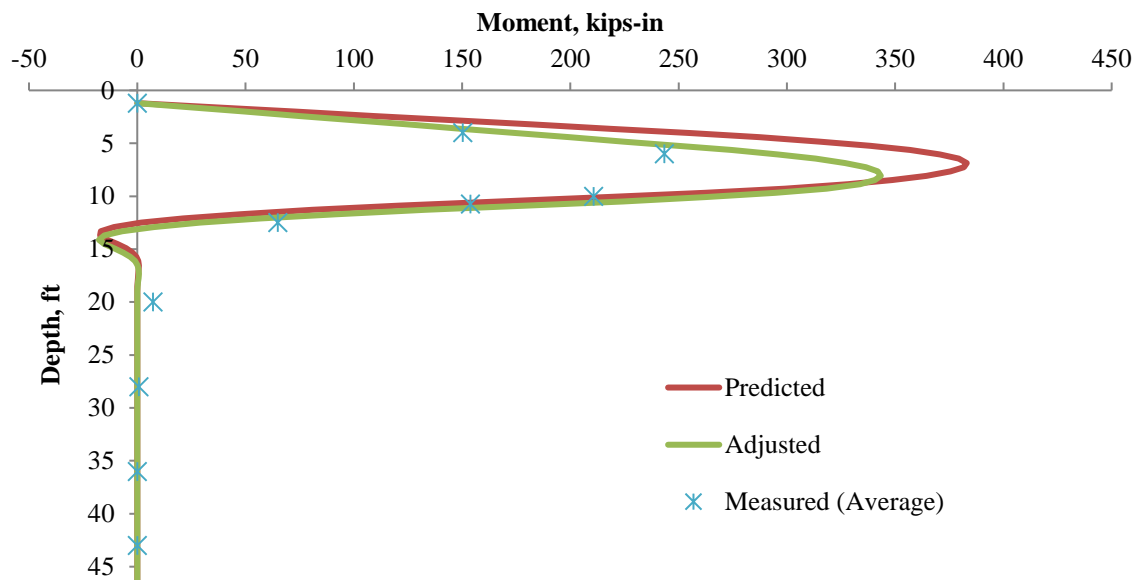
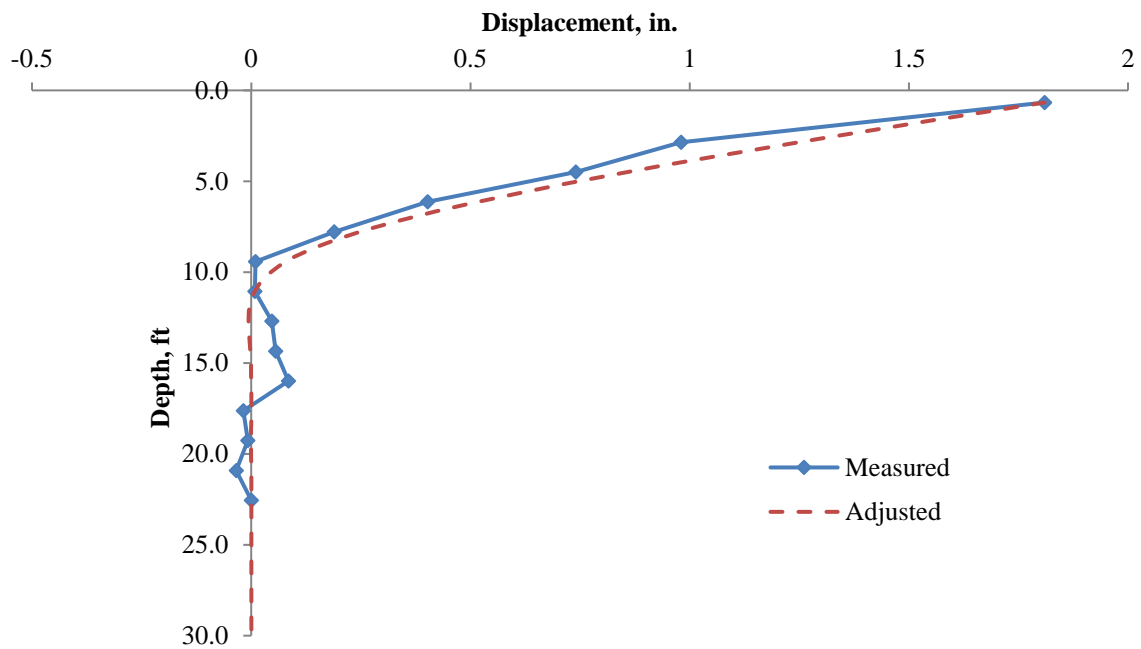**Figure E-2. Moments along length of P3 at 5.0 kip load step during lateral load test**
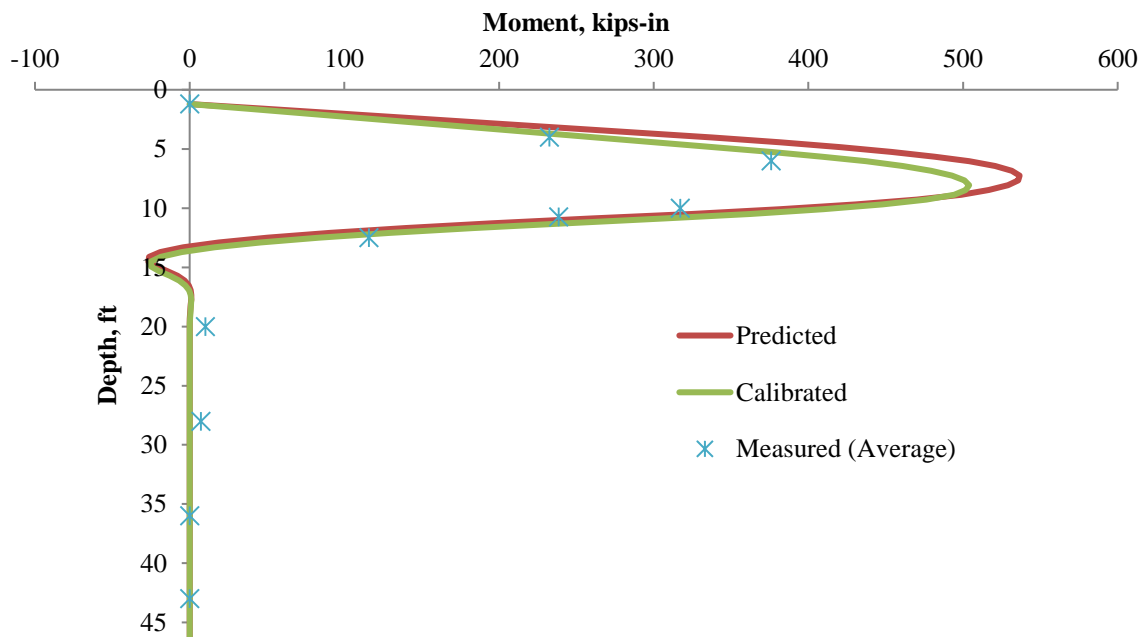
Figure E-3. Moments along length of P3 at 7.5 kip load step during lateral load test
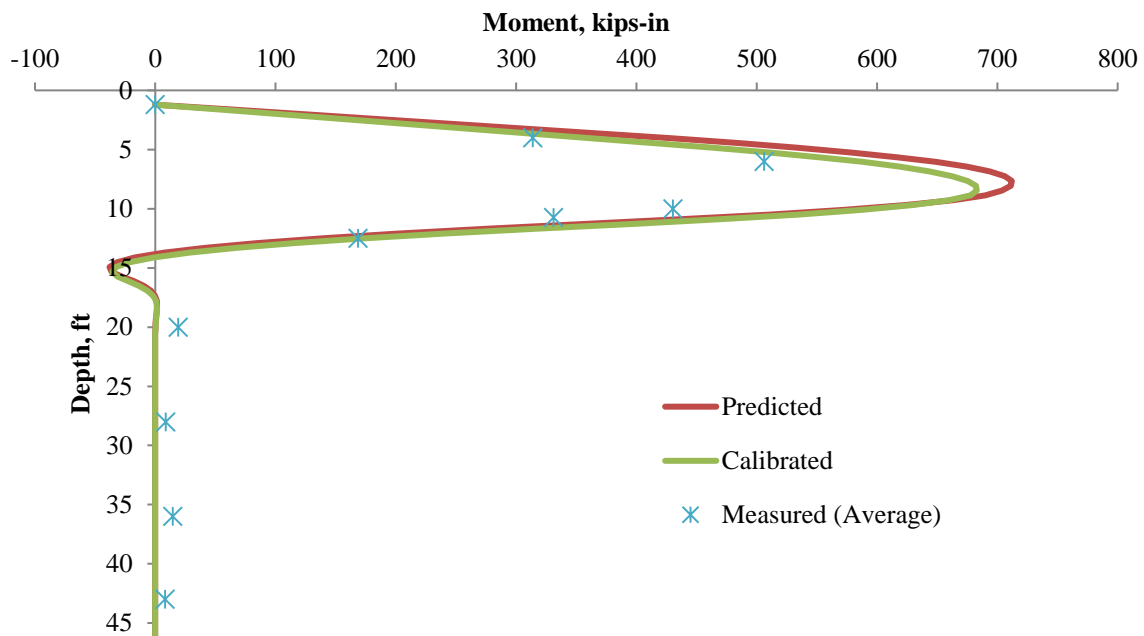
Figure E-4. Moments along length of P3 at 10.0 kip load step during lateral load test
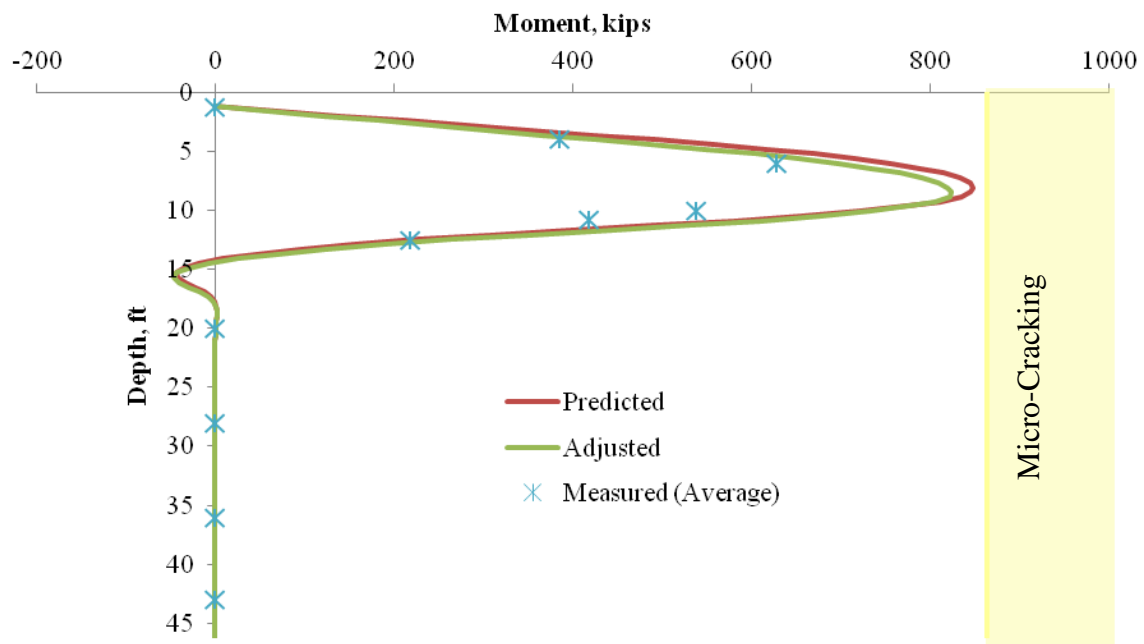
Figure E-5. Moments along length of P3 at 12.5 kip load step during lateral load test
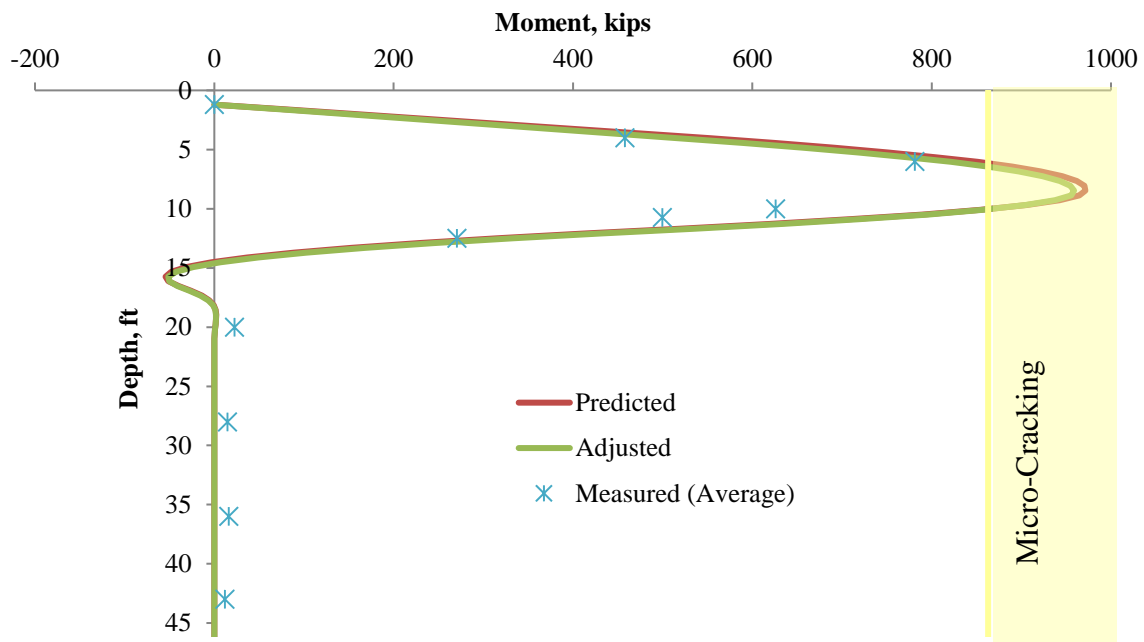
Figure E-6. Moments along length of P3 at 15.0 kip load step during lateral load test
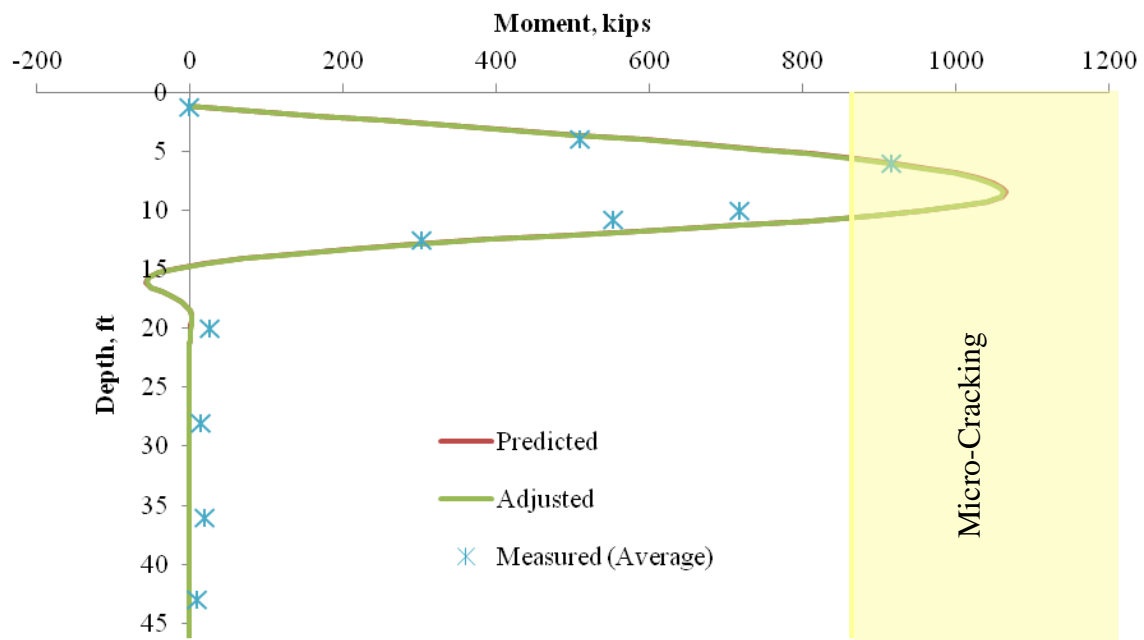
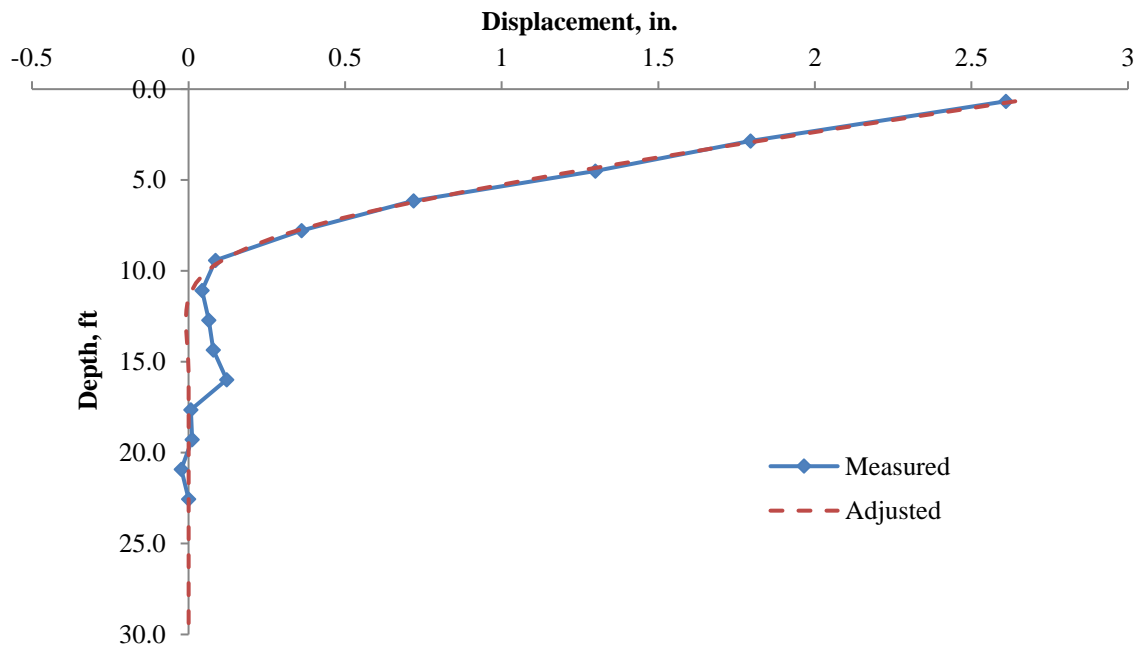**Figure E-7. Moments along length of P3 at 17.0 kip load step during lateral load test**

278
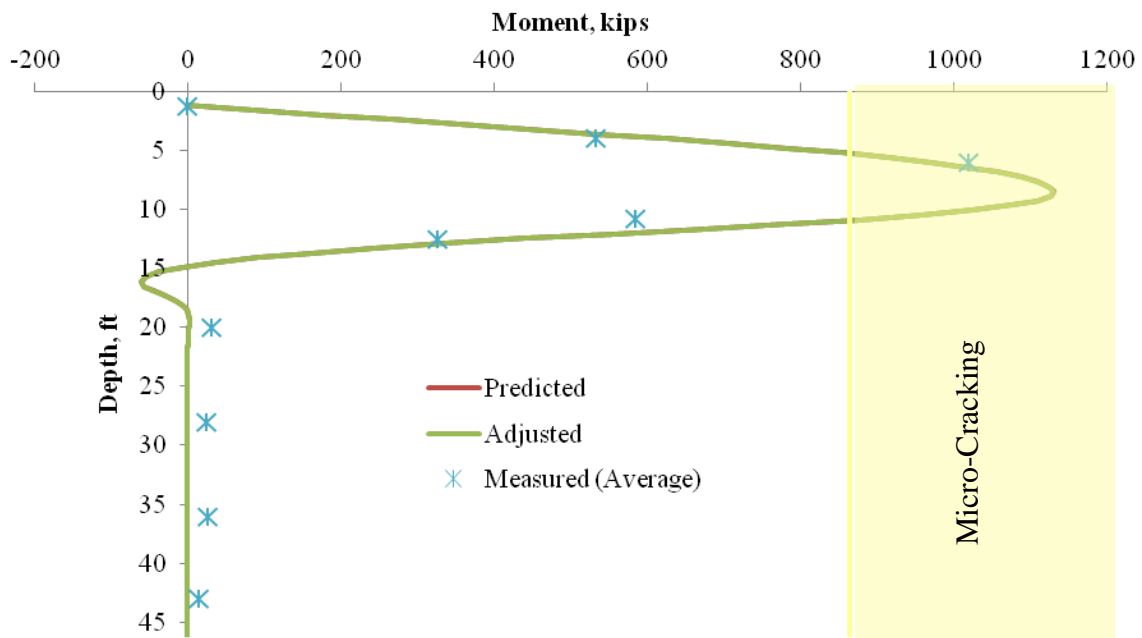
Figure E-8. Moments along length of P3 at 18.0 kip load step during lateral load test
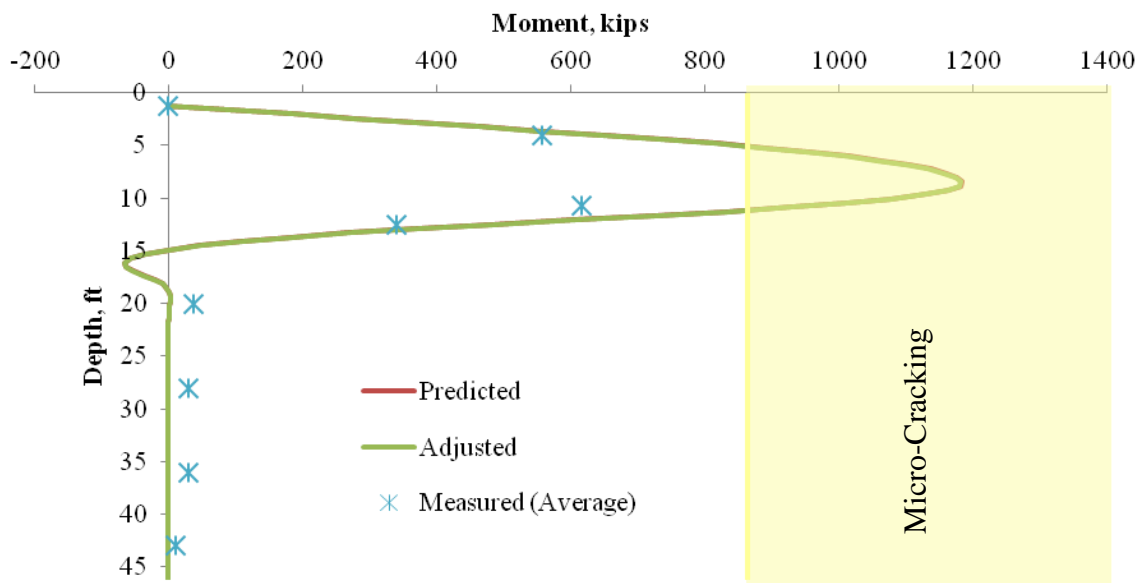
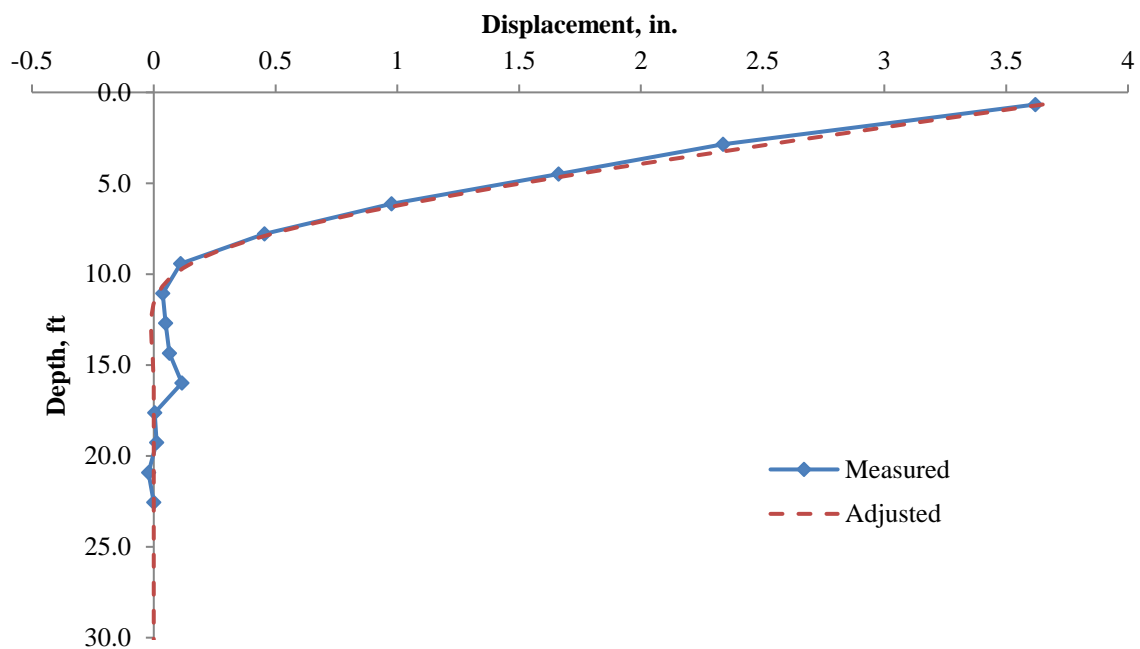**Figure E-9. Moments along length of P3 at 19.0 kip load step during lateral load test**

279

E.2. Predicted, Adjusted, and Average Measured Moments along the Length of P4
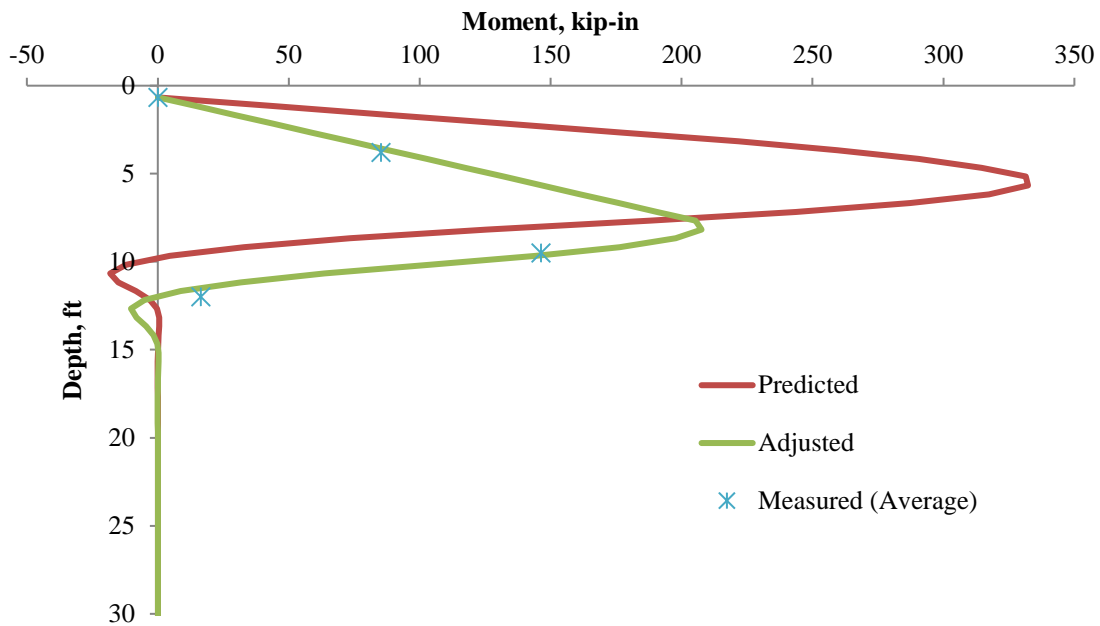
Figure E-10. Moments along length of P4 at 2.5 kip load step during lateral load test
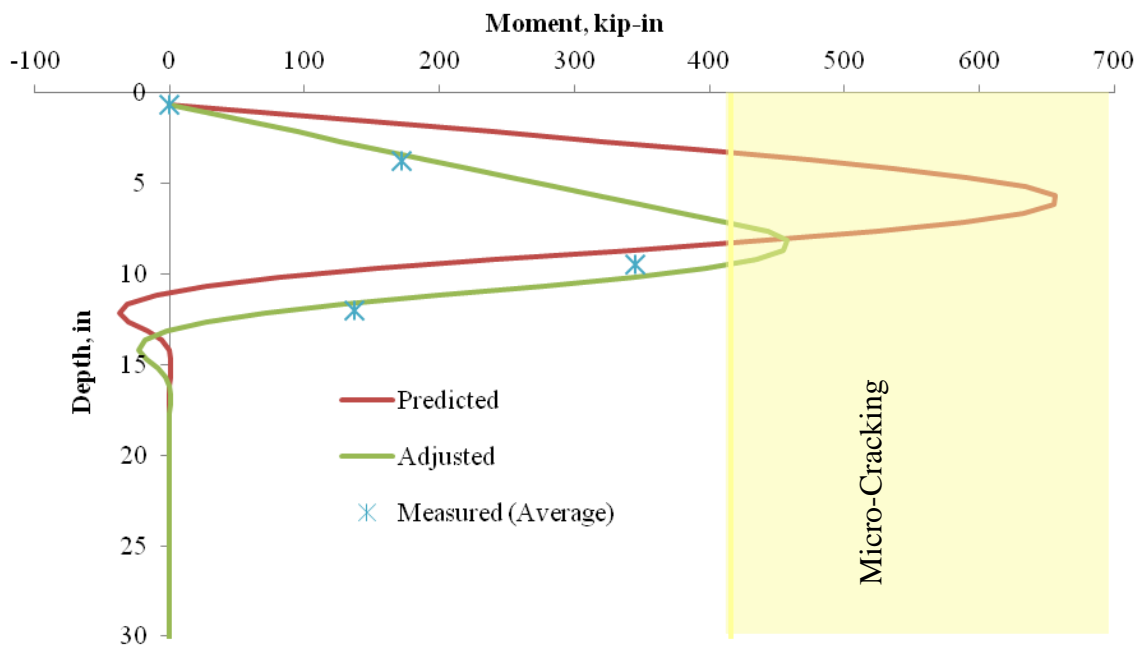
Figure E-11. Moments along length of P4 at 5.0 kip load step during lateral load test
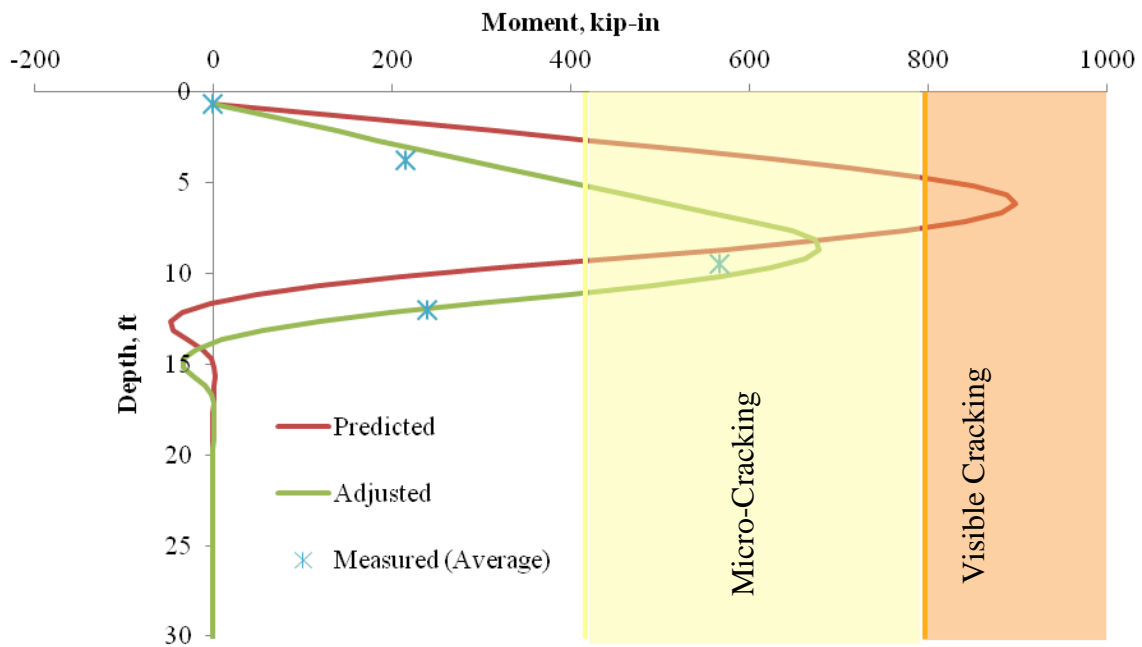
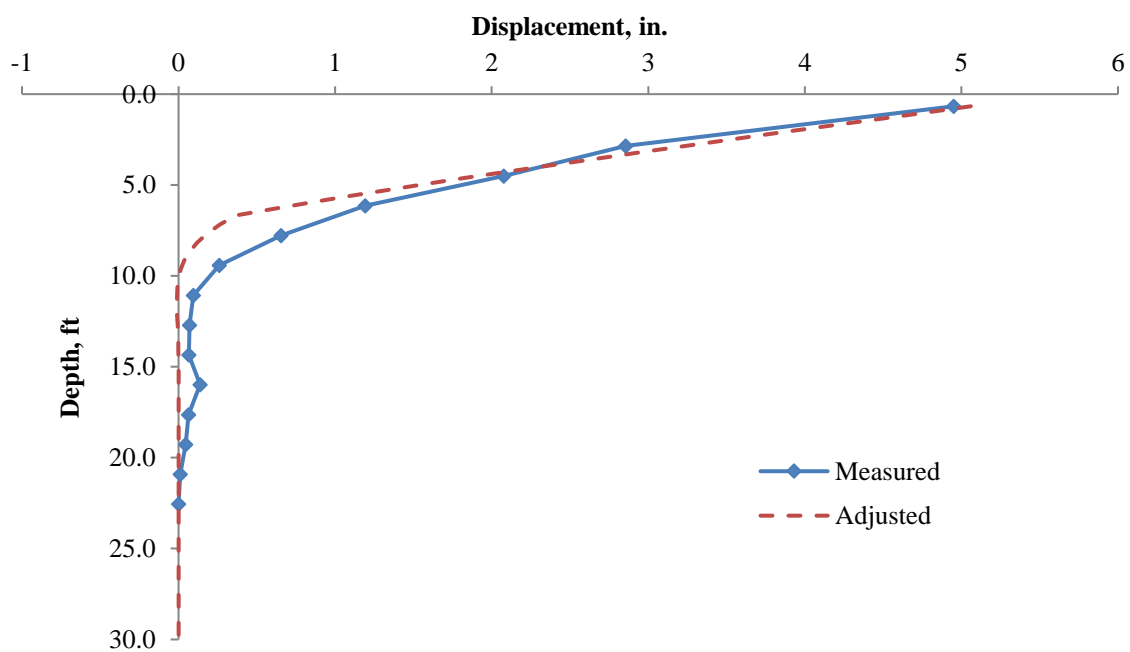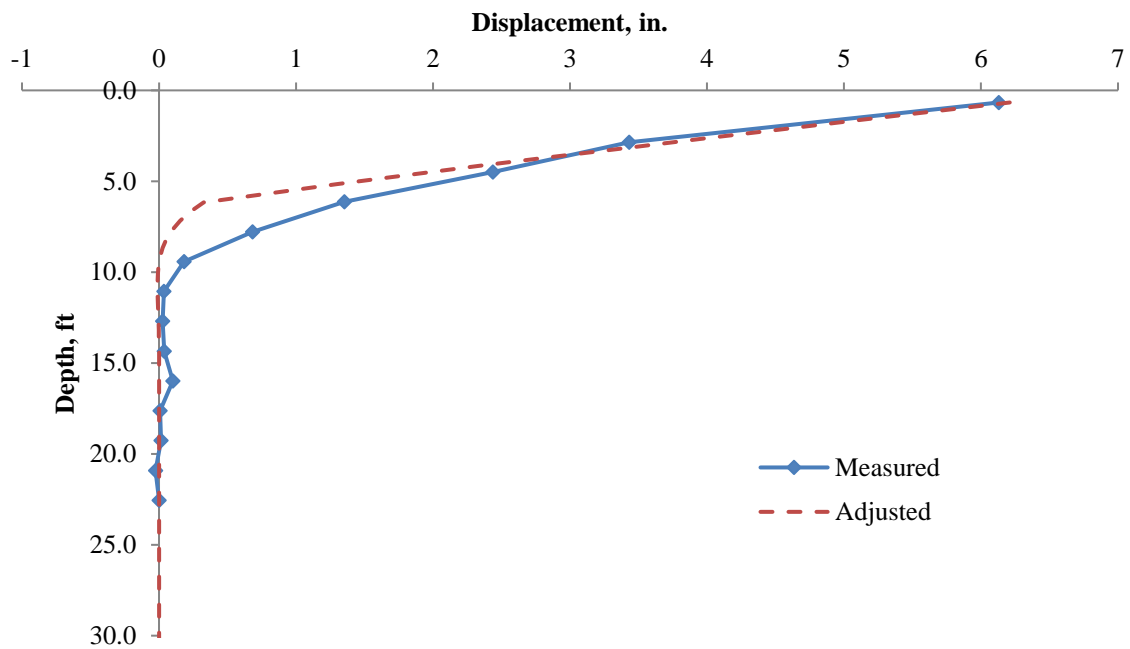**Figure E-12. Moments along length of P4 at 7.5 kip load step during lateral load test**
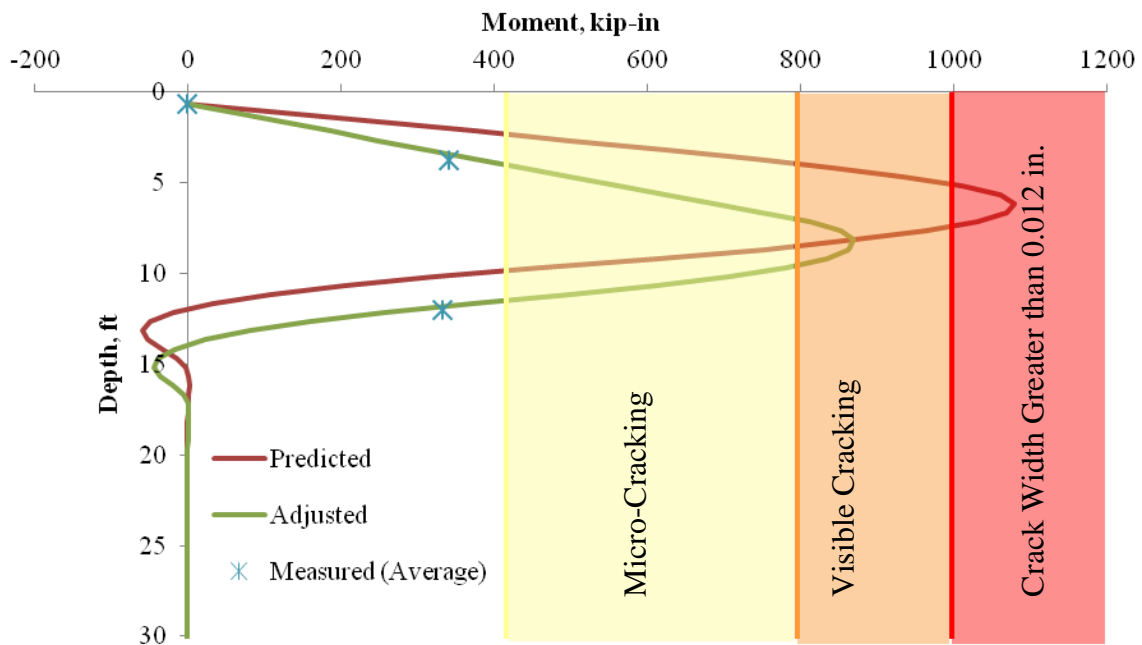
Figure E-13. Moments along length of P4 at 10.0 kip load step during lateral load test
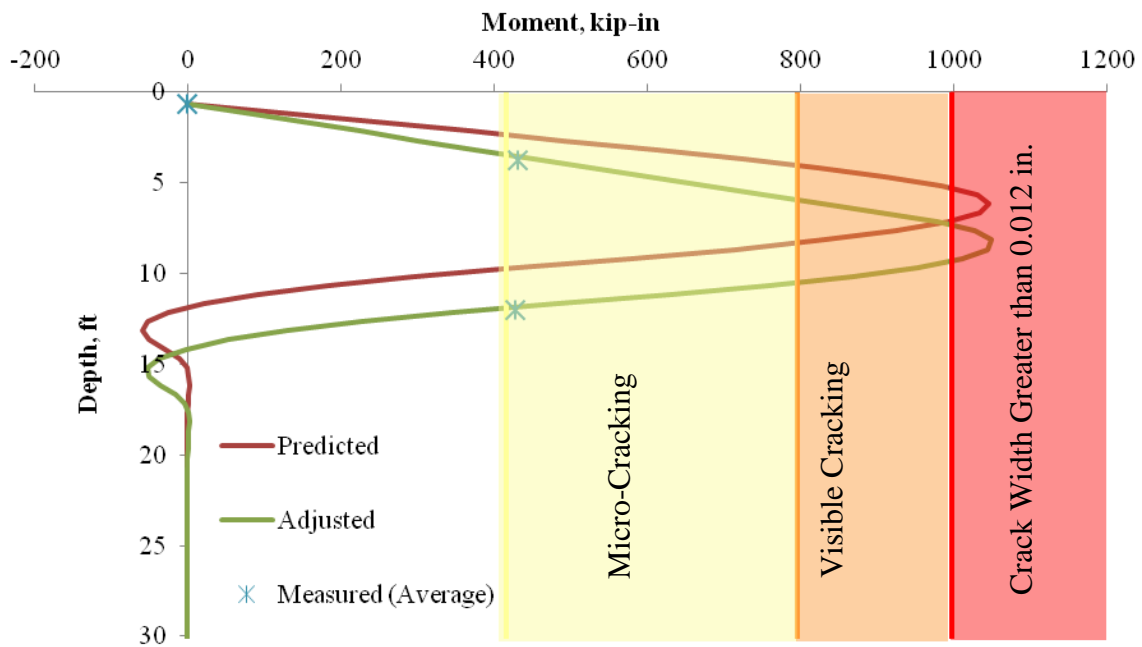
Figure E-14. Moments along length of P4 at 12.5 kip load step during lateral load test
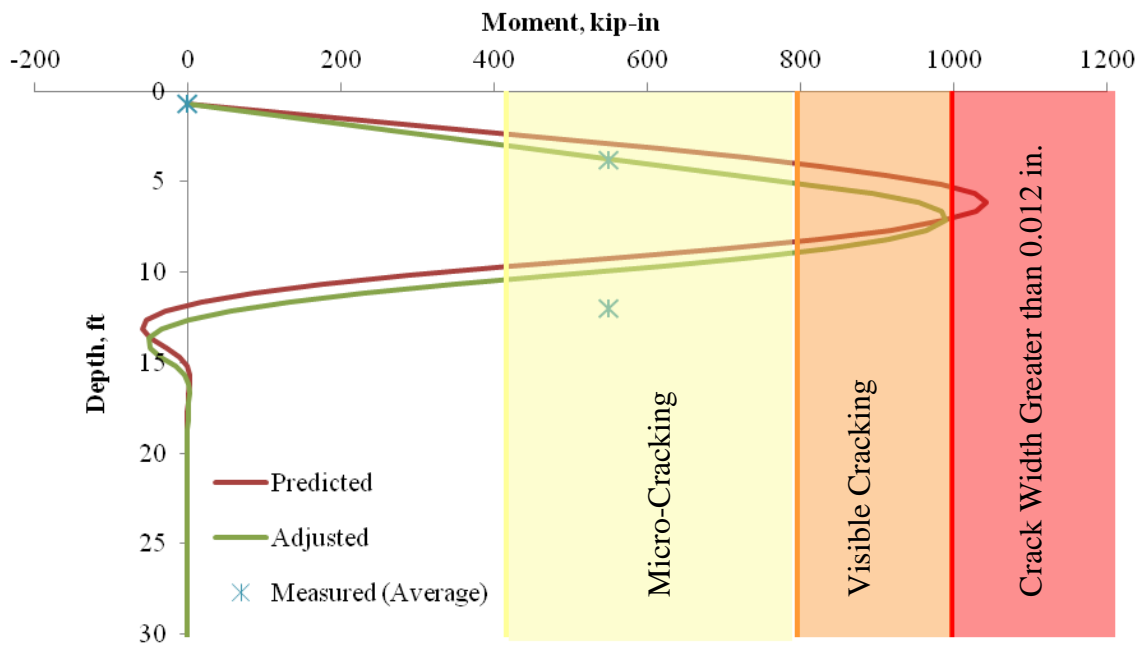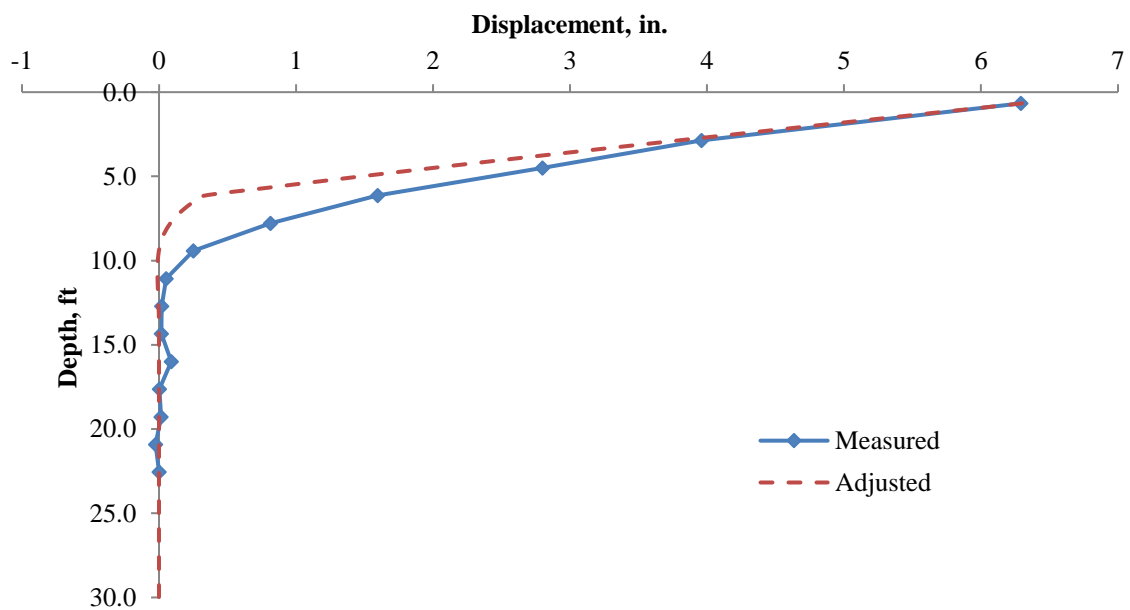

Figure E-15. Moments along length of P4 at 15.0 kip load step during lateral load test

282
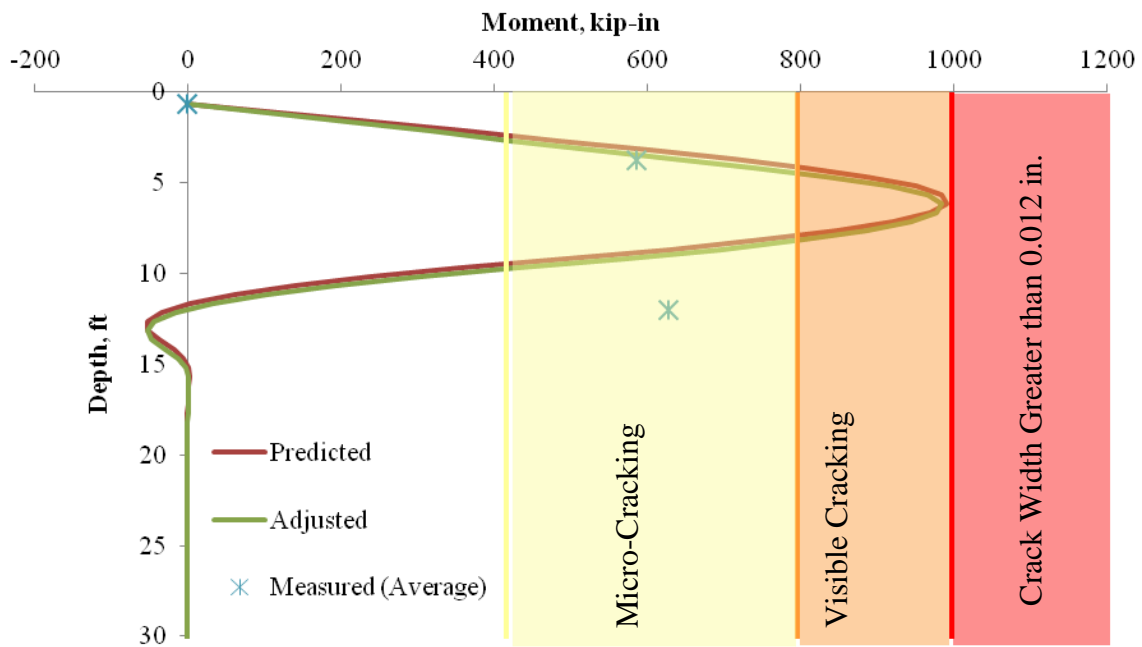
Figure E-16. Moments along length of P4 at 17.0 kip load step during lateral load test
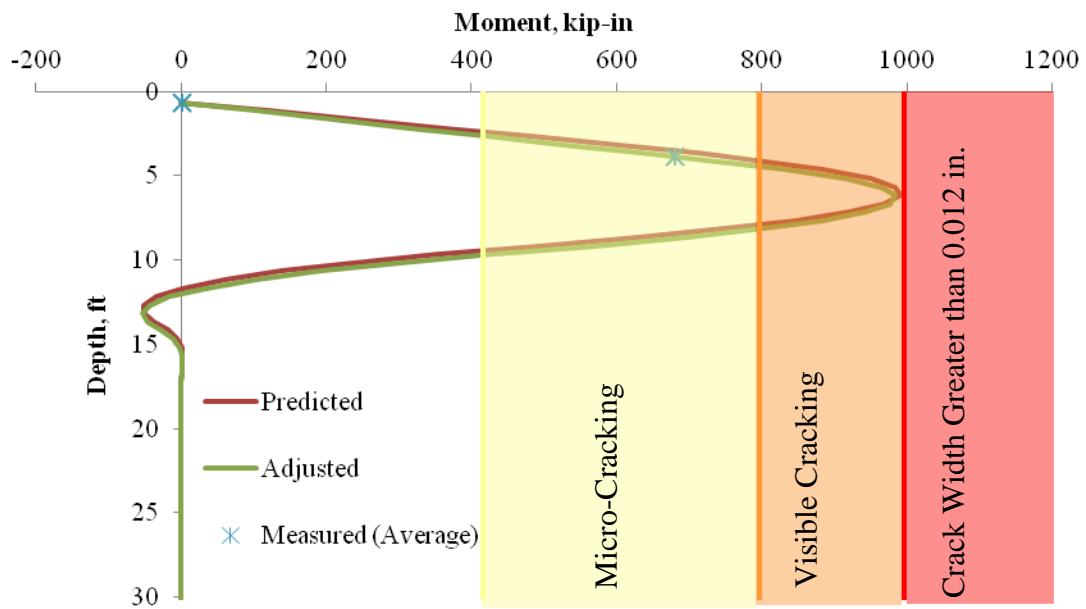
Figure E-17. Moments along length of P4 at 18.0 kip load step during lateral load test

E.3. Adjusted and Measured Displacement along the Length of P4
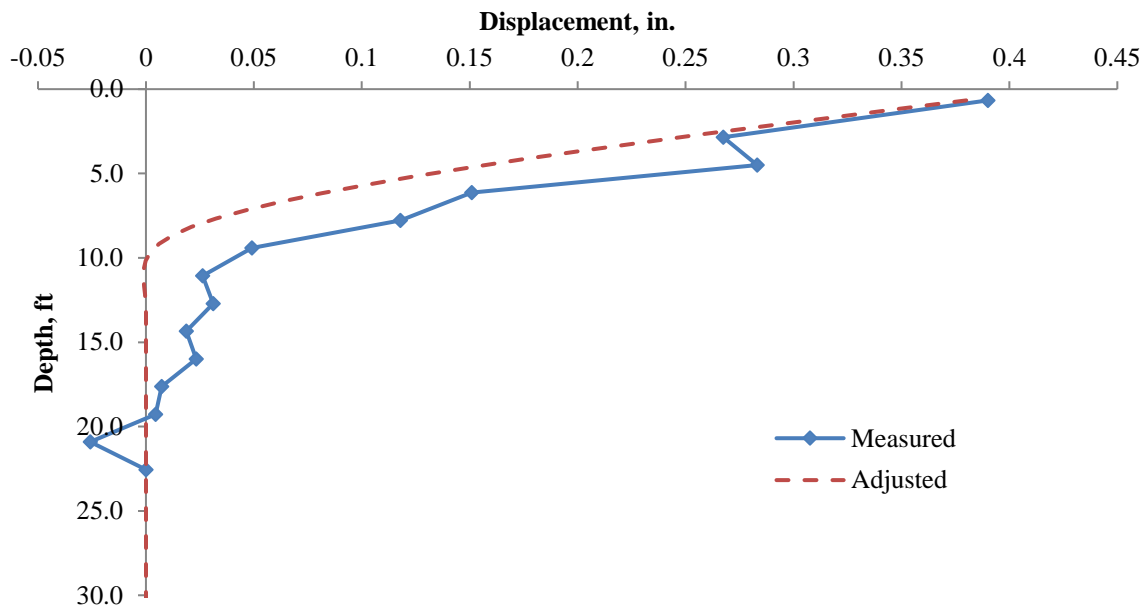
Figure E-18. Displacements along length of P4 at 2.5 kip load step during lateral load test

Figure E-19. Displacements along length of P4 at 5.0 kip load step during lateral load test

Figure E-20. Displacements along length of P4 at 7.5 kip load step during lateral load test

Figure E-21. Displacements along length of P4 at 10.0 kip load step during lateral load test

Figure E-22. Displacements along length of P4 at 12.5 kip load step during lateral load test

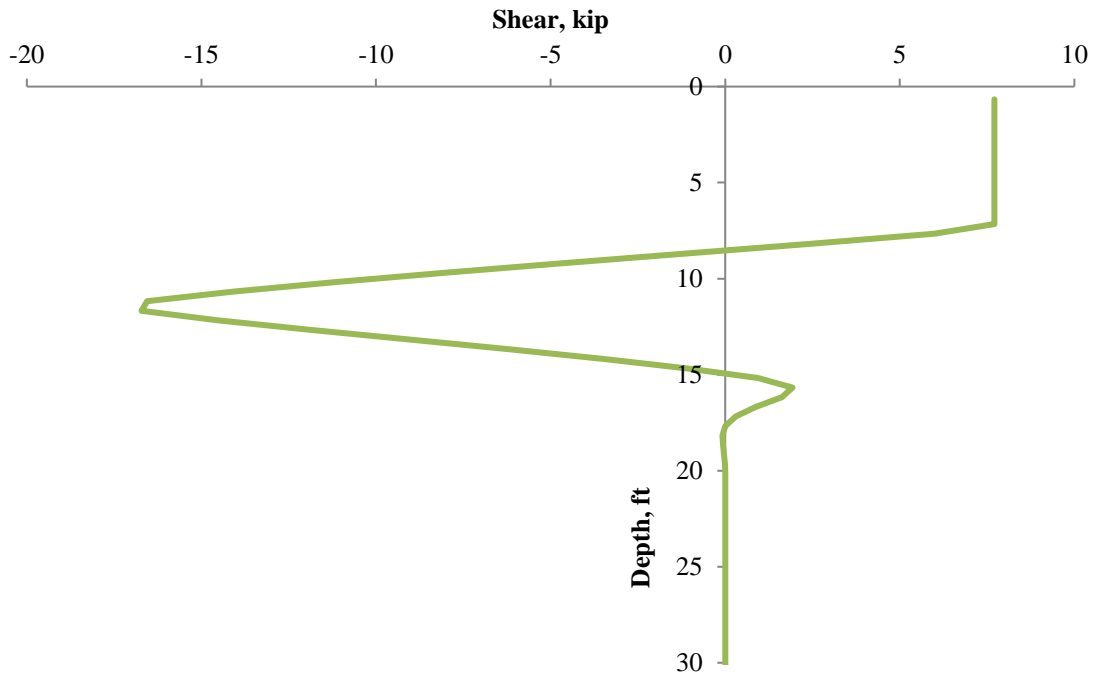**Figure E-23. Displacements along length of P4 at 15.0 kip load step during lateral load test**

286

Figure E-24. Displacements along length of P4 at 17.0 kip load step during lateral load test

Figure E-25. Displacements along length of P4 at 18.0 kip load step during lateral load test

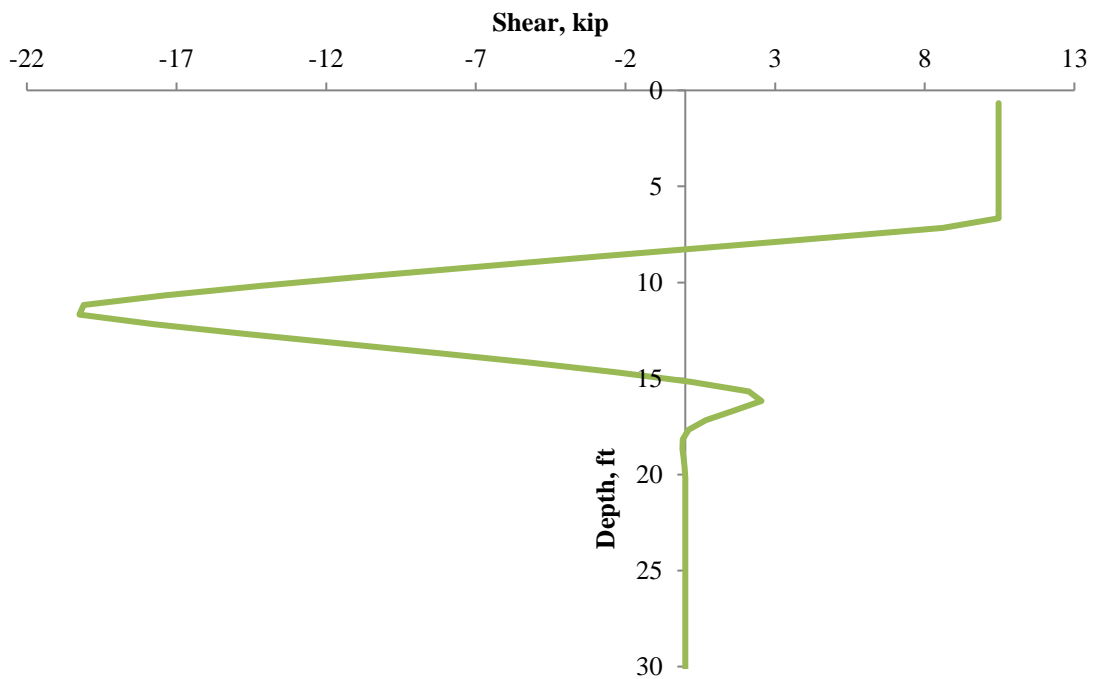## E.4. Adjusted Shear Force along the Length of P4
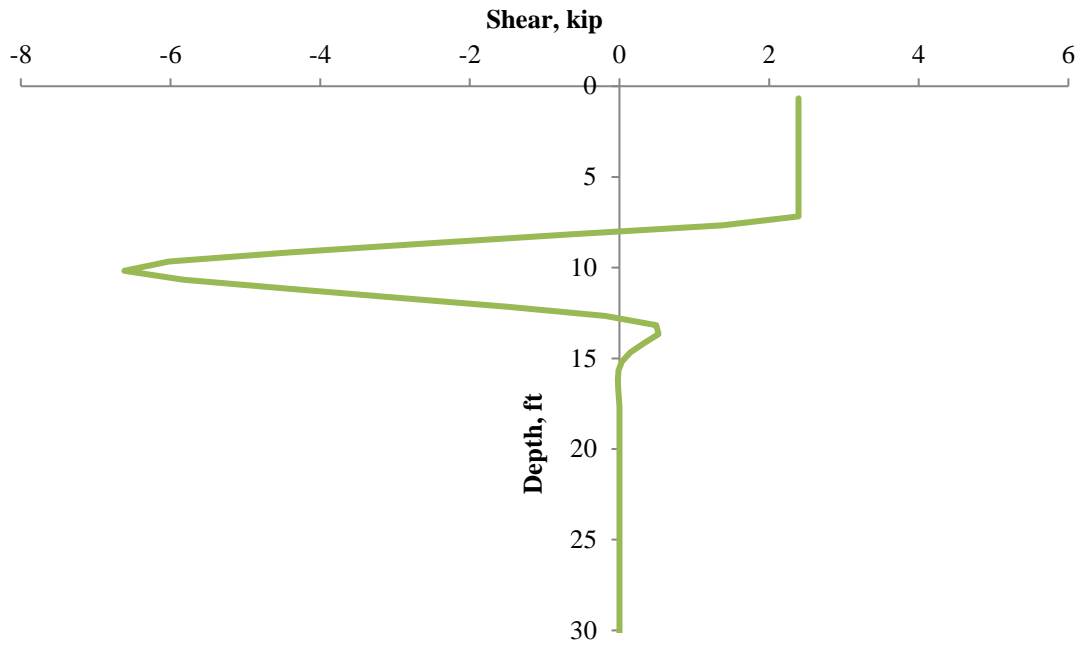
Figure E-26. Adjusted shear force along length of P4 at 2.5 kip load step during lateral load test
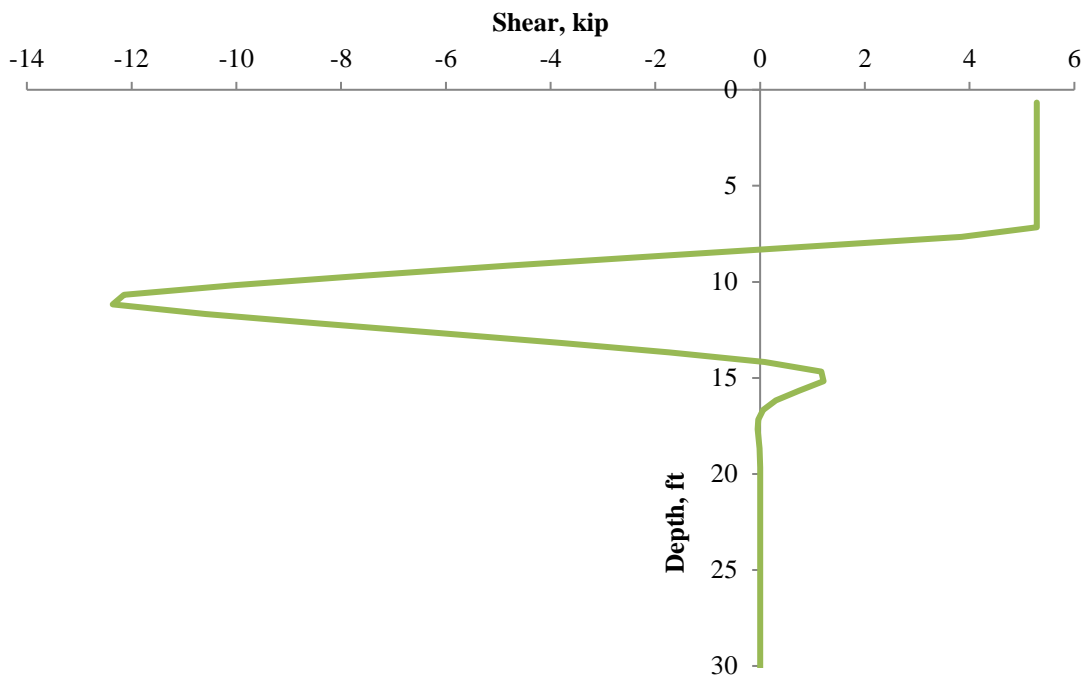
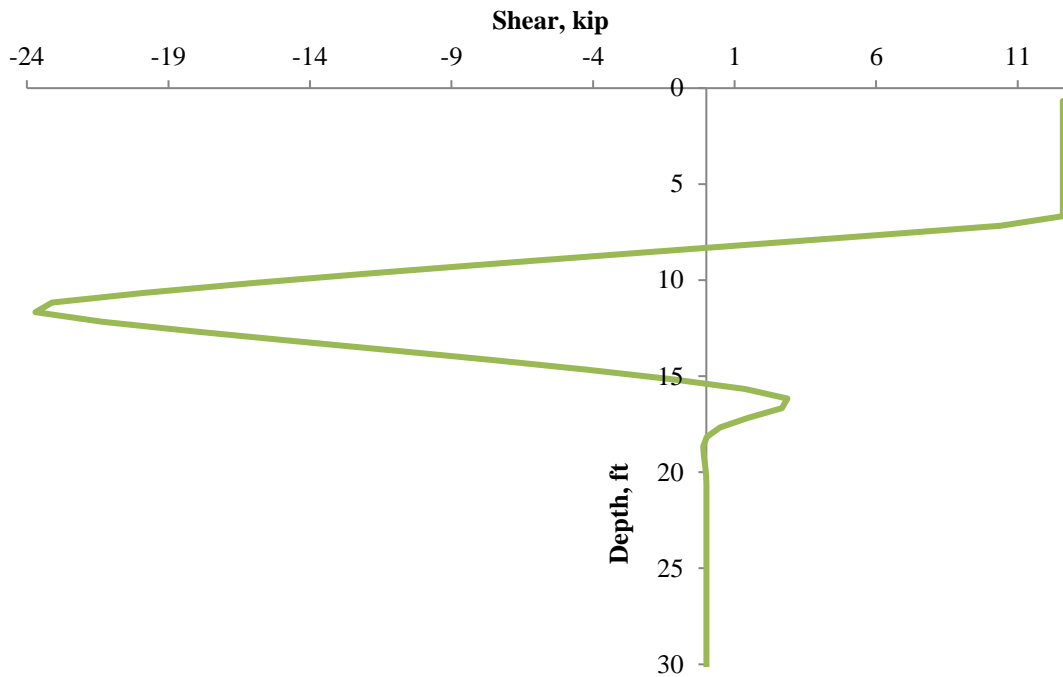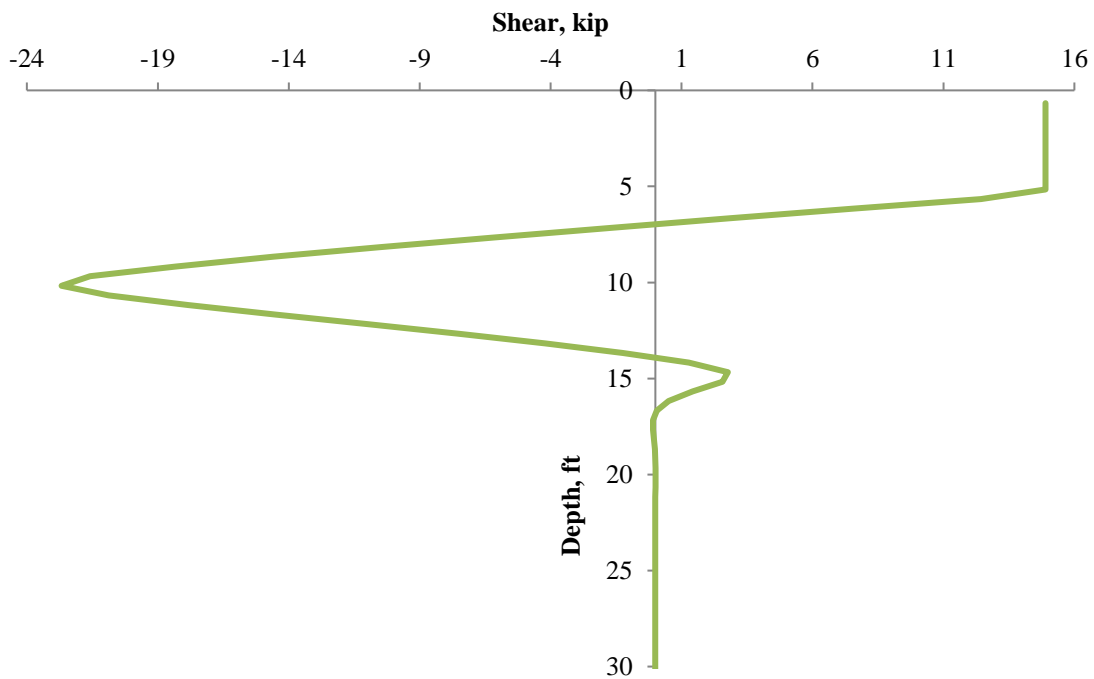**Figure E-27. Adjusted shear force along length of P4 at 5.0 kip load step during lateral load test**

Figure E-28. Adjusted shear force along length of P4 at 7.5 kip load step during lateral load test

Figure E-29. Adjusted shear force along length of P4 at 10.1 kip load step during lateral load test

289

Figure E-30. Adjusted shear force along length of P4 at 12.5 kip load step during lateral load test

Figure E-31. Adjusted shear force along length of P4 at 15.0 kip load step during lateral load test
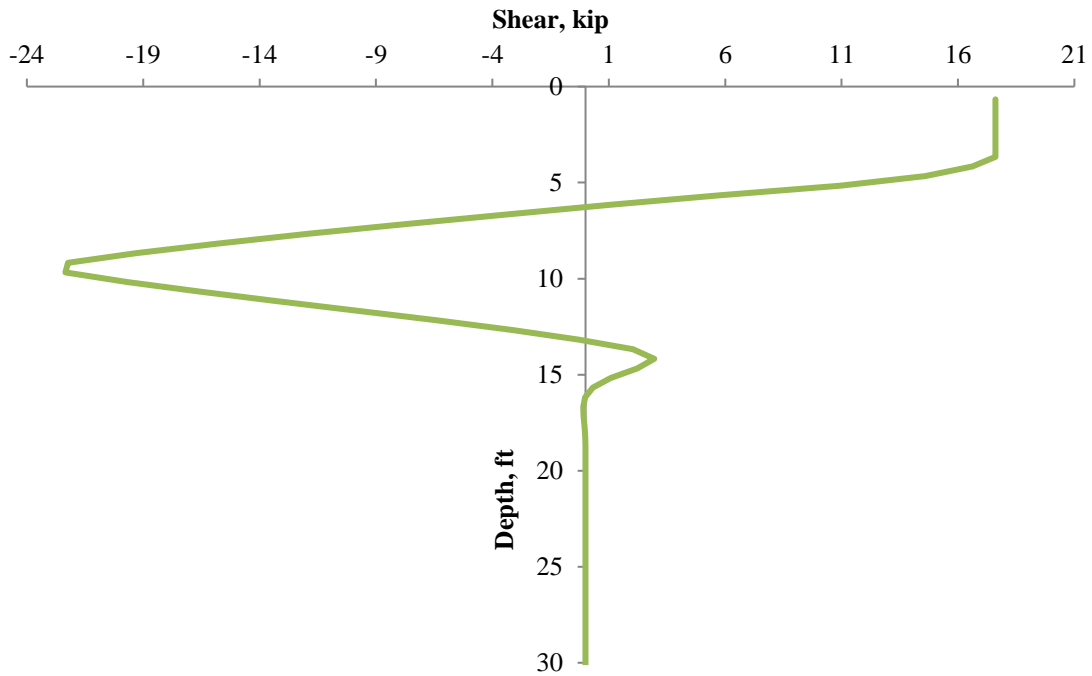
Figure E-32. Adjusted shear force along length of P4 at 17.0 kip load step during lateral load test
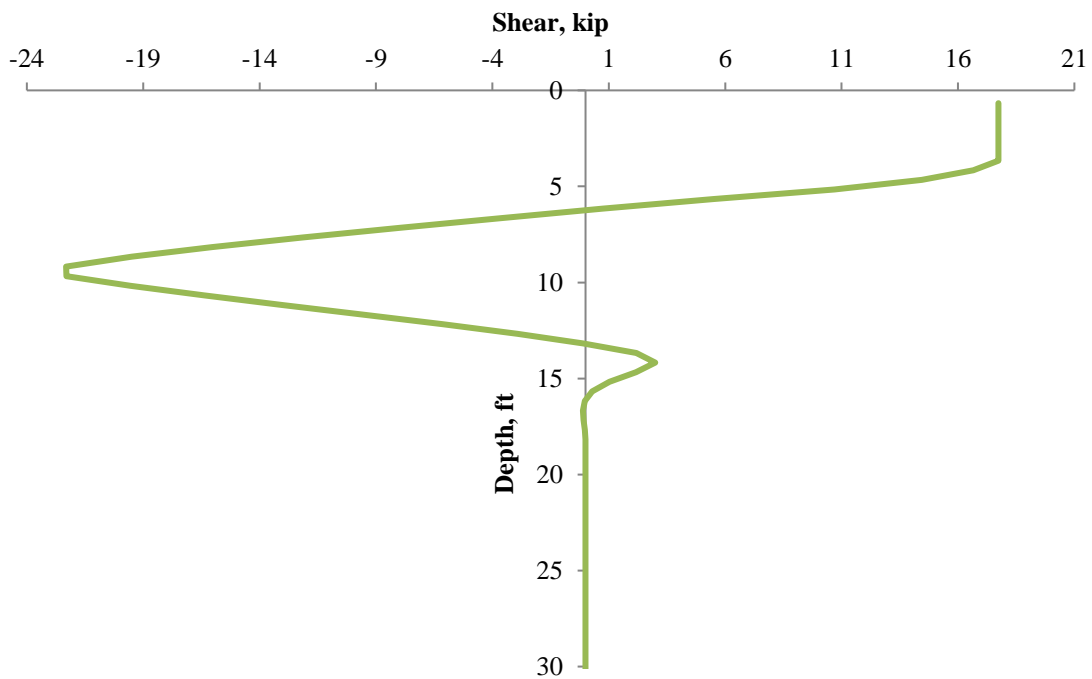

Figure E-33. Adjusted shear force along length of P4 at 18.0 kip load step during lateral load test

THE INSTITUTE FOR TRANSPORTATION IS THE FOCAL POINT FOR TRANSPORTATION AT IOWA STATE UNIVERSITY.

InTrans centers and programs perform transportation research and provide technology transfer services for government agencies and private companies;

InTrans contributes to ISU's educational programs for transportation students and provides K–12 outreach; and

InTrans conducts local, regional, and national transportation services and continuing education programs.

INSTITUTE FOR TRANSPORTATION

IOWA STATE UNIVERSITY

Visit **InTrans.iastate.edu** for color pdfs of this and other research reports.